Theoretical Investigation of Diradicals and Carbenes

By

Benjamin Christian Haenni

A dissertation submitted in partial fulfillment of

the requirements for the degree of

Doctor of Philosophy

(Chemistry)

at the

UNVIERSITY OF WISCONSIN-MADISON

2016

Date of final oral examination: 8/17/2016

The dissertation is approved by the following members of the Final Oral Committee:

Robert J. McMahon, Professor, Chemistry

Samuel H. Gellman, Professor, Chemistry

Edwin L. Sibert, III, Professor, Chemistry

Clark R. Landis, Professor, Chemistry

R. Claude Woods, Professor, Chemistry

For Mary. <3 (^^^)

Theoretical Investigations of Diradicals and Carbenes

Benjamin Christian Haenni

Under the supervision of Professor Robert J. McMahon

at the University of Wisconsin-Madison

This thesis focuses on a variety of computational work on a range of different organic diradical and carbene species. Chapter 1 gives an introduction to using computational chemistry to predict rate constants for a tunneling reaction. The installation and use of Polyrate and Gaussrate software is discussed from the perspective of teaching a new graduate student the use of the software. Though the number of publications using this software is increasing every year, there remains a lack of easily obtainable resources for the novice user. The chapter also provides an overview of transition state theory (TST) and the many different tunneling approximations available in the software.

Chapters 2 and 3 detail the two main investigations into tunneling. Chapter 2 outlines the study of a hydrogen migration reaction of triplet *o*-tolylcarbene and several naphthylcarbene species. Tunneling rates and the potential energy surface (PES) of these species

were explored computationally in comparison to experimental matrix and spectroscopy work. This work explores the differences in the PES of the carbenes in an attempt to rationalize the observed experimental differences in tunneling rates. Chapter 3 explores the heavy-atom tunneling present in the ring expansion of benzazirine to ketenimine, an important process along the long studied phenylnitrene pathway. The role of heavy-atom tunneling will be discussed in comparison to other substituted benzazirine species, and previously studied systems.

Chapter 4 introduces the study of two families of (σ,σ) diradical species on the C_8H_4 PES; didehydropentalene (DDP) and didehydrobenzocyclobutadiene (DDB). CASSCF and CASMP2 calculations were performed to evaluate the differences in through-bond and through-space coupling of the two spins in the singlet state.

Chapter 5 discusses the use of computational chemistry to better understand and explain the observed spectroscopy of three matrix isolated species; HC_7H, MeC_7H, and MeC_3Me. High-level coupled-cluster calculations were used to explore the PES of these species to discover the most likely ground state structure. Harmonic vibrational frequency and excited state calculations carried out in Gaussian09 and CFOUR allow for comparison of predicted and experimental IR and UV/Vis spectra, respectively. Natural Bond Orbital (NBO) and Natural Resonance Theory (NRT) calculations were performed to rationalize the large spin delocalization present in the triplet diradical species.

Acknowledgements

The completion of my thesis is in large part due to the love and support of so many people.

I would like to start by thanking my advisor, Robert J. McMahon. I still remember the first time we met at recruitment weekend. There I was, tremendously unsure of myself and the chemistry I wanted to explore. I very clearly recall calling my future wife on the phone and excitingly telling her about this "cool astrochemistry professor" who just gave a presentation. From then on I knew which research group I was going to join. Bob helped me explore a field of chemistry I never expected to dive into. He helped me become a better writer, scientist, and thinker. He supported my crazy and last minute move to La Crosse, even though it made things more difficult, which I am greatly appreciative.

I would like to thank the many members of the UW Madison faculty and staff. Nick Hill helped me become a better TA over 5 years. Desiree Bates spent many, many, many hours helping me with both my work and my understanding of computational chemistry, for which I am incredibly grateful. Paul McGuire also spent many hours helping me with problems I encountered (or created) using the PHOENIX cluster. Professor John Stanton of the University of Texas proved invaluable for guiding me through using CFOUR and coupled-cluster calculations. I greatly enjoyed the time I got to spend with Claude Woods, whose stories always made group dinners just that much more fun.

I would like to thank the McMahon group, past and present. You made my day-to-day life in the office enjoyable. Enjoyable! How many graduate students can brag about that? I have never met a more funny, goofy, and incredible group of people. I am happy to say as I was able to work in an office of friends for five years. Thanks to Brian, for helping me grow as a

teacher and a computational chemist. Thanks to Terese, for putting up with me. To Brent, for all the great times we had together in Madison. Thanks to Thomas, who stayed in touch all these years even from the other side of the world. Thanks to Steph, for becoming a better friend than I could of possibly imagined. Thanks to Laura, for baking me that delicious challah. Thanks to Cara, Zach, Maria, Vanessa, Nick, Matisha, Andrew, and George for making the McMahon group the friendliest and silliest group in Madison.

Next, I have to thank my family. I do not think my parents fully understood what I had gotten into when I started graduate school (neither did I, truly) but they were always excited and supported me in every way they could. Thanks Mom, thanks Dad, I loves ya the most. Thanks to my brother Joe for being there to talk to when I needed. It was good to know that if we got in touch I could count on taking a couple of hours to catch up, no matter how long it had been or how great the distance. I am so happy for you, Kelsey, and Maeve. This thesis is long enough without naming all of my family (thanks Lonergan family), but know that trips back to St. Louis and Jacksonville where often just the bit of fun I needed to keep me going.

I must also thank the Olsens. It was great to live so nearby for so long and see each other so often. Ann and Marv were always super supportive, and kept me very well fed. I am so happy that I was able to be so close to Chris and Sara and watch Maryn grow up a little, even if she is a dork. To Laura and Neal, don't worry, we are moving closer! To Sarah Olsen, sorry, we are moving away! Thanks to Auntie, Woody, and Greg for making me feel part of the family since I first walked through that door on Jamesway so many years ago.

I must thank my friends. Scott, best man and Star Trek partner for life, has been listening to my complaining since elementary school, and seems content to continue for the foreseeable future. My Drake crew of Lizzy, Andrew, and Jamie; isn't it funny that we all ended up teaching

one way or another? To my Madison bros Andrei, Brent, Jon, Derek, Joe, Sarah, Chris, Caroline, Anna, Alex, and Allice, and Will; Thanks for filling in the gaps of work with the fun memories of Madison that I will never forget. Times that I will never regret, besides perhaps the hours of LoL and one fifth qualifier.

I must end with, of course, my wife Mary. She has been there every step of the way with me after following me to Madison after we graduated from Drake. From the time I started stressing and panicking about taking the GRE she has been there with her support. Never backing down, never letting me give up, and never making me regret or feel guilty for dragging her along for this wild ride that is graduate school. She was always there to pick me up and tell me that no matter what it would be O.K, and I cannot tell her enough how much I appreciated that. The tacos didn't hurt either. I love you, I love you, I love you.

Table of Contents

List of Schemes

List of Tables

Chapter 1: Introduction to Tunneling Calculations using Gaussrate and Polyrate

Chapter 2: Tunneling Reactions in Arylcarbenes

Chapter 3: Quantum Mechanical Tunneling in Benzazirines

Chapter 4: Diradicals on the C_8H_4 Potential Energy Surface

List of Figures

Chapter 1: Introduction to Tunneling Calculations using Gaussrate and Polyrate

Chapter 2: Tunneling Reactions in Arylcarbenes

Chapter 3: Quantum Mechanical Tunneling in Benzazirines

Chapter 4: Diradicals on the C_8H_4 Potential Energy Surface

Chapter 1: Introduction to Tunneling Calculations using Gaussrate and Polyrate

Introduction

Almost ninety years ago, Hund predicted that light particles could pass "through" a potential energy barrier instead of thermodynamically passing over the barrier.[1] This process eventually became known as quantum mechanical tunneling (QMT), or simply as tunneling. Shortly after, several papers demonstrated tunneling in chemical reactions involving the hydrogen atom.[2,3] Since then, tunneling in chemical reactions is a well-accepted and studied quantum mechanical phenomenon. In the McMahon research group, tunneling (or the possibility of tunneling) is of particular interest to us for its relevance to our work matrix isolating reactive intermediates. When a molecule is trapped in a cryogenic matrix of an inert gas at extremely low temperatures (4-20 K), classical or "over the barrier" reactions are often impossible. However, tunneling reactions, which are independent of temperature, can still occur. The observation of the decay of a matrix-isolated species is often very indicative of a tunneling reaction taking place. As such, the ability to calculate and predict rate constants of these tunneling reactions becomes an incredibly powerful tool for us.

In more recent years, a wide range of tunneling reactions in organic systems has been studied both experimentally and computationally.[4-6] Scheme 1.1 shows several examples of tunneling reactions whose study was augmented by calculated rate constants. Zuev *et al*. studied the decay of two halocarbenes,**1a** and **1b**, under matrix isolation conditions, both involving heavy-atom tunneling.[7] The chlorocarbene **1a** was not detected in the matrix, and only the product of the ring expansion 2a was observed. Calculated CVT / SCT rate constants predicted a very fast rate for the tunneling reaction ($k = 1.4 \times 10^4$ s^{-1}), demonstrating why the chlorocarbene could not be detected. In contrast, the decay of fluorocarbene **1b** was slow enough to be

observed via IR spectroscopy. DFT calculations demonstrated that a larger barrier was responsible for the slower rate of $k = 4.0 \times 10^{-6}$ s^{-1} at 8 K compared to the ring expansion of **1a**. The calculated rate constant for the tunneling reaction from **1b** to **2b** was $k = 9.1 \times 10^{-6}$ s^{-1} at 8 K, which closely correlates with experiment. In a joint study between Truhlar and Borden,[8] experimental results for the life time of carbene **3** were rationalized with the discovery of a very fast 1,2 hydrogen shift to from the product **4** in the gas phase. The barrier to the reaction derived experimentally from the Arrhenius plot was 4.9 kcal/mol, much smaller than the calculated barrier of 11.4 kcal/mol. CVT / SCT constants demonstrated that tunneling was a major contributor to the rate constant, even at higher temperatures (>298 K). Schreiner *et al*. were able to use calculated rate constants to explain the observed reactivity of methylhydroxycarbene **5**.[9] They found that the controlling factor was not the height of the barrier (kinetic control) or relative energy of the products (thermodynamic control), but the width of the barrier (tunneling control). As the barrier to **7** was found to be much narrower than the barrier to **6**, tunneling to **7** was the observed major product at low temperatures. Overall, computational study of the potential energy surface (PES) and calculated rate constants, including contributions from tunneling, have been shown to be critical in the study of tunneling in organic reactions.

Scheme 1.1. Organic reactions involving QMT.

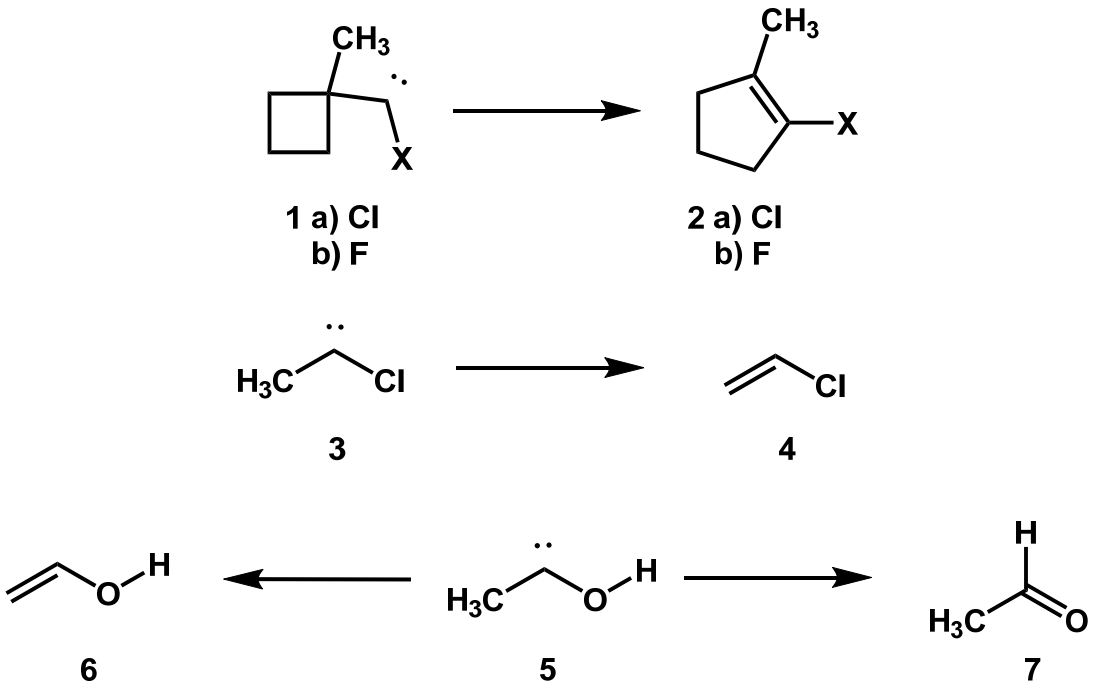

This chapter will serve as an introduction to tunneling calculations using Polyrate and Gaussrate software. Though many in the physical organic chemistry field are familiar with the common types of DFT calculations in computational chemistry software packages, such as Gaussian, tunneling calculations have their own unique language and background. Furthermore, guides and resources outside of the Polyrate and Gaussrate manuals are scarce. Whereas most common problems with Gaussian calculations have been answered many times over in easy-to-find online sources, finding help with Polyrate can be challenging outside of directly contacting another research group. With this in mind, this chapter will be dedicated to explaining the background and procedure necessary for performing and understanding these calculations.

Transition State Theory and Tunneling Approximations

Though there are other popular methods for calculating rate constants, such as instanton theory,[10] Polyrate employs variational transition state theory (VTST) and canonical variational transition state theory (CVT). In generalized transition state theory (TST), it is assumed that the transition state (sometimes referred to as saddle point) is a dividing surface that separates the reaction and product regions of the PES.[11,12] For TST, it is also assumed that all trajectories that connect the reactant and the transition state will proceed to the product side of the dividing surface without recrossing back to the reactant region. As such, the product side of the surface does not contribute to the rate constant *k*. In reality this assumption is false; pathways connected to the reactant and product can recross the transition state multiple times. Because of this, TST gives only an upper bound of the classical rate constant. While useful due to the small amount of information needed of the total PES (small regions around the reactant and product), variational transition state theory improves on generalized TST. In VTST, recrossing is included by altering the position of the transition state (the region known as the "bottleneck") to minimize recrossing of the dividing surface, thus lowering the classical rate constant to a more physical value. While not accounting for all of the recrossing that can occur, rate constants calculated by VTST provide values that much more closely correlate with experiment.[13,14] The specific type of VTST used in Polyrate is canonical variational theory (CVT), where one single transition state is found and used for any given temperature.[15]

For classical reactions, CVT uses the minimum energy pathway (MEP) to calculate rate constants. The MEP is defined as the steepest descent path in mass-weighted Cartesian coordinates connecting the transition state and reactants and products.[16] However, all the methods discussed thus far do not include corrections for non-classical trajectories through the

barrier, as is the case in a tunneling reaction. Tunneling has a strong dependence on the width of the tunneling pathway, and as a result, tunneling reactions do not necessarily follow the MEP. This is demonstrated in Figure 1.1. The black dotted line represents the MEP between the reactant and product side of the PES, passing through the transition state TS. The green dotted line represents one possible tunneling pathway that goes through a higher energy, though ultimately shorter, pathway on the dividing surface.

Figure 1.1. Demonstrative potential energy surface of a tunneling reaction of A–B + C → A + B–C.

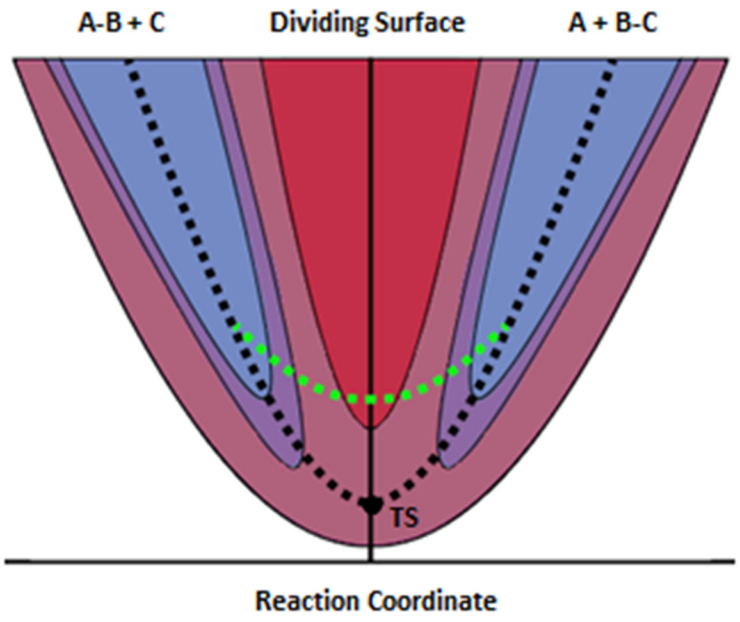

The degree of this deviation from the MEP is described at the "curvature" of the tunneling reaction. Different types of tunneling approximations have been formulated to model different reactions depending on the degree of curvature in the tunneling system. If the tunneling

path does not deviate from the MEP but instead follows the same pathway, then the minimum energy path semiclassical adiabatic ground state (MEPSAG) tunneling approximation is used.[17] This is more often referred to as the zero-curvature tunneling (ZCT) method. However, as most tunneling reactions typically follow shorter pathways through the dividing surface, the ZCT approximation has been shown to often severely underestimate the contribution of tunneling to a reaction.[18] To predict rate constants in reactions where tunneling takes a shorter pathway than the MEP, the centrifugal-dominant small curvature semiclassical adiabatic ground state (CD-SCSAG) method is used.[19] Often referred to as small-curvature tunneling (SCT), this method is appropriate when the tunneling pathway is close to the MEP but deviates by a small amount. Lastly, for cases where the deviation from the MEP is significant, as in a straight line tunneling pathway from reactants to products, the large-curvature tunneling (LCT) approximation is used.[20] Such a large curvature away from the MEP is often seen when a light atom is transferred between two heavy atoms in a bimolecular reaction, and the tunneling pathway is essentially a straight line between the reactant and product wells. While the LCT approximation appears to be valid when used to model specific types of bimolecular reactions, the contribution of large-curvature pathways in other systems has been shown to be negligible.[21] While all three of these tunneling approximations have been used with success, the focus of this work will be on the SCT approximation. The SCT approximation has been found to accurately calculate rate constants for a variety of unimolecular hydrogen transfer reactions and ring-opening reactions involving heavy atoms, the subjects of Chapters 2 and 3 respectively.[5,6]

To calculate rate constants for tunneling reactions we used Polyrate.[22] Polyrate calculates rate constants and tunneling approximations using ZCT, SCT, and LCT for a given PES. Gaussrate[23] is a separate program that links Gaussian 09[24] and Polyrate. This allows for

Gaussian09 to generate the data for the MEP and directly feed this information to Polyrate for the rate calculations.

Installation of Polyrate and Gaussrate

With an incredible amount of help from the Chemistry Departments High-Performance Computing (HPC) Systems Administrator, Paul McGuire, both Polyrate and Gaussrate were installed on the PHOENIX cluster. Polyrate and Gaussrate were compiled and installed following the Polyrate user's manual (http://comp.chem.umn.edu/polyrate/) and Gaussrate Quickstart Guide (http://comp.chem.umn.edu/gaussrate/), the only difference being they were compiled in bash (Bourne Again Shell) instead of csh (C shell). Due to complications with file sharing permissions, individual users must have Polyrate and Gaussrate installed in their own home directory. Future users of Polyrate and Gaussrate must contact Paul McGuire for installation in their home directory.

Overview of Input Files

Though manuals and guides can be found for Polyrate and Gaussrate at the links above, overall I found it challenging to learn the software on my own. Unlike the ubiquitous Gaussian09, Gaussrate is more of a niche computational chemistry package used by only a handful of research groups. Though this is slowly changing, with the number of published papers utilizing this software slowly increasing every year, little is written for the novice or beginner user. When I started my research in the McMahon group, it took me a significant amount of time to eventually reproduce the results of Truhlar's study of the 1,2-hydrogen

migration in methylchlorocarbene.[8] For these reasons, I believe it would be greatly beneficial to lay out a guideline for using this software here.

To carry out a tunneling calculation for a given reaction using Gaussrate, two main components are needed: the optimized geometry of the reactants, products, and saddle point (transition state), as well as the MEP connecting the reactant and products through the saddle point. Gaussrate can be used to generate both of those components and then feed that information directly to Polyrate to find the rate constants. Using Gaussrate requires several different input files for Polyrate, Gaussrate, and Gaussian09. Table 1.1 shows the different files. Each one will be described in detail in the following section.

Table 1.1. Main Input files for Gaussrate.

File Name	Description
esp.fu70	General Gaussrate input date
esp.fu71	Gaussian09 input file for geometry optimization of reactant 1
esp.fu72	Gaussian09 input file for geometry optimization of reactant 2
esp.fu73	Gaussian09 input file for geometry optimization of product 1
esp.fu74	Gaussian09 input file for geometry optimization of product 2
esp.fu75	Gaussian09 input file for geometry optimization of the saddle point
esp.fu83	Gaussrate restart file used to restart or extend a calculation
esp.dat	Polyrate input file

The esp.fu70 input file

An example of a typical esp.fu70 input file is shown below in Figure 2.1, followed by explanations of the relevant sections and keywords. While some input files can vary depending on how the rate constant calculation is set up, a esp.fu70 file is required for every calculation using Gaussrate.

Figure 1.2. Sample esp.fu70 Gaussrate input file.

```
*GRGENERAL

 GRRESTART

*GRSTART

 CHARGE          0
 MULTIPLICITY  1

*GRCOMMON

 GRENER
    #b3lyp/6-31g(d) UNITS=AU FCHK NOSYMM INT=GRID=ULTRAFINE
 END

 GRFIRST
    #b3lyp/6-31g(d) FORCE UNITS=AU FCHK NOSYMM INT=GRID=ULTRAFINE
 END

 GRSEC
    #b3lyp/6-31g(d) FREQ=NORAMAN UNITS=AU FCHK NOSYMM INT=GRID=ULTRAFINE
 END

 GRLINK0
    %nproc=12
    %mem=24GB
 END
```

***GRGENERAL**

GRRESTART: The use of this keyword instead of NOGRRESTART creates an esp.fu84 output file after the calculations. This allows the calculation to be restarted if there is an error, or to make a longer PES or otherwise extend the calculation. It is strongly recommended to always run calculations with GRERESTART=ON as no extra computational cost is required.

***GRSTART**

The charge and multiplicity for the reaction.

CHARGE: The charge for the molecules to be studied.

MULTIPLICITY: The multiplicity for the molecules to be studied.

***GRCOMMON**

The keywords in this field specify the level of theory and basis set used to calculated the energy, first derivative, and second derivative for the stationary points. These are essentially Gaussian input lines and should be treated as such. For example, it is recommended for DFT calculations to use the keyword INT=GRID=ULTRAFINE when using tight convergence criteria so that keyword would be included in this section. The level of theory and basis must be consistent for all three.

UNITS=AU: This is very important for using Gaussrate, as all geometries in all input files must be given in bohr instead of the more common Angstrom (the default in most other computational

chemistry software). UNITS=ANG is not a useable option. Many common errors arise from not properly converting from one unit to the other.

NOSYMM: Removes any symmetry in the calculation, treating the molecule as C_1 regardless of its actual point group. It is not required, but very highly recommended. Severe complications can arise from symmetry across the changing PES, and using the NOSYMM keyword helps avoid these complications.

FCHK: Generates FCHK files from the stationary points for use in the rest of the PES and rate calculation. This keyword is required for normal use.

FORCE: Required for calculation of first-ordered derivatives in GRFIRST.

FREQ=NORAMAN: Not required, but strongly recommend. This saves computational resources by not calculating intensities of Raman transitions, which are often not desired or required.

GRLINK0

The keywords here specify the information for running the job on the PHOENIX cluster.

%nproc: The number of processers used for the calculation. Given the scale of the IRC calculations carried out, the maximum number of processors for a typical node on PHOENIX

should be used. This is currently at 12, but can be updated if PHOENIX gets larger nodes. As installed, Gaussrate and Polyrate cannot be parallelized across multiple nodes.

%mem: Memory for the calculation. 24 GB, as shown in the example, is a low and safe value of memory allocation. Speak to the current Computational Chemistry Leader to assign the proper largest amount of memory.

The esp.dat input file

Most of the data for the calculation will be in the esp.dat file. This is the Polyrate input file and will have a bulk of the information for the calculation. Some of the fields in esp.dat are straightforward enough or explained well enough in the manual that they will not be discussed in depth here. The rest of the sections and keywords will be described below.

Figure 1.3. Sample esp.dat Polyrate input file.

```
*General

 TITLE
 Ring expansion
 END

 ATOMS
  1   C  13.0033548378
  2   C
  3   C
  4   C
  5   C
  6   C
  7   N
  8   H
  9   H
  10  H
  11  H
  12  H
 END

 NOSUPERMOL

 INPUNIT AU

*OPTIMIZATION

 OPTMIN  OHOOK
 OPTTS   OHOOK

*SECOND

 HESSCAL HHOOK

 *REACT1

 STATUS   2

 # Geometry in a.u.
 GEOM
1            -1.41230750   -1.57814797    0.22339396
2             1.05273422   -2.68487355    0.40114725
3             2.86404603   -0.90581181   -0.06706827
4             2.28386992    1.75053255   -0.41266324
5            -0.04056486    2.76549682    0.10569993
6            -2.11854724    1.08808533    0.77591582
7            -3.17062762   -0.83977722   -1.21065484
8             1.43069454   -4.65260554    0.82503547
9             4.83594675   -1.47804918   -0.15296009
10            3.84643520    2.99752683   -0.88256251
11           -0.25173040    4.80606641    0.26220137
12           -3.44235321    1.59381380    2.26430558
 END

 ELEC
  1   0.000
 END

 SPECIES  NONLINRP

*PROD1

 STATUS   2

# Geometry in a.u.
 GEOM
 1             0.00884770   -2.48567942   -0.06045233
 2             2.33389474   -1.90515560    0.65699348
 3             2.97396383    0.63133856   -0.28238553
 4             1.19042722    2.48678491   -0.32917326
 5            -1.45615293    2.29010790    0.43832572
 6            -3.00138754    0.24425275    0.27966433
 7            -2.16481907   -2.04552823   -0.87461621
 8             3.51098805   -3.01766564    1.90929410
 9              4.88269102       1.04369566     -0.93914090
10             1.78183397    4.35721869   -0.95223293
11            -2.34120987    4.04262089    1.05256415
12            -4.97812407    0.32291638    0.83398899
 END

 ELEC
  1   0.000
 END

 SPECIES  NONLINRP

*START

 STATUS 2

 # Geometry in a.u.
 GEOM
1             1.03302627   -2.01837097   -0.07102535
2            -1.47058287   -2.49797587   -0.56354653
3            -2.96282957   -0.41939823    0.15028235
4            -1.96872976    2.01599181    0.48591091
5             0.50533730    2.67147917   -0.24247074
6             2.45572538    0.93776518   -0.61016418
7             2.87238917   -1.23256622    1.17093469
8            -2.17495934   -4.19997270   -1.45413659
9            -4.99688527   -0.68068686    0.30325378
10            -3.28338379    3.53100781    0.92224486
11             0.83254524    4.59923212   -0.88987197
12             3.96426907    1.24142525   -1.97196875
END

 ELEC
  1   0.000
 END

 SPECIES  NONLINTS

# end of start section

*PATH

 SCALEMASS  1.00

 INTMU   3
 SSTEP   0.005
 INH     10

 SRANGE
  SLP  1.70
  SLM -2.90
 END

 RPM       PAGEM

 SIGN    REACTANT

 IDIRECT  1
```

```
 COORD  CURV3

 INTDEF
 2-1
 3-2 3-2-1
 4-3 4-3-2 4-3-2-1
 5-4 5-4-3 5-4-3-2
 6-5 6-5-4 6-5-4-3
 7-6 7-6-5 7-6-5-4
 8-2 8-2-3 8-2-3-4
 9-3 9-3-4 9-3-4-5
 10-4 10-4-5 10-4-5-6
 11-5 11-5-6 11-5-6-7
 12-6 12-6-7 12-6-7-1
END

PRPATH
  INTERVAL 1
 END

 PRINTSTEP

*TUNNEL

 QRST
  harmonic
  srw -2.90
  mode 30
  states all
 END

  ZCT
  SCT

 *RATE


  FORWARDK
  GTLOG
  SIGMAF      1
  CVT

  TEMP
    10.
    20.
    30.
    40.
    50.
    60.
    70.
    80.
    90.
   100.
   110.
   120.
   130.
   380.
   390.
   400.
END
```

***General section**

ATOMS: List of the atoms for the molecules(s) of the reaction. The order of the atoms must be consistent across all input files.

If a kinetic isotope effect (KIE) is needed, this is also where different isotopes must be specified. If left blank, the naturally abundant isotope for the element will be used by default. Listing another mass in a.m.u. will change the mass of the atom to the appropriate value. Note that any value can be used, not just those of actual isotopes. This can be taken advantage of by giving individual atoms unrealistic masses to mimic the effect of large, computationally demanding substituents. This technique was used quite cleverly by Kozuch when studying the automerization of pentalene.[25] Large *tert*-butyl groups substituents added too much computational cost to the calculations, so instead a hydrogen atom with a mass of 57 was used to test to effects of that mass on the tunneling reaction.

INPUNIT: Specifies the units for the input geometries, if any. As in the esp.fu70 input file, bohr should be used.

***REACT 1, REACT2, PROD1, PROD2, and START section**

Each section specifies the required information for the respective reactant, product, or transition state (referred to as START in Polyrate). For the tunneling calculations in this work, all reactions are unimolecular and only *REACT1, *PROD1 and *START are required. If calculating a bimolecular reaction, the *REACT2 and/or *PROD2 fields will be needed.

STATUS: The STATUS keyword determines how much information for the stationary points is read into Polyrate from the input files, and how much must be calculated on the fly. The choices for STATUS are shown in Table 1.2.

Table 1.2. Options for the STATUS keyword.

Option	For reactants of products	For transition state (START)
0	Calculate geometry, energy, and frequencies	Calculate geometry, energy, frequencies, and eigenvectors
2	Read in geometry; Calculate energy and frequencies	Read in geometry; Calculate energy, frequencies and eigenvectors
4	Not Available	Read in geometry, energy, and Hessian; Calculate frequencies and eigenvectors
6	Read in geometry, energy, and frequencies.	Read in geometry, energy, frequencies, and eigenvectors.

From personal experience and demonstrated from published papers, STATUS = 0 or STATUS = 2 are often the most convenient options. While this does lead to some unnecessary recalculation of properties of the stationary points, the bulk of the computational workload is generating the PES and the extra time taken is largely insignificant.

The example in Figure 1.2 uses STATUS = 2, so the geometry for each stationary point (in a.u.) is given. If STATUS = 0, then the list of the numbered atoms for each structure should be given with no further information.

ELEC: This keyword specifies the degeneracy and energy of the electronic state of each species. Typically one electronic state is listed and denoted the ground state by listing a relative energy of zero.

SPECIES: Denotes if the reactant or product is linear (LINRP) or not linear (NONLINRP), or if the transition state is linear (LINNTS) or not linear (NONLINTS).

PATH Section

Most of the variables in this section are at their default settings. The important variables are explained below.

SRANGE: This specifies the limits of the reaction coordinate to be explored for the generation of the MEP, with the units dictated by the INPUNIT keyword. An IRC calculation should be done in Gaussian with large step sizes to quickly get a good starting guess at these values before running the more computationally demanding Polyrate and Gaussrate calculation. SLP is the positive limit and SLM is the negative limit.

RPM: This is the method for following the integrator from the transition state downhill to generate the MEP. PAGEM stands for Page-McIver integrator method.[26,27] While I have not personally tested and compared the various methods extensively, PAGEM is universally preferred by those using Gaussrate.

SIGN: Designates the reactant on the positive or negative side of the reaction coordinate. By default, $s < 0$ is the reactant side and $s > 0$ is the product side. This is not always true, however, and the MEP should be manually examined for each new calculation. SIGN = REACTANT by default.

COORD: This keyword determines whether Cartesian or Curvilinear coordinates are used for generalized normal mode analyses. Curvilinear coordinates have been shown to give more physical values for vibrational modes calculated along the reaction path, and are preferred.[28] The options of curv1, curv2, and curv3 are different methods discussed in-depth in the Polyrate manual. The curv3 method is the preferred option for systems larger than 3 atoms.

PRPATH: Off by default, this keyword ensures that the reaction path information is printed to the esp.fu25 output file (see later section for details on this file). The reaction path information is very important for assessing the accuracy of the calculation, and as such this keyword should always be enabled.

PRINTSTEP: This keyword prints the xyz coordinates for the geometry of each step along the MEP to the esp.fu6 output file. It is strongly recommended to take advantage of PRINSTEP, as this is the only way to visualize the geometry of the reactants/products at a given point on the pathway, and for ensuring the generated pathway connects to the proper minimum.

***TUNNEL Section**

The keywords in this section control the properties for the tunneling approximations applied to the calculation.

QRST: Quantized-reactant-state-tunneling[29] is a keyword that must be used when performing calculations of unimolecular reactions at low temperatures. Normally, tunneling is assumed to occur from a series of continuous tunneling energies, which is a fine approximation for higher temperatures. At lower temperatures, QRST only performs tunneling calculations at energies corresponding to the eigenstates of the reaction-coordinate mode of the reactant. SRW is the position on the reaction coordinate of the reactant. STATES determines the number of quantized reactant states to be included (ALL by default). MODE is the number of vibrational modes in the molecule. It is important to note that the end result of including QRST increases the magnitude of the rate constants. In my experience, QRST rate constants were consistently around 100 times larger than rate constants calculated without QRST.

ZCT and SCT: This is where the tunneling approximations to be performed are listed. For most of the types of tunneling reactions of interest to the McMahon group, ZCT and SCT are the most appropriate. While ZCT often underestimates contributions from tunneling, it is useful as a point of comparison between CVT rate constants with no tunneling approximation and CVT rate constants using the SCT approximation.

***RATE section**

The *RATE section contains all the keywords needed to control the rate constant calculations.

FORWARDK: This keyword controls whether rate constants are calculated for the forward reaction or for both the forward and reverse reaction (BOTHK).

GTLOG: This keyword specifies that "generalized free energy of activation should be calculated by using the logarithms of the vibrational partition functions."[22] This keyword is needed when doing calculations at low temperatures or very large systems.

SIGMAF: SIGMAF is the symmetry number representing the number of equivalent pathways that a reaction can proceed in the forward reaction. This essentially multiplies the calculated rate constant from the calculation by the symmetry number. For example, most of the arylcarbenes in Chapter 2 have two equivalent pathways for hydrogen migration; clockwise rotation of the methyl group to donate one hydrogen atom, or counter-clockwise rotation to donate another hydrogen atom. In that instance, SIGMAF 2 would be appropriate.

CVT: Determines if canonical vibrational transition state theory is used when calculating rate constants. CVT, combined with a tunneling approximation like SCT, is currently the golden standard for tunneling calculations of hydrogen and carbon tunneling. If not present, TST (transition state theory) will be used instead. As discussed in the introduction, CVT is considered an improvement on generalized TST and should be used by default.

TEMP: This keyword determines the temperature at which rate constants will be calculated. Up to 40 temperatures can be listed.

Input files esp.71-75: Gaussian Input Files

If the keyword STATUS=0 is used in the esp.dat input file, then the appropriate Gaussian inputs must be provided for the reactants, products, and the saddle point. These files should be identical in construction to general Gaussian09 input files and will not be discussed in-depth here. Care should be taken that the level of theory, basis set, charge, and multiplicity of the system described in the esp.fu70 input file matches all used Gaussian input files and the esp.dat file.

Setting up a Rate Calculation

Before attempting to use Gaussrate/Polyrate, it is important to make sure that the stationary points and MEP is thoroughly investigated.

1) Find optimized structures of the stationary points

Perform an optimization and harmonic frequency calculation on all stationary points (reactants, products, and transitions state) using Gaussian09. This data will be needed for comparison to the output files for the Gaussrate calculation.

2) Map the PES from transition state to reactant(s) and product(s) with an IRC calculation

The bulk of the needed Gaussrate computational resources will be accurately mapping out the MEP connecting the reactant and the product. It is not uncommon in computational

chemistry for the MEP starting from a transition state to connect to different structures than what is obvious or predicted. To check that the predicted reactant(s), transition state, and product(s) are all connected by a single MEP, an intrinsic reaction coordinate (IRC) calculation in Gaussian should be run before attempting Gaussrate. IRC calculations, though using a different method for mapping the path of steepest descent from the transition state to the reactants and products, often find identical pathways as those in Gaussrate. The step size along the MEP for a typical IRC calculation is often much smaller than those in used in Gaussrate. Thus, running an IRC calculation to find errors can save days' worth of computational time.

2) Prepare stationary point geometries for rate.dat

If using a STATUS keyword where the geometry is read in the esp.dat file, care must be taken to input the geometry of each stationary point properly. The units of the given Cartesian coordinates must be in bohr, and the connectivity of the atoms must stay consistent for all geometries. For example, if the atom to be transferred in a tunneling reaction is labeled number 14 in the reactant, it must also be listed as number 14 in the transition state and products.

The easiest way to accomplish this is to open the optimized stationary point in GaussView, then save it as a new file with the UNITS=AU in the input line. The **Connection** tool in the **Edit** tab can then be used to renumber the atoms as needed.

4) Submitting the job to the PHOENIX cluster

All input files should be in the same directory on PHOENIX. In this directory, a file named "grinputlist" must be made. In this file, all input files being used for the calculation must be listed, one on each line. The files esp.fu70 and esp.dat are always required. If a STATUS

keyword is being used that requires inputs for reactants or products, those files must be present as well (esp.fu71-75). If an old calculation is being restarted, then esp.fu83 must be present (see the section on restarting calculations). Note that for the input files, the label of "esp" is the default used by Gaussrate and Polyrate, but any title can be chosen by the user as long as it is properly labeled in the grinputlist.

Typical use of the script would look like:

qgaussrate –np X jobname

where *–np* designates the number of processors to use for the job and *jobname* your designated title for that job. The chosen jobname will replace the "esp" label in the output files. For most calculations, even a modest B3LYP/6-31G(d) calculation can takes several days. It is recommended that the maximum amount of available processors on a single node on the PHOENIX cluster be used (currently 12).

Description of Output files / Reading results

At the end of the calculation, there is a wide array of different output files (Table 1.3).

Table 1.3. Main output files for Gaussrate.

File Name	Description
esp.fu61	Geometry, Energy, Vibrational Frequencies and for reactants, products, and transition state
esp.fu82	Temporary Gaussian09 output file for transition state calculations
esp.fu84	Restart file for further calculations
esp.fu14	Reserved for future use (not used)
esp.fu15	Summary of rate constants
esp.fu25	PES data generated if PRPATH is used
esp.fu6	Polyrate output file

The esp.fu61 file contains the geometry, energy, and vibrational frequencies for the stationary points. The data in this file must be vigorously checked to match previously calculated results for the stationary points. If they are not matching, then an error may have occurred in the optimization or frequency calculation of the stationary points that must be addressed.

The esp.fu82 file is the Gaussian output file for the transition state calculation. Again, the data in this file must be checked against previously calculated data to ensure accuracy. The

esp.fu15 file simply contains a short summary of the calculated rate constants at the specified temperatures and levels of theory.

The esp.fu25 file, generated by the PRPATH keyword in the esp.dat input file is critically important. This output file prints the pathway information connecting the transition state structure to the products and reactants. There are a variety of important pieces of data to check from this file.

1) **The MEP successfully connects to reactant**: Depending on the calculation, the reactant can lie on either the positive or reactant side of the reaction coordinate (negative or positive *s* values). The "Vmep" column shows the relative energy of each point of the pathway compared to the reactant. If the Vmep value converges to zero on one side of the barrier, then this is confirmation that the MEP made it to the reactant.

2) **The MEP successfully connects to the product**: Unlike the reactant side, it is not critical that the MEP reaches all the way to the product for the sake of the calculation. Once the MEP reaches the point where it is lower in relative energy on product side compared to the reactant, the calculation can be stopped. This is the result of the tunneling process taking place from the minimum on the reactant side through the barrier. Once it is across, the products simply relaxes in energy down the slope to the products, so calculation of the rest of the path is unnecessary. As long as the Vmep value is negative on the product side, the calculation has reached far enough for an accurate rate constant. If the product side of the MEP is wide (as demonstrated by several methylnaphthylcarbenes is Chapter 2), cutting off the calculation early is a great way to save computational resources.

3) **Visual inspection of the MEP**: The data in the file allows one to graph *s* vs. Vmep to visually inspect the generated MEP in comparison to previously calculated IRC data using Gaussian09.

The final output file is esp.fu6, which is the Polyrate output file that contains the greatest wealth of information that needs to be checked. It contains all the information on the stationary points, the MEP, and detailed reporting of the calculated rate constants. The first part of the output file prints the calculated geometries, energies, and vibrational frequencies of the stationary points. These must be thoroughly compared with previous calculations for accuracy. A particularly useful section of the output automatically compares the relative energies of all the stationary points after the calculation. Assuming the potential energy surface has been properly explored ahead of time, this is a quick way to check that everything matches up in this calculation.

Table 1.4. Sample saddle point energetics table from esp.fu6 output file.

Saddle point energetics (V = classical energy, ZPE = zero point energy)

	hartrees	eV	cm**-1	kcal
V w/re reactants V	0.03098	0.84307	6799.79	19.4416
V w/re product V	0.04666	1.26978	10241.42	29.2817
V+ZPE w/re reactant V	0.20291	5.52150	44533.51	127.3277
V+ZPE w/re product V	0.21859	5.94821	47975.15	137.1678
V+ZPE w/re reactant V+ZPE	0.02611	0.71042	5729.84	16.3824
V+ZPE w/re product V+ZPE	0.04303	1.17080	9443.07	26.9991
V+ZPE w/re saddle point V	0.17193	4.67842	37733.72	107.8861

The final section of interest in the esp.fu6 output file is the section labeled "Space-fixed Cartesian coordinates vs reaction coordinate (a.u.)". This is the geometry data for every point along the generated MEP. The geometry can be copied from the output file to view in GaussView, MOLDEN, or any other visualization program. This is valuable when doing calculations where the reactant is on a very flat region of the PES. If several subtly different minima exist of the reactant side, then visual inspection of the geometry along the MEP might be necessary to ensure the proper reactant is reached. For example, if another rotamer of the reactant is similar in energy, inspection of the Vmep value from the esp.fu25 output file may make it appear that the proper rotamer was reached when in fact the pathway diverged to a different reactant. Taking the geometry of that point and visualizing it in a program like GaussView or MOLDEN can then confirm that the proper rotamer was reached.

Restarting a calculation

The most common reason to restart a calculation is to extend the MEP that did not fully reach the reactant or product. The restart file will store the current MEP and simply add points onto the end, extending the calculation and saving an incredible amount of computational resources.

To restart a calculation, the keyword GRRESTART must be enabled in the *GRGENERAL section of the esp.fu70 input file. Even if one is not planning on restarting a future calculation, enabling GRRESTART does not increase that amount of computational resources needed, and as such should always be enabled for safety. This will generate the esp.fu84 output file at the end of the calculation. This file needs to be copied and renamed to esp.83 and listed in the grinputlist file for the next calculation.

Summary

Quantum mechanical tunneling involving hydrogen atoms in low-temperature matrices have been observed for decades. Once thought impossible, heavy-atom tunneling involving carbon has been demonstrated in more and more examples both experimentally and computationally. Theoretically calculated rate constants using canonical variational transition state theory (CVT) and several types of tunneling approximations (namely ZCT and SCT) have demonstrated impressive accuracy in predicting the rates of these tunneling reactions. The Polyrate and Gaussrate computational software packages provide a powerful tool for predicting rate constants of tunneling calculations.

References

1. Hund, F. Zur deutung der molekelspektren. III. *Z Phys* **1927**, *43*, 805-826.

2. Gurney, E. W.; Condon, E. U. Wave mechanics and radioactive distegration. *Nature* **1928**, *122*.

3. Bell, R. The application of quantum mechanics to chemical kinetics. *Proc. R. Soc. Lond. A Math. Phys. Sci.* **1933**, *139*, 466-474.

4. McMahon, R. J. Chemical Reactions Involving Quantum Tunneling. *Science* **2003**, *299*, 833-834.

5. Borden, W. T. Reactions that involve tunneling by carbon and the role that calculations have played in their study. *Wiley Interdisciplinary Reviews: Computational Molecular Science* **2016**, *6*, 20-46.

6. Sheridan, R. S. In *Reviews of Reactive Intermediate Chemistry*; John Wiley & Sons, Inc.: 2006, p 415-463.

7. Zuev, P. S.; Sheridan, R. S.; Albu, T. V.; Truhlar, D. G.; Hrovat, D. A.; Borden, W. T. Carbon Tunneling from a Single Quantum State. *Science* **2003**, *299*, 867-870.

8. Albu, T. V.; Lynch, B. J.; Truhlar, D. G.; Goren, A. C.; Hrovat, D. A.; Borden, W. T.; Moss, R. A. Dynamics of 1,2-Hydrogen Migration in Carbenes and Ring Expansion in Cyclopropylcarbenes. *J. Phys. Chem. A.* **2002**, *106*, 5323-5338.

9. Schreiner, P. R.; Reisenauer, H. P.; Ley, D.; Gerbig, D.; Wu, C.-H.; Allen, W. D. Methylhydroxycarbene: Tunneling Control of a Chemical Reaction. *Science* **2011**, *332*, 1300-1303.

10. Mills, G.; Schenter, G. K.; Makarov, D. E.; Jónsson, H. Generalized path integral based quantum transition state theory. *Chem. Phys. Lett.* **1997**, *278*, 91-96.

11. Rossi, I.; Truhlar, D. G. *Transition State Theory*; John Wiley & Sons, Inc: New York, 1986.

12. Truhlar, D. G.; Garrett, B. C.; Klippenstein, S. J. Current Status of Transition-State Theory. *J. Chem. Phys.* **1996**, *100*, 12771-12800.

13. Klippenstein, S. J.; Pande, V. S.; Truhlar, D. G. Chemical Kinetics and Mechanisms of Complex Systems: A Perspective on Recent Theoretical Advances. *J. Am. Chem. Soc.* **2014**, *136*, 528-546.

14. Truhlar, D. G.; Garrett, B. C. Variational transition-state theory. *Acc. Chem. Res.* **1980**, *13*, 440-448.

15. Truhlar, D. G.; Isaacson, A. D.; Garrett, B. C. *Theory of Chemical Reaction Dynamics*; CRC Press: Boca Raton, FL, 1985; Vol. 4.

16. Miller, W. H.; Handy, N. C.; Adams, J. E. Reaction path Hamiltonian for polyatomic molecules. *J. Chem. Phys.* **1980**, *72*, 99-112.

17. Garrett, B. C.; Truhlar, D. G.; Grev, R. S.; Magnuson, A. W. Improved treatment of threshold contributions in variational transition-state theory. *J. Chem. Phys.* **1980**, *84*, 1730-1748.

18. Kuppermann, A.; Truhlar, D. G. Exact tunneling calculations. *J. Am. Chem. Soc.* **1971**, *93*, 1840-1851.

19. Liu, Y. P.; Lynch, G. C.; Truong, T. N.; Lu, D. H.; Truhlar, D. G.; Garrett, B. C. Molecular modeling of the kinetic isotope effect for the [1,5]-sigmatropic rearrangement of cis-1,3-pentadiene. *J. Am. Chem. Soc.* **1993**, *115*, 2408-2415.

20. Garrett, B. C.; Joseph, T.; Truong, T. N.; Truhlar, D. G. Application of the large-curvature tunneling approximation to polyatomic molecules: Abstraction of H or D by methyl radical. *Chem. Phys.* **1989**, *136*, 271-293.

21. Tishchenko, O.; Truhlar, D. G. Optimizing the Performance of the Multiconfiguration Molecular Mechanics Method. *J. Phys. Chem. A.* **2006**, *110*, 13530-13536.

22. Corchado, J. C. *POLYRATE 2010-A* University of Minnesota, Minneapolis, MN, 2010.

23. Corchado, J. C. *GAUSSRATE 2009-A* University of Minnesota, Minneapolis, MN, 2010.

24. Frisch, M. J.; Trucks, G. W.; Schlegel, H. B.; Scuseria, G. E.; Robb, M. A.; Cheeseman, J. R.; Scalmani, G.; Barone, V.; Mennucci, B.; Petersson, G. A.; Nakatsuji, H.; Caricato, M.; Li, X.; Hratchian, H. P.; Izmaylov, A. F.; Bloino, J.; Zheng, G.; Sonnenberg, J. L.; Hada, M.; Ehara, M.; Toyota, K.; Fukuda, R.; Hasegawa, J.; Ishida, M.; Nakajima, T.; Honda, Y.; Kitao, O.; Nakai, H.; Vreven, T.; Montgomery Jr., J. A.; Peralta, J. E.; Ogliaro, F.; Bearpark, M. J.; Heyd, J.; Brothers, E. N.; Kudin, K. N.; Staroverov, V. N.; Kobayashi, R.; Normand, J.; Raghavachari, K.; Rendell, A. P.; Burant, J. C.; Iyengar, S. S.; Tomasi, J.; Cossi, M.; Rega, N.; Millam, N. J.; Klene, M.; Knox, J. E.; Cross, J. B.; Bakken, V.; Adamo, C.; Jaramillo, J.; Gomperts, R.; Stratmann, R. E.; Yazyev, O.; Austin, A. J.; Cammi, R.; Pomelli, C.; Ochterski, J. W.; Martin, R. L.; Morokuma, K.; Zakrzewski, V. G.; Voth, G. A.; Salvador, P.; Dannenberg, J. J.; Dapprich, S.; Daniels, A. D.; Farkas, Ö.; Foresman, J. B.; Ortiz, J. V.; Cioslowski, J.; Fox, D. J.; *Gaussian 09; Revision B.1*, 2009.

25. Kozuch, S. Heavy atom tunneling in the automerization of pentalene and other antiaromatic systems. *RSC Advances* **2014**, *4*, 21650-21656.

26. Page, M.; Doubleday, C.; McIver, J. W. Following steepest descent reaction paths. The use of higher energy derivatives with abinitio electronic structure methods. *J. Chem. Phys.* **1990**, *93*, 5634-5642.

27. Page, M.; McIver, J. W. On evaluating the reaction path Hamiltonian. *J. Chem. Phys.* **1988**, *88*, 922-935.

28. Natanson, G. A.; Garrett, B. C.; Truong, T. N.; Joseph, T.; Truhlar, D. G. The definition of reaction coordinates for reaction-path dynamics. *J. Chem. Phys.* **1991**, *94*, 7875-7892.

29. Lauderdale, J. G.; Truhlar, D. G. Diffusion of hydrogen, deuterium, and tritium on the (100) plane of copper: Reaction-path formulation, variational transition state theory, and tunneling calculations. *Surf. Sci.* **1985**, *164*, 558-588.

Chapter 2: Tunneling Reactions in Arylcarbenes

Introduction

Through years of investigation, arylcarbenes have demonstrated a complex pathway of both inter- and intramolecular reactions, studied using a wide array of spectroscopy and computational methods.[1-10] Among these transformations, many carbenes have demonstrated a 1,2 and 1,4-hydrogen shift reactivity. Scheme 2.1 shows a variety of arylcarbenes that have displayed this reactivity. Platz *et al*. demonstrated a longer 1,4 hydrogen shift in triplet 1,8-naphthoquinodimethane.[11-13] Upon irradiation of a diazo precursor, the diradical **2** was observed as the sole EPR active species in the matrix at 4.2 K. Platz theorized that the reaction proceeded by a very facile tunneling process due to a very small barrier for the hydrogen shift. Even upon deuteration, intermediate **1** could not be detected. Though impossible to exclude other mechanisms, such as hydrogen transfer from an excited diazo species, a narrow calculated barrier suggested tunneling from **1** as a possibility. Several other studies also show evidence for 1,4 hydrogen shifts[14,15] in arylcarbenes, though like the study by Platz *et al*., direct observation of these reactions is rare.

Chapman and McMahon[16] were able to directly observe the decay of triplet *o*–tolylcarbene (^{3}**3**) to singlet *o*-xylyene (^{1}**4**) in an argon matrix at 4.6 K (Scheme 2.1). Upon generation and matrix isolation of ^{3}**3** in an Ar matrix from a diazo precursor, the decay of ^{3}**3** and the growth of signals corresponding to *o*-xylene (^{1}**4**) were monitored using IR, ESR, and UV/Vis spectroscopy. While the Arrhenius plot of the reaction was mostly non-linear, below 12 K the plot displayed a mostly linear, temperature independent region. Furthermore, the reaction is spin-forbidden (triplet to singlet). Discussion of possible points for intersystem crossing (ISC) will be discussed later in depth. Upon addition of a $-CD_3$ group to ^{3}**3**, thermal decay of the carbene could not be observed, even upon heating of the matrix up to 60 K. The deviation from

Arrhenius behavior at low temperature, combined with the other factors, strongly suggested a tunneling mechanism.

Similarly, Sheridan *et al*. were able to matrix isolate triplet carbene **5** in an Ar matrix doped with H_2.[17] Upon warming of the matrix to 30 K, disappearance of **5** and appearance of the H_2 adduct **7** was observed via IR spectroscopy. B3LYP calculations demonstrated that the barrier for the reaction (5.7 kcal/mol) was too high for cryogenic temperatures. While the intermediate **6** was not observed, lack of a reaction in a D_2 doped matrix (implying a very high KIE) and high calculated barrier led to the conclusion that a tunneling process may be responsible for the reaction.

Wierlacher *et al.* were able to observe evidence for the intramolecular 1,2-hydrogen shift in singlet carbene **8**.[18] Photolysis of a precursor benzylchlorodiazirine in an Ar matrix at 10 K generated the singlet carbene **8**. Using IR spectroscopy, the growth of the hydrogen shift product **9** was observed both in the dark and after irradiation at $\lambda > 360$ nm. Later calculations demonstrated that tunneling heavily contributed to the rate constant at low temperatures.[19]

Scheme 2.1. Hydrogen shift reactions of arylcarbenes involving tunneling.

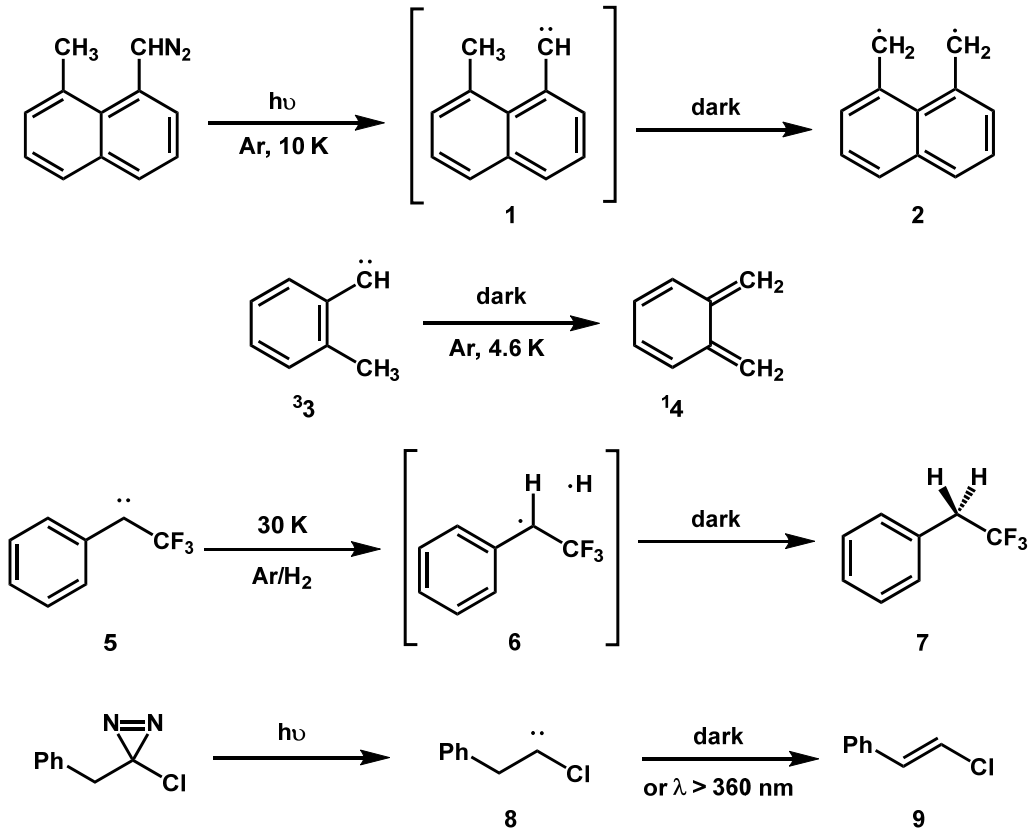

To further the investigation of the tunneling reaction observed by Chapman and McMahon, Albrecht matrix isolated the series of methylnaphthylcarbenes ^{3}**10**, ^{3}**12**, and ^{3}**13** (Scheme 2.2).[20] Carbenes ^{3}**10** and ^{3}**13** were observed to decay in an argon matrix at 10 K to the corresponding naphthoquinodimethane products ^{1}**11** and ^{1}**14**, with a similar rate of the decay to that of ^{3}**3** to ^{1}**4**. As with *o*-tolylcarbene, the inclusion of a –CD_3 group to carbene ^{3}**13** showed no decay in the matrix, with measured lower bound of the KIE of at least 371 for the main rotational isomer. Again, this large primary KIE effect upon deuteration at low temperatures suggested that a quantum mechanical tunneling process was involved.

Scheme 2.2. 1,2-hydrogen shifts in naphthylcarbenes.

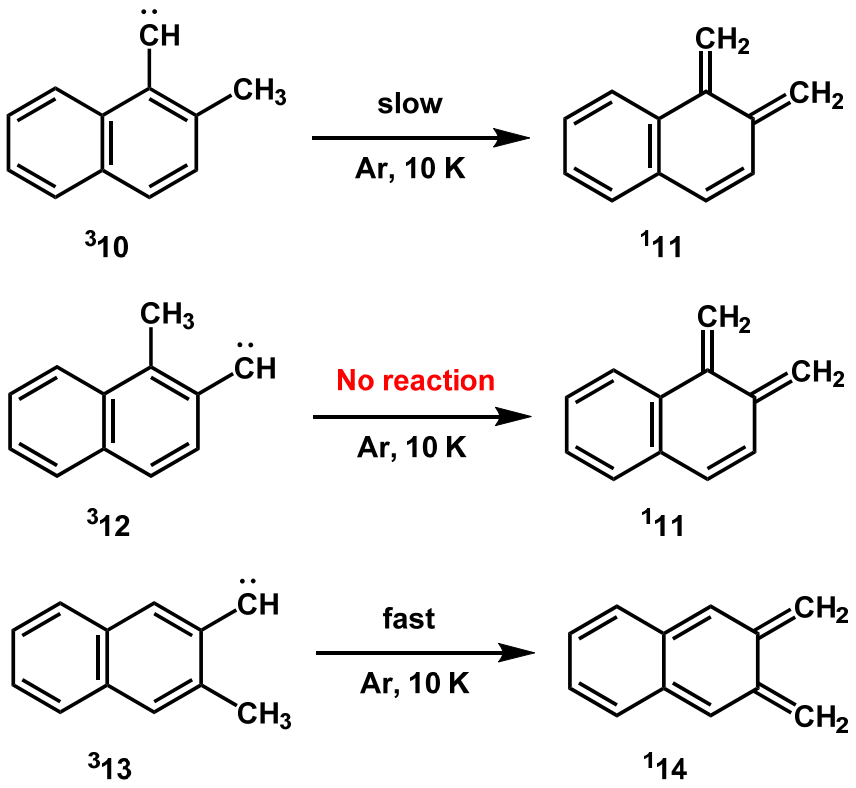

Quite surprisingly, ^{3}**12** proved to be stable in the matrix at 10 K, and no decay to ^{1}**11** was observed. Albrecht reported that the carbene remained stable even when warmed to higher temperatures such as 65 K. This was an unexpected result, as no clear reason for the difference between the naphthylcarbenes could be deduced. In an attempt to gain new insight into the tunneling mechanism of these triplet carbenes, and to determine why carbene ^{3}**12** proved stable in the matrix compared to such similar species, Bonvallet conducted an extensive computational study of all three methylnaphthylcarbenes on the B3LYP/6-31G* potential energy surface (PES), as well as performing further deuteration experiments.[21] Unfortunately, Bonvallet's computational and experimental results were unable to satisfactorily explain the discrepancy in the observed tunneling rates. The computational results focus on the width and height of the

barrier of reaction, two properties which influence the rate of tunneling processes. The calculated barrier height for the hydrogen migration was found to be highest for the rearrangement of ^{3}**13** to ^{1}**14**, which was observed to have the fastest tunneling rate of the methylnaphthylcarbenes. Similarly, comparing the width of the reaction by measuring the total distance traveled by the migratory hydrogen atom yielded conflicting results. To probe the impact of the methyl torsional barrier on the hydrogen migration, the decay of 3-(dideuteriometyhl)-2-naphthylcarbene in a solid argon matrix was observed. If only 33 % of the carbene was seen to decay (representing only the protio hydrogen reacting, with the two deuterium atoms locked in place), then the reactivity could be explained by the methyl rotation being hindered in the matrix. An EPR experiment of di-deuterated ^{3}**13** revealed the major isomer decaying at least 66 %, ruling out the possibility of a frozen methyl group (Table 2.1).

Table 2.1. Comparison of the kinetic parameters of ^{3}**13** and its deuteratred counterparts.

	Measured rate constants (s^{-1})	KIE
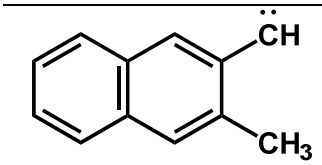	2.6×10^{-5}	-
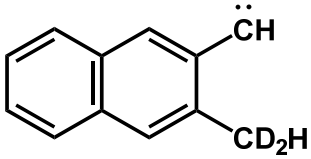	1.4×10^{-5}	19
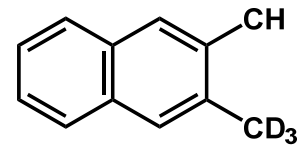	$\leq 7 \times 10^{-8}$	≥ 371

Since the studies of Albrecht and Bonvallet, computational chemistry software Polyrate and Gaussrate allows chemists to readily calculate rate constants for chemical reactions. Using

these software packages, contributions to the rate from tunneling can be included. Several studies have been able to show remarkable agreement between theory and experiment for a variety of tunneling reactions.[22] With this new software installed on the PHOENIX cluster here at the UW-Madison, we investigated these arylcarbene rearrangements depicted in Scheme 2.2 in an effort to better understand the tunneling phenomenon, and to understand the discrepancy in tunneling amongst the methylnaphthylcarbenes.

Computational Methods

All optimizations and harmonic frequency calculations were completed using Gaussian09,[23] with the nature of each stationary point determined by assessing the harmonic frequency calculations. The B3LYP[24] functional was used as an efficient level of theory for the computationally demanding SCT calculations, along with the smaller 6-31G(d)[25] basis set. All optimizations were ran with OPT=TIGHT and an ultrafine grid. Intrinsic reaction coordinate (IRC) calculations were used to verify that all stationary points were connected. Earlier examples have shown that B3LYP/6-31G(d) calculations have been effective for accurately predicting tunneling rates for organic reactions .[26,27] Stability of the diradical species was evaluated with the STABLE=OPT keyword.

To calculate the rate constants, Polyrate[28] was used. Gaussrate[29] was used as an interface between Gaussian09 (stationary point and PES data) and Polyrate. Semi-classical rate constants without a tunneling approximation were carried out with canonical variational transition state theory (CVT).[30] Rate constants including a multi-dimensional tunneling approximation were also calculated with both zero curvature tunneling (ZCT)[31] and small curvature tunneling (SCT).[30] SCT in particular has demonstrated considerable accuracy for unimolecular tunneling

reactions at cryogenic temperatures.[32] As is appropriate for low-temperature unimolecular reactions, quantized-reactant-state-tunneling (QRST)[33] was enabled for all tunneling approximations.

Results and Discussion

Potential Energy Surface of Arylcarbenes

Scheme 2.3. Major and minor rotamers of *o*-tolycarbene.

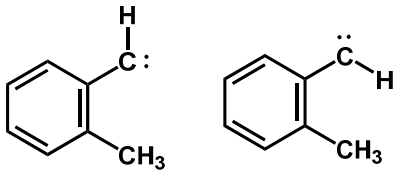

^{3}**3-major** ^{3}**3-minor**

As noted in work of Chapman and McMahon for *o*-tolylcarbene, and Albrecht and Bonvallet for the various methylnaphthylcarbenes, two rotamers of the triplet carbene were detected in the matrix by EPR spectroscopy (Scheme 2.3). Furthermore, in each instance the two isomers were found to decay at different rates. In order to properly calculate rate constants using Polyrate and Gaussrate, a transition state must be found connecting the reactants and products of the reaction. Despite vigorous searching, no transition state leading to any of the minor isomers (with the carbene hydrogen pointing towards the methyl group) could be found for any of the four carbenes studied. Without a minimum energy pathway (MEP) connecting the minor isomers to the products, the focus of the work will be on pathways connecting the transition state to the major rotamers. Calculations concerning the rate of interconversion between major and minor rotamers will be discussed in a later section.

The potential energy surface (PES) for the various arylcarbenes is shown in Figures 2.1-2.4. Starting with *o*-tolylcarbene, the singlet surface is relatively straightforward, with a single transition state connecting the reactant and product side of the PES. The transition state barrier is 12.2 kcal/mol, yielding the product ^{1}**4**, 41.6 kcal/mol lower in energy than ^{1}**3**. The triplet surface, however, shows much more complexity. The transition state for the hydrogen transfer does not immediately reach the reactant and product minima. Using an intrinsic reaction coordinate (IRC) calculation to follow the path of steepest descent from the transition state towards the reactant, the early portion of the reaction coordinate represents the motion of the hydrogen atom from the methyl group to the carbene carbon. Once the transfer is complete, this conformation (**^{3}3-syn**) with the methyl hydrogen pointing directly at the carbene carbon was found to be a transition state along the reaction coordinate of methyl rotation. From **^{3}3-syn**, the system will continue to relax by rotation of the methyl group to the react side minimum **^{3}3-anti.**

A similar situation is seen on the product side of the hydrogen transfer barrier. The early portion of the reaction coordinate correlates to the transfer of the tunneling hydrogen atom to the carbene to make the diradical ^{3}**15**. With $–CH_2$ group in the plane of the ring and the other perpendicular, this structure was found to be a transition state along the rotation of the $–CH_2$ reaction coordinate. This structure then relaxes by rotating the $–CH_2$ group to the planar diradical ^{3}**16**.

While the transition states on the triplet and singlet surfaces are similar to one another energetically (difference of 1.7 kcal/mol), the higher energy of the singlet reactant ^{1}**3** gives the hydrogen transfer a lower barrier on the singlet surface. The geometry of carbene ^{1}**3** is such that methyl hydrogen atom is pointing almost directly at the carbene carbon, only slightly twisted out of the plane. The lower barrier and more favorable geometry would predict a faster tunneling

rate for the singlet carbene. However, with the triplet carbene ^{3}**3** more stable by 6.8 kcal/mol, it would be unexpected for a meaningful population of the singlet carbene to exist in matrix conditions. Thus, the focus of this work will be calculating tunneling rates on the triplet surface.

Shown in Figures 2.2-2.4, the PES's for the three methylnaphthylcarbenes species studied are similar to that of *o*-tolylcarbene, both in the overall relative energies of the species and complexity of the triplet surface. While differences exist, the main tenants seen in *o*-tolylcarbene remain; A triplet ground state for the carbene favored by around 5-7 kcal/mol, a very exothermic singlet product, and a complex triplet surface involving methyl rotation, hydrogen transfer, and -CH_2 rotation. The obvious difference is the 1-methyl-2-napthylcarbene (^{3}**12**) triplet surface. Due to steric repulsion of the *peri* hydrogen[34] on the naphthalene ring, the structure of the triplet carbene reactant has one of its hydrogen atoms pointing directly at the carbene carbon in the perfect position for the tunneling reaction. In this case, no extra rotation of the methyl group is needed.

Figure 2.1. PES for the singlet and triplet *o*-tolylcarbene (B3LYP/6-31G(d)).

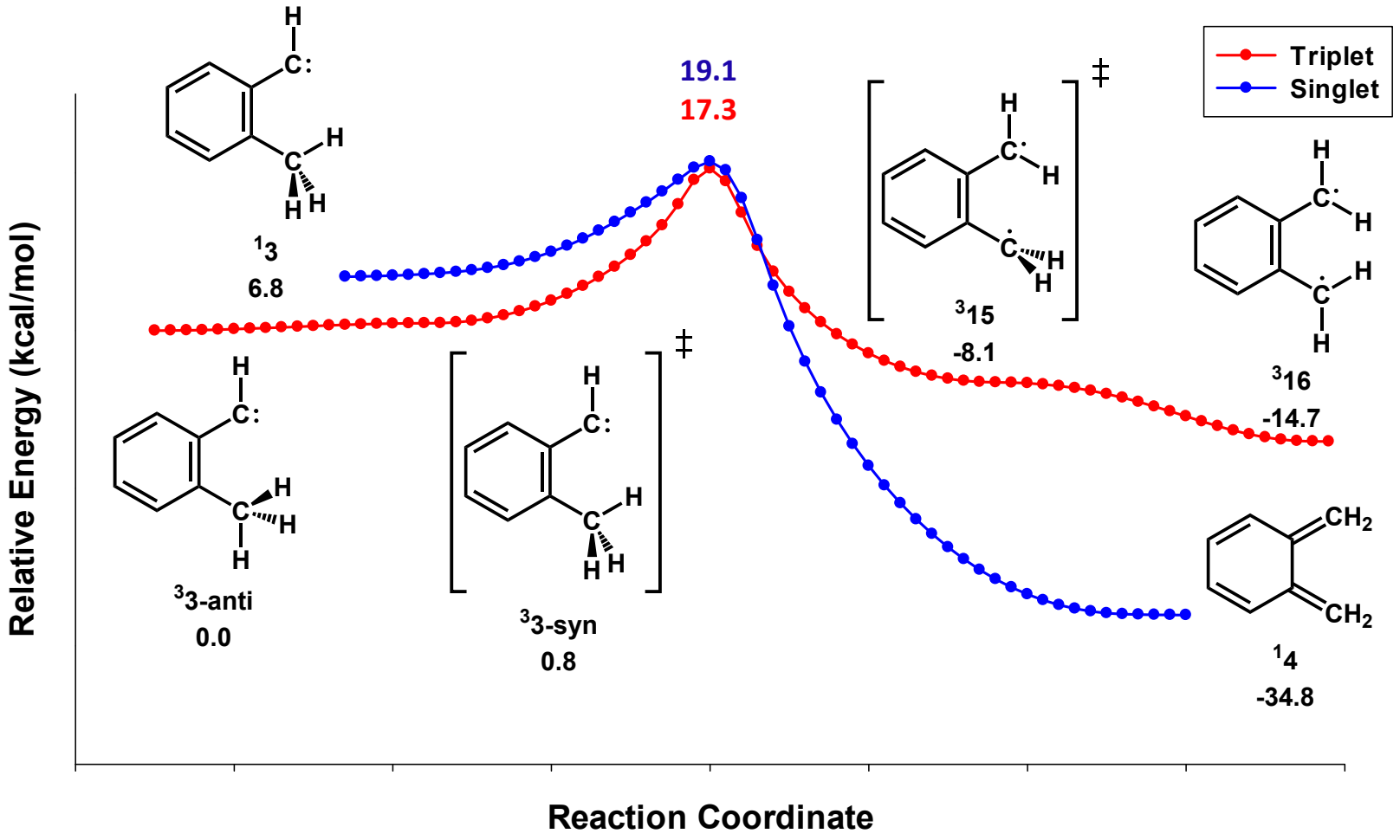

Figure 2.2. PES for the singlet and triplet 2-methyl-1-naphthylcarbene (B3LYP/6-31G(d)).

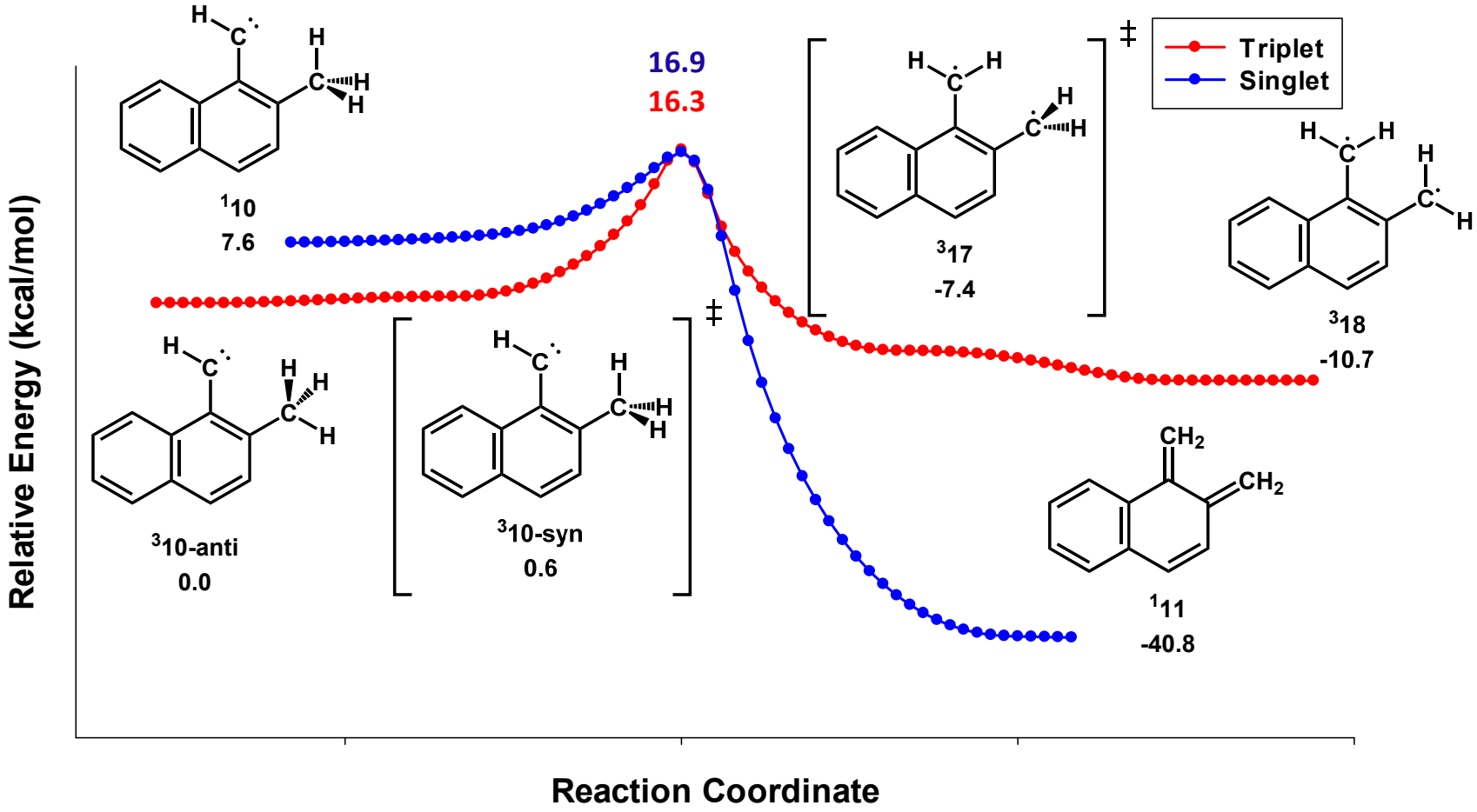

Figure 2.3. PES for the singlet and triplet 1-methyl-2-naphthylcarbene. (B3LYP/6-31G(d)).

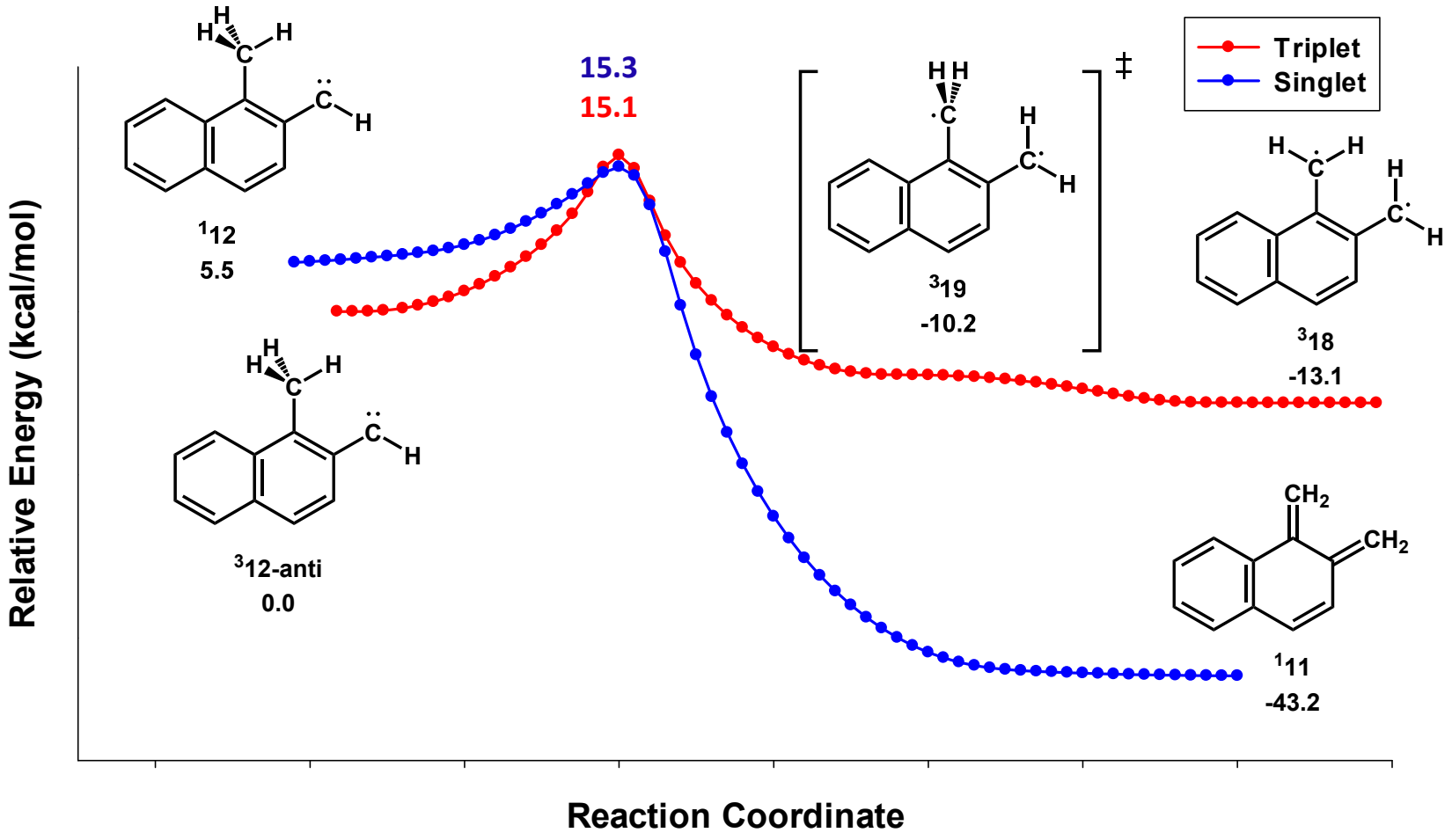

Figure 2.4. PES for the singlet and triplet 3-methyl-2-naphthylcarbene (B3LYP/6-31G(d)).

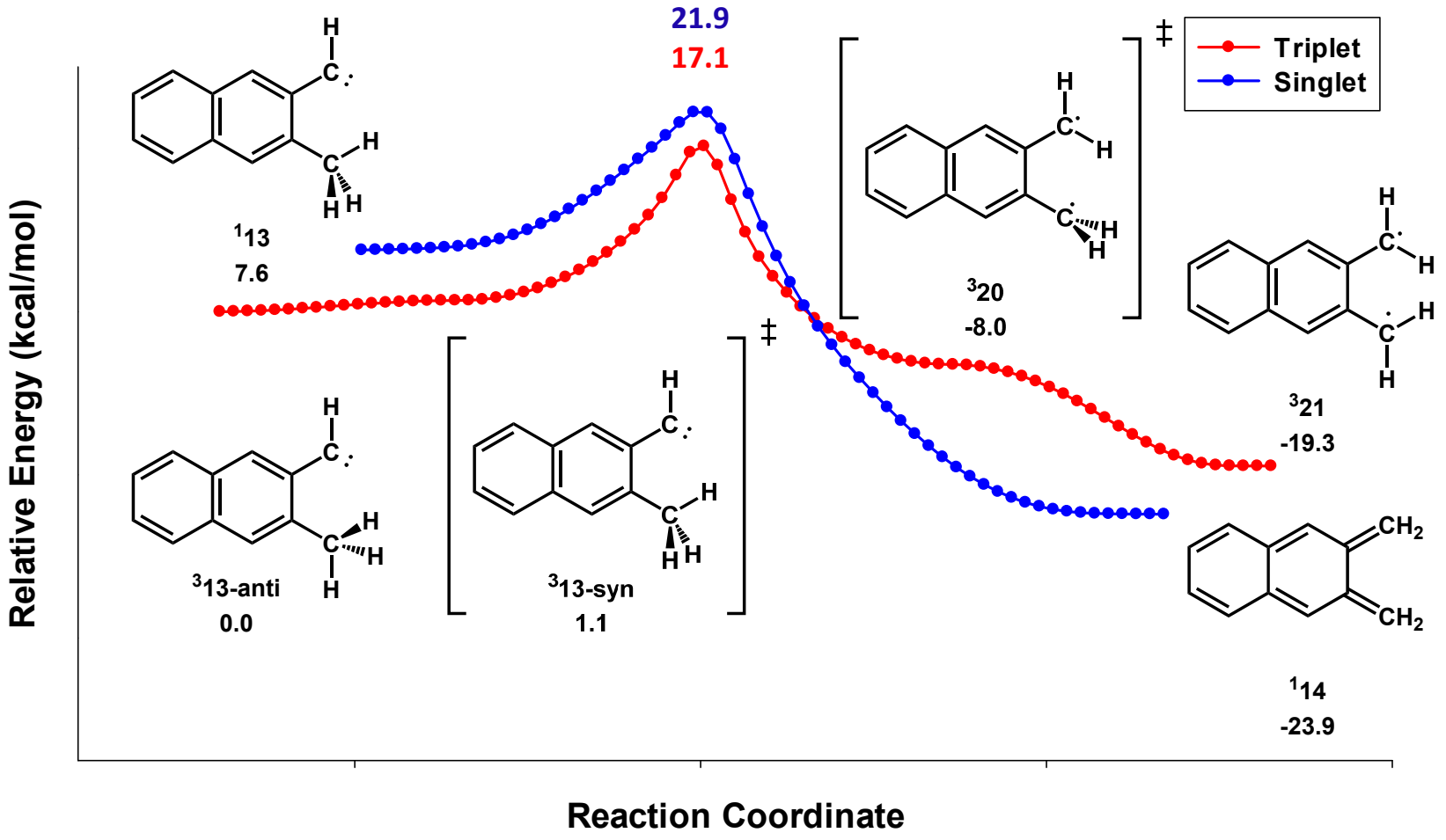

It should be noted that the complexity of the PES is a reason for uncertainty as we first attempted these tunneling calculations. Though not chemically unique, published tunneling reactions studied using Gaussrate and Polyrate usually have comparatively simple pathways, where the full reaction coordinate is essentially mapped to one atomic motion. The capabilities of Gaussrate to correctly predict tunneling constants for a reaction coordinate with two distinct portions of the PES (methyl rotation and hydrogen transfer) has yet to be demonstrated in the literature. Additionally, the calculated methyl torsional barriers in this study are between 0.6 and 1.1 kcal/mol, similar to other substituted benzenes.[35] With a very low barrier, exactly how the potential for rotational tunneling[36] of the methyl group impacts these calculations is not fully understood.

Further complicating this study is the addition of the ISC from triplet to singlet. While it is clear that the ISC must occur at some point along the pathway, we can only calculate rate constants on the triplet or singlet surface. Though it is reasonable to assume that a tunneling reaction might occur from the more stable triplet carbene and then ISC at some point after the tunneling process, it cannot be known with certainty.[37,38] To search for a possible point of ISC, singlet single-point energy calculations of triplet geometries along the IRC pathway were performed It was found that a crossing occurs after the hydrogen transfer on the product side of the barrier during the $-CH_2$ group rotation. This is demonstrated for *o*-tolylcarbene in Figure 2.5. Though this gives some evidence that the tunneling process can be modeled completely on the triplet surface, it must be stressed that this is not conclusive as density functionals such as B3LYP often struggle with open-shelled singlet diradicals.

Figure 2.5. Singlet single-point energy calculations of triplet geometries along the IRC pathway. Relative energy values for B3LYP/6-31G(d) energy surface.

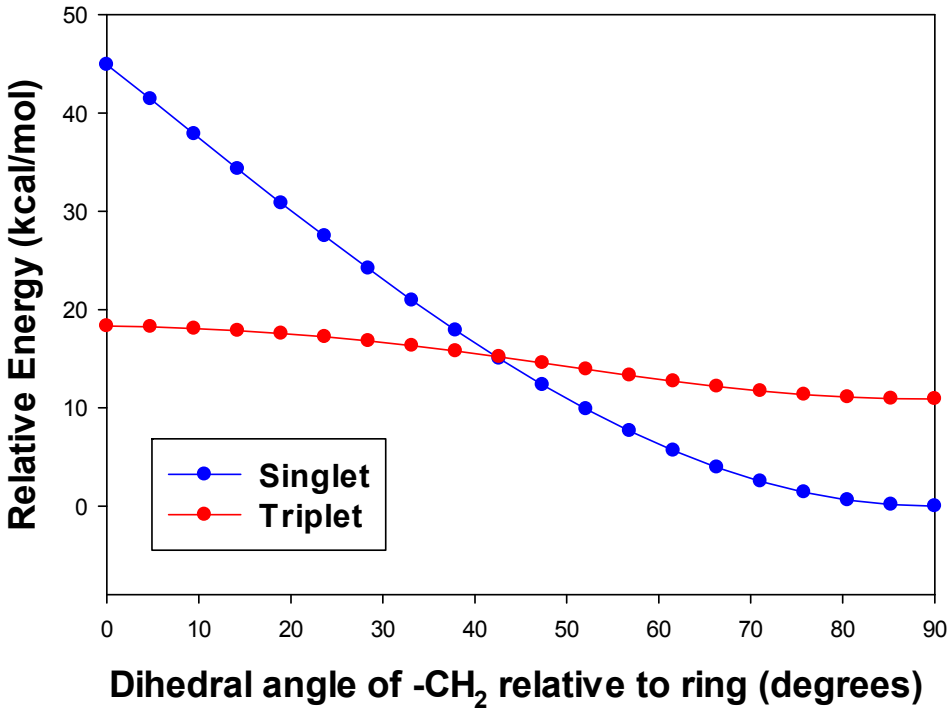

Calculated Tunneling Rates

Table 2.2 summarizes the calculated rate constants of the various arylcarbenes. For each species, the calculated rate was found for the PES starting from the lowest energy rotamer of the triplet carbene. Starting with *o*-tolylcarbene, the CVT rate constants show the rate of thermal decay of ^{3}**3** without contributions from tunneling. The larger barrier (17.3 kcal/mol) prohibits the hydrogen transfer reaction from happening thermally until much higher temperatures. The CVT / ZCT rate constants, now including approximations for tunneling, show a profound increase in the rate (~10^{168}). As expected, the ability of the SCT to account for "corner cutting" of the MEP leads to higher rate constants when compared to ZCT, where the tunneling pathway

is the MEP and thus longer. In particular, the CVT / SCT rate constants show good agreement with the observed tunneling rates. Considering the level of theory employed and the inability for Polyrate to account for matrix effects on rate, the results presented implies that the MEP presented in Figure 2.1 is reasonably close to the actual tunneling pathway. While not fully understood, the effect of the matrix on rates must be considered when comparing these values, especially for reactions involving ISC. In their study of the ring opening of a cyclopropene, Sander *et al*. observed the rate for ring opening to be 30 times faster in Xe than Ar, most likely due to the heavy-atom effect of xenon increasing the ISC rate.[38] These matrix effects are not accounted for in Polyrate calculations. These results also demonstrate the ability of Polyrate to calculate rate constants for a complicated MEP that strongly correlates to two completely different atomic motions. Lastly, this also implies that the tunneling takes place completely on the triplet surface, with the ISC occurring sometime after the tunneling event.

Table 2.2. Rate constants for the intramolecular 1,2-hydrogen shift reaction for listed triplet arylcarbenes. All rate constants in (s^{-1}) on the B3LYP/6-31G(d) surface.

	o-tolylcarbene (^{3}**3**)			2-methyl-1-naphthylcarbene (^{3}**10**)		
T (K)	CVT	CVT / ZCT	CVT / SCT	CVT	CVT / ZCT	CVT / SCT
20	3.91×10^{-178}	6.20×10^{-14}	1.09×10^{-7}	3.97×10^{-168}	3.98×10^{-12}	6.91×10^{-6}
50	3.65×10^{-64}	2.49×10^{-11}	1.17×10^{-6}	2.29×10^{-60}	1.28×10^{-9}	3.57×10^{-5}
100	4.49×10^{-26}	1.24×10^{-8}	1.00×10^{-4}	2.21×10^{-24}	2.29×10^{-7}	9.64×10^{-4}
150	2.28×10^{-13}	9.82×10^{-6}	6.53×10^{-3}	2.19×10^{-12}	6.63×10^{-5}	2.90×10^{-2}
200	5.08×10^{-7}	4.92×10^{-3}	3.63×10^{-1}	2.16×10^{-6}	1.79×10^{-2}	8.99×10^{-1}
250	3.27×10^{-3}	7.82×10^{-1}	1.18×10^{1}	8.48×10^{-3}	1.89×10^{0}	2.03×10^{1}
300	1.13×10^{0}	4.18×10^{1}	2.29×10^{2}	2.11×10^{0}	7.49×10^{1}	3.12×10^{2}
350	7.43×10^{1}	9.50×10^{2}	2.86×10^{3}	1.09×10^{2}	1.36×10^{3}	3.29×10^{3}
	Experiment at 18 K = 4.9×10^{-6}			Experiment at 14 K = 2.0×10^{-5}		

	1-methyl-2-naphthylcarbene (^{3}**12**)			3-methyl-2-naphthylcarbene (^{3}**13**)		
T (K)	CVT	CVT / ZCT	CVT / SCT	CVT	CVT / ZCT	CVT / SCT
20	4.14×10^{-163}	1.74×10^{-7}	3.29×10^{-3}	1.46×10^{-175}	1.48×10^{-15}	7.53×10^{-9}
50	2.51×10^{-58}	2.38×10^{-7}	4.10×10^{-3}	3.96×10^{-63}	4.36×10^{-12}	1.79×10^{-7}
100	2.72×10^{-23}	2.40×10^{-6}	1.57×10^{-2}	1.54×10^{-25}	1.42×10^{-8}	9.07×10^{-5}
150	1.34×10^{-11}	2.96×10^{-4}	1.88×10^{-1}	5.38×10^{-13}	1.52×10^{-5}	9.08×10^{-3}
200	9.43×10^{-6}	6.06×10^{-2}	4.01×10^{0}	1.01×10^{-6}	7.82×10^{-3}	5.48×10^{-1}
250	3.03×10^{-2}	5.63×10^{0}	7.66×10^{1}	5.83×10^{-3}	1.22×10^{0}	1.81×10^{1}
300	6.63×10^{0}	2.07×10^{2}	1.06×10^{3}	1.89×10^{0}	6.40×10^{1}	3.52×10^{2}
350	3.12×10^{2}	3.54×10^{3}	1.03×10^{4}	1.18×10^{2}	1.42×10^{3}	4.34×10^{3}
	Experiment at 18 K = No reaction			Experiment at 18 K = 2.6×10^{-5}		

The rate constants for two of the methylnaphthylcarbenes show modest agreement with experiment. While the rates for ^{3}**13** differ most from experiment ($k = 7.53 \times 10^{-9}$ s^{-1} compared to $k = 2.6 \times 10^{-5}$), the results for ^{3}**10** show fairly good agreement. We believe that the relative accuracy of these calculations also indicates that the general tunneling pathway for these two methylnaphthylcarbenes is close to the MEP described in Figures 2.2 and 2.4. At this point, further investigation with different density functionals and basis sets could be performed to find more accurate rate constants. Tunneling is very dependent on the overall shape of the PES. The

region of the PES corresponding to the methyl torsional barrier is very flat, and could be sensitive to the level of theory and basis set employed.

The Arrhenius plots for the various arylcarbenes are shown in Figure 2.6 and 2.7. Linear portions of the plot indicate the rate of reaction is temperature dependent, with a non-linear or curved portion indicating temperature independence. The plot of CVT rate constants without a tunneling approximation shows complete linearity throughout the range of calculated temperatures. The plot of CVT with the SCT approximation shows significant deviation from linearity, indicating the presence of tunneling at lower temperatures. Even at 200 K, large deviation of CVT / SCT compared to CVT shows that a tunneling mechanism contributes to the rate constant even at high temperatures.

Figure 2.6. Arrhenius plots for a) ^{3}**3**→ ^{1}**4** and b) ^{3}**10** → ^{1}**11.**

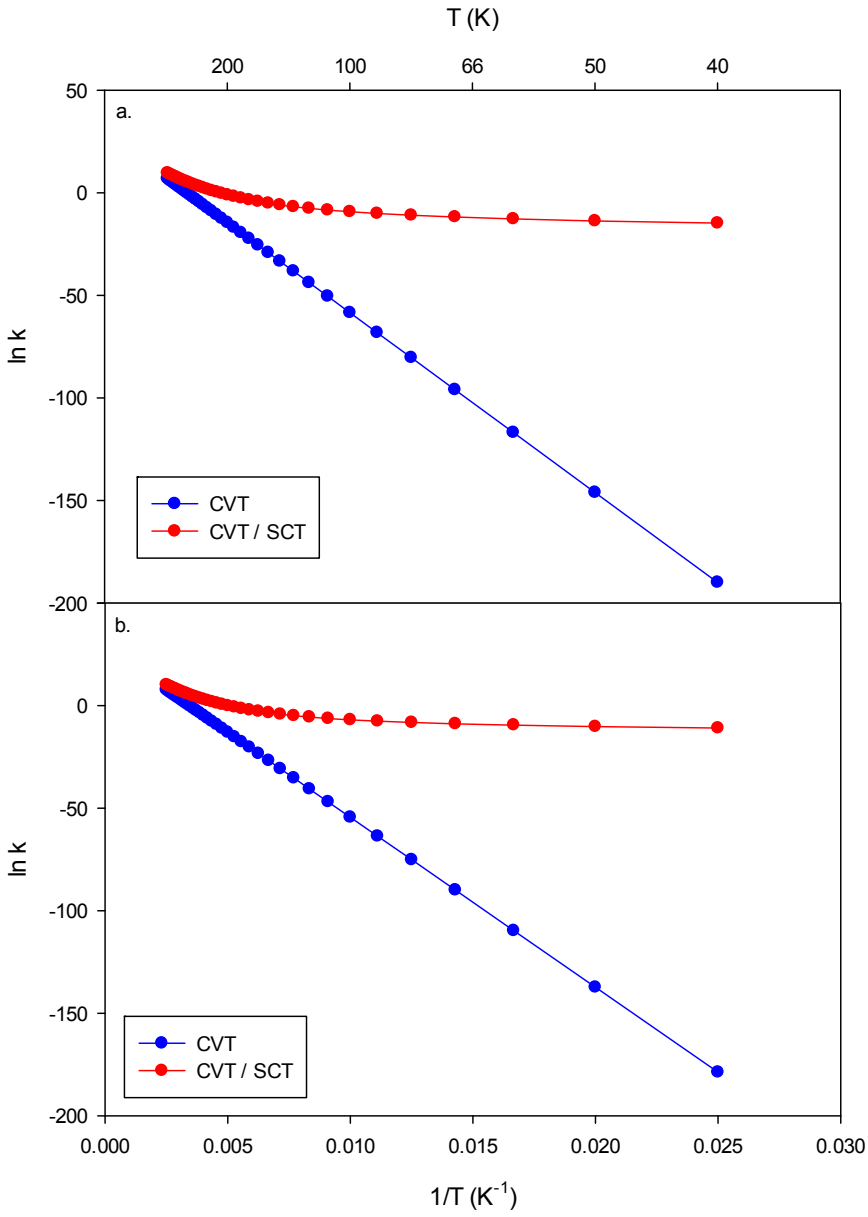

Figure 2.7. Arrhenius plots for a) ^{3}**12** → ^{1}**11** and b) ^{3}**13** → ^{1}**14.**

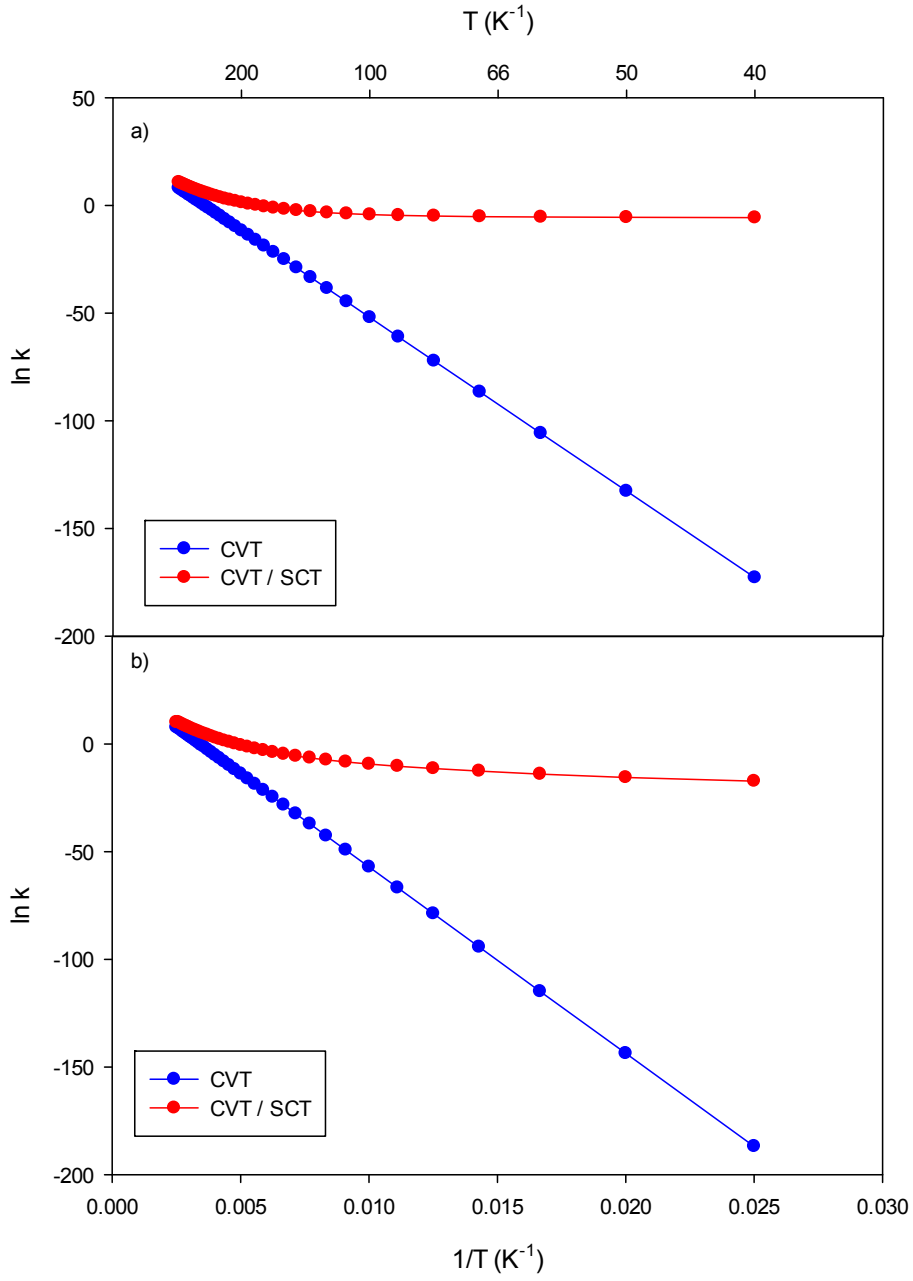

Though triplet *o*-tolylcarbene (**^{3}3**) was found to be more stable than singlet *o*-tolylcarbene (**^{1}4**) by 6.8 kcal/mol (Figure 2.1), tunneling on the singlet surface was investigated for comparison. The results of the calculation are shown in Table 2.3. At 10 K, the rate of tunneling on the singlet surface is calculated to be much faster than on the triplet surface. This can be easily explained by two factors. As the singlet carbene is higher in energy, the resulting barrier to the hydrogen migration is lower by approximately 5 kcal/mol. Furthermore, the geometry of the singlet carbene has a hydrogen atom pointing almost directly at the carbene, with the hydrogen only slightly out of the plane. With the hydrogen atom in prime position for tunneling, it avoids the requirement for methyl rotation to get into the optimal position. This observation lends some evidence that the triplet tunneling paths shown in Figure 2.1-Figure 2.4 is close to the actual tunneling pathways; the requirement of the methyl group rotation explains the slower hydrogen migration seen in **^{3}3**, **^{3}10**, and **^{3}13**. This result is also quite similar to the calculated rate for the decay of **^{3}12**, where the hydrogen atom is also pointing directly at the carbene center due to sterics of the *peri* hydrogen on the naphthylene ring.

Table 2.3. Rate constants for the reaction of **^{1}3 to ^{1}4** on the singlet PES. All rate constants in (s^{-1}).

T (K)	CVT	CVT / ZCT	CVT / SCT
10	1.87×10^{-257}	5.96×10^{-7}	8.47×10^{-3}
20	3.83×10^{-123}	8.51×10^{-7}	8.51×10^{-3}
50	2.27×10^{-42}	1.81×10^{-6}	1.25×10^{-2}
100	2.15×10^{-15}	7.79×10^{-5}	7.32×10^{-2}
150	2.06×10^{-6}	1.16×10^{-2}	1.49×10^{0}
200	6.21×10^{-2}	2.66×10^{0}	5.32×10^{1}
250	2.98×10^{1}	2.41×10^{2}	1.42×10^{3}
300	1.81×10^{3}	7.01×10^{3}	2.16×10^{4}
350	3.41×10^{4}	8.85×10^{4}	1.91×10^{5}

As mentioned previously, rate constant calculations for interconversion of the carbene hydrogen rotamer were carried out for the various triplet carbenes. Scheme 2.4 shows a representative case for the arylcarbenes studied using *o*-tolylcarbene. McMahon and Chapman[16] observed **^{3}3-major** and **^{3}3-minor** decaying at different rates in the matrix using ESR measurements. For this observation to be possible, the interconversion between the more stable **^{3}3-major** and the less stable **^{3}3-minor** must be slow on the hydrogen transfer time scale. The calculated rate with CVT / SCT was found to be $k = 6.56 \times 10^6$ s^{-1} at 10 K, many orders of magnitude faster than both the predicted and observed rate of hydrogen transfer.

Several factors could account for this large discrepancy. Though no direct evidence for the rate of rotation in phenylcarbene or naphthylcarbene exists to the our knowledge, the best study available is a series of matrix experiments by Platz. *et al.*[39] They found that the barrier for the interconversion from *syn* to *anti* 1-naphthylcarbene and 2-napthylcarbene to be greater than 4.5-6.3 kcal/mol. The B3LYP/6-31G(d) barrier was calculated to be between 3.8-4.1 amongst the studied arylcarbenes. In the same study, Platz also concludes that the rate of interconversion must be slower than the rates measured for naphthylcarbenes hydrogen-abstraction reaction with the matrix, which ranged from an order of 1×10^{-3} s^{-1} and 1×10^{-4} s^{-1}. Though the differences in barrier heights between theory and experiments explain some of the difference in the rates, the magnitude of that difference is surprising. While no published work has demonstrated the accuracy of CVT and SCT methodology to accurately predict rate constants for similar rotations, we see no reason why this could not be the case.

Scheme 2.4. Relative rates of tunneling of the major and minor isomer of *o*-tolylcarbene.

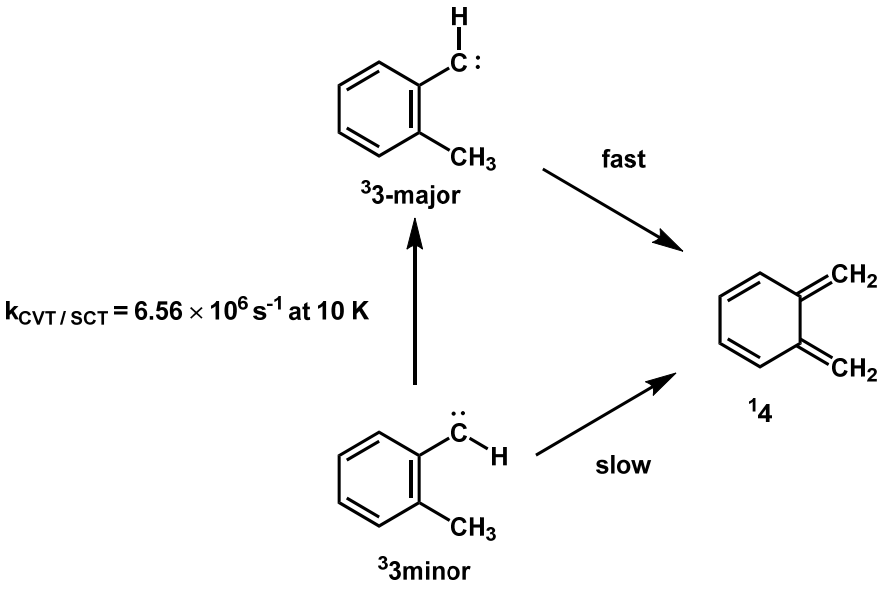

Due to the mass dependence on tunneling rates, the kinetic isotope effect (KIE) upon deuteration can be much higher than normal. The magnitude of the KIE is temperature dependent; the KIE will be largest at lower temperatures where the tunneling mechanism contributes most to the rate constant. Calculated CVT / SCT KIE's for the various arylcarbenes are shown in Table 2.4. For each calculated KIE, when monodeuteration is shown, the deuterium atom is the tunneling atom. The results of monodeuteration for all the carbenes is a KIE of around 10^4. Since the overall impact of the deuteration on the arylcarbenes that must first rotate the methyl group to the proper orientation for tunneling (^{3}**8**, ^{3}**10**, and ^{3}**13**) is similar to the impact on carbenes that avoid such methyl rotation (^{3}**12**), we can assume the heavier isotope has minimal impact on methyl rotation.

Table 2.4. Comparison of theoretical KIE data for the various deuterated arylcarbenes compared to experimental values (if performed). All *k* values in s^{-1} at CVT / SCT on B3LYP/6-31G(d) surface. a) Tunneling atom is deuterium b) Tunneling atom is hydrogen.

	Theoretical KIE	Experimental KIE
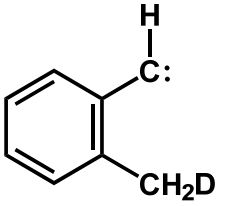	6.81×10^4	No tunneling observed with –CD3.
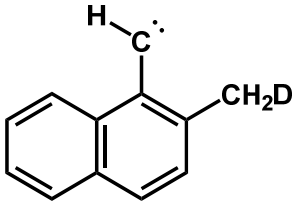	3.32×10^4	-
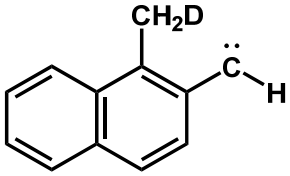	1.70×10^4	-
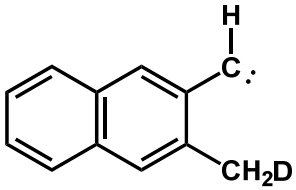	7.89×10^4	-
a) 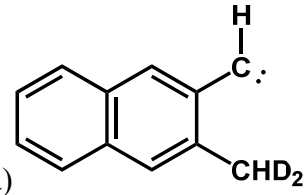	5.58×10^5	19
b) 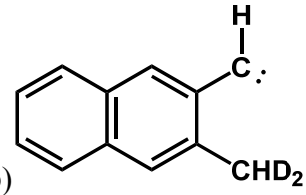	836	19
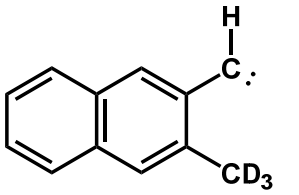	6.33×10^7	$\geq$ 371

Providing more insight into the role of methyl rotation, Albrecht performed studies with a tri-deuterio sample of ^{3}**13**, and Bonvallet performed studies with a di-deuterio samples of ^{3}**13** **(**Tables 1 and 4). Combined, these two studies give us data for a system where methyl rotation can avoid tunneling of the heavier isotope (-CD_2H) and an instance where it cannot (-CD_3). Two KIE were calculated for di-deuterated ^{3}**13**: one calculation where one of the two deuterium atoms was the tunneling atom, and one calculation where the lone hydrogen was tunneled. As seen in Table 4, the later calculation is much closer to the experimentally determined KIE. This demonstrates that even at low temperatures, the methyl group is free enough to avoid having to donate the heavier deuterium atom.

Though the calculated KIE's are very large, they are not without precedent. In their study of possible tunneling pathways of cyclopropylmethylcarbene (Scheme 2.5), Schreiner *et al*. calculated a KIE of a similar magnitude as the arylcarbenes in this study. Using the B3PW91/cc-pVTZ calculations, the CVT / SCT KIE was calculated to be 1.44×10^4.[40] Such high KIE values seem to be possible at low temperatures for intramolecular hydrogen transfer reactions carbenes.

Scheme 2.5. KIE of the 1,2-hydrogen shift in cyclopropylcarbene.

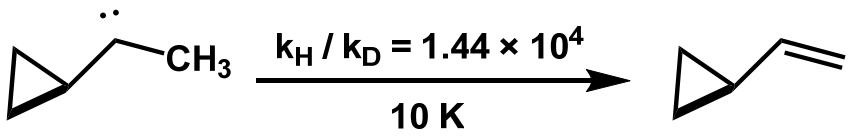

Summary

The tunneling process in a family of arylcarbenes was investigated using rate constant calculations. Using Polyrate and Gaussrate, CVT rate constants with ZCT and SCT tunneling approximations for the hydrogen migration of *o*-tolylcarbene and several naphthylcarbenes were calculated. Using the B3LYP density functional and a small basis set (6-31G(d)), good to modest agreement between rate constants observed from decay in the matrix and calculated rate constants was found. Comparison of calculated tunneling rates on the triplet and singlet surface demonstrates that ISC most likely occurs after the tunneling event. Unfortunately, the discrepancy between the observed lack of tunneling in ^{3}**12** and a large calculated rate constant (relative to the other methylnaphthylcarbenes) has not been resolved. The lack of methyl group rotation to allow tunneling and similar barrier height to hydrogen migration reconcile the computational result, but not the experimental. Non-linear Arrhenius plots and very large KIE further demonstrate the large role of tunneling on the rate constant, even at higher temperatures.

References

1. Chapman, O. L.; McMahon, R. J.; West, P. R. Rearrangements of tolylmethylenes via cycloheptatetraenes: formation of benzocyclobutene and styrene. *J. Am. Chem. Soc.* **1984**, *106*, 7973-7974.

2. West, P. R.; Mooring, A. M.; McMahon, R. J.; Chapman, O. L. Benzobicyclo[4.1.0]hepta-2,4,6-trienes. *J. Org. Chem.* **1986**, *51*, 1316-1320.

3. McMahon, R. J.; Abelt, C. J.; Chapman, O. L.; Johnson, J. W.; Kreil, C. L.; LeRoux, J. P.; Mooring, A. M.; West, P. R. 1,2,4,6-Cycloheptatetraene: the key intermediate in arylcarbene interconversions and related C_7H_6 rearrangements. *J. Am. Chem. Soc.* **1987**, *109*, 2456-2469.

4. Pharr, C. R.; Kopff, L. A.; Bennett, B.; Reid, S. A.; McMahon, R. J. Photochemistry of Furyl- and Thienyldiazomethanes: Spectroscopic Characterization of Triplet 3-Thienylcarbene. *J. Am. Chem. Soc.* **2012**, *134*, 6443-6454.

5. Albrecht, S. W.; McMahon, R. J. Photoequilibration of 2-naphthylcarbene and 2,3-benzobicyclo[4.1.0]hepta-2,4,6-triene. *J. Am. Chem. Soc.* **1993**, *115*, 855-859.

6. Nicolaides, A.; Matsushita, T.; Yonezawa, K.; Sawai, S.; Tomioka, H.; Stracener, L. L.; Hodges, J. A.; McMahon, R. J. The Elusive Benzocyclobutenylidene: A Combined Computational and Experimental Attempt. *J. Am. Chem. Soc.* **2001**, *123*, 2870-2876.

7. Bonvallet, P. A.; Todd, E. M.; Kim, Y. S.; McMahon, R. J. Access to the Naphthylcarbene Rearrangement Manifold via Isomeric Benzodiazocycloheptatrienes. *J. Org. Chem.* **2002**, *67*, 9031-9042.

8. Sheridan, R. S. Heteroarylcarbenes. *Chem. Rev.* **2013**, *113*, 7179-7208.

9. Hirai, K.; Itoh, T.; Tomioka, H. Persistent Triplet Carbenes. *Chem. Rev.* **2009**, *109*, 3275-3332.

10. Platz, M. S. A Perspective on Physical Organic Chemistry. *J. Org. Chem.* **2014**, *79*, 2341-2353.

11. Platz, M. S.; Burns, J. R. Heteroatomic biradicals. Electron spin resonance spectroscopy of a nitrogen analog of 1,8-naphthoquinodimethane. *J. Am. Chem. Soc.* **1979**, *101*, 4425-4426.

12. Platz, M. S. The mechanism of intersystem crossing and ring closure of the triplet 1,8-naphthoquinodimethane biradical. *J. Am. Chem. Soc.* **1980**, *102*, 1192-1194.

13. Fritz, M. J.; Ramos, E. L.; Platz, M. S. Triplet ground states of 4-substituted 1,8-naphthoquinodimethanes. *J. Org. Chem.* **1985**, *50*, 3522-3526.

14. Karney, W. L.; Borden, W. T. Ab Initio Study of the Ring Expansion of Phenylnitrene and Comparison with the Ring Expansion of Phenylcarbene. *J. Am. Chem. Soc.* **1997**, *119*, 1378-1387.

15. Tomioka, H.; Okada, H.; Watanabe, T.; Banno, K.; Komatsu, K.; Hirai, K. Polymethylated and Poly(tert)butylated Diphenylcarbenes. Generation, Reactions, Kinetics, and Deuterium Isotope Effects of Sterically Congested Triplet Carbenes. *J. Am. Chem. Soc.* **1997**, *119*, 1582-1593.

16. McMahon, R. J.; Chapman, O. L. Direct spectroscopic observation of intramolecular hydrogen shifts in carbenes. *J. Am. Chem. Soc.* **1987**, *109*, 683-692.

17. Zuev, P. S.; Sheridan, R. S. Low-Temperature Hydrogenation of Triplet Carbenes and Diradicaloid Biscarbenes Electronic State Selectivity. *J. Am. Chem. Soc.* **2001**, *123*, 12434-12435.

18. Wierlacher, S.; Sander, W.; Liu, M. T. H. Photolysis of alkylhalodiazirines and direct observation of benzylchlorocarbene in cryogenic matrixes. *J. Am. Chem. Soc.* **1993**, *115*, 8943-8953.

19. Albu, T. V.; Lynch, B. J.; Truhlar, D. G.; Goren, A. C.; Hrovat, D. A.; Borden, W. T.; Moss, R. A. Dynamics of 1,2-Hydrogen Migration in Carbenes and Ring Expansion in Cyclopropylcarbenes. *J. Phys. Chem. A.* **2002**, *106*, 5323-5338.

20. Albrecht, S. W., Ph.D. Dissertation, University of Wisconsin-Madison, 1995.

21. Bonvallet, P. A., Ph.D. Dissertation, University of Wisconsin-Madison, 2001.

22. Sheridan, R. S. In *Reviews of Reactive Intermediate Chemistry*; John Wiley & Sons, Inc.: 2006, p 415-463.

23. Frisch, M. J.; Trucks, G. W.; Schlegel, H. B.; Scuseria, G. E.; Robb, M. A.; Cheeseman, J. R.; Scalmani, G.; Barone, V.; Mennucci, B.; Petersson, G. A.; Nakatsuji, H.; Caricato, M.; Li, X.; Hratchian, H. P.; Izmaylov, A. F.; Bloino, J.; Zheng, G.; Sonnenberg, J. L.; Hada, M.; Ehara, M.; Toyota, K.; Fukuda, R.; Hasegawa, J.; Ishida, M.; Nakajima, T.; Honda, Y.; Kitao, O.; Nakai, H.; Vreven, T.; Montgomery Jr., J. A.; Peralta, J. E.; Ogliaro, F.; Bearpark, M. J.; Heyd, J.; Brothers, E. N.; Kudin, K. N.; Staroverov, V. N.; Kobayashi, R.; Normand, J.; Raghavachari, K.; Rendell, A. P.; Burant, J. C.; Iyengar, S. S.; Tomasi, J.; Cossi, M.; Rega, N.; Millam, N. J.; Klene, M.; Knox, J. E.; Cross, J. B.; Bakken, V.; Adamo, C.; Jaramillo, J.; Gomperts, R.; Stratmann, R. E.; Yazyev, O.; Austin, A. J.; Cammi, R.; Pomelli, C.; Ochterski, J. W.; Martin, R. L.; Morokuma, K.; Zakrzewski, V. G.; Voth, G. A.; Salvador, P.; Dannenberg, J. J.; Dapprich, S.; Daniels, A. D.; Farkas, Ö.; Foresman, J. B.; Ortiz, J. V.; Cioslowski, J.; Fox, D. J.; *Gaussian 09; Revision B.1*, 2009.

24. Becke, A. D. Density-functional thermochemistry. III. The role of exact exchange. *J. Chem. Phys.* **1993**, *98*, 5648-5652.

25. Hariharan, P. C.; Pople, J. A. Influence of polarization functions on MO hydrogenation energies. *Theor. Chim. Acta* **1973**, *28*, 213-222.

26. Kozuch, S.; Zhang, X.; Hrovat, D. A.; Borden, W. T. Calculations on Tunneling in the Reactions of Noradamantyl Carbenes. *J. Am. Chem. Soc.* **2013**, *135*, 17274-17277.

27. Datta, A.; Hrovat, D. A.; Borden, W. T. Calculations Predict Rapid Tunneling by Carbon from the Vibrational Ground State in the Ring Opening of Cyclopropylcarbinyl Radical at Cryogenic Temperatures. *J. Am. Chem. Soc.* **2008**, *130*, 6684-6685.

28. Corchado, J. C. *POLYRATE 2010-A* University of Minnesota, Minneapolis, MN, 2010.

29. Corchado, J. C. *GAUSSRATE 2009-A* University of Minnesota, Minneapolis, MN, 2010.

30. Fernandez-Ramos, A.; Ellingson, B. A.; Garrett, B. C.; Truhlar, D. G. In *Rev. Comput. Chem.*; John Wiley & Sons, Inc.: 2007, p 125-232.

31. Kuppermann, A.; Truhlar, D. G. Exact tunneling calculations. *J. Am. Chem. Soc.* **1971**, *93*, 1840-1851.

32. Borden, W. T. Reactions that involve tunneling by carbon and the role that calculations have played in their study. *Wiley Interdisciplinary Reviews: Computational Molecular Science* **2016**, *6*, 20-46.

33. Lauderdale, J. G.; Truhlar, D. G. Diffusion of hydrogen, deuterium, and tritium on the (100) plane of copper: Reaction-path formulation, variational transition state theory, and tunneling calculations. *Surf. Sci.* **1985**, *164*, 558-588.

34. Balasubramaniyan, V. peri Interaction in Naphthalene Derivatives. *Chem. Rev.* **1966**, *66*, 567-641.

35. Breen, P. J.; Warren, J. A.; Bernstein, E. R.; Seeman, J. I. Torsional motion in aromatic molecules. Conformational analysis of methyl-, ethyl-, and n-propylbenzenes. *J. Am. Chem. Soc.* **1987**, *109*, 3453-3455.

36. Prager, M.; Heidemann, A. Rotational Tunneling and Neutron Spectroscopy: A Compilation. *Chem. Rev.* **1997**, *97*, 2933-2966.

37. Morawietz, J.; Sander, W.; Traeubel, M. Intramolecular Hydrogen Transfer in (2-Aminophenyl)carbene and 2-Tolylnitrene. Matrix Isolation of 6-Methylene-2,4-cyclohexadien-1-imine. *J. Org. Chem.* **1995**, *60*, 6368-6378.

38. Ertelt, M.; Hrovat, D. A.; Borden, W. T.; Sander, W. Heavy-Atom Tunneling in the Ring Opening of a Strained Cyclopropene at Very Low Temperatures. *Chem. Eur. J.* **2014**, *20*, 4713-4720.

39. Senthilnathan, V. P.; Platz, M. S. Conformational barriers in triplet 1- and 2-naphthylcarbene. 2. Absolute rate of decay of arylcarbenes by electron spin resonance spectroscopy. *J. Am. Chem. Soc.* **1981**, *103*, 5503-5511.

40. Gerbig, D.; Ley, D.; Schreiner, P. R. Light- and Heavy-Atom Tunneling in Rearrangement Reactions of Cyclopropylcarbenes. *Org. Lett.* **2011**, *13*, 3526-3529.

Supporting Information

Chapter 2: Tunneling in Aryl Carbenes

Table 2.S1. Full rate constant data for ^{1}**3** → ^{1}**4**.

T (K)	TST (s^{-1})	CVT (s^{-1})	CVT / ZCT (s^{-1})	CVT / SCT (s^{-1})
10	8.68-257	1.87-257	5.96E-07	8.47E-03
14	2.96-180	9.90-181	5.96E-07	8.47E-03
20	8.24-123	3.83-123	6.06E-07	8.51E-03
30	4.44E-78	2.66E-78	7.12E-07	8.97E-03
40	1.10E-55	7.50E-56	1.05E-06	1.02E-02
50	3.08E-42	2.27E-42	1.81E-06	1.25E-02
60	2.87E-33	2.22E-33	3.46E-06	1.62E-02
70	7.35E-27	5.91E-27	7.01E-06	2.19E-02
80	4.70E-22	3.88E-22	1.49E-05	3.11E-02
90	2.57E-18	2.17E-18	3.33E-05	4.65E-02
100	2.51E-15	2.15E-15	7.79E-05	7.32E-02
110	7.00E-13	6.09E-13	1.92E-04	1.22E-01
120	7.62E-11	6.71E-11	4.98E-04	2.14E-01
130	4.03E-09	3.58E-09	1.37E-03	3.93E-01
140	1.21E-07	1.08E-07	3.91E-03	7.54E-01
150	2.29E-06	2.06E-06	1.16E-02	1.49E+00
160	3.00E-05	2.73E-05	3.50E-02	3.02E+00
170	2.91E-04	2.65E-04	1.06E-01	6.19E+00
180	2.19E-03	2.00E-03	3.19E-01	1.27E+01
190	1.33E-02	1.22E-02	9.38E-01	2.62E+01
200	6.73E-02	6.21E-02	2.66E+00	5.32E+01
210	2.92E-01	2.70E-01	7.22E+00	1.07E+02
220	1.11E+00	1.03E+00	1.87E+01	2.10E+02
230	3.74E+00	3.48E+00	4.61E+01	4.06E+02
240	1.14E+01	1.07E+01	1.08E+02	7.68E+02
250	3.18E+01	2.98E+01	2.41E+02	1.42E+03
260	8.19E+01	7.68E+01	5.13E+02	2.56E+03
270	1.97E+02	1.85E+02	1.05E+03	4.52E+03
280	4.44E+02	4.18E+02	2.05E+03	7.79E+03
290	9.46E+02	8.92E+02	3.86E+03	1.31E+04
300	1.92E+03	1.81E+03	7.01E+03	2.16E+04
310	3.71E+03	3.51E+03	1.23E+04	3.47E+04
320	6.90E+03	6.54E+03	2.10E+04	5.47E+04
330	1.24E+04	1.17E+04	3.48E+04	8.45E+04
340	2.14E+04	2.03E+04	5.62E+04	1.28E+05
350	3.59E+04	3.41E+04	8.85E+04	1.91E+05
360	5.84E+04	5.55E+04	1.36E+05	2.79E+05
370	9.28E+04	8.82E+04	2.05E+05	4.02E+05
380	1.44E+05	1.37E+05	3.03E+05	5.70E+05
390	2.18E+05	2.07E+05	4.40E+05	7.97E+05

Table 2.S2. Full rate constant data for ^{3}**3** → ^{3}**4**

T (K)	TST (s^{-1})	CVT (s^{-1})	CVT / ZCT (s^{-1})	CVT / SCT (s^{-1})
10	0.00E+00	0.00E+00	NaN	NaN
14	2.13-259	2.02-259	4.86E-14	1.07E-07
20	4.05-178	3.91-178	6.20E-14	1.09E-07
30	7.59-115	7.41-115	4.58E-13	1.58E-07
40	3.55E-83	3.49E-83	4.24E-12	3.99E-07
50	3.71E-64	3.65E-64	2.49E-11	1.17E-06
60	1.81E-51	1.79E-51	1.04E-10	3.19E-06
70	2.11E-42	2.09E-42	3.58E-10	8.04E-06
80	1.34E-35	1.33E-35	1.15E-09	1.91E-05
90	2.63E-30	2.62E-30	3.71E-09	4.39E-05
100	4.52E-26	4.49E-26	1.24E-08	1.00E-04
110	1.32E-22	1.31E-22	4.38E-08	2.28E-04
120	1.02E-19	1.01E-19	1.64E-07	5.22E-04
130	2.83E-17	2.81E-17	6.42E-07	1.21E-03
140	3.51E-15	3.49E-15	2.53E-06	2.81E-03
150	2.29E-13	2.28E-13	9.82E-06	6.53E-03
160	8.84E-12	8.81E-12	3.70E-05	1.51E-02
170	2.22E-10	2.21E-10	1.34E-04	3.44E-02
180	3.91E-09	3.89E-09	4.66E-04	7.72E-02
190	5.07E-08	5.06E-08	1.55E-03	1.69E-01
200	5.10E-07	5.08E-07	4.92E-03	3.63E-01
210	4.11E-06	4.10E-06	1.49E-02	7.62E-01
220	2.74E-05	2.73E-05	4.30E-02	1.56E+00
230	1.55E-04	1.55E-04	1.18E-01	3.12E+00
240	7.59E-04	7.57E-04	3.11E-01	6.12E+00
250	3.27E-03	3.27E-03	7.82E-01	1.18E+01
260	1.26E-02	1.26E-02	1.88E+00	2.21E+01
270	4.40E-02	4.39E-02	4.33E+00	4.08E+01
280	1.41E-01	1.40E-01	9.57E+00	7.38E+01
290	4.14E-01	4.13E-01	2.04E+01	1.31E+02
300	1.14E+00	1.13E+00	4.18E+01	2.29E+02
310	2.92E+00	2.91E+00	8.30E+01	3.92E+02
320	7.07E+00	7.06E+00	1.59E+02	6.60E+02
330	1.63E+01	1.62E+01	2.97E+02	1.09E+03
340	3.56E+01	3.55E+01	5.38E+02	1.78E+03
350	7.45E+01	7.43E+01	9.50E+02	2.86E+03
360	1.50E+02	1.49E+02	1.63E+03	4.51E+03
370	2.90E+02	2.89E+02	2.75E+03	7.02E+03
380	5.42E+02	5.41E+02	4.51E+03	1.08E+04
390	9.83E+02	9.80E+02	7.27E+03	1.63E+04

.

Table 2.S3. Full rate constant data for ^{3}**10** → ^{3}**11**

T (K)	TST (s^{-1})	CVT (s^{-1})	CVT / ZCT (s^{-1})	CVT / SCT (s^{-1})
10	0.00E+00	0.00E+00	NaN	NaN
20	3.97-168	3.85-168	3.98E-12	6.91E-06
30	2.75-108	2.70-108	4.17E-11	9.54E-06
40	2.43E-78	2.40E-78	2.99E-10	1.76E-05
50	2.32E-60	2.29E-60	1.28E-09	3.57E-05
60	2.27E-48	2.24E-48	4.13E-09	7.18E-05
70	8.36E-40	8.29E-40	1.16E-08	1.40E-04
80	2.23E-33	2.22E-33	3.11E-08	2.67E-04
90	2.23E-28	2.21E-28	8.31E-08	5.07E-04
100	2.22E-24	2.21E-24	2.29E-07	9.64E-04
110	4.16E-21	4.14E-21	6.61E-07	1.86E-03
120	2.22E-18	2.21E-18	2.00E-06	3.63E-03
130	4.49E-16	4.47E-16	6.32E-06	7.19E-03
140	4.26E-14	4.24E-14	2.04E-05	1.44E-02
150	2.20E-12	2.19E-12	6.64E-05	2.90E-02
160	6.94E-11	6.92E-11	2.14E-04	5.84E-02
170	1.46E-09	1.45E-09	6.78E-04	1.17E-01
180	2.18E-08	2.17E-08	2.09E-03	2.34E-01
190	2.45E-07	2.45E-07	6.23E-03	4.61E-01
200	2.17E-06	2.16E-06	1.79E-02	8.99E-01
210	1.55E-05	1.55E-05	4.94E-02	1.73E+00
220	9.32E-05	9.29E-05	1.31E-01	3.27E+00
230	4.78E-04	4.77E-04	3.32E-01	6.10E+00
240	2.14E-03	2.14E-03	8.09E-01	1.12E+01
250	8.51E-03	8.48E-03	1.89E+00	2.03E+01
260	3.04E-02	3.03E-02	4.24E+00	3.61E+01
270	9.88E-02	9.85E-02	9.17E+00	6.33E+01
280	2.95E-01	2.94E-01	1.91E+01	1.09E+02
290	8.18E-01	8.16E-01	3.84E+01	1.86E+02
300	2.12E+00	2.11E+00	7.49E+01	3.12E+02
310	5.16E+00	5.15E+00	1.41E+02	5.14E+02
320	1.19E+01	1.19E+01	2.59E+02	8.36E+02
330	2.61E+01	2.60E+01	4.62E+02	1.34E+03
340	5.46E+01	5.45E+01	8.02E+02	2.11E+03
350	1.10E+02	1.09E+02	1.36E+03	3.29E+03
360	2.12E+02	2.11E+02	2.25E+03	5.05E+03
370	3.95E+02	3.94E+02	3.65E+03	7.64E+03
380	7.13E+02	7.11E+02	5.80E+03	1.14E+04
390	1.25E+03	1.25E+03	9.03E+03	1.68E+04
400	2.13E+03	2.12E+03	1.38E+04	2.45E+04

Table 2.S4. Full rate constant data for ^{3}**12** → ^{3}**11**

T (K)	TST (s^{-1})	CVT (s^{-1})	CVT / ZCT (s^{-1})	CVT / SCT (s^{-1})
10	0.00E+00	0.00E+00	NaN	NaN
14	1.26-237	7.80-238	1.73E-07	3.28E-03
20	5.81-163	4.14-163	1.74E-07	3.29E-03
30	7.74-105	6.17-105	1.80E-07	3.37E-03
40	9.64E-76	8.14E-76	1.99E-07	3.62E-03
50	2.88E-58	2.51E-58	2.38E-07	4.10E-03
60	1.31E-46	1.17E-46	3.10E-07	4.88E-03
70	2.83E-38	2.57E-38	4.42E-07	6.09E-03
80	5.07E-32	4.65E-32	6.95E-07	7.97E-03
90	3.72E-27	3.45E-27	1.22E-06	1.09E-02
100	2.91E-23	2.72E-23	2.40E-06	1.57E-02
110	4.48E-20	4.20E-20	5.31E-06	2.37E-02
120	2.03E-17	1.91E-17	1.31E-05	3.74E-02
130	3.58E-15	3.39E-15	3.51E-05	6.19E-02
140	3.02E-13	2.87E-13	1.00E-04	1.06E-01
150	1.41E-11	1.34E-11	2.96E-04	1.88E-01
160	4.08E-10	3.89E-10	8.83E-04	3.42E-01
170	7.92E-09	7.58E-09	2.63E-03	6.29E-01
180	1.11E-07	1.06E-07	7.68E-03	1.17E+00
190	1.17E-06	1.13E-06	2.19E-02	2.17E+00
200	9.81E-06	9.43E-06	6.06E-02	4.01E+00
210	6.70E-05	6.45E-05	1.62E-01	7.39E+00
220	3.84E-04	3.70E-04	4.17E-01	1.35E+01
230	1.89E-03	1.83E-03	1.03E+00	2.43E+01
240	8.18E-03	7.89E-03	2.46E+00	4.34E+01
250	3.14E-02	3.03E-02	5.63E+00	7.66E+01
260	1.09E-01	1.05E-01	1.24E+01	1.33E+02
270	3.44E-01	3.32E-01	2.64E+01	2.29E+02
280	1.00E+00	9.67E-01	5.42E+01	3.87E+02
290	2.70E+00	2.62E+00	1.08E+02	6.45E+02
300	6.85E+00	6.63E+00	2.07E+02	1.06E+03
310	1.63E+01	1.58E+01	3.85E+02	1.72E+03
320	3.69E+01	3.57E+01	6.98E+02	2.75E+03
330	7.94E+01	7.69E+01	1.23E+03	4.32E+03
340	1.63E+02	1.58E+02	2.11E+03	6.71E+03
350	3.22E+02	3.12E+02	3.54E+03	1.03E+04
360	6.13E+02	5.94E+02	5.80E+03	1.55E+04
370	1.13E+03	1.09E+03	9.31E+03	2.32E+04
380	2.01E+03	1.94E+03	1.46E+04	3.41E+04
390	3.47E+03	3.36E+03	2.26E+04	4.96E+04

Table 2.S5. Full rate constant data for ^{3}**13** → ^{3}**14**

T (K)	TST (s^{-1})	CVT (s^{-1})	CVT / ZCT (s^{-1})	CVT / SCT (s^{-1})
10	0.00E+00	0.00E+00	NaN	NaN
14	9.53-256	9.49-256	1.32E-15	7.36E-09
20	1.47-175	1.46-175	1.48E-15	7.53E-09
30	3.87-113	3.87-113	9.15E-15	1.03E-08
40	6.81E-82	6.80E-82	2.95E-13	3.21E-08
50	3.96E-63	3.96E-63	4.36E-12	1.79E-07
60	1.31E-50	1.31E-50	3.44E-11	8.89E-07
70	1.17E-41	1.16E-41	1.89E-10	3.49E-06
80	6.04E-35	6.04E-35	8.50E-10	1.14E-05
90	1.01E-29	1.01E-29	3.51E-09	3.34E-05
100	1.54E-25	1.54E-25	1.42E-08	9.07E-05
110	4.05E-22	4.05E-22	5.74E-08	2.37E-04
120	2.87E-19	2.87E-19	2.35E-07	6.04E-04
130	7.43E-17	7.43E-17	9.58E-07	1.52E-03
140	8.69E-15	8.69E-15	3.87E-06	3.74E-03
150	5.38E-13	5.38E-13	1.52E-05	9.08E-03
160	1.99E-11	1.99E-11	5.79E-05	2.16E-02
170	4.81E-10	4.81E-10	2.12E-04	5.03E-02
180	8.17E-09	8.17E-09	7.39E-04	1.14E-01
190	1.03E-07	1.03E-07	2.46E-03	2.53E-01
200	1.01E-06	1.01E-06	7.82E-03	5.48E-01
210	7.92E-06	7.92E-06	2.36E-02	1.16E+00
220	5.16E-05	5.16E-05	6.81E-02	2.38E+00
230	2.86E-04	2.86E-04	1.87E-01	4.79E+00
240	1.38E-03	1.38E-03	4.89E-01	9.42E+00
250	5.83E-03	5.83E-03	1.22E+00	1.81E+01
260	2.21E-02	2.21E-02	2.92E+00	3.41E+01
270	7.61E-02	7.61E-02	6.70E+00	6.30E+01
280	2.40E-01	2.40E-01	1.48E+01	1.14E+02
290	6.98E-01	6.98E-01	3.13E+01	2.02E+02
300	1.89E+00	1.89E+00	6.40E+01	3.52E+02
310	4.81E+00	4.81E+00	1.26E+02	6.02E+02
320	1.15E+01	1.15E+01	2.42E+02	1.01E+03
330	2.63E+01	2.63E+01	4.49E+02	1.67E+03
340	5.70E+01	5.70E+01	8.10E+02	2.71E+03
350	1.18E+02	1.18E+02	1.42E+03	4.34E+03
360	2.36E+02	2.36E+02	2.44E+03	6.83E+03
370	4.54E+02	4.54E+02	4.09E+03	1.06E+04
380	8.43E+02	8.43E+02	6.69E+03	1.62E+04
390	1.52E+03	1.52E+03	1.07E+04	2.44E+04

Symm.	Frequency (cm^{-1})	Intensity
A"	121.37	0.1937
A"	166.44	0.0902
A"	252.1566	4.3366
A'	293.2973	1.434
A'	397.2321	0.7819
A"	430.6167	9.2184
A"	498.919	8.1206
A'	512.2896	0.8047
A"	533.33	4.9065
A'	587.2061	0.5335
A"	715.2016	7.0656
A'	748.6453	1.1494
A"	757.1135	42.9482
A"	857.3943	0.6462
A'	865.6191	0.3271
A'	896.8437	20.2631
A"	930.5981	1.0812
A"	968.1897	0.0632
A'	1011.0855	1.4758
A'	1066.5731	4.5527
A"	1071.7294	2.926
A'	1141.0393	0.626
A'	1187.5824	0.021
A'	1198.6092	0.6923
A'	1299.968	1.77
A'	1318.3219	0.2186
A'	1340.7166	0.0606
A'	1442.2057	1.0335
A'	1462.4502	0.6259
A'	1493.9023	9.1266
A"	1507.8568	6.2821
A'	1523.021	9.0607
A'	1580.4042	0.2448
A'	1620.235	5.7031
A'	3039.241	24.2371
A"	3088.1495	17.7091
A'	3124.6454	17.3456
A'	3175.999	10.8881
A'	3182.9581	4.7929
A'	3197.1927	27.5079
A'	3208.9039	24.3608
A'	3247.9107	2.9756

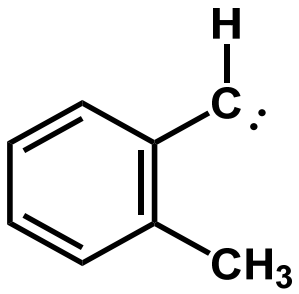

Charge	Multiplicity	Theory/Basis Set
0	3	UB3LYP/6-31G(d)
Zero-point Energy		**Electronic Energy**
0.129999		-309.5480235
Electronic and Zero-Point Energy		
-309.418024		
Full Point Group		**Dipole Moment (D)**
C_S		0.3563

(Energies in Hartrees/particle)

Atom	Coordinates (Angstroms)		
	X	Y	Z
C	1.848531	-0.710076	0.000000
C	0.949337	-1.783681	0.000000
C	-0.415724	-1.546217	0.000000
C	-0.933022	-0.211715	0.000000
C	0.000000	0.882409	0.000000
C	1.361853	0.604108	0.000000
H	2.919488	-0.891943	0.000000
H	1.318763	-2.805919	0.000000
H	-1.116429	-2.376756	0.000000
H	2.065776	1.433505	0.000000
C	-0.512193	2.299482	0.000000
C	-2.306636	0.009573	0.000000
H	-1.13787	2.497000	0.879776
H	0.312172	3.019413	0.000000
H	-1.13787	2.497000	-0.879776
H	-3.176909	-0.635601	0.000000

Symm.	Frequency (cm^{-1})	Intensity
A'	-1862.8542	25.3693
A''	179.287	0.0238
A''	241.097	4.3287
A''	399.6844	0.1726
A'	414.9253	0.5714
A''	421.0727	9.4263
A''	519.4287	3.7574
A''	564.7692	9.1617
A'	566.3836	2.0068
A'	583.3114	0.0529
A'	613.4039	3.9136
A''	721.993	11.7452
A''	766.004	41.2826
A'	782.8883	0.5874
A''	861.5139	0.7621
A'	877.5706	0.4674
A''	928.6063	1.3885
A''	971.3658	0.0279
A'	975.8569	27.41
A'	1023.9382	2.3379
A'	1050.9004	8.8116
A''	1054.5147	0.6211
A'	1124.3656	0.3664
A'	1179.8646	0.1024
A'	1198.2092	2.5769
A''	1211.5366	5.8984
A'	1278.1619	3.6844
A'	1317.9077	0.2174
A'	1360.3201	0.9188
A'	1456.4591	0.5184
A'	1479.4715	4.7448
A'	1503.052	9.4741
A'	1586.0237	1.8504
A'	1614.1566	3.5182
A'	1720.5028	2.4969
A'	3096.8557	20.0537
A''	3167.7099	13.177
A'	3179.7641	2.14
A'	3186.209	8.3848
A'	3198.6073	30.5274
A'	3208.7732	24.8568
A'	3231.5439	7.6169

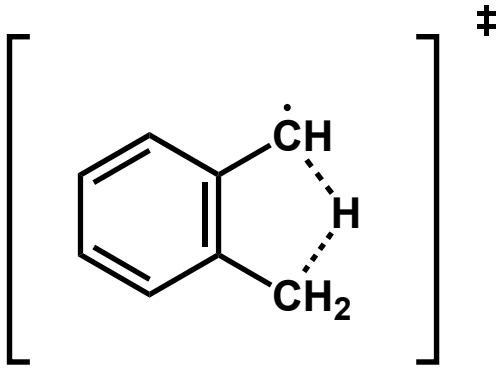

Charge	Multiplicity	Theory/Basis Set
0	3	UB3LYP/6-31G(d)
Zero-point Energy		**Electronic Energy**
0.124885		-309.5152733
Electronic and Zero-Point Energy		
-309.390389		
Full Point Group		**Dipole Moment (D)**
C_S		0.3487

Atom	Coordinates (Angstroms)		
	X	Y	Z
C	-1.072846	-1.724220	0.000000
C	0.309748	-1.579852	0.000000
C	-1.374570	0.695977	0.000000
C	-1.914649	-0.601825	0.000000
H	-1.508606	-2.720161	0.000000
H	0.957729	-2.452171	0.000000
H	-2.035994	1.559131	0.000000
H	-2.992812	-0.736093	0.000000
C	2.216381	0.121785	0.000000
C	0.869963	-0.277675	0.000000
C	0.791641	2.137990	0.000000
H	0.751292	2.745983	0.907147
H	1.979360	1.486043	0.000000
H	0.751292	2.745983	-0.907147
C	0.000000	0.863109	0.000000
H	3.143730	-0.440456	0.000000

Symm.	Frequency (cm^{-1})	Intensity
A2	137.2409	0.0000
B1	262.9792	3.1319
A2	342.8887	0.0000
A1	368.1833	0.8312
B1	369.9778	0.1232
B2	413.2744	0.0376
B1	462.3381	12.1197
B2	502.9096	1.1483
A2	525.8060	0.0000
A1	596.5445	0.0489
A2	633.6416	0.0000
B1	651.1197	58.7086
B1	750.1654	68.3160
A2	752.5979	0.0000
A1	760.3394	0.3592
B2	866.2000	2.7484
A2	872.1129	0.0000
B1	915.4824	4.9797
A2	959.2935	0.0000
B2	977.4155	0.0404
A1	990.3664	0.9454
A1	1074.7371	0.3299
B2	1136.0102	0.1285
A1	1176.3071	1.7998
A1	1212.4691	0.3094
B2	1270.8549	2.4810
B2	1311.7878	1.9277
A1	1394.9389	6.0701
B2	1466.4304	3.2448
B2	1499.8923	0.8996
A1	1515.1000	0.3237
A1	1542.6157	9.1700
B2	1550.9375	3.1688
A1	1609.8316	0.0524
B2	3178.0569	9.2178
A1	3181.7585	0.5942
B2	3187.6904	11.2027
A1	3194.0689	9.5365
B2	3196.1067	26.5882
A1	3211.3797	23.7652
B2	3282.6354	10.8152
A1	3293.4430	6.0985

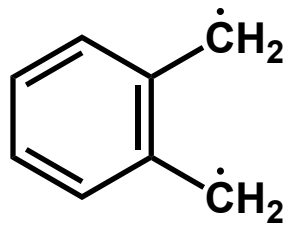

Charge	Multiplicity
0	3
Zero-point Energy	**Electronic Energy**
0.12894	-309.5704436
Electronic and Zero-Point Energy	
-309.441504	
Full Point Group	**Dipole Moment (D)**
C_{2V}	0.2044

(Energies in Hartrees/particle)

Atom	Coordinates (Angstroms)		
	X	Y	Z
C	0.000000	0.727285	-0.582198
C	0.000000	-0.727285	-0.582198
C	0.000000	-1.387959	0.657259
C	0.000000	-0.693024	1.880891
C	0.000000	0.693024	1.880891
C	0.000000	1.387959	0.657259
C	0.000000	1.486329	-1.784406
C	0.000000	-1.486329	-1.784406
H	0.000000	-2.475392	0.662594
H	0.000000	-1.247373	2.815160
H	0.000000	1.247373	2.815160
H	0.000000	2.475392	0.662594
H	0.000000	2.570403	-1.739818
H	0.000000	-1.034609	-2.767218
H	0.000000	-2.570403	-1.739818
H	0.000000	1.034609	-2.767218

Charge	Multiplicity	Theory/Basis Set	Full Point Group
0	3	UB3LYP/6-31G(d)	C_S
Zero-point Energy	**Electronic Energy**	**Electronic and Zero-Point Energy**	**Dipole Moment (D)**
0.176835	-463.193048	-463.016213	0.3146

(Energies in Hartrees/particle)

Symm.	Frequency (cm^{-1})	Intensity	Symm.	Frequency (cm^{-1})	Intensity
A"	89.5471	0.1066	A'	1069.8252	2.6286
A"	111.5880	0.3865	A'	1125.1812	2.9747
A"	133.2181	0.2868	A'	1177.3806	0.6525
A"	228.1806	1.1431	A'	1185.6757	0.2429
A'	276.4945	0.5354	A'	1218.8918	2.0229
A"	298.3032	3.1401	A'	1245.2236	3.3136
A'	331.8682	0.2965	A'	1271.3334	1.7290
A"	422.0910	1.7357	A'	1314.2902	0.5462
A'	426.3581	1.0009	A'	1353.0789	1.6398
A'	456.8644	1.6800	A'	1356.3900	3.5397
A"	470.6397	11.1852	A'	1403.8161	0.7204
A"	520.7080	1.3266	A'	1441.4905	1.8127
A'	522.0931	1.2743	A'	1468.4327	1.1604
A"	554.1613	17.6530	A'	1491.9180	0.6316
A'	593.8501	0.9843	A"	1506.8627	6.4948
A"	663.9311	4.6354	A'	1518.1044	3.1581
A'	702.2378	0.5977	A'	1554.2650	18.8337
A'	740.9605	3.8535	A'	1567.4702	1.5458
A"	750.1866	9.7784	A'	1611.0307	4.7123
A"	784.3399	12.5416	A'	1662.4737	2.3941
A"	811.9036	37.4158	A'	3037.7677	28.4154
A'	820.6769	14.1845	A"	3085.8835	16.6347
A'	878.5573	0.2768	A'	3123.8772	18.5756
A"	879.0252	2.8706	A'	3176.2300	8.9844
A"	939.7207	0.7147	A'	3178.0721	3.3349
A"	946.3424	0.6639	A'	3187.9420	4.9045
A'	966.5740	14.3660	A'	3196.2740	26.9152
A"	982.1091	0.0380	A'	3201.2578	31.2134
A'	1039.8157	0.8855	A'	3211.1090	25.2902
A"	1065.2495	2.9015	A'	3272.3014	1.0971

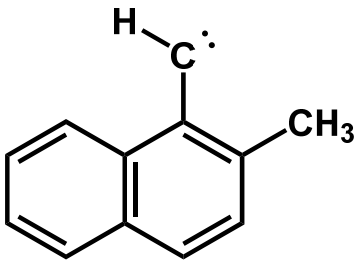

Charge	Multiplicity	Theory/Basis Set	Full Point Group
0	3	UB3LYP/6-31G(d)	C_S
Zero-point Energy	**Electronic Energy**	**Electronic and Zero-Point Energy**	**Dipole Moment (D)**
0.175513	-463.208712	-463.033200	0.2407

(Energies in Hartrees/particle)

Symm.	Frequency (cm^{-1})	Intensity	Symm.	Frequency (cm^{-1})	Intensity
A"	74.8493	0.0615	A'	1042.3876	1.0815
A"	117.9492	0.3499	A'	1075.9463	0.9857
A"	197.0752	0.4851	A'	1091.2796	1.7855
A"	267.3154	1.7904	A'	1171.6978	1.5215
A"	295.2550	0.0024	A'	1195.6158	0.0486
A'	301.3251	1.5482	A'	1226.1409	6.5623
A"	329.4408	3.3288	A'	1248.5068	0.0472
A'	410.3650	0.4521	A'	1268.4348	0.3811
A"	423.4987	4.3243	A'	1300.7154	1.6292
A'	430.5678	0.0764	A'	1335.2563	8.1363
A'	469.3172	0.4399	A'	1367.8978	1.7948
A'	518.5693	0.5263	A'	1417.2721	1.0425
A"	519.3578	3.2522	A'	1461.4148	3.0427
A"	533.0222	0.0390	A'	1500.6077	0.7123
A'	582.5576	1.7447	A'	1505.3412	3.2878
A"	588.6039	13.7624	A'	1539.0372	1.7206
A"	628.8025	68.5223	A'	1554.5178	6.2152
A"	690.8405	2.2485	A'	1584.4822	2.3917
A'	703.2123	1.6795	A'	1607.3230	8.7234
A'	741.6450	1.1302	A'	1666.3022	3.9239
A"	751.7245	21.1998	A'	3177.6984	2.0473
A"	792.9475	0.0239	A'	3179.7370	5.2170
A"	824.0964	44.8961	A'	3189.1964	13.0759
A"	870.0024	6.6178	A'	3194.3581	8.9113
A'	878.2568	0.3985	A'	3197.9975	31.1486
A'	880.7002	0.1298	A'	3206.0246	29.8405
A"	937.7811	1.0084	A'	3217.9160	9.0270
A"	948.4255	0.5060	A'	3231.8346	13.8173
A"	982.3001	0.0614	A'	3295.0841	9.6050
A'	990.7155	0.8845	A'	3310.5654	6.1177

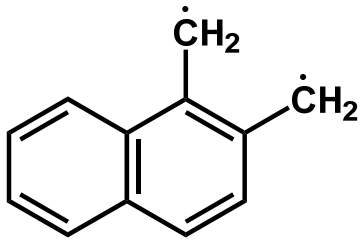

Charge	Multiplicity	Theory/Basis Set	Full Point Group
0	3	UB3LYP/6-31G(d)	C_S
Zero-point Energy	**Electronic Energy**	**Electronic and Zero-Point Energy**	**Dipole Moment (D)**
0.171859	-463.162069	-462.990210	0.3451

(Energies in Hartrees/particle)

Symm.	Frequency (cm^{-1})	Intensity	Symm.	Frequency (cm^{-1})	Intensity
A'	-1855.8764	24.5960	A''	1049.5767	0.5204
A''	113.9583	0.5156	A'	1063.9349	5.9024
A''	130.3714	0.4569	A'	1116.1104	5.5378
A''	224.9791	1.6461	A'	1167.9274	0.0892
A'	272.6527	0.6479	A'	1188.3115	0.1964
A''	291.1409	2.7614	A''	1211.9292	5.9075
A''	401.0405	1.2061	A'	1224.8707	4.6946
A''	436.5553	1.7286	A'	1237.1313	3.0904
A'	438.6374	1.1201	A'	1256.7924	1.5918
A'	467.4206	0.4924	A'	1312.1206	0.6957
A''	493.4187	3.0946	A'	1345.8257	0.731
A'	524.5296	0.808	A'	1376.0988	4.879
A''	534.2188	0.0075	A'	1427.944	2.0784
A''	590.5369	24.1304	A'	1465.055	2.7823
A'	600.4541	3.4655	A'	1474.6414	0.3725
A'	638.9473	2.3058	A'	1494.2875	1.0424
A''	673.3907	6.934	A'	1550.9816	8.7235
A'	712.7431	0.3967	A'	1571.2271	2.0141
A''	751.2291	7.551	A'	1604.2126	2.337
A'	757.6263	2.2978	A'	1662.9924	4.1869
A''	793.1855	16.1227	A'	1721.7714	3.4804
A''	813.5857	37.851	A'	3092.8853	26.4745
A''	884.1655	2.413	A''	3163.0152	13.3372
A'	885.2147	0.2859	A'	3176.8635	2.5766
A'	912.6192	11.137	A'	3180.508	3.9558
A''	936.7505	0.6101	A'	3186.4958	2.3272
A''	949.9021	0.9925	A'	3196.98	10.7852
A''	984.4696	0.0165	A'	3198.0752	48.2743
A'	1026.9377	14.9306	A'	3209.0938	28.1025
A'	1031.7488	4.8224	A'	3237.4534	4.7724

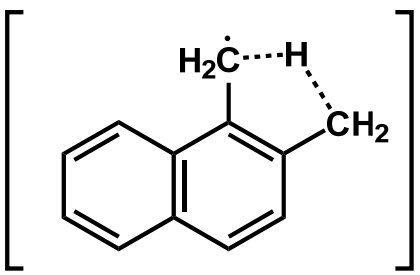

Charge	Multiplicity	Theory/Basis Set	Full Point Group
0	3	UB3LYP/6-31G(d)	C_S
Zero-point Energy	**Electronic Energy**	**Electronic and Zero-Point Energy**	**Dipole Moment (D)**
0.177142	-463.190870	-463.013728	0.3861

(Energies in Hartrees/particle)

Symm.	Frequency (cm^{-1})	Intensity	Symm.	Frequency (cm^{-1})	Intensity
A"	106.2800	0.0355	A'	1080.3474	0.0447
A"	128.2564	0.0643	A'	1108.6678	2.8285
A"	150.5478	0.3050	A'	1176.2223	0.1660
A"	215.6776	3.1392	A'	1188.3159	1.6796
A'	279.3103	0.4403	A'	1200.0279	0.9665
A"	303.1094	2.3125	A'	1243.7289	1.4001
A'	324.3194	0.9092	A'	1280.4018	3.8774
A"	416.0415	1.8663	A'	1319.6019	0.1178
A'	447.6035	0.2274	A'	1376.3323	3.2636
A'	462.4078	0.4922	A'	1396.4882	1.6881
A"	485.5976	17.3376	A'	1407.8712	6.1181
A'	506.8493	1.1131	A'	1436.6712	3.6926
A"	529.3893	0.3672	A'	1456.7729	0.1113
A"	537.5057	9.2797	A'	1481.6216	6.6764
A'	571.3691	3.9196	A"	1513.7876	5.8378
A"	658.1041	0.0089	A'	1519.6221	8.5786
A'	695.9916	0.2800	A'	1544.7268	6.1163
A'	744.0279	0.3714	A'	1578.3184	3.4859
A"	757.9493	15.1216	A'	1640.7340	0.7386
A"	783.2325	10.1752	A'	1657.0704	0.9598
A"	820.3642	46.4697	A'	3035.4180	22.3735
A'	859.7258	1.6808	A"	3083.9276	19.3596
A"	878.1150	2.1787	A'	3130.1333	8.8180
A'	899.1274	29.2254	A'	3175.2482	0.0559
A'	915.1082	1.3331	A'	3178.3433	8.2860
A"	946.2037	1.5454	A'	3187.7940	12.9404
A"	964.4339	0.5033	A'	3200.4442	25.0971
A"	983.7277	0.0645	A'	3204.6439	32.7772
A'	1055.7861	3.0767	A'	3217.2715	18.3794
A"	1059.6266	0.4468	A'	3250.1021	2.4167

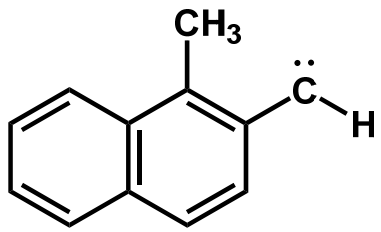

Charge	Multiplicity	Theory/Basis Set	Full Point Group
0	3	UB3LYP/6-31G(d)	C_S
Zero-point Energy	**Electronic Energy**	**Electronic and Zero-Point Energy**	**Dipole Moment (D)**
0.175513	-463.208712	-463.033200	0.2407

(Energies in Hartrees/particle)

Symm.	Frequency (cm^{-1})	Intensity	Symm.	Frequency (cm^{-1})	Intensity
A"	74.8493	0.0615	A'	1042.3876	1.0815
A"	117.9492	0.3499	A'	1075.9463	0.9857
A"	197.0752	0.4851	A'	1091.2796	1.7855
A"	267.3153	1.7904	A'	1171.6978	1.5215
A"	295.2549	0.0024	A'	1195.6158	0.0486
A'	301.3251	1.5482	A'	1226.1409	6.5623
A"	329.4408	3.3288	A'	1248.5068	0.0472
A'	410.3650	0.4521	A'	1268.4349	0.3811
A"	423.4987	4.3243	A'	1300.7154	1.6292
A'	430.5678	0.0764	A'	1335.2562	8.1363
A'	469.3172	0.4399	A'	1367.8978	1.7948
A'	518.5692	0.5263	A'	1417.2721	1.0424
A"	519.3578	3.2522	A'	1461.4148	3.0427
A"	533.0222	0.0390	A'	1500.6077	0.7123
A'	582.5576	1.7447	A'	1505.3412	3.2878
A"	588.6039	13.7624	A'	1539.0372	1.7206
A"	628.8025	68.5223	A'	1554.5178	6.2152
A"	690.8405	2.2485	A'	1584.4821	2.3917
A'	703.2123	1.6795	A'	1607.3230	8.7234
A'	741.6450	1.1302	A'	1666.3021	3.9239
A"	751.7245	21.1998	A'	3177.6983	2.0473
A"	792.9475	0.0239	A'	3179.7370	5.2170
A"	824.0964	44.8961	A'	3189.1964	13.0760
A"	870.0024	6.6179	A'	3194.3581	8.9114
A'	878.2568	0.3985	A'	3197.9975	31.1486
A'	880.7002	0.1298	A'	3206.0245	29.8405
A"	937.7811	1.0084	A'	3217.9161	9.0269
A"	948.4255	0.5060	A'	3231.8347	13.8173
A"	982.3001	0.0614	A'	3295.0842	9.6050
A'	990.7155	0.8845	A'	3310.5655	6.1177

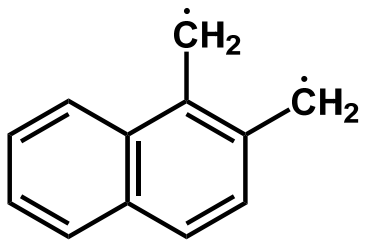

Charge	Multiplicity	Theory/Basis Set	Full Point Group
0	3	UB3LYP/6-31G(d)	C_S
Zero-point Energy	**Electronic Energy**	**Electronic and Zero-Point Energy**	**Dipole Moment (D)**
0.171948	-463.160304	-462.988356	0.3757

(Energies in Hartrees/particle)

Symm.	Frequency (cm^{-1})	Intensity	Symm.	Frequency (cm^{-1})	Intensity
A'	-1867.0143	19.9109	A''	1047.0518	0.054
A''	118.1716	0.3915	A'	1068.2668	2.0772
A''	140.366	0.0637	A'	1091.6744	2.1943
A''	227.0543	2.8215	A'	1171.5107	0.1832
A'	261.0208	0.3489	A'	1185.0794	0.0041
A''	285.9517	2.8126	A'	1191.68	4.1213
A''	403.4533	0.0246	A''	1208.166	6.7632
A''	439.6896	4.2829	A'	1239.4498	2.475
A'	448.6917	1.0772	A'	1290.6878	5.903
A'	471.138	1.559	A'	1317.4612	1.7001
A''	504.9411	3.5987	A'	1379.9833	0.0242
A'	520.7218	0.4793	A'	1390.8255	3.4953
A''	540.6789	0.4774	A'	1419.957	6.0505
A''	562.2127	21.2781	A'	1464.6639	0.8661
A'	600.5032	4.636	A'	1479.3063	1.2914
A'	624.3121	0.9612	A'	1479.7442	2.5703
A''	669.7861	0.0197	A'	1551.7548	9.0722
A'	714.1418	1.0008	A'	1576.6498	0.1629
A'	746.6416	0.4092	A'	1628.0451	1.3398
A''	761.8716	20.1881	A'	1655.8992	1.9055
A''	784.8285	5.3099	A'	1716.4871	4.082
A''	827.7071	45.3691	A'	3089.4125	18.3693
A'	865.6949	0.0549	A''	3158.9878	13.221
A''	879.2198	2.2432	A'	3175.8347	0.0237
A''	946.6162	1.529	A'	3178.8248	11.2188
A''	967.4513	0.3786	A'	3185.3412	4.0472
A'	971.745	4.3284	A'	3197.9611	25.9538
A'	975.3797	27.8542	A'	3202.3214	27.0877
A''	984.3809	0.0945	A'	3209.5064	30.4467
A'	1045.9384	7.4772	A'	3233.7399	6.3509

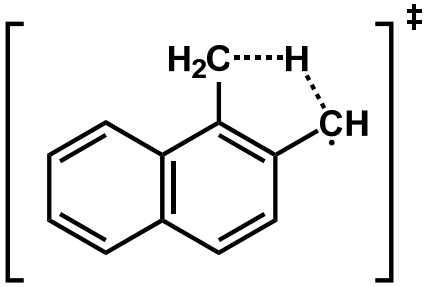

Charge	Multiplicity	Theory/Basis Set	Full Point Group
0	3	UB3LYP/6-31G(d)	C_S
Zero-point Energy	**Electronic Energy**	**Electronic and Zero-Point Energy**	**Dipole Moment (D)**
0.177076	-463.193725	-463.016648	0.3032

(Energies in Hartrees/particle)

Symm.	Frequency (cm^{-1})	Intensity	Symm.	Frequency (cm^{-1})	Intensity
A"	110.2589	0.1925	A"	1076.2076	2.9263
A"	118.8030	1.0783	A'	1138.7742	0.1886
A"	153.6118	0.0014	A'	1183.3150	0.7998
A"	263.2860	0.0318	A'	1186.0667	1.0075
A'	264.8611	0.1682	A'	1226.6270	1.3901
A'	294.8599	2.2379	A'	1247.1499	0.9752
A"	302.9286	1.6547	A'	1296.2153	4.4245
A"	408.1916	4.8675	A'	1317.4639	0.5212
A'	409.1744	1.5327	A'	1341.4458	1.4522
A'	451.0696	0.1175	A'	1396.4768	0.1179
A"	481.1414	4.1357	A'	1410.9869	0.3384
A"	523.6336	15.9118	A'	1442.2015	0.2987
A'	527.1267	1.1772	A'	1463.7230	1.2924
A"	554.1116	6.2170	A'	1485.9665	5.6730
A'	633.6921	2.8365	A"	1506.4375	6.6785
A'	679.9408	1.2660	A'	1518.0905	6.9174
A"	682.5177	1.7816	A'	1536.5520	5.8462
A'	754.1879	0.2288	A'	1587.6697	1.6743
A"	759.1280	23.9334	A'	1647.1303	7.9966
A"	769.0623	4.0620	A'	1656.8105	2.8088
A'	814.8926	4.6763	A'	3040.1891	31.1052
A"	843.3687	19.4723	A"	3089.5134	17.4507
A"	872.3861	15.8490	A'	3126.8206	15.9458
A'	898.6384	9.9938	A'	3169.9817	14.4741
A"	908.0028	4.4045	A'	3176.6098	8.9882
A'	948.4296	12.4165	A'	3180.3393	4.7066
A"	949.1530	3.9094	A'	3184.6707	6.8648
A"	982.1015	0.0389	A'	3194.7399	34.7618
A'	1030.6050	2.6254	A'	3208.2202	34.4202
A'	1053.0112	1.0056	A'	3248.9108	2.9479

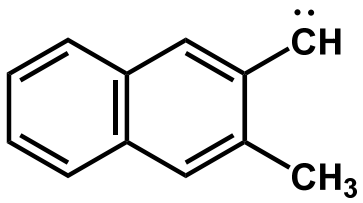

Charge	Multiplicity	Theory/Basis Set	Full Point Group
0	3	UB3LYP/6-31G(d)	C_{2V}
Zero-point Energy	**Electronic Energy**	**Electronic and Zero-Point Energy**	**Dipole Moment (D)**
0.176457	-463.223850	-463.047393	0.2577

(Energies in Hartrees/particle)

Symm.	Frequency (cm^{-1})	Intensity	Symm.	Frequency (cm^{-1})	Intensity
A2	86.8282	0.0000	A1	1026.4368	0.0116
B1	119.0314	1.0118	A1	1062.3198	1.7161
A2	233.5084	0.0000	B2	1145.4578	0.6348
B2	269.9111	0.0339	A1	1177.9613	0.3570
B1	312.9423	0.0673	B2	1218.8071	0.5849
A1	370.3269	0.5812	A1	1221.8838	2.0810
B1	396.7895	3.1520	A1	1251.0203	1.6905
B2	411.5954	0.9855	B2	1297.6728	6.2829
A2	444.9934	0.0000	B2	1313.0595	0.3243
A1	457.5595	0.0186	B2	1347.4430	0.0016
B1	468.0409	2.6738	A1	1364.5484	0.0256
B2	526.2519	0.0056	A1	1446.5199	0.0182
B1	533.2980	6.8742	B2	1463.0726	3.7448
A2	548.3287	0.0000	A1	1491.6306	0.8543
A1	631.1247	3.8770	B2	1510.3956	4.0490
A2	685.5557	0.0000	A1	1523.8237	0.5623
B2	691.4596	0.5013	B2	1545.3095	0.0188
B1	729.2142	84.7924	A1	1548.7311	17.9469
A1	741.3958	0.0106	A1	1608.6278	0.0337
A2	746.3025	0.0000	B2	1632.8214	1.3759
B1	758.2273	15.2027	B2	3173.6525	9.3296
A2	758.3932	0.0000	A1	3175.1327	0.1139
A1	840.2275	2.2036	B2	3178.1438	16.4389
A2	848.0725	0.0000	A1	3182.3186	0.2023
B1	858.2394	53.6989	B2	3185.0589	18.1533
A2	893.4768	0.0000	A1	3190.6090	8.5303
B2	916.2195	0.0483	B2	3195.6122	29.8193
B1	939.7610	4.8909	A1	3209.6215	36.0122
A2	976.6202	0.0000	B2	3275.3798	10.6289
B2	1013.7573	0.0044	A1	3285.1261	3.6837

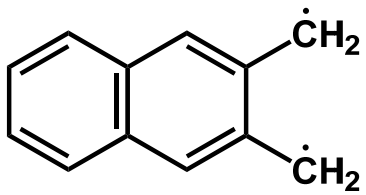

Charge	Multiplicity	Theory/Basis Set	Full Point Group
0	3	UB3LYP/6-31G(d)	C_S
Zero-point Energy	**Electronic Energy**	**Electronic and Zero-Point Energy**	**Dipole Moment (D)**
0.171805	-463.161231	-462.989426	0.2327

(Energies in Hartrees/particle)

Symm.	Frequency (cm^{-1})	Intensity	Symm.	Frequency (cm^{-1})	Intensity
A'	-1855.0431	27.7263	A'	1054.3807	0.8648
A''	117.549	0.8301	A''	1056.0262	1.0432
A''	122.6719	0.4429	A'	1127.1689	0.0359
A''	246.7177	0.0499	A'	1175.6726	0.5435
A'	284.258	0.4454	A'	1183.3223	0.2686
A''	297.2439	1.3702	A'	1215.6165	1.4853
A''	396.2238	2.0309	A''	1217.2774	5.9432
A''	400.8551	3.542	A'	1241.0807	0.63
A'	408.8288	0.1062	A'	1282.3337	2.9798
A'	442.6827	0.3502	A'	1292.4877	7.0226
A''	482.387	5.8126	A'	1360.4841	2.0379
A''	540.8088	4.1967	A'	1392.4722	0.2651
A'	575.4442	0.1277	A'	1430.674	2.7204
A''	583.1212	17.5698	A'	1457.0153	1.9842
A'	615.6775	8.3625	A'	1471.5005	4.7682
A'	629.7879	1.6599	A'	1490.7713	1.5225
A''	694.2442	2.552	A'	1535.0458	7.4292
A'	717.7061	0.8458	A'	1588.5196	1.3065
A''	760.162	22.443	A'	1645.2437	7.5291
A'	767.7005	0.25	A'	1655.9156	2.1344
A''	771.5814	4.0992	A'	1724.6859	2.4436
A'	836.3252	1.4129	A'	3099.2137	23.1757
A''	846.6676	17.4651	A''	3170.5932	11.8783
A''	872.6683	20.8181	A'	3174.7514	0.5817
A''	905.6283	3.2935	A'	3177.1543	15.6378
A'	913.3147	0.8076	A'	3180.2673	6.0488
A''	948.8712	3.9194	A'	3186.6652	7.0906
A''	982.0149	0.0238	A'	3194.4463	36.3173
A'	995.9423	26.601	A'	3208.038	35.1759
A'	1037.2633	5.2757	A'	3230.4097	7.6005

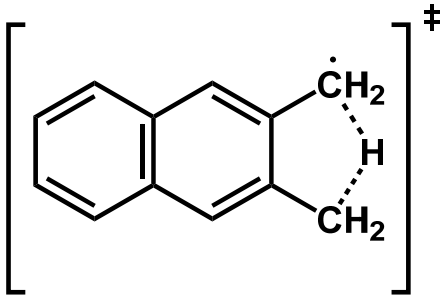

Chapter 3: Quantum Mechanical Tunneling in Benzazirines

Introduction

The study of phenylnitrenes (**2**) and their photochemistry has been the subject of a great many theoretical and spectroscopic studies over the years.[1,2] The exact nature of the intermediates and reaction pathway for the phenylnitrene system has been often been controversial. Many different arylnitrenes have been studied for years through spectroscopy,[3,4] matrix studies[5-9], and computational work.[2,10] Though debated for some time, the current generally accepted pathway of rearrangements is shown in Scheme 3.1. Singlet phenylnitrene is generated from photolysis of the corresponding phenyl azide (**1**). At lower temperatures, intersystem crossing (ISC) to the more stable triplet nitrene (^{3}**2**) is favored. At higher temperatures, the singlet phenylnitrene will quickly rearrange to form the intermediate benzazirine (**3**).

Scheme 3.1. Rearrangements on the phenylnitrene energy surface.

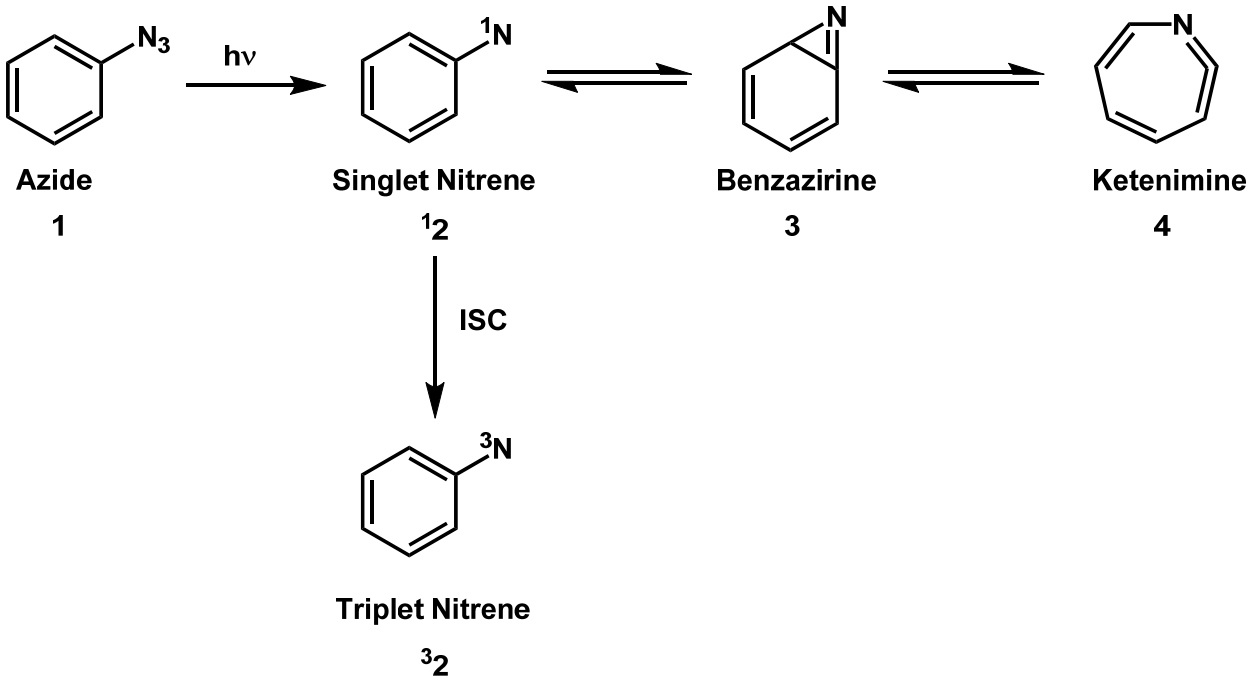

From **3**, ring expansion to ketenimine **4** occurs. Computational studies have shown that the barrier to forming the ketenimine is lower than that for the formation of the benzazirine.[10] Furthermore, the rate of intersystem crossing (ISC) from singlet phenylnitrene ^{1}**2** to triplet ^{3}**2** becomes faster than the formation of **3** at lower temperatures, making observation of the parent benzazirine difficult. Though the parent benzazirine has never been observed experimentally, trapped products from nucleophilic solvents[11,12] and computational studies[10] imply its existence. In a few cases, bulky or strong electron withdrawing substituents have raised the barrier to ring expansion sufficiently to allow observation of different substituted benzazirines.[5,7]

In a recent study of Inui *et al.*, a methylthio substituted benzazirine was observed via IR spectroscopy in an argon matrix.[13] Surprisingly, the observed benzazirine **5** was found to rearrange in the dark at 10 K to the more stable ketenimine **6** (Scheme 3.2). Based on the low temperature, the barrier to rearrangement (calc. 3.4 kcal/mol), and a negligible change in rate with increasing temperature, it was concluded that this rearrangement occurred via a heavy-atom tunneling process. To our knowledge, no other studied benzazirine has demonstrated this ability to rearrange via heavy-atom tunneling. In the same study, the methoxy substituted benzazirine **7** was shown to be stable in the matrix under the same conditions. A higher and wider barrier of reaction was cited as evidence for the lack of tunneling to ketenimine **8**.

Scheme 3.2. Ring expansion of substituted benzazirines.

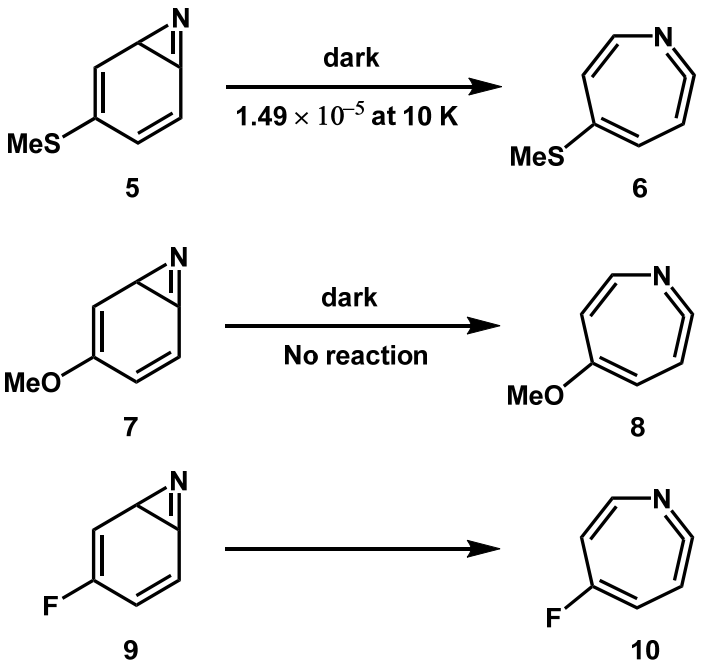

Once thought to be impossible due to its large mass in comparison to hydrogen,[14] reactions involving carbon tunneling have been observed with increasing frequency in the past decade, either through experimental or computational study.[15-20] Due to the 12-fold increase in mass compared to hydrogen, these tunneling reactions necessitate a low and more importantly, narrow barrier to reaction. Intrigued by the results of Inui *et al.*, we investigated the possibility of heavy-atom tunneling in the parent benzazirine **3**.

Computational Methods

All optimizations and harmonic frequency calculations were completed using Gaussian09,[21] with the nature of each stationary point determined by a harmonic frequency calculation. Due to the large computational demands of the rate constant calculations including

tunneling corrections, the B3LYP[22] functional was used as an efficient level of theory for these calculations with a small 6-31G(d)[23] basis set. All optimizations were run with OPT=TIGHT and an ultrafine grid. Intrinsic reaction coordinate (IRC) calculations were used to verify that all stationary points were connected. Earlier studies have shown B3LYP/6-31G(d)to be effective at accurately modeling the potential energy surface (PES) for carbon tunneling calculations.[19,20] The geometries and relative energies of the stationary points on the PES at B3LYP/6-31G(d) are similar to those obtained in previous studies using to higher-level (CASPT2(8,8)/6-311G(2d,p)//CASSCF(8,8)/6-31G*) calculations.[10,24]

Semi-classical rate constants were carried out with canonical variational transition state theory (CVT)[25] as implemented by the Polyrate[26] and Gaussrate[27] software packages. Rate constants including a multi-dimensional tunneling approximation were also calculated with both zero curvature tunneling (ZCT)[28] and small curvature tunneling (SCT).[25] SCT in particular has demonstrated considerable accuracy for unimolecular tunneling reactions at cryogenic temperatures[29]. As is appropriate for low-temperature unimolecular reactions, quantized-reactant-state-tunneling (QRST)[30] was enabled for all tunneling approximations.

Results and Discussion

The PES for the tunneling reaction of **3** to **4** is shown in Figure 3.1. The barrier calculated at B3LYP/6-31G(d) was found to be 3.7 kcal/mol, similar to the value found by Borden et al. using CASPT2 calculations of 3.1 kcal/mol.[10] The reaction was found to exothermic by 5.1 kcal/mol, again similar to the other published work of 5.7 kcal/mol.

The results of the rate calculations are shown below in Table 3.1. The CVT rate constants demonstrate that, without tunneling, the ring expansion of benzazirine is impossible for

a classical thermally activated reaction at cryogenic temperatures. The addition of ZCT and SCT tunneling approximations to the CVT rate constant shows the impact tunneling has on the reaction. The addition of the ZCT approximation was found to dramatically increase the rate by a factor of ~10^{75}. As expected, rate constants with the SCT approximation are slightly larger compared to ZCT, accounting for "corner cutting" of the MEP by a shorter tunneling pathway. Even at 10 K, the ring expansion is predicted to be very fast ($k = 1.17 \times 10^5$ s^{-1} at CVT / SCT). This fast tunneling process adds further complications to the isolation of **3**. The barrier to formation of ^{1}**2** to **3** is predicted computationally to be higher than the barrier of **3** to **4**. Furthermore, at lower temperatures the rate of ISC from ^{1}**2** to ^{3}**2** is known to be faster than the rate of formation of **3**. Therefore, at low temperatures not only is the formation of benzazirine **3** not favored, but any that is formed would immediately tunnel to the ketenimine **4**, making the observation of benzazirine all but impossible.

Figure 3.1. Potential energy surface of the ring expansion of benzazirine **(3)** to ketenimine (**4**) at B3LYP/6-31G(d).

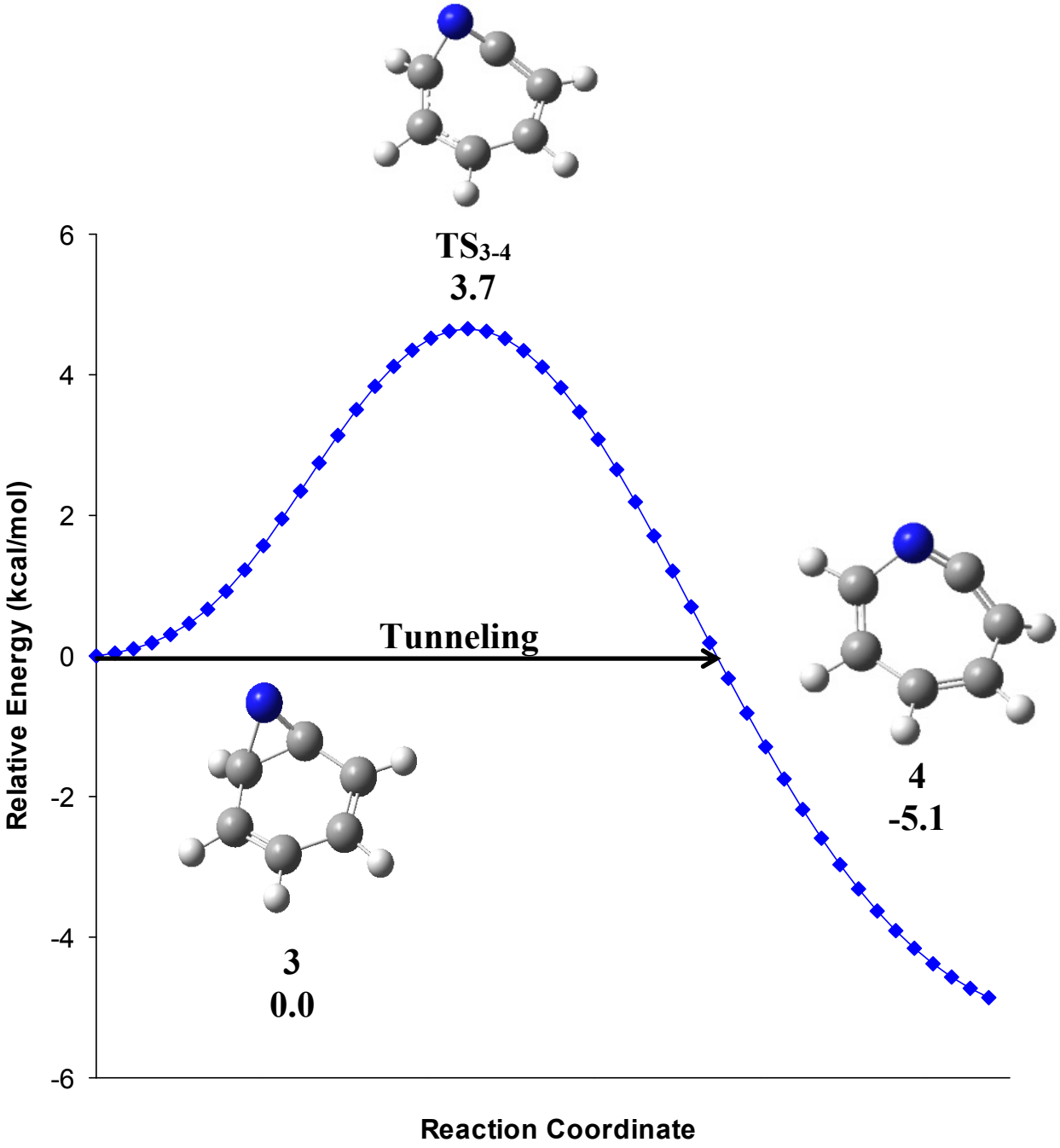

Table 3.1. Calculated rate constants for the ring expansion of benzazirine (**3**) to ketenimine (**4**) at selected temperatures. All rate constants at B3LYP/6-31G(d).

T (K)	CVT (s^{-1})	CVT / ZCT (s^{-1})	CVT / SCT (s^{-1})
10	9.37×10^{-71}	2.53×10^{4}	1.17×10^{5}
20	8.82×10^{-30}	2.53×10^{4}	1.17×10^{5}
50	5.61×10^{-5}	2.70×10^{4}	1.21×10^{5}
100	1.50×10^{4}	3.62×10^{5}	6.25×10^{5}
150	1.12×10^{7}	3.43×10^{7}	3.72×10^{7}
200	3.24×10^{8}	6.14×10^{8}	6.33×10^{8}
250	2.53×10^{9}	3.88×10^{9}	3.95×10^{9}
300	1.02×10^{10}	1.39×10^{10}	1.41×10^{10}

Several other examples of carbon tunneling in the literature also demonstrate calculated rate constants similar to that of benzazirine. Scheme 3.3 highlights several of these cases. Schreiner *et al.*[15] studied the ring expansion of cyclopropylcarbene **11** to cyclobutene **12.** CVT / SCT results found the reaction to proceed at even a higher rate than the ring expansion of benzazirine ($k = 1.17 \times 10^{5}$ s^{-1} to $k = 5.42 \times 10^{6}$ s^{-1}, respectively). The main factor cited for such fast carbon tunneling is a low barrier to reaction at 2.4 kcal/mol. Similarly, Zuev *et al.*[17] calculated rate constants for the ring expansion of the chlorocarbene **13** to the cyclopropene **14**. Again, a low barrier of 3.1 kcal/mol is cited to explain the large carbon tunneling. A narrow barrier of 0.44 Å for the longest distance moved by a heavy-atom during the tunneling event also explains the high rate of $k = 1.4 \times 10^{4}$ s^{-1} at 8 K. This large rate constant is consistent with their inability to detect **13** in matrix isolation experiments. Lastly, Kozuch[16] calculated rate constants for the automerization of several anti-aromatic species including pentalene (**15**). CVT / SCT calculations predict an incredibly high rate constant of $k = 2.2 \times 10^{8}$ s^{-1} at only 10 K. M06-2X/6-31G(d) optimized geometries of pentalene indicate the difference in length between single and double-bonds in pentalene to be only 0.128 Å. Kozuch concludes that this small atomic

movement is what facilitates the carbon tunneling. In relation to these examples, the low barrier and small width to the reaction of **3** to **4** is well within the range of these other calculated rate constants.

Scheme 3.3. Calculated CVT / SCT rate constants for carbon tunneling reactions (in s^{-1}).

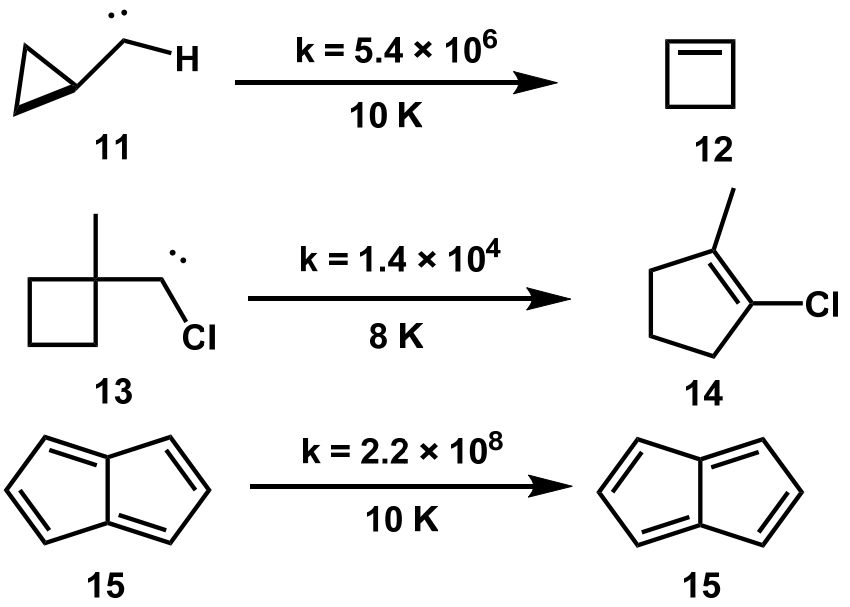

Tunneling reactions are often accompanied by large kinetic isotope effects (KIE) with substitution of heavier isotopes. While the KIE of heavy atoms are not as dramatic as the substitution of hydrogen with deuterium due to the smaller percent change in mass, noticeable KIE's are still observable at low temperatures. To measure this, rate constants with ^{13}C and ^{15}N substitutions for the three-membered ring atoms were calculated, with the results displayed in Table 3.2 and Figure 3.2. For both carbon atoms, at 10 K they display a very high KIE of 1.34 and 1.48, whereas ^{15}N substitution shows a small KIE of 1.09. The large difference in the calculated KIE can be explained by the distance each atom moves from the reactant to the other side of the reaction barrier. Carbons 1 and 2 move a total of 0.28 and 0.29 Å, respectively,

whereas the nitrogen atom moves only 0.16 Å. It has been demonstrated that for heavy-atom tunneling, the tunneling probability is strongly correlated with distance the heavy atom must move. As noted by Inui *et. al.* in their study of the methylthio substituted benzazirine[13], the largest distance any heavy atom moves in the reaction is 0.33 Å. They conclude that this small tunneling distance contributes to the tunneling observed in the matrix. Figure 3.2 demonstrates the dependence of KIE on temperature. As the temperature increases out of the tunneling dominant region, the KIE quickly falls to more standard KIE values of 1.07, 1.04, and 1.04 for C_1, C_2, and N, respectively.

Table 3.2. KIE of the ring expansion of benzazirine **3** to ketenimine **4**. KIE's based off CVT / SCT rate constants of B3LYP/6-31G(d) PES.

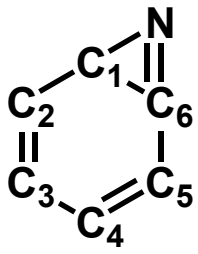

T (K)	$^{13}C_1$	$^{13}C_6$	^{15}N
10	1.34	1.48	1.09
20	1.34	1.48	1.09
50	1.34	1.47	1.09
100	1.20	1.30	1.04
150	1.08	1.13	1.02
200	1.05	1.10	1.03
250	1.04	1.08	1.03
300	1.04	1.07	1.04
Distance Moved (Å)	0.28	0.29	0.16

Arrhenius plots can also be used to demonstrate tunneling. For classic thermally activated organic reactions, plots of ln *k* vs. 1/T are linear, demonstrating temperature dependence on the rate. If a tunneling process contributes to the reaction, the curve will flatten out in the low temperature region of the plot where tunneling dominates, demonstrating independence from temperature on the rate.[31] The Arrhenius plot for the tunneling from **3** to **4** is

shown in Figure 3.3. The plot for the CVT data without any tunneling approximations shows temperature dependence for the full range of temperatures. Around 150 K, the CVT / SCT plot, taking tunneling into account, begins to deviate from the CVT line. Though tunneling is commonly associated with cryogenic temperatures, here tunneling is shown to have important contributions to the rate constant even at 100 K. As expected, the plot of CVT / ZCT is similar to that of CVT / SCT and underestimates the impact of tunneling on the rate constants.

Figure 3.2. KIE for select heavy atoms in the ring expansion of **3** to **4**. Rate constants found using CVT / SCT on the B3LYP/6-31G(d) surface.

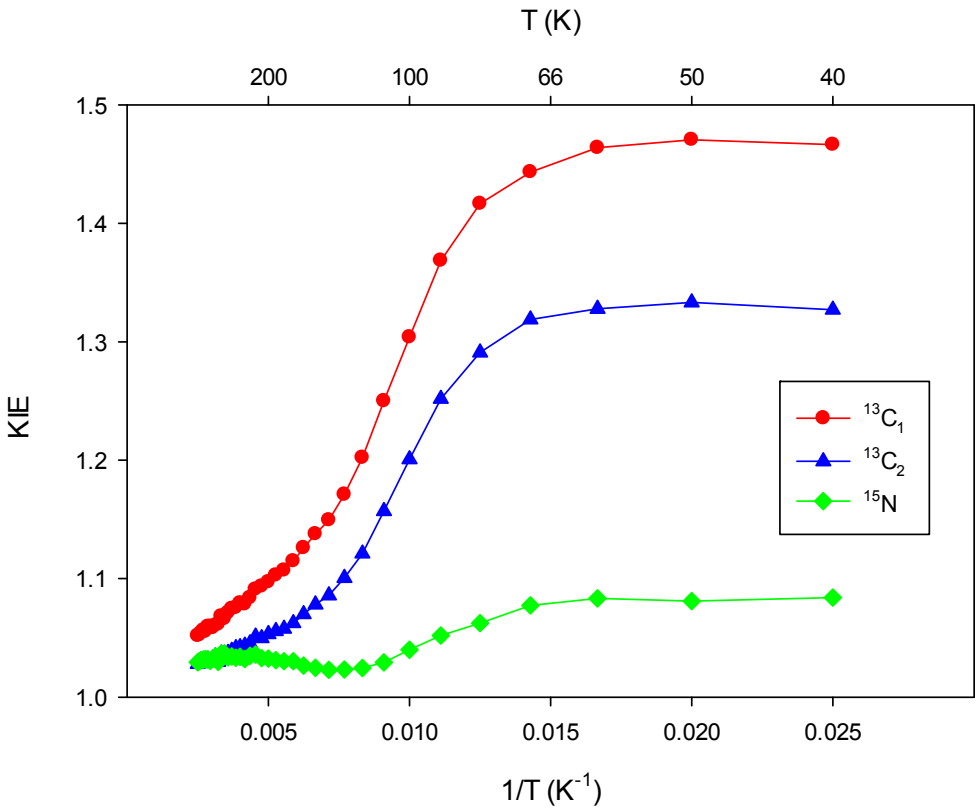

Figure 3.3. Arrhenius plot for the reaction of **3** to **4**. Rate constants found using CVT / SCT on the B3LYP/6-31G(d) surface.

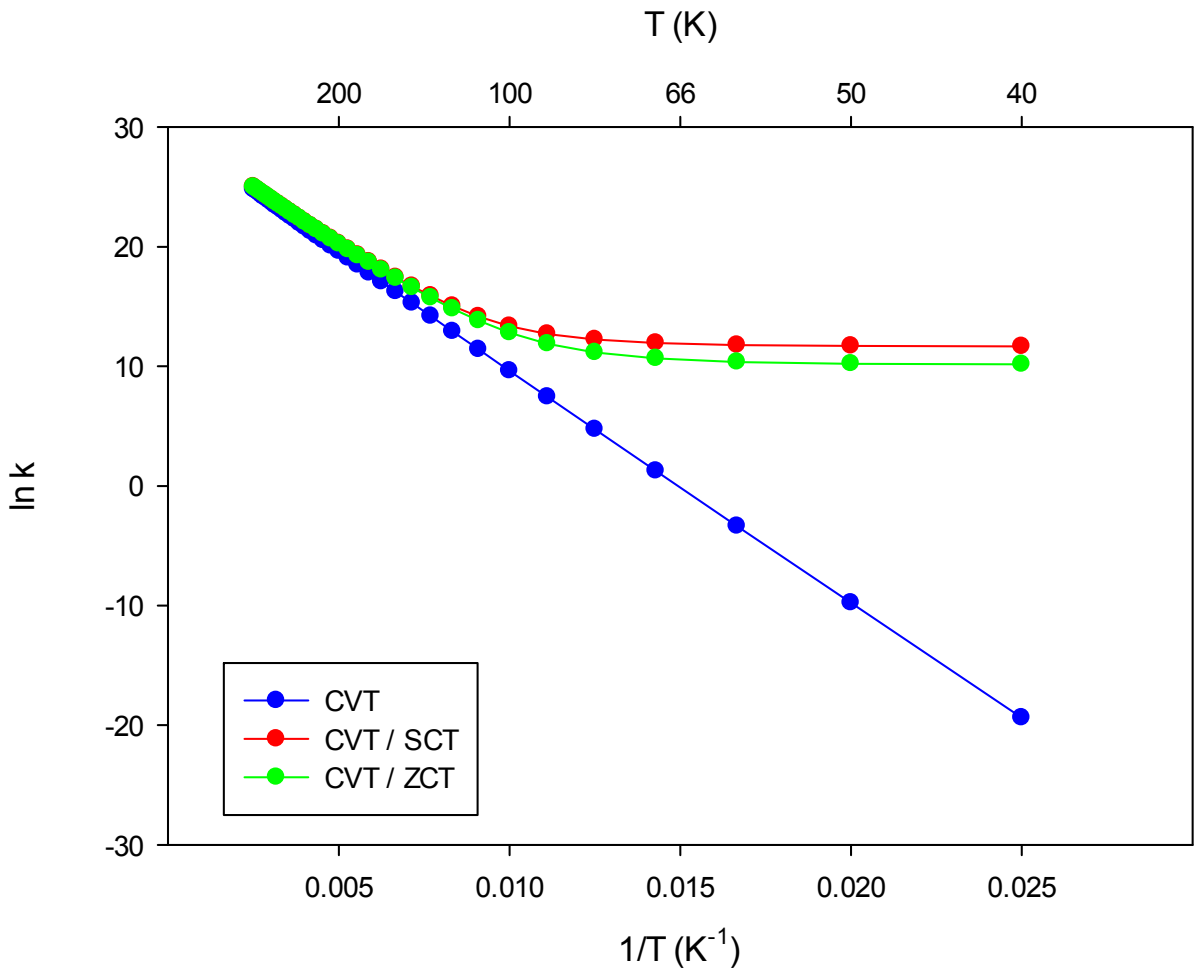

To evaluate the impact of an electron-withdrawing group (EWG) on the tunneling of benzazirine without introducing additional complications from large steric or conformational effects, tunneling calculations were performed on the ring expansion of fluorine substituted benzazirine **9** to ketenimine **10** (Figure 3.4). As a result of the fluorine substitution, the barrier to the reaction increases to 4.7 kcal/mol. The width of the barrier, measured by the largest distance moved by a heavy atom through the barrier, also increased to 0.31 Å when compared to the ring expansion of **3** to **4**. The net result of both of these factors is an overall decrease in the

tunneling rate (Table 3.3). The overall comparison of CVT, ZCT, and SCT rate constants also shows the same patterns as the parent benzazirine system.

Figure 3.4. Potential Energy Surface of the ring expansion of benzazirine **9** to ketenimine **10** at B3LYP/6-31G(d).

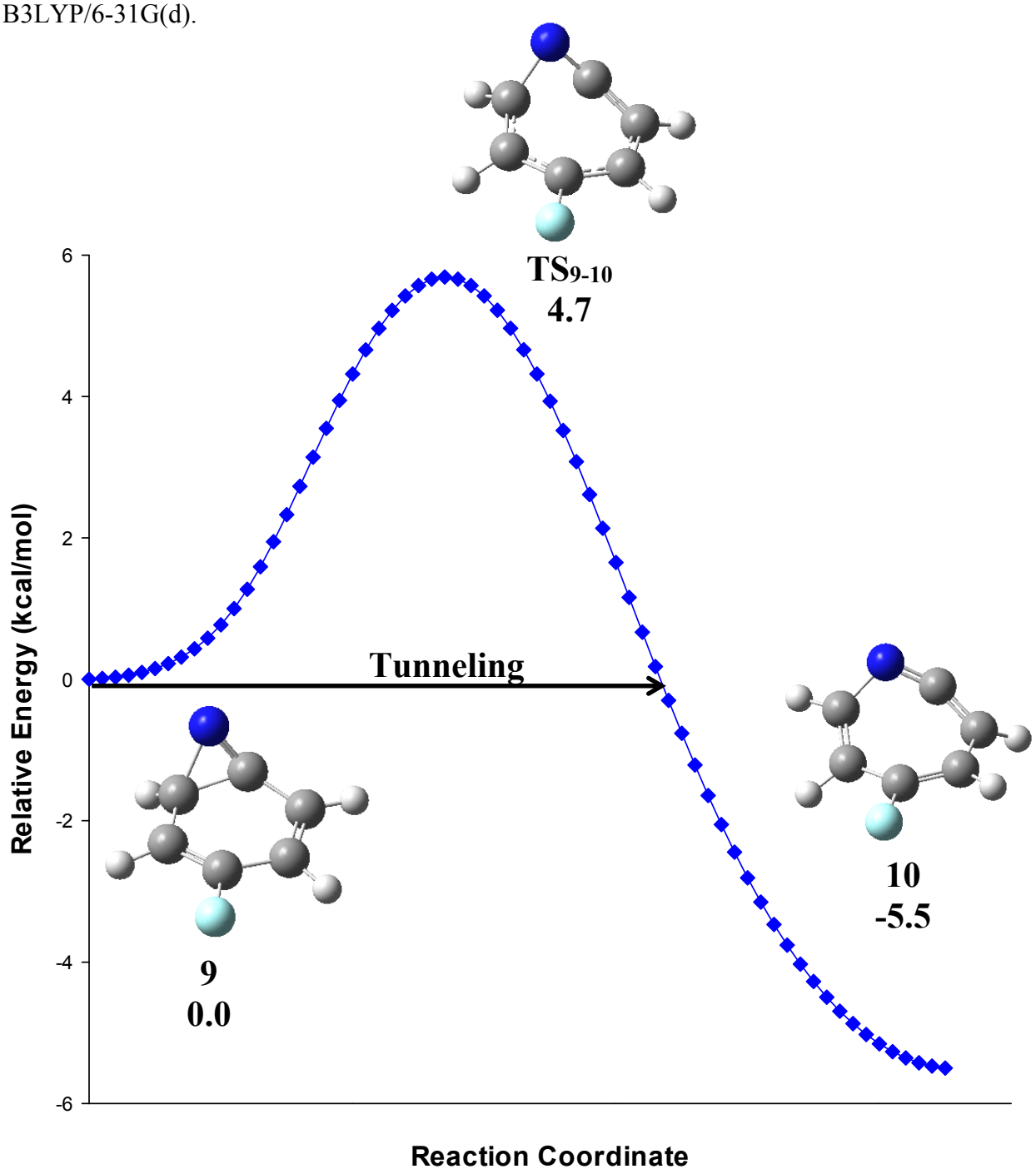

Table 3.3. Calculated rate constants for the ring expansion of benzazirine (**9**) to ketenimine (**10**) at selected temperatures. All rate constants at B3LYP/6-31G(d).

T (K)	CVT (s^{-1})	CVT / ZCT (s^{-1})	CVT / SCT (s^{-1})
10	7.48×10^{-92}	2.96×10^{2}	2.15×10^{3}
20	2.50×10^{-40}	2.96×10^{2}	2.15×10^{3}
50	3.38×10^{-9}	3.42×10^{2}	2.33×10^{3}
100	1.15×10^{2}	6.13×10^{3}	1.35×10^{4}
150	4.30×10^{5}	1.56×10^{6}	1.73×10^{6}
200	2.80×10^{7}	5.93×10^{7}	6.15×10^{7}
250	3.55×10^{8}	6.02×10^{8}	6.14×10^{8}
300	1.97×10^{9}	2.96×10^{9}	2.99×10^{9}

Comparing the parent benzazirine to the methylthio substituted benzazirine, one would expect similar tunneling rates based off of the height and width of the barrier (Figure 3.5). The barrier heights are within 0.3 kcal/mol of each other, and though the largest tunneling distance for a heavy atom is larger (0.33 Å from **5** to **6)**, it is still relatively small. However, the calculated rate for the ring expansion of **3** to **4** is many orders of magnitude faster than the experimentally observed rate constant for **5** to **6** (Scheme 3.2). This discrepancy can be explained by the required torsional motion of the thiomethyl substituent. The reaction coordinate for the ring expansion of **3** to **4** is mainly associated with one motion: the C-N-C bending mode. For the ring expansion of **5** to **6**, the reaction coordinate involves this motion in addition to a significant rotation of the methylthio arm. According to B3LYP/6-31G(d) calculations of the PES, the dihedral angle of the methylthio group changes from 3.5° in the lowest energy conformation of the reactant to 80.5° in the transition state.[13] As noted by Borden *et al.* in their study of tunneling in noradamantyl carbenes, slow rotation of a ethyl substituent was found to greatly lower the calculated rate constant ($k = 3.0 \times 10^{-7}$ s^{-1}).[19] We believe this additional complexity is responsible for the slower observed tunneling rate of the ring expansion of **5** to **6**.

However, our calculated rate constants for **5** to **6** are much larger than experiment (Table 3.4). The additional portion of the reaction coordinate related to the torsion of the thiomethyl arm is very flat and possibly not modeled correctly at this level of theory. Similarly, the calculated rate for the ring expansion of **7** to **8** is also found to tunnel, albeit slowly, when it was observed to not react at low temperatures in experiment. The larger calculated height (6.9 kcal/mol) and width (0.43 Å) of the barrier for the ring expansion explains the lower calculated rate constants compared to the ring expansion of **5** to **6**. Both systems predict much faster tunneling through theory than experiment, though the relative rates between them are appropriate.

Table 3.4. Calculated rate constants for the ring expansion of substituted benzazirines. All rate constants at B3LYP/6-31G(d).

5 → 6			
T (K)	CVT (s^{-1})	CVT / ZCT (s^{-1})	CVT / SCT (s^{-1})
10	2.61×10^{-56}	2.18×10^{3}	1.97×10^{4}
20	1.29×10^{-22}	9.17×10^{3}	4.95×10^{4}
50	2.95×10^{-2}	8.79×10^{4}	3.00×10^{5}
100	2.48×10^{5}	3.39×10^{6}	5.25×10^{6}
150	5.82×10^{7}	1.43×10^{8}	1.59×10^{8}
200	9.50×10^{8}	1.50×10^{9}	1.57×10^{9}
250	5.26×10^{9}	6.93×10^{9}	7.11×10^{9}
300	1.68×10^{10}	2.02×10^{10}	2.06×10^{10}
7 → 8			
T (K)	CVT (s^{-1})	CVT / ZCT (s^{-1})	CVT / SCT (s^{-1})
10	8.73×10^{-140}	2.04×10^{-4}	1.28×10^{-2}
20	2.71×10^{-64}	2.08×10^{-4}	1.29×10^{-2}
50	9.30×10^{-19}	5.69×10^{-4}	2.11×10^{-2}
100	2.15×10^{-3}	1.97×10^{-1}	6.13×10^{-1}
150	3.35×10^{2}	1.11×10^{3}	1.30×10^{3}
200	1.42×10^{5}	2.51×10^{5}	2.67×10^{5}
250	5.58×10^{6}	7.73×10^{6}	8.00×10^{6}
300	6.61×10^{7}	8.11×10^{7}	8.29×10^{7}

Figure 3.5. Potential Energy Surface of the ring expansion of substituted benzazirines at B3LYP/6-31G(d).

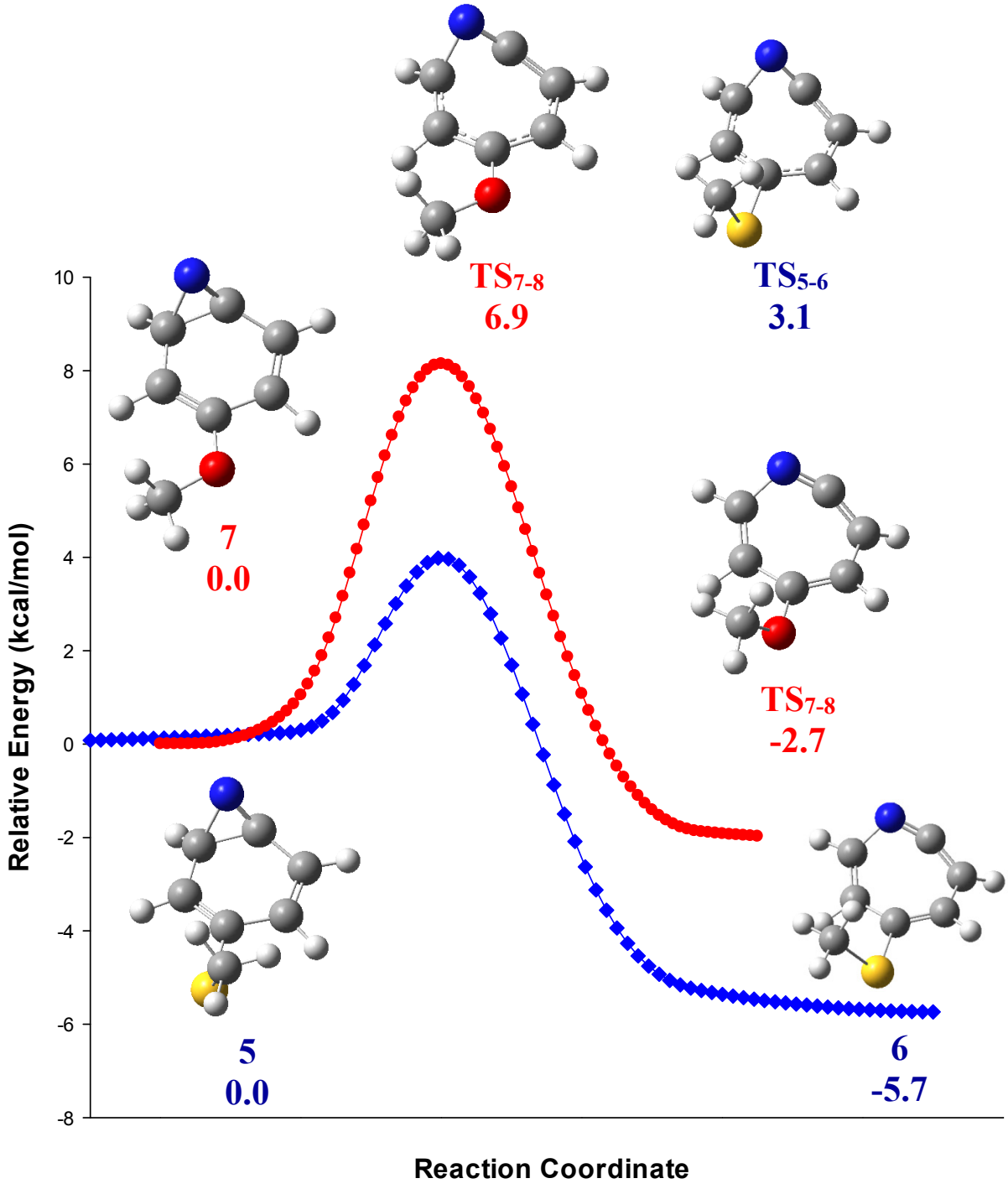

Summary

Rate constants for the ring expansion of benzazirine **3** to ketenimine **4**, including contributions from tunneling, have been completed. CVT / SCT rate constants on the B3LYP/6-31G(d) potential energy surface using Gaussrate and Polyrate software show large contributions from carbon tunneling. Due to a low and narrow reaction barrier, even at very low temperatures (10 K), the rate for heavy-atom tunneling was found to be significant ($k = 1.16\times 10^5\ s^{-1}$). Further evidence for tunneling is supported by comparison to other carbon tunneling systems, KIE's, and non-linear Arrhenius plots. Substitution of fluorine raises and widens the barrier of the reaction, leading to lower rate constants compared to the parent benzazirine system. Tunneling calculations of methoxy and methylthio substituted benzazirines **7** and **9** show poor agreement with experimental results, most likely from complications involving the additional torsion of the substituents on the reaction coordinate.

References

1. Gritsan, N. P.; Platz, M. S. Kinetics, Spectroscopy, and Computational Chemistry of Arylnitrenes. *Chem. Rev.* **2006**, *106*, 3844-3867.

2. Borden, W. T.; Gritsan, N. P.; Hadad, C. M.; Karney, W. L.; Kemnitz, C. R.; Platz, M. S. The Interplay of Theory and Experiment in the Study of Phenylnitrene. *Acc. Chem. Res.* **2000**, *33*, 765-771.

3. Tsao, M.-L.; Platz, M. S. Photochemistry of Ortho, Ortho‘ Dialkyl Phenyl Azides. *J. Am. Chem. Soc.* **2003**, *125*, 12014-12025.

4. Maltsev, A.; Bally, T.; Tsao, M.-L.; Platz, M. S.; Kuhn, A.; Vosswinkel, M.; Wentrup, C. The Rearrangements of Naphthylnitrenes: UV/Vis and IR Spectra of Azirines, Cyclic Ketenimines, and Cyclic Nitrile Ylides. *J. Am. Chem. Soc.* **2004**, *126*, 237-249.

5. Grote, D.; Sander, W. Photochemistry of Fluorinated 4-Iodophenylnitrenes: Matrix Isolation and Spectroscopic Characterization of Phenylnitrene-4-yls. *J. Org. Chem.* **2009**, *74*, 7370-7382.

6. Pritchina, E. A.; Gritsan, N. P.; Bally, T. Matrix isolation and computational study of the photochemistry of p-azidoaniline. *PCCP* **2006**, *8*, 719-727.

7. Morawietz, J.; Sander, W. Photochemistry of Fluorinated Phenyl Nitrenes: Matrix Isolation of Fluorinated Azirines. *J. Org. Chem.* **1996**, *61*, 4351-4354.

8. Chapman, O. L.; Le Roux, J. P. 1-Aza-1,2,4,6-cycloheptatetraene. *J. Am. Chem. Soc.* **1978**, *100*, 282-285.

9. Hayes, J. C.; Sheridan, R. S. The IR spectrum of triplet phenylnitrene. On the origin of didehydroazepine in low temperature matrices. *J. Am. Chem. Soc.* **1990**, *112*, 5879-5881.

10. Karney, W. L.; Borden, W. T. Ab Initio Study of the Ring Expansion of Phenylnitrene and Comparison with the Ring Expansion of Phenylcarbene. *J. Am. Chem. Soc.* **1997**, *119*, 1378-1387.

11. Carroll, S. E.; Nay, B.; Scriven, E. F. V.; Suschitzky, H.; Thomas, D. R. Decomposition of aromatic azides in ethanethiol. *Tetrahedron Lett.* **1977**, *18*, 3175-3178.

12. Carroll, S. E.; Nay, B.; Scriven, E. F. V.; Suschitzky, H. Decomposition of arylazides in piperidine: the effect of tetramethylethylenediamine on the nature of the products. *Tetrahedron Lett.* **1977**, *18*, 943-946.

13. Inui, H.; Sawada, K.; Oishi, S.; Ushida, K.; McMahon, R. J. Aryl Nitrene Rearrangements: Spectroscopic Observation of a Benzazirine and Its Ring Expansion to a Ketenimine by Heavy-Atom Tunneling. *J. Am. Chem. Soc.* **2013**, *135*, 10246-10249.

14. Bell, R. The application of quantum mechanics to chemical kinetics. *Proc. R. Soc. Lond. A Math. Phys. Sci.* **1933**, *139*, 466-474.

15. Gerbig, D.; Ley, D.; Schreiner, P. R. Light- and Heavy-Atom Tunneling in Rearrangement Reactions of Cyclopropylcarbenes. *Org. Lett.* **2011**, *13*, 3526-3529.

16. Kozuch, S. Heavy atom tunneling in the automerization of pentalene and other antiaromatic systems. *RSC Advances* **2014**, *4*, 21650-21656.

17. Zuev, P. S.; Sheridan, R. S.; Albu, T. V.; Truhlar, D. G.; Hrovat, D. A.; Borden, W. T. Carbon Tunneling from a Single Quantum State. *Science* **2003**, *299*, 867-870.

18. Kozuch, S. A Quantum Mechanical "Jack in the Box": Rapid Rearrangement of a Tetrahedryl-Tetrahedrane via Heavy Atom Tunneling. *Org. Lett.* **2014**, *16*, 4102-4105.

19. Kozuch, S.; Zhang, X.; Hrovat, D. A.; Borden, W. T. Calculations on Tunneling in the Reactions of Noradamantyl Carbenes. *J. Am. Chem. Soc.* **2013**, *135*, 17274-17277.

20. Datta, A.; Hrovat, D. A.; Borden, W. T. Calculations Predict Rapid Tunneling by Carbon from the Vibrational Ground State in the Ring Opening of Cyclopropylcarbinyl Radical at Cryogenic Temperatures. *J. Am. Chem. Soc.* **2008**, *130*, 6684-6685.

21. Frisch, M. J.; Trucks, G. W.; Schlegel, H. B.; Scuseria, G. E.; Robb, M. A.; Cheeseman, J. R.; Scalmani, G.; Barone, V.; Mennucci, B.; Petersson, G. A.; Nakatsuji, H.; Caricato, M.; Li, X.; Hratchian, H. P.; Izmaylov, A. F.; Bloino, J.; Zheng, G.; Sonnenberg, J. L.; Hada, M.; Ehara, M.; Toyota, K.; Fukuda, R.; Hasegawa, J.; Ishida, M.; Nakajima, T.; Honda, Y.; Kitao, O.; Nakai, H.; Vreven, T.; Montgomery Jr., J. A.; Peralta, J. E.; Ogliaro, F.; Bearpark, M. J.; Heyd, J.; Brothers, E. N.; Kudin, K. N.; Staroverov, V. N.; Kobayashi, R.; Normand, J.; Raghavachari, K.; Rendell, A. P.; Burant, J. C.; Iyengar, S. S.; Tomasi, J.; Cossi, M.; Rega, N.; Millam, N. J.; Klene, M.; Knox, J. E.; Cross, J. B.; Bakken, V.; Adamo, C.; Jaramillo, J.; Gomperts, R.; Stratmann, R. E.; Yazyev, O.; Austin, A. J.; Cammi, R.; Pomelli, C.; Ochterski, J. W.; Martin, R. L.; Morokuma, K.; Zakrzewski, V. G.; Voth, G. A.; Salvador, P.; Dannenberg, J. J.; Dapprich, S.; Daniels, A. D.; Farkas, Ö.; Foresman, J. B.; Ortiz, J. V.; Cioslowski, J.; Fox, D. J.; *Gaussian 09; Revision B.1*, 2009.

22. Becke, A. D. Density-functional thermochemistry. III. The role of exact exchange. *J. Chem. Phys.* **1993**, *98*, 5648-5652.

23. Hariharan, P. C.; Pople, J. A. Influence of polarization functions on MO hydrogenation energies. *Theor. Chim. Acta* **1973**, *28*, 213-222.

24. Karney, W. L.; Borden, W. T. Why Does o-Fluorine Substitution Raise the Barrier to Ring Expansion of Phenylnitrene? *J. Am. Chem. Soc.* **1997**, *119*, 3347-3350.

25. Fernandez-Ramos, A.; Ellingson, B. A.; Garrett, B. C.; Truhlar, D. G. In *Rev. Comput. Chem.*; John Wiley & Sons, Inc.: 2007, p 125-232.

26. Corchado, J. C. *POLYRATE 2010-A* University of Minnesota, Minneapolis, MN, 2010.

27. Corchado, J. C. *GAUSSRATE 2009-A* University of Minnesota, Minneapolis, MN, 2010.

28. Kuppermann, A.; Truhlar, D. G. Exact tunneling calculations. *J. Am. Chem. Soc.* **1971**, *93*, 1840-1851.

29. Borden, W. T. Reactions that involve tunneling by carbon and the role that calculations have played in their study. *Wiley Interdisciplinary Reviews: Computational Molecular Science* **2016**, *6*, 20-46.

30. Lauderdale, J. G.; Truhlar, D. G. Diffusion of hydrogen, deuterium, and tritium on the (100) plane of copper: Reaction-path formulation, variational transition state theory, and tunneling calculations. *Surf. Sci.* **1985**, *164*, 558-588.

31. Caldin, E. F. Tunneling in proton-transfer reactions in solution. *Chem. Rev.* **1969**, *69*, 135-156.

Supporting Information

Quantum Mechanical Tunneling in Benzazirine

Table 3.S1. Full rate data for the tunneling of **3** to **4. (**B3LYP/6-31G(d))

T(K)	TST (s^{-1})	CVT (s^{-1})	CVT / ZCT (s^{-1})	CVT / SCT (s^{-1})
10	1.35E-70	9.31E-71	2.53E+04	1.17E+05
20	1.06E-29	8.82E-30	2.53E+04	1.17E+05
30	5.43E-16	4.79E-16	2.54E+04	1.17E+05
40	4.22E-09	3.84E-09	2.56E+04	1.17E+05
50	6.04E-05	5.61E-05	2.70E+04	1.21E+05
60	3.68E-02	3.46E-02	3.13E+04	1.30E+05
70	3.67E+00	3.48E+00	4.21E+04	1.54E+05
80	1.18E+02	1.12E+02	6.94E+04	2.05E+05
90	1.77E+03	1.70E+03	1.44E+05	3.24E+05
100	1.56E+04	1.50E+04	3.62E+05	6.25E+05
110	9.33E+04	9.01E+04	9.87E+05	1.40E+06
120	4.16E+05	4.03E+05	2.67E+06	3.34E+06
130	1.48E+06	1.44E+06	6.77E+06	7.89E+06
140	4.43E+06	4.31E+06	1.59E+07	1.77E+07
150	1.15E+07	1.12E+07	3.43E+07	3.72E+07
160	2.64E+07	2.58E+07	6.88E+07	7.33E+07
170	5.54E+07	5.41E+07	1.29E+08	1.36E+08
180	1.07E+08	1.05E+08	2.28E+08	2.38E+08
190	1.94E+08	1.90E+08	3.83E+08	3.97E+08
200	3.31E+08	3.24E+08	6.14E+08	6.33E+08
210	5.39E+08	5.27E+08	9.45E+08	9.70E+08
220	8.39E+08	8.22E+08	1.41E+09	1.44E+09
230	1.26E+09	1.23E+09	2.03E+09	2.07E+09
240	1.83E+09	1.79E+09	2.84E+09	2.89E+09
250	2.58E+09	2.53E+09	3.88E+09	3.95E+09
260	3.55E+09	3.48E+09	5.20E+09	5.27E+09
270	4.78E+09	4.69E+09	6.81E+09	6.91E+09
280	6.30E+09	6.18E+09	8.78E+09	8.89E+09
290	8.16E+09	8.00E+09	1.11E+10	1.13E+10
300	1.04E+10	1.02E+10	1.39E+10	1.41E+10
310	1.30E+10	1.28E+10	1.71E+10	1.73E+10
320	1.61E+10	1.58E+10	2.09E+10	2.11E+10
330	1.97E+10	1.93E+10	2.52E+10	2.54E+10
340	2.38E+10	2.33E+10	3.00E+10	3.02E+10
350	2.85E+10	2.79E+10	3.55E+10	3.57E+10
360	3.37E+10	3.30E+10	4.15E+10	4.18E+10
370	3.96E+10	3.88E+10	4.83E+10	4.86E+10
380	4.61E+10	4.52E+10	5.57E+10	5.60E+10
390	5.33E+10	5.22E+10	6.38E+10	6.42E+10
400	6.12E+10	6.00E+10	7.27E+10	7.30E+10

Table 3.S2. Full rate data for the tunneling of **3** to **4** with $C_1=^{13}C$**. (**B3LYP/6-31G(d))

T(K)	TST (s^{-1})	CVT (s^{-1})	CVT / ZCT (s^{-1})	CVT / SCT (s^{-1})
10	4.28E-71	2.92E-71	1.76E+04	7.93E+04
20	5.99E-30	4.94E-30	1.76E+04	7.93E+04
30	3.70E-16	3.26E-16	1.76E+04	7.93E+04
40	3.17E-09	2.88E-09	1.78E+04	7.98E+04
50	4.81E-05	4.45E-05	1.88E+04	8.22E+04
60	3.04E-02	2.85E-02	2.19E+04	8.94E+04
70	3.12E+00	2.95E+00	3.00E+04	1.07E+05
80	1.02E+02	9.73E+01	5.08E+04	1.45E+05
90	1.56E+03	1.49E+03	1.10E+05	2.38E+05
100	1.39E+04	1.34E+04	2.88E+05	4.79E+05
110	8.41E+04	8.12E+04	8.16E+05	1.12E+06
120	3.79E+05	3.67E+05	2.26E+06	2.78E+06
130	1.36E+06	1.32E+06	5.85E+06	6.73E+06
140	4.09E+06	3.97E+06	1.39E+07	1.54E+07
150	1.06E+07	1.04E+07	3.04E+07	3.28E+07
160	2.47E+07	2.40E+07	6.14E+07	6.52E+07
170	5.19E+07	5.06E+07	1.16E+08	1.22E+08
180	1.01E+08	9.84E+07	2.06E+08	2.15E+08
190	1.83E+08	1.79E+08	3.48E+08	3.60E+08
200	3.14E+08	3.06E+08	5.60E+08	5.76E+08
210	5.11E+08	5.00E+08	8.66E+08	8.88E+08
220	7.98E+08	7.81E+08	1.29E+09	1.32E+09
230	1.20E+09	1.18E+09	1.87E+09	1.90E+09
240	1.75E+09	1.71E+09	2.63E+09	2.67E+09
250	2.47E+09	2.42E+09	3.60E+09	3.66E+09
260	3.41E+09	3.34E+09	4.83E+09	4.90E+09
270	4.59E+09	4.50E+09	6.35E+09	6.43E+09
280	6.06E+09	5.94E+09	8.20E+09	8.30E+09
290	7.86E+09	7.70E+09	1.04E+10	1.05E+10
300	1.00E+10	9.81E+09	1.30E+10	1.32E+10
310	1.26E+10	1.23E+10	1.61E+10	1.63E+10
320	1.56E+10	1.53E+10	1.97E+10	1.98E+10
330	1.91E+10	1.87E+10	2.37E+10	2.39E+10
340	2.30E+10	2.26E+10	2.83E+10	2.85E+10
350	2.76E+10	2.70E+10	3.35E+10	3.38E+10
360	3.27E+10	3.20E+10	3.93E+10	3.96E+10
370	3.84E+10	3.76E+10	4.58E+10	4.60E+10
380	4.48E+10	4.39E+10	5.29E+10	5.32E+10
390	5.19E+10	5.08E+10	6.06E+10	6.10E+10
400	5.96E+10	5.83E+10	6.91E+10	6.95E+10

Table 3.S3. Full rate data for the tunneling of **3** to **4** with C_6=^{13}C**. (**B3LYP/6-31G(d))

T(K)	TST (s^{-1})	CVT (s^{-1})	CVT / ZCT (s^{-1})	CVT / SCT (s^{-1})
10	7.84E-71	5.40E-71	1.89E+04	8.73E+04
20	8.11E-30	6.73E-30	1.89E+04	8.73E+04
30	4.53E-16	4.00E-16	1.89E+04	8.73E+04
40	3.69E-09	3.36E-09	1.91E+04	8.78E+04
50	5.43E-05	5.03E-05	2.02E+04	9.05E+04
60	3.37E-02	3.16E-02	2.36E+04	9.84E+04
70	3.40E+00	3.22E+00	3.23E+04	1.17E+05
80	1.10E+02	1.05E+02	5.49E+04	1.59E+05
90	1.67E+03	1.60E+03	1.18E+05	2.59E+05
100	1.48E+04	1.42E+04	3.10E+05	5.20E+05
110	8.89E+04	8.58E+04	8.72E+05	1.21E+06
120	3.98E+05	3.86E+05	2.41E+06	2.97E+06
130	1.42E+06	1.38E+06	6.21E+06	7.16E+06
140	4.27E+06	4.15E+06	1.47E+07	1.63E+07
150	1.11E+07	1.08E+07	3.20E+07	3.46E+07
160	2.56E+07	2.49E+07	6.46E+07	6.86E+07
170	5.37E+07	5.24E+07	1.22E+08	1.28E+08
180	1.04E+08	1.02E+08	2.16E+08	2.25E+08
190	1.89E+08	1.84E+08	3.63E+08	3.76E+08
200	3.23E+08	3.16E+08	5.84E+08	6.01E+08
210	5.25E+08	5.14E+08	9.02E+08	9.24E+08
220	8.19E+08	8.02E+08	1.34E+09	1.37E+09
230	1.23E+09	1.21E+09	1.94E+09	1.98E+09
240	1.79E+09	1.75E+09	2.72E+09	2.77E+09
250	2.53E+09	2.48E+09	3.73E+09	3.79E+09
260	3.48E+09	3.41E+09	5.00E+09	5.07E+09
270	4.68E+09	4.59E+09	6.56E+09	6.65E+09
280	6.18E+09	6.06E+09	8.47E+09	8.56E+09
290	8.00E+09	7.84E+09	1.07E+10	1.09E+10
300	1.02E+10	9.99E+09	1.34E+10	1.36E+10
310	1.28E+10	1.25E+10	1.66E+10	1.67E+10
320	1.58E+10	1.55E+10	2.02E+10	2.04E+10
330	1.93E+10	1.90E+10	2.44E+10	2.46E+10
340	2.34E+10	2.29E+10	2.91E+10	2.93E+10
350	2.80E+10	2.74E+10	3.44E+10	3.46E+10
360	3.32E+10	3.25E+10	4.03E+10	4.06E+10
370	3.89E+10	3.82E+10	4.69E+10	4.72E+10
380	4.54E+10	4.45E+10	5.41E+10	5.44E+10
390	5.25E+10	5.14E+10	6.20E+10	6.24E+10
400	6.03E+10	5.91E+10	7.07E+10	7.10E+10

Table 3.S4. Full rate data for the tunneling of **3** to **4** with ^{15}N**. (**B3LYP/6-31G(d))

T(K)	TST (s^{-1})	CVT (s^{-1})	CVT / ZCT (s^{-1})	CVT / SCT (s^{-1})
10	1.78E-70	1.21E-70	2.35E+04	1.07E+05
20	1.22E-29	1.01E-29	2.35E+04	1.07E+05
30	5.94E-16	5.23E-16	2.36E+04	1.07E+05
40	4.51E-09	4.10E-09	2.38E+04	1.08E+05
50	6.38E-05	5.90E-05	2.52E+04	1.11E+05
60	3.85E-02	3.61E-02	2.94E+04	1.21E+05
70	3.81E+00	3.61E+00	3.98E+04	1.43E+05
80	1.22E+02	1.16E+02	6.62E+04	1.93E+05
90	1.82E+03	1.74E+03	1.39E+05	3.09E+05
100	1.60E+04	1.54E+04	3.52E+05	6.01E+05
110	9.54E+04	9.21E+04	9.66E+05	1.36E+06
120	4.25E+05	4.11E+05	2.61E+06	3.26E+06
130	1.51E+06	1.47E+06	6.63E+06	7.71E+06
140	4.50E+06	4.38E+06	1.55E+07	1.73E+07
150	1.16E+07	1.13E+07	3.35E+07	3.63E+07
160	2.68E+07	2.61E+07	6.70E+07	7.14E+07
170	5.61E+07	5.48E+07	1.25E+08	1.32E+08
180	1.09E+08	1.06E+08	2.21E+08	2.31E+08
190	1.96E+08	1.92E+08	3.71E+08	3.85E+08
200	3.35E+08	3.27E+08	5.94E+08	6.13E+08
210	5.44E+08	5.32E+08	9.15E+08	9.40E+08
220	8.46E+08	8.29E+08	1.36E+09	1.39E+09
230	1.27E+09	1.24E+09	1.96E+09	2.00E+09
240	1.84E+09	1.81E+09	2.74E+09	2.80E+09
250	2.60E+09	2.55E+09	3.75E+09	3.82E+09
260	3.58E+09	3.51E+09	5.02E+09	5.10E+09
270	4.81E+09	4.71E+09	6.59E+09	6.68E+09
280	6.34E+09	6.21E+09	8.49E+09	8.60E+09
290	8.20E+09	8.03E+09	1.08E+10	1.09E+10
300	1.04E+10	1.02E+10	1.35E+10	1.36E+10
310	1.31E+10	1.28E+10	1.66E+10	1.68E+10
320	1.62E+10	1.59E+10	2.02E+10	2.04E+10
330	1.98E+10	1.94E+10	2.44E+10	2.46E+10
340	2.39E+10	2.34E+10	2.91E+10	2.93E+10
350	2.85E+10	2.80E+10	3.43E+10	3.46E+10
360	3.38E+10	3.31E+10	4.03E+10	4.05E+10
370	3.97E+10	3.89E+10	4.68E+10	4.71E+10
380	4.62E+10	4.53E+10	5.40E+10	5.43E+10
390	5.34E+10	5.23E+10	6.19E+10	6.23E+10
400	6.14E+10	6.01E+10	7.05E+10	7.09E+10

Table 3.S5. Full rate data for the tunneling of **5** to **6. (**B3LYP/6-31G(d))

T(K)	TST (s^{-1})	CVT (s^{-1})	CVT/ZCT (s^{-1})	CVT/SCT (s^{-1})
10	3.72E-56	2.61E-56	2.18E+03	1.97E+04
20	1.54E-22	1.29E-22	9.17E+03	4.95E+04
50	3.16E-02	2.95E-02	8.79E+04	3.00E+05
60	6.10E+00	5.75E+00	1.61E+05	4.85E+05
70	2.67E+02	2.54E+02	3.06E+05	7.98E+05
80	4.61E+03	4.42E+03	6.33E+05	1.39E+06
90	4.28E+04	4.12E+04	1.43E+06	2.60E+06
100	2.57E+05	2.48E+05	3.39E+06	5.25E+06
110	1.12E+06	1.09E+06	8.02E+06	1.10E+07
120	3.85E+06	3.74E+06	1.81E+07	2.28E+07
130	1.10E+07	1.07E+07	3.85E+07	4.58E+07
140	2.71E+07	2.65E+07	7.65E+07	8.74E+07
150	5.95E+07	5.82E+07	1.43E+08	1.59E+08
160	1.19E+08	1.16E+08	2.50E+08	2.73E+08
170	2.19E+08	2.15E+08	4.18E+08	4.49E+08
180	3.79E+08	3.72E+08	6.65E+08	7.07E+08
190	6.19E+08	6.08E+08	1.02E+09	1.07E+09
200	9.66E+08	9.50E+08	1.50E+09	1.57E+09
210	1.45E+09	1.42E+09	2.14E+09	2.23E+09
220	2.09E+09	2.06E+09	2.97E+09	3.08E+09
230	2.93E+09	2.89E+09	4.03E+09	4.16E+09
240	4.00E+09	3.94E+09	5.33E+09	5.49E+09
250	5.34E+09	5.26E+09	6.93E+09	7.11E+09
260	6.97E+09	6.87E+09	8.84E+09	9.05E+09
270	8.93E+09	8.80E+09	1.11E+10	1.13E+10
280	1.12E+10	1.11E+10	1.37E+10	1.40E+10
290	1.40E+10	1.38E+10	1.68E+10	1.71E+10
300	1.71E+10	1.69E+10	2.02E+10	2.06E+10
310	2.07E+10	2.04E+10	2.42E+10	2.46E+10
320	2.47E+10	2.44E+10	2.86E+10	2.90E+10
330	2.93E+10	2.89E+10	3.35E+10	3.39E+10
340	3.43E+10	3.39E+10	3.89E+10	3.94E+10
350	3.99E+10	3.93E+10	4.48E+10	4.53E+10
360	4.61E+10	4.54E+10	5.12E+10	5.18E+10
370	5.28E+10	5.20E+10	5.83E+10	5.89E+10
380	6.01E+10	5.92E+10	6.59E+10	6.66E+10
390	6.80E+10	6.70E+10	7.40E+10	7.48E+10
400	7.64E+10	7.53E+10	8.28E+10	8.36E+10

Table 3.S6. Full rate data for the tunneling of **7** to **9. (**B3LYP/6-31G(d))

T(K)	TST (s^{-1})	CVT (s^{-1})	CVT/ZCT (s^{-1})	CVT/SCT (s^{-1})
10	1.42-139	8.73-140	2.04E-04	1.28E-02
20	3.46E-64	2.71E-64	2.08E-04	1.29E-02
30	5.62E-39	4.77E-39	2.39E-04	1.38E-02
40	2.50E-26	2.21E-26	3.35E-04	1.63E-02
50	1.03E-18	9.30E-19	5.69E-04	2.11E-02
60	1.27E-13	1.17E-13	1.16E-03	2.98E-02
70	5.66E-10	5.26E-10	2.85E-03	4.72E-02
80	3.14E-07	2.95E-07	8.81E-03	8.66E-02
90	4.34E-05	4.10E-05	3.60E-02	1.98E-01
100	2.26E-03	2.15E-03	1.97E-01	6.13E-01
110	5.80E-02	5.52E-02	1.30E+00	2.61E+00
120	8.73E-01	8.33E-01	8.62E+00	1.33E+01
130	8.70E+00	8.32E+00	5.10E+01	6.78E+01
140	6.27E+01	6.01E+01	2.58E+02	3.16E+02
150	3.49E+02	3.35E+02	1.11E+03	1.30E+03
160	1.57E+03	1.51E+03	4.14E+03	4.67E+03
170	5.96E+03	5.72E+03	1.35E+04	1.49E+04
180	1.95E+04	1.88E+04	3.94E+04	4.28E+04
190	5.66E+04	5.44E+04	1.04E+05	1.11E+05
200	1.48E+05	1.42E+05	2.51E+05	2.67E+05
210	3.53E+05	3.39E+05	5.61E+05	5.92E+05
220	7.80E+05	7.50E+05	1.17E+06	1.23E+06
230	1.61E+06	1.55E+06	2.31E+06	2.41E+06
240	3.14E+06	3.02E+06	4.33E+06	4.50E+06
250	5.81E+06	5.58E+06	7.73E+06	8.00E+06
260	1.03E+07	9.86E+06	1.32E+07	1.36E+07
270	1.74E+07	1.67E+07	2.18E+07	2.25E+07
280	2.84E+07	2.73E+07	3.48E+07	3.57E+07
290	4.49E+07	4.31E+07	5.39E+07	5.52E+07
300	6.88E+07	6.61E+07	8.11E+07	8.29E+07
310	1.03E+08	9.87E+07	1.19E+08	1.22E+08
320	1.50E+08	1.44E+08	1.71E+08	1.74E+08
330	2.14E+08	2.05E+08	2.40E+08	2.44E+08
340	2.99E+08	2.86E+08	3.31E+08	3.37E+08
350	4.09E+08	3.92E+08	4.49E+08	4.56E+08
360	5.52E+08	5.28E+08	5.99E+08	6.08E+08
370	7.33E+08	7.01E+08	7.87E+08	7.98E+08
380	9.58E+08	9.16E+08	1.02E+09	1.03E+09
390	1.24E+09	1.18E+09	1.30E+09	1.32E+09
400	1.58E+09	1.50E+09	1.65E+09	1.67E+09

Table 3.S7. Full rate data for the tunneling of **9** to **10. (**B3LYP/6-31G(d))

T(K)	TST (s^{-1})	CVT (s^{-1})	CVT/ZCT (s^{-1})	CVT/SCT (s^{-1})
10	1.32E-91	7.48E-92	2.96E+02	2.15E+03
20	3.33E-40	2.50E-40	2.96E+02	2.15E+03
30	5.39E-23	4.46E-23	2.97E+02	2.15E+03
40	2.36E-14	2.05E-14	3.08E+02	2.19E+03
50	3.79E-09	3.38E-09	3.42E+02	2.33E+03
60	1.16E-05	1.05E-05	4.26E+02	2.63E+03
70	3.64E-03	3.35E-03	6.12E+02	3.22E+03
80	2.76E-01	2.57E-01	1.05E+03	4.39E+03
90	8.11E+00	7.60E+00	2.26E+03	6.96E+03
100	1.22E+02	1.15E+02	6.13E+03	1.35E+04
110	1.13E+03	1.07E+03	1.95E+04	3.23E+04
120	7.28E+03	6.93E+03	6.45E+04	8.86E+04
130	3.53E+04	3.37E+04	2.04E+05	2.51E+05
140	1.37E+05	1.32E+05	5.91E+05	6.82E+05
150	4.48E+05	4.30E+05	1.56E+06	1.73E+06
160	1.26E+06	1.21E+06	3.75E+06	4.06E+06
170	3.16E+06	3.04E+06	8.30E+06	8.83E+06
180	7.16E+06	6.91E+06	1.70E+07	1.79E+07
190	1.49E+07	1.44E+07	3.27E+07	3.41E+07
200	2.89E+07	2.80E+07	5.93E+07	6.15E+07
210	5.28E+07	5.10E+07	1.02E+08	1.05E+08
220	9.12E+07	8.84E+07	1.68E+08	1.73E+08
230	1.51E+08	1.46E+08	2.66E+08	2.73E+08
240	2.39E+08	2.32E+08	4.07E+08	4.15E+08
250	3.66E+08	3.55E+08	6.02E+08	6.14E+08
260	5.42E+08	5.26E+08	8.66E+08	8.81E+08
270	7.82E+08	7.58E+08	1.22E+09	1.23E+09
280	1.10E+09	1.07E+09	1.67E+09	1.69E+09
290	1.51E+09	1.46E+09	2.24E+09	2.27E+09
300	2.03E+09	1.97E+09	2.96E+09	2.99E+09
310	2.68E+09	2.61E+09	3.84E+09	3.88E+09
320	3.49E+09	3.39E+09	4.90E+09	4.95E+09
330	4.46E+09	4.33E+09	6.17E+09	6.23E+09
340	5.63E+09	5.46E+09	7.68E+09	7.75E+09
350	7.01E+09	6.81E+09	9.44E+09	9.52E+09
360	8.64E+09	8.38E+09	1.15E+10	1.16E+10
370	1.05E+10	1.02E+10	1.38E+10	1.39E+10
380	1.27E+10	1.23E+10	1.65E+10	1.66E+10
390	1.51E+10	1.47E+10	1.95E+10	1.96E+10
400	1.79E+10	1.74E+10	2.28E+10	2.30E+10

Charge	Multiplicity	Theory/Basis Set	Full Point Group
0	1	UB3LYP/6-31G(d)	C_1
ZPVE	**Electronic Energy**	**Electronic and ZPVE**	**Dipole Moment (D)**
0.091890	-286.276590	-286.184700	2.6620

(Energies in Hartrees/particle)

Symm.	Frequency (cm^{-1})	Intensity
A	245.3987	11.3360
A	357.8429	0.6604
A	409.8129	4.4323
A	559.0998	3.9754
A	590.6104	0.8869
A	605.3252	3.4879
A	642.4257	16.9912
A	728.6413	26.4246
A	798.1042	24.3204
A	900.6740	1.7109
A	927.2843	14.5126
A	941.1303	3.9408
A	968.3150	2.4859
A	981.4120	1.6526
A	990.3537	2.9662
A	1040.0822	15.7793
A	1116.6560	6.3345
A	1172.8461	1.6781
A	1209.4858	2.2837
A	1337.4199	1.4228
A	1398.7966	4.8376
A	1462.7655	2.2761
A	1534.1933	7.3943
A	1633.2087	1.4139
A	1822.1908	32.5231
A	3164.1323	10.9366
A	3174.6335	22.7862
A	3186.6707	15.4575
A	3202.1627	17.7693
A	3233.3003	3.9781

Atom	Coordinates (Angstroms)		
	X	Y	Z
C	1.208572	0.926342	-0.218372
C	1.515588	-0.479335	-0.035491
C	0.557083	-1.420774	0.212278
C	-0.747361	-0.835120	0.118215
C	-1.121087	0.575790	0.410597
C	-0.021466	1.463438	0.055934
H	2.559073	-0.782150	-0.080943
H	0.757091	-2.462053	0.436590
H	-1.821615	0.843410	1.198219
H	-0.133210	2.543261	0.138751
N	-1.677824	-0.444391	-0.640651
H	2.035446	1.586223	-0.467032

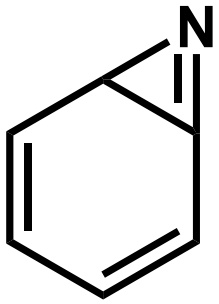

3

Charge	Multiplicity	Theory/Basis Set	Full Point Group
0	1	UB3LYP/6-31G(d)	C_1
ZPVE	**Electronic Energy**	**Electronic and ZPVE**	**Dipole Moment (D)**
0.091814	-286.284705	-286.192891	1.9752

(Energies in Hartrees/particle)

Symm.	Frequency (cm^{-1})	Intensity
A	300.6237	7.6479
A	317.3595	0.6237
A	388.9612	13.1425
A	455.7092	1.1743
A	526.5537	8.3498
A	603.7903	10.9616
A	674.9747	14.6184
A	702.5476	38.3200
A	773.7362	51.9883
A	851.4920	1.9208
A	874.8040	4.1655
A	923.8891	1.2865
A	964.7555	4.7939
A	969.8446	2.9702
A	1013.6265	22.0301
A	1042.3134	2.3208
A	1148.6357	14.4901
A	1222.0690	1.9000
A	1243.3182	2.8784
A	1347.8438	2.7890
A	1388.7311	17.2002
A	1450.7588	0.2647
A	1588.5044	1.1246
A	1637.7584	1.7168
A	1968.0611	164.0963
A	3147.8861	9.1230
A	3165.2128	19.4221
A	3176.3740	21.6988
A	3202.1540	25.8941
A	3229.2638	4.1200

Atom	Coordinates (Angstroms)		
	X	Y	Z
C	0.004682	-1.315365	-0.031990
C	1.235044	-1.008165	0.347666
C	-1.588266	0.129253	0.147992
C	1.573754	0.334090	-0.149432
C	-0.770563	1.211873	0.231952
C	0.629947	1.315950	-0.174191
H	1.857935	-1.596880	1.010355
H	-2.634310	0.170880	0.441328
H	2.583809	0.552300	-0.496972
H	-1.238915	2.139263	0.556993
N	-1.145573	-1.082447	-0.462827
H	0.942906	2.305741	-0.503900

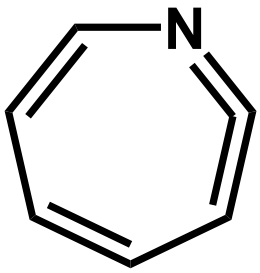

4

Charge	Multiplicity	Theory/Basis Set	Full Point Group
0	1	UB3LYP/6-31G(d)	C_1
ZPVE	**Electronic Energy**	**Electronic and ZPVE**	**Dipole Moment (D)**
0.090353	-286.269134	-286.178780	2.1626

(Energies in Hartrees/particle)

Symm.	Frequency (cm^{-1})	Intensity
A	-483.9899	14.1656
A	306.4968	3.7849
A	376.9701	0.8042
A	439.8507	1.4074
A	520.5444	1.7205
A	609.2937	15.6577
A	641.1254	5.4412
A	685.3427	41.6443
A	769.8375	32.4279
A	857.1654	3.7296
A	868.2942	5.9199
A	910.7322	3.9767
A	938.8660	3.0771
A	965.3034	3.1954
A	1009.4988	1.2367
A	1050.5794	12.3361
A	1104.7226	5.6028
A	1191.7523	1.5925
A	1217.0061	1.9808
A	1343.1714	10.8937
A	1390.9391	13.5346
A	1461.1506	1.7331
A	1528.9955	4.8789
A	1580.2111	3.6841
A	1932.0960	75.2420
A	3155.3342	5.3924
A	3177.3721	7.3784
A	3185.9307	27.1602
A	3201.3300	16.5509
A	3240.5703	1.3145

Atom	Coordinates (Angstroms)		
	X	Y	Z
C	-1.041807	1.066817	0.257133
C	-1.567862	-0.221936	0.079526
C	-0.778199	-1.321872	-0.298216
C	0.546654	-1.068076	-0.037585
C	1.299514	0.496244	-0.322885
C	0.267413	1.413686	-0.128310
H	-2.644238	-0.360204	0.160475
H	-1.150939	-2.222530	-0.769496
H	2.097801	0.656934	-1.043521
H	0.440564	2.433809	-0.470900
N	1.520003	-0.652246	0.619632
H	-1.737492	1.868529	0.488031

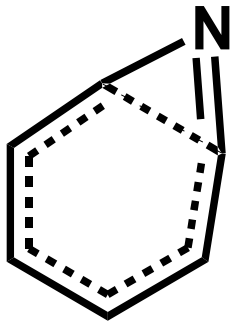

$TS_{3\text{-}4}$

Charge	Multiplicity	Theory/Basis Set	Full Point Group
0	1	RB3LYP/6-31G(d)	C_1
ZPVE	**Electronic Energy**	**Electronic and ZPVE**	**Dipole Moment (D)**
0.120666	-723.776667	-723.656001	1.6270

Symm.	Frequency (cm^{-1})	Intensity
A	30.1878	4.2673
A	100.7957	2.7516
A	157.3563	0.0406
A	213.0859	4.8628
A	282.5440	5.8725
A	299.4466	0.7394
A	369.1590	0.1893
A	426.1142	7.6722
A	470.0431	0.9253
A	602.0872	5.1159
A	622.9835	13.7209
A	636.6688	6.2676
A	660.5153	2.9982
A	698.8408	0.5998
A	732.0657	14.1580
A	864.5097	11.3203
A	915.6317	12.0900
A	933.3109	12.8827
A	954.1178	1.3181
A	986.9763	4.2886
A	998.1867	2.0876
A	1006.1835	30.2891
A	1038.5755	17.6798
A	1047.1083	1.1054
A	1139.1985	8.9950
A	1175.9688	2.8302
A	1316.7165	4.5083
A	1358.1313	4.5032
A	1385.6091	6.3490
A	1411.4446	3.3381
A	1496.1289	9.7327
A	1512.9300	11.2506
A	1516.1953	3.9052
A	1603.9373	2.3871
A	1826.5576	38.8752
A	3065.0576	25.2032
A	3152.0003	10.4734
A	3159.0932	7.7961
A	3172.2658	22.7961
A	3191.4519	8.0856
A	3202.8855	0.9889

(Energies in Hartrees/particle)

Atom	Coordinates (Angstroms)		
	X	**Y**	**Z**
C	0.335210	-0.087403	-0.335473
C	-0.224034	1.257656	-0.422329
C	-1.550475	1.525259	-0.247626
C	-2.252375	0.339290	0.144764
C	-1.904413	-1.060002	-0.218765
C	-0.458992	-1.209331	-0.312521
H	0.461529	2.066285	-0.660057
H	-2.003155	2.500080	-0.386995
H	-2.568062	-1.697005	-0.798257
H	-0.009581	-2.182597	-0.495890
C	2.673687	0.209230	1.162636
H	3.765517	0.149035	1.155161
H	2.375817	1.232684	1.405868
H	2.278811	-0.480491	1.912565
N	-2.547286	-0.454842	1.079681
S	2.113655	-0.265768	-0.519642

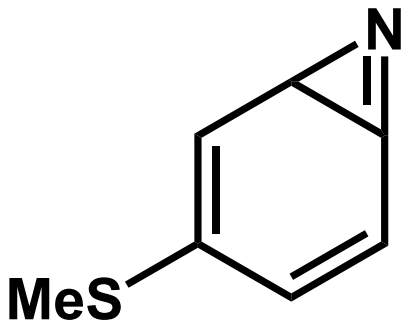

5

Charge	Multiplicity	Theory/Basis Set	Full Point Group
0	1	UB3LYP/6-31G(d)	C_1
ZPVE	**Electronic Energy**	**Electronic and ZPVE**	**Dipole Moment (D)**
0.120713	-723.785814	-723.665101	0.7781

Symm.	Frequency (cm^{-1})	Intensity
A	58.3519	4.4119
A	103.5098	2.0350
A	149.1241	0.2687
A	228.6983	2.3099
A	297.6497	3.1363
A	304.0189	0.8735
A	360.2703	4.7894
A	388.3116	8.6164
A	424.2480	6.3998
A	514.5896	12.6543
A	584.0154	4.3597
A	633.4567	4.7777
A	683.1556	29.3281
A	700.1991	0.9939
A	722.9368	24.6950
A	820.5657	25.9298
A	886.1564	12.2759
A	898.7710	0.7683
A	968.5802	2.3171
A	984.1267	13.3795
A	992.2331	6.9470
A	1008.7362	10.7045
A	1016.1971	17.7347
A	1069.2260	5.6181
A	1150.0770	15.6300
A	1241.1997	3.8358
A	1327.0672	18.6262
A	1344.8122	8.9582
A	1385.5861	3.8804
A	1419.4609	4.0264
A	1495.3720	10.1097
A	1513.0010	11.0577
A	1562.8347	3.2551
A	1606.2449	11.0154
A	1970.6220	171.4264
A	3067.4163	23.2589
A	3155.4150	9.4160
A	3159.4888	6.9399
A	3173.5323	9.7079
A	3182.9560	1.4316
A	3204.2146	19.9827
A	3230.5416	4.2366

(Energies in Hartrees/particle)

Atom	Coordinates (Angstroms)		
	X	Y	Z
C	-2.360471	0.248304	0.391447
C	-1.916237	1.441939	0.031397
C	-1.430252	-1.524483	-0.392210
C	-0.449391	1.454635	0.122088
C	-0.274900	-0.911364	-0.760324
C	0.273189	0.358630	-0.264234
H	-2.521162	2.257249	-0.346738
H	-1.719137	-2.492773	-0.793533
H	0.074469	2.333366	0.494339
H	0.367863	-1.460945	-1.443834
N	-2.268596	-0.976312	0.623220
C	2.581873	-0.858090	0.792534
H	3.675066	-0.870012	0.776379
H	2.237693	-0.695343	1.816777
H	2.210005	-1.817791	0.424785
S	2.063282	0.520188	-0.300932

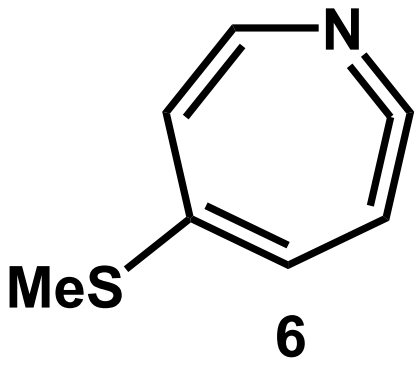

6

Charge	Multiplicity	Theory/Basis Set	Full Point Group
0	1	RB3LYP/6-31G(d)	C_1
ZPVE	**Electronic Energy**	**Electronic and ZPVE**	**Dipole Moment (D)**
0.119170	-723.770308	-723.651138	0.7364

Symm.	Frequency (cm^{-1})	Intensity
A	-466.8373	10.9767
A	52.3497	3.5161
A	103.8850	2.4527
A	151.7095	0.0667
A	240.5535	1.5309
A	296.1040	0.5220
A	317.4164	1.8857
A	393.1976	0.6632
A	436.5616	3.4966
A	474.2229	1.7048
A	582.0745	12.0848
A	629.9709	8.3572
A	660.2371	8.0826
A	694.2291	19.6148
A	701.3632	6.1431
A	832.9071	11.8001
A	869.0219	20.4510
A	909.2496	1.0544
A	937.0254	4.3231
A	942.9868	7.1332
A	986.7530	3.3411
A	1006.8141	18.6937
A	1047.7999	13.0698
A	1074.6861	4.0772
A	1130.0191	6.6490
A	1204.3262	5.5618
A	1314.9509	13.6306
A	1383.3347	11.2692
A	1387.3748	11.8215
A	1406.4995	0.8822
A	1467.8216	2.1393
A	1496.0037	9.3322
A	1513.0981	10.5654
A	1561.5284	3.2615
A	1930.6660	103.2925
A	3064.6385	27.2354
A	3154.7185	9.8596
A	3155.4358	9.5300
A	3170.3049	1.3965
A	3191.0199	20.4913
A	3194.0391	0.6083
A	3242.5808	0.8073

(Energies in Hartrees/particle)

Atom	Coordinates (Angstroms)		
	X	Y	Z
C	0.318777	0.220570	-0.255516
C	-0.382411	1.403923	0.054255
C	-1.781894	1.462753	0.138645
C	-2.302143	0.202782	0.323326
C	-1.696349	-1.209572	-0.508086
C	-0.345903	-0.938150	-0.719524
H	0.189484	2.322861	0.158163
H	-2.371657	2.365956	0.046416
H	-2.289266	-1.786313	-1.213510
H	0.184780	-1.559012	-1.439689
C	2.663016	-0.685612	0.982740
H	3.755992	-0.700402	0.943503
H	2.342994	-0.239181	1.927586
H	2.288483	-1.709807	0.910479
N	-2.365967	-0.940903	0.811609
S	2.101400	0.322004	-0.444328

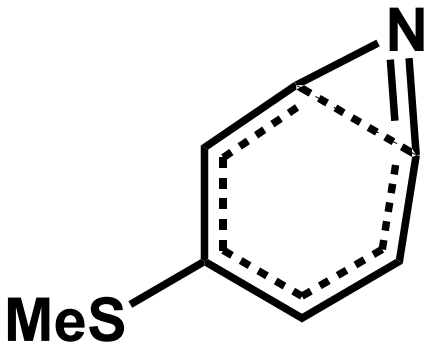

$TS_{5\text{-}6}$

Charge	Multiplicity	Theory/Basis Set	Full Point Group
0	1	RB3LYP/6-31G(d)	C_1
ZPVE	**Electronic Energy**	**Electronic and ZPVE**	**Dipole Moment (D)**
0.124983	-400.800338	-400.675355	2.8197

Symm.	Frequency (cm^{-1})	Intensity
A	98.0511	3.7747
A	172.7517	9.2746
A	249.2083	4.3469
A	270.4458	0.1891
A	294.3828	4.6999
A	392.2660	2.2223
A	444.4717	2.7892
A	459.8106	2.5888
A	554.9926	6.0403
A	600.2839	7.6894
A	631.0353	12.4199
A	662.1740	2.3941
A	738.7392	5.9753
A	748.4932	23.7982
A	827.6874	35.8754
A	898.3017	0.8404
A	941.9816	12.8874
A	949.9184	1.2675
A	1004.1003	6.7243
A	1055.9373	36.9565
A	1068.6018	16.3460
A	1162.8968	16.9860
A	1173.8893	15.5454
A	1186.3939	1.2918
A	1218.9235	9.9821
A	1272.9842	185.9635
A	1330.7082	11.3563
A	1369.4487	4.3746
A	1433.3970	48.4705
A	1498.0827	4.2004
A	1517.8555	7.5372
A	1535.4970	15.1898
A	1559.1205	44.8090
A	1646.5178	78.9472
A	1807.7613	24.9080
A	3027.2728	39.5421
A	3086.6393	39.5328
A	3160.0581	31.4212
A	3162.4914	25.1101
A	3207.2867	6.6263
A	3208.0510	8.2299
A	3232.1679	4.1369

(Energies in Hartrees/particle)

Atom	Coordinates (Angstroms)		
	X	**Y**	**Z**
C	0.667414	0.254802	-0.042771
C	-0.168179	1.452508	-0.089999
C	-1.526537	1.404028	-0.124588
C	-1.986452	0.045954	-0.016629
C	-1.265472	-1.164999	-0.433970
C	0.178131	-1.009245	-0.252811
H	0.358423	2.402633	-0.086263
H	-2.163616	2.277292	-0.206343
H	-1.651988	-1.827960	-1.204872
H	0.847496	-1.848697	-0.412042
C	2.927419	-0.483049	0.132879
H	3.893738	-0.025625	0.352214
H	2.689139	-1.229836	0.901655
H	2.971904	-0.977589	-0.846535
O	1.983070	0.575726	0.136285
N	-2.252513	-0.910860	0.768463

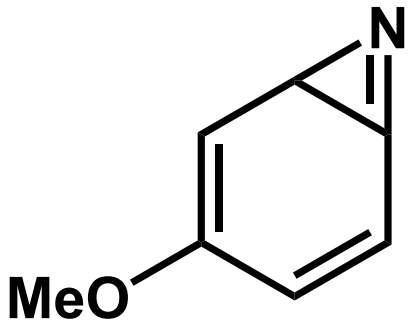

7

Charge	Multiplicity	Theory/Basis Set	Full Point Group
0	1	RB3LYP/6-31G(d)	C_1
ZPVE	**Electronic Energy**	**Electronic and ZPVE**	**Dipole Moment (D)**
0.124319	-400.804002	-400.679683	1.4969

Symm.	Frequency (cm^{-1})	Intensity
A	75.2619	5.8271
A	128.4645	2.9885
A	168.3178	1.8009
A	272.0120	4.3096
A	328.8629	0.6279
A	372.3936	6.3660
A	434.7640	4.8046
A	437.0994	4.2469
A	459.2548	9.4503
A	535.0570	13.9028
A	623.5817	14.5798
A	689.4165	30.2477
A	716.9125	10.9406
A	739.6455	30.8524
A	830.1564	17.1064
A	876.3409	11.0763
A	906.5095	4.1549
A	970.2500	2.3930
A	1011.2345	19.3100
A	1029.5850	39.8124
A	1068.7553	1.2999
A	1148.1021	20.3858
A	1179.6147	59.6948
A	1192.3609	64.9153
A	1226.2071	40.6203
A	1254.0250	94.2290
A	1318.6082	7.9220
A	1352.2233	26.4969
A	1427.1578	17.6518
A	1500.7065	1.9180
A	1516.3645	7.8101
A	1533.3445	13.8062
A	1586.9917	11.7176
A	1637.9628	80.2397
A	1969.3402	159.9367
A	3030.5643	51.6909
A	3090.8071	38.1763
A	3153.9964	30.5760
A	3174.3002	16.2809
A	3179.5068	2.8521
A	3201.1512	22.3929
A	3222.5197	6.0579

(Energies in Hartrees/particle)

Atom	Coordinates (Angstroms)		
	X	**Y**	**Z**
C	-2.032523	0.294438	0.349482
C	-1.578514	1.444205	-0.124647
C	-1.085906	-1.547725	-0.256793
C	-0.115536	1.476818	-0.017490
C	0.079272	-0.971618	-0.649670
C	0.606863	0.348693	-0.280494
H	-2.181481	2.205580	-0.605753
H	-1.361856	-2.551229	-0.572139
H	0.422739	2.381901	0.258351
H	0.747318	-1.576645	-1.258706
N	-1.952945	-0.911695	0.676467
C	2.705497	-0.389622	0.566907
H	3.763493	-0.191388	0.382605
H	2.469280	-0.173360	1.617134
H	2.495278	-1.447867	0.367010
O	1.980115	0.475468	-0.305942

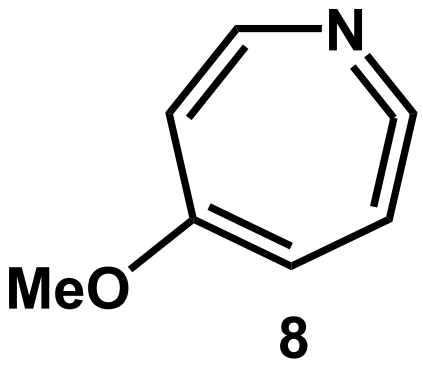

8

Charge	Multiplicity	Theory/Basis Set	Full Point Group
0	1	RB3LYP/6-31G(d)	C_1
ZPVE	**Electronic Energy**	**Electronic and ZPVE**	**Dipole Moment (D)**
0.123004	-400.787365	-400.664362	2.2538

Symm.	Frequency (cm^{-1})	Intensity
A	-520.8224	29.0626
A	74.3547	4.8608
A	184.1644	2.7552
A	251.6925	1.6967
A	270.2653	0.5165
A	322.2817	3.0127
A	408.1180	0.3131
A	464.7596	3.4945
A	474.6648	2.0489
A	524.2285	2.8858
A	589.1157	11.9664
A	649.0874	9.4645
A	700.3414	18.3850
A	721.8427	35.7812
A	800.7036	22.8659
A	855.4539	16.6930
A	890.8775	2.4810
A	935.1007	4.2751
A	955.9278	1.1552
A	1049.9101	12.7961
A	1072.3311	25.8096
A	1127.1767	17.1177
A	1184.0723	3.0025
A	1209.1511	2.2490
A	1215.0436	32.4611
A	1279.8102	269.8815
A	1325.8843	15.2777
A	1399.9389	42.2221
A	1426.8285	9.4813
A	1495.8744	2.1130
A	1504.9942	0.2653
A	1519.7756	15.7283
A	1539.1425	16.9974
A	1604.6514	74.7164
A	1928.8531	78.6818
A	3017.4918	52.0917
A	3074.8621	45.3611
A	3149.6339	29.6715
A	3172.2699	14.2899
A	3189.4708	14.3639
A	3196.6666	2.4869
A	3235.4943	2.1650

(Energies in Hartrees/particle)

Atom	Coordinates (Angstroms)		
	X	Y	Z
C	0.632231	0.320939	-0.015314
C	-0.194227	1.455545	-0.057496
C	-1.589958	1.376715	-0.219027
C	-2.049453	0.135890	0.124775
C	-1.175075	-1.343530	-0.345792
C	0.166882	-0.966587	-0.370798
H	0.296719	2.425147	-0.031810
H	-2.207569	2.177316	-0.606903
H	-1.577190	-2.079090	-1.039301
H	0.853503	-1.636283	-0.883063
C	2.890241	-0.467989	0.139148
H	3.838556	-0.055959	0.490821
H	2.574480	-1.283965	0.803253
H	3.033080	-0.867594	-0.874749
O	1.965533	0.604489	0.161695
N	-2.088527	-0.940197	0.759316

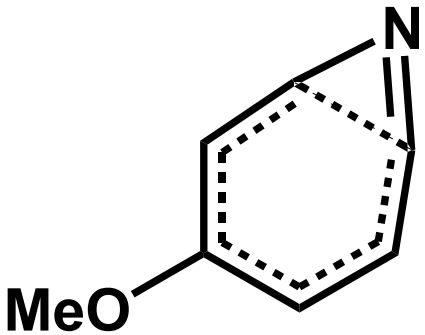

$TS_{7\text{-}8}$

Charge	Multiplicity	Theory/Basis Set	Full Point Group
0	1	RB3LYP/6-31G(d)	C_1
ZPVE	**Electronic Energy**	**Electronic and ZPVE**	**Dipole Moment (D)**
0.083767	-385.508650	-385.424883 (Energies in Hartrees/particle)	2.4165

Symm.	Frequency (cm^{-1})	Intensity
A	181.7017	5.6895
A	285.9879	6.6704
A	387.8390	4.2755
A	403.3304	2.4241
A	449.2790	2.2154
A	520.2841	5.7392
A	601.5069	7.9131
A	623.6091	8.4985
A	661.5094	2.3803
A	726.3053	15.3845
A	756.9875	23.3056
A	848.9365	28.6417
A	910.8869	2.6618
A	935.6067	5.8452
A	941.7917	11.3843
A	996.8494	6.2127
A	1043.0635	17.0129
A	1144.2168	13.3183
A	1154.0900	7.6301
A	1240.2415	88.2690
A	1311.7690	1.0475
A	1365.0597	1.5785
A	1432.5896	41.9967
A	1552.8274	6.4002
A	1650.9991	57.4070
A	1814.9931	24.2472
A	3172.6214	23.7789
A	3203.0602	6.0892
A	3213.5770	0.4321
A	3237.9962	1.5705

Atom	Coordinates (Angstroms)		
	X	Y	Z
C	1.094149	-0.130144	0.030475
C	0.646430	1.242384	-0.075958
C	-0.675959	1.556605	-0.187035
C	-1.484057	0.377372	-0.056368
C	-1.106662	-1.010939	-0.411565
C	0.318470	-1.229423	-0.182493
H	1.411811	2.012866	-0.073202
H	-1.053436	2.560098	-0.344623
H	-1.633080	-1.578090	-1.175235
H	0.791091	-2.199297	-0.313058
N	-2.012822	-0.451200	0.738753
F	2.424349	-0.274700	0.225836

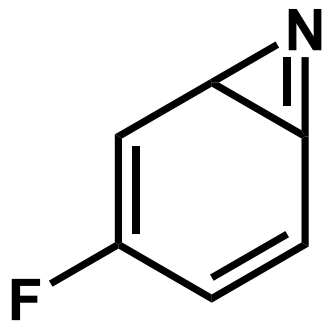

9

Charge	Multiplicity	Theory/Basis Set	Full Point Group
0	1	RB3LYP/6-31G(d)	C_1
ZPVE	**Electronic Energy**	**Electronic and ZPVE**	**Dipole Moment (D)**
0.083802	-385.517425	-385.433623 (Energies in Hartrees/particle)	1.5228

Symm.	Frequency (cm^{-1})	Intensity
A	192.3663	3.3766
A	292.9623	4.7533
A	357.9999	4.8651
A	387.6776	5.8882
A	437.3475	3.0701
A	468.9121	2.2568
A	527.0772	7.7607
A	628.5194	18.6899
A	669.0556	6.7320
A	705.4134	40.4853
A	747.0539	27.5602
A	820.4562	33.3675
A	864.5768	19.1278
A	904.0644	2.8739
A	967.9511	2.2704
A	1013.7005	19.0308
A	1070.4226	1.1610
A	1151.3597	14.3366
A	1190.6404	97.3933
A	1242.4356	17.2199
A	1318.4242	7.8133
A	1355.2951	20.6267
A	1434.6796	20.3541
A	1600.8546	7.2248
A	1651.9118	84.5351
A	1972.8621	168.3486
A	3180.4587	12.6971
A	3193.2696	3.3328
A	3211.1274	14.9639
A	3225.9423	3.8718

Atom	Coordinates (Angstroms)		
	X	Y	Z
C	1.534512	0.695191	-0.131039
C	0.710463	1.625622	0.324262
C	1.058276	-1.401294	0.148109
C	-0.671670	1.282679	-0.035507
C	-0.267684	-1.203142	0.369406
C	-1.049169	-0.020298	0.026850
H	0.990573	2.451485	0.967537
H	1.541888	-2.341414	0.400822
H	-1.398906	2.028004	-0.351648
H	-0.848642	-2.038971	0.750287
N	1.847598	-0.444288	-0.543504
F	-2.345163	-0.317959	-0.241661

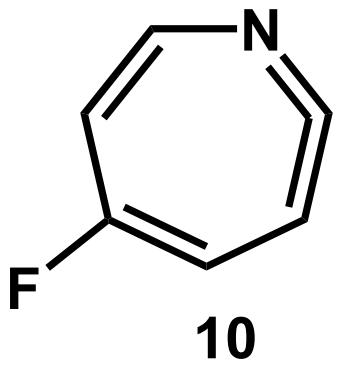

10

Charge	Multiplicity	Theory/Basis Set	Full Point Group
0	1	RB3LYP/6-31G(d)	C_1
ZPVE	**Electronic Energy**	**Electronic and ZPVE**	**Dipole Moment (D)**
0.082150	-385.499581	-385.417430 (Energies in Hartrees/particle)	2.1938

Symm.	Frequency (cm^{-1})	Intensity
A	-504.5538	23.2995
A	206.9445	2.1003
A	329.3207	2.3210
A	402.9819	1.3100
A	422.3584	1.2687
A	461.5598	2.1149
A	507.7858	3.7140
A	577.4449	11.6083
A	647.8017	8.3368
A	695.4040	30.2080
A	741.8973	26.6549
A	816.8775	22.0056
A	860.2673	21.6183
A	890.7006	1.6235
A	938.9220	3.7188
A	959.8924	3.9688
A	1046.2505	10.3191
A	1121.2738	13.3928
A	1180.9579	9.8761
A	1252.1449	105.5320
A	1310.5418	6.9691
A	1393.7117	28.0744
A	1424.5936	10.1203
A	1518.3185	1.9389
A	1600.5577	46.8669
A	1928.2847	67.5851
A	3179.9757	5.7470
A	3193.7512	13.5021
A	3205.8998	1.3666
A	3243.3652	0.3205

Atom	Coordinates (Angstroms)		
	X	Y	Z
C	1.071866	-0.087066	0.065709
C	0.650848	1.240227	-0.040915
C	-0.697908	1.567440	-0.270244
C	-1.513515	0.512566	0.050704
C	-1.101167	-1.161705	-0.327960
C	0.292215	-1.202554	-0.271374
H	1.410397	2.016998	-0.019101
H	-1.037083	2.502553	-0.697426
H	-1.670464	-1.774607	-1.022344
H	0.813799	-2.060188	-0.691527
N	-1.906856	-0.464096	0.721051
F	2.401923	-0.294393	0.238613

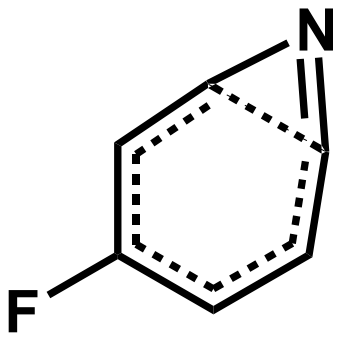

$TS_{9\text{-}10}$

Full reference for Polyrate

POLYRATE 2010-A: Computer Program for the Calculations of Chemical Reaction Rate for Polyatomics

Jingjing Zheng, Shuxia Zhang, Benjamin J. Lynch, José C. Corchado, Yao-Yuan Chuang, Patton L. Fast, Wei-Ping Hu, Yi-Ping Liu, Gillian C. Lynch, Kiet A. Nguyen, Charles F. Jackels, Antonio Fernandez Ramos, Benjamin A. Ellingson, Vasilios S. Melissas, Jordi Villà, Ivan Rossi, Elena. L. Coitiño, Jingzhi Pu, Titus V. Albu
Department of Chemistry and Supercomputing Institute
University of Minnesota, Minneapolis, Minnesota 55455

Artur Ratkiewicz
Institute of Chemistry, University of Bialystok, Poland

Rozeanne Steckler
Northwest Alliance for Computational Science & Engineering
Oregon State University, Corvallis, Oregon 97331

Bruce C. Garrett
Environmental Molecular Sciences Laboratory
Pacific Northwest Laboratory
Richland, Washington 99352

Alan D. Isaacson
Department of Chemistry and Biochemistry
Miami University Oxford, Ohio 45056

and Donald G. Truhlar
Department of Chemistry and Supercomputing Institute
University of Minnesota, Minneapolis, Minnesota 55455

Full reference for Gaussrate

GAUSSRATE 2009-A

Jingjing Zheng, Shuxia Zhang, José C. Corchado, Yao-Yuan Chuang, Elena L. Coitiño, Benjamin A. Ellingson, and Donald G. Truhlar
Department of Chemistry and Supercomputing Institute,
University of Minnesota, Minneapolis, MN 55455-0431, USA

Chapter 4: Diradicals on the C_8H_4 Potential Energy Surface

Includes the work of a collaborator:

Brian Esselman

Introduction

The study of arynes dates back more than a century to the early work on the formation of 2-ethoxybenzofuran from 3-bromobenzofuran via a postulated *ortho*-didehydrobenzofuran.[1] The rigid cyclic framework of aromatic species allows for the unique opportunity to study (σ,σ) diradicals, where two non-bonding electrons occupy separate σ orbitals in the plane of the molecule. This makes arynes an ideal system to study the through-space and through-bond interactions between two radical centers. In their landmark paper,[2] Hoffman, Imamura, and Hehre used extended Hückel calculations to predict patterns in through-bond coupling for a number of aryne species which has served as a model for studying didehydroarenes.

Figure 4.1. *Ortho,meta*, and *para*-benzyne, respectively.

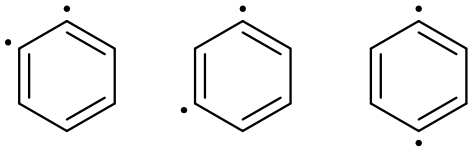

More recent interest in didehydroarenes has been connected to the role of several diradiacal arynes that play an important role in the cleavage of double-stranded DNA with enediyne cytstostatics.[3,4] In calichaemicin for example, a *p*-benzyne intermediate is formed from a Bergman cyclization that then performs radical chemistry to cleave DNA. Understanding the formation of these diradical species and their reactivity has been a key focus for drug-design as potential anti-tumor drugs. For physical organic chemists, arynes have always served as fascinating models for the study of the interactions of two radical centers across a molecule, pushing the limits of spectroscopy and computational methods.

To compare different diradicals, the reactivity of these species is often best understood by the $\Delta E_{S\text{-}T}$ splitting. For triplet diradicals, the two spins are not able to strongly interact. Singlet diradicals, however, can be greatly stabilized by through-space and through-bond interactions. Thus, the $\Delta E_{S\text{-}T}$ splitting strongly correlates to the degree of interaction between the two spins. A larger $\Delta E_{S\text{-}T}$ implies more interaction between spins in the singlet state, resulting in a less reactive and less diradicaloid species. Using the benzyne family as an example, *o*-benzyne (Figure 4.1) has strong orbital overlap between the two spins on adjacent carbon atoms and has a large $\Delta E_{S\text{-}T}$ splitting of 38 kcal/mol (based on photoelectron spectroscopy measurements).[5] For *m*-benzyne, the greater distance allows for less overlap of the radical orbitals, and a smaller $\Delta E_{S\text{-}T}$ splitting of 21 kcal/mol. With no direct orbital overlap between orbitals, *p*-benzyne has only a weak interaction between the two spins and thus a $\Delta E_{S\text{-}T}$ splitting of 3.8 kcal/mol.

While arynes have been studied using matrix-isolation spectroscopy,[6-11] negative-ion photoelectron spectroscopy,[5,12] and mass spectrometry,[13,14] much of the work on arynes has been done computationally due to the challenge of their synthesis and characterization. Didehydroindene,[15] didehydronaphthalene (DDN),[16] didehydrophenanthrenes (DDPh),[17] many substituted benzynes[18,19] and didehydropyridines[20] have all been studied computationally. With a rich catalogue of computational work on a variety of didehydroarenes, the interactions between the two radicals across a carbon framework is well documented for six-membered rings.

Scheme 4.1, Coalescence and annealing model towards fullerene formation.

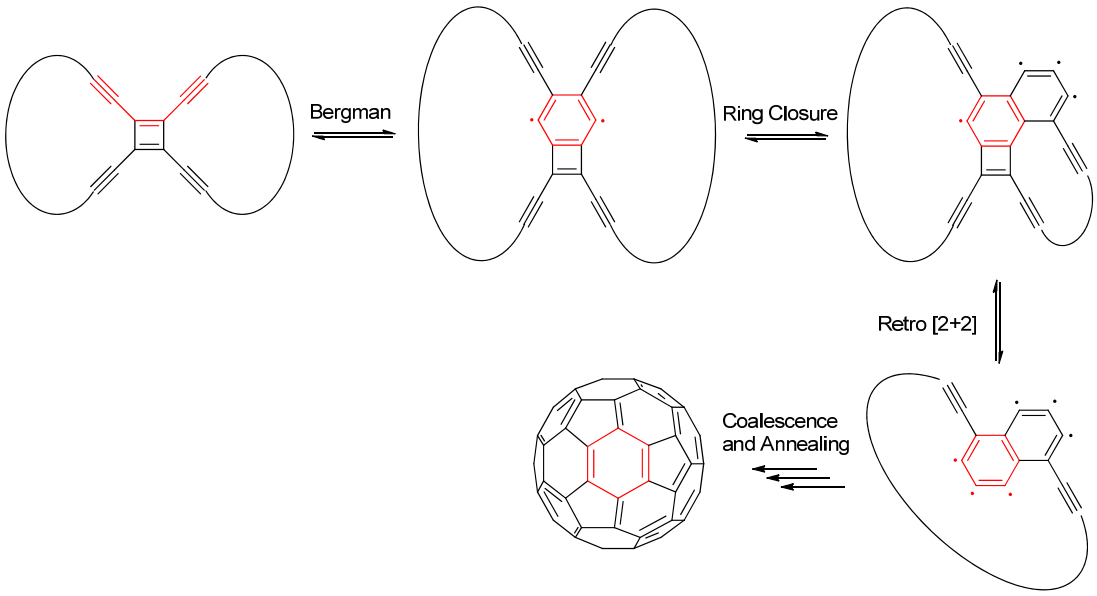

Our interest in didehydropentalene (DDP) started with Esselman's exploration of a carbon condensation pathway towards fullerene (Scheme 4.1).[21] Exploring this pathway, another diradical, 1,4-didehydrobenzocyclobutadiene (1,4-DDB), was investigated as a possible intermediate (Scheme 4.2). It was found at several levels of theory that the diradical intermediate was not a stable minimum on the potential energy surface, and would readily undergo a ring expansion to cyclooctadienediyne with either no barrier or a very shallow barrier,[21] depending on the level of theory. The diradical 3,6-DDP was then investigated as a potential next step from the thermodynamically stable cyclooctadienediyne. This reaction would serve as a pathway to generate five-membered rings, allowing for possible Stone-Walls rearrangements to propagate these five-membered rings for fullerene formation.[22-24] Though the diradical was found to be very high in energy (Scheme 4.2) to be reasonable as the next step along the pathway, we continued our investigation of the family of DDP (σ,σ) diradicals.

Scheme 4.2. Possible intermediates along the carbon-condensation pathway towards the formation of fullerene. Values in kcal/mol calculated at B3LYP/6-31G(d).

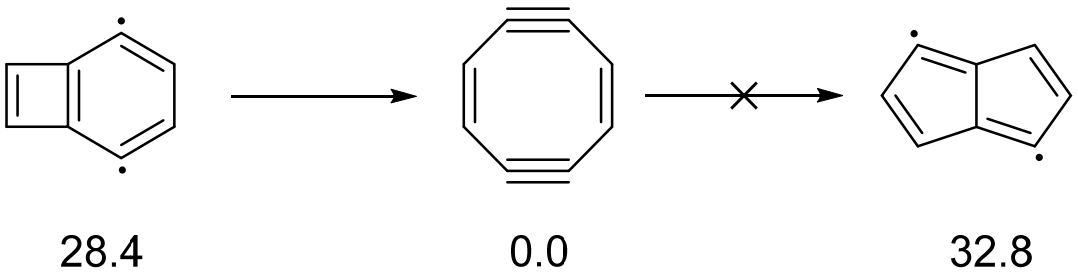

While matrix-isolation spectroscopy and electronic-structure calculations of pentalene have been reported,[25] and one study of didehydrohetero-substituted pentalenes was conducted computationally,[26] a detailed study of all didehydropentalene (DDP) isomers has not been completed with modern computational techniques. Extending the chemical space around (σ,σ) diradicals with DDP provides several unique opportunities, chiefly in the 5,5- bicyclic motif. The large majority of (σ,σ) diradicals that have been studied to date are six-membered or 6,6-bicyclic structures, and the change in the geometry will have a large impact on the through-space and through-bond interactions that govern the relative stability of these diradicals. Additionally, most of the other studied (σ,σ) diradicals are aromatic compounds with a great degree of bond delocalization. In contrast, in pentalene the large degree of bond localization results in large differences in bond lengths compared to most arenes. The bond localization in pentalene allows for nine unique (σ,σ) diradicals. The goal of this study is to use electronic-structure calculations to evaluate the stability and structure of all nine DDP species, and to evaluate the $\Delta E_{S\text{-}T}$ splitting as a measure of reactivity and interaction between the two separated spins.

During his exploration of the C_8H_4 potential energy surface, Esselman also optimized the full family of nine didehydrobenzocyclobutadienes (DDB) using B3LYP/6-31G(d). Esselman attempted optimizations for all nine possible diradical species, but was unable to find a minimum structure for singlets 1,4-DDB and 5,6-DDB. With our experience performing calculations on similar diradical species for DDP, and to further test the capabilities of CASSCF calculations to model these systems, the full family of DDB species was investigated. Despite an aromatic six-membered ring, the four-membered ring is anti-aromatic and thus highly reactive. This reactivity means benzocyclobutadiene readily dimerizes at room temperatures, and has only be observed in matrix-isolation experiments of Chapman *et al.*[27] and fast-flow NMR experiments.[28] Derivatives of benzocyclobutadiene with several bulky substituents, such as multiple tert-butyl[29] and trimethylsilane groups,[30] have also been isolated. The DDB family also provides a unique opportunity to study (σ,σ) diradicals in a 6,4-bicyclic motif.

Computational Methods

All optimized geometries and harmonic frequencies were obtained with the B3LYP[31] density functional as well as the complete active space self-consistent field (CASSCF) method with the 6-31G(d) basis set[32] using Gaussian 09.[33] All optimizations were carried out with OPT=TIGHT and an ultrafine grid (INT=GRID=ULTRAFINE). Harmonic vibrational frequency calculations were used to ensure that all geometries were minima on the potential energy surface. For the singlet 1,2-diradicals, both a restricted and a broken symmetry spin unrestricted wavefunction was used for the optimizations, and the lower energy structure was used. Unrestricted wavefunctions were used for all other singlet and triplet diradicals. Instabilities in the wavefunction were checked and optimized using the STABLE=OPT keyword

available in Gaussian. The shortcomings of DFT methodology when handling singlet open-shell diradicals are well known, namely the prevalence for spin contamination of the wavefunction.[34,35] Spin contamination is measured by the value of the $\langle \hat{S}^2 \rangle$ operator for the open-shell diradical species. Under ideal conditions, $\langle \hat{S}^2 \rangle$ should be 0.00 for singlets and 2.00 for triplets. Large discrepancies from these ideal values indicate the presence of spin contamination from higher spin states. For many of the triplet diradicals, $\langle \hat{S}^2 \rangle$ after annihilation of the spin contaminant was close to or exactly 2.00. In the case of the singlet species, $\langle \hat{S}^2 \rangle$ varies wildly with many singlet diradicals showing a $\langle \hat{S}^2 \rangle$ value that is very large (>3).

To more properly address the issue of open-shell singlet diradicals and to examine the level at which spin contamination affected the geometry and energy of the singlets, all DDP and DDB species were optimized at the multiconfiguration self-consistent field (MCSCF) level of theory. For all DDP and DDB species, the complete active space of 10 electrons in 10 orbitals (CASSCF (10,10)) was used, representing the full π-system (bonding and anti-bonding orbitals) and both radical centers. Other monoradicals and diradicals studied for comparison used a similarly appropriate active space. Second-order perturbation theory single-point energy corrections of the CASSCF geometries were carried out using the CASMP2 method. To further evaluate through-bond coupling in several DDP species, Natural Bond Orbital (NBO) and Natural Resonance Theory (NRT) calculations were performed to using NBO 6.0[36] to elucidate donor-acceptor interactions between the two radical centers.[36-39] All NBO calculations were performed on the optimized CASSCF(10,10)/6-31G(d) geometry using B3LYP/6-31G(d).

Didehydropentalenes - Results

Pentalene, both monodehydropentalenes, and all nine DDP species were successfully optimized using both B3LYP/6-31G(d) and CASSCF(10,10)/6-31G(d) methods. As mentioned previously, DFT methods are known to struggle with open-shell singlet diradicals. The STABLE=OPT keyword was employed to attempt to correct instabilities in the wavefunction, and optimized minima for singlet and triplet diradicals of all nine DDP isomers were found. This removed some of the more obviously erroneous results, such as overly stable triplet diradicals (Figure 4.S1). Despite this improvement, problems still remained. Though spin contamination was within acceptable boundaries for most singlets, several singlet diradicals demonstrated serious spin contamination ($\langle \hat{S}^2 \rangle > 3$). For a full list of $\langle \hat{S}^2 \rangle$ values, see Table 4.S3. In light of these results, the focus of this study is evaluating the geometries and energies from CASSCF and CASMP2 calculations.

Our geometry for pentalene is consistent with previously reported calculations at the MP2 and QCFF[25] levels. To our knowledge no experimental determination of the parent pentalene geometry is available outside of an x-ray crystal structure of several substituted pentalenes and organometallic complexes where pentalene serves as a ligand.[40] The anti-aromaticity of pentalene leads to a rather large bond alternation (Figure 4.2) between the single and double-bonds. The bond alternation in addition to the C_{2h} symmetry allows for nine possible didehydro species from the parent pentalene. All species (non-radicals and radicals) where found to be planar.

Figure 4.2. Calculated CASSCF(8,8)/6-31G(d) bond lengths (in Å) in pentalene (C_{2v}).

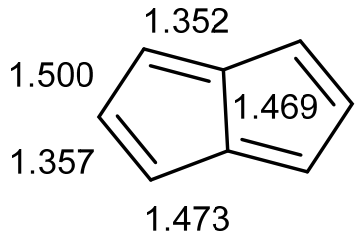

For nearly all the triplet diradical species, the optimized geometries show only small deviations from pentalene (Table 4.S4). The two parallel spins cannot participate in the same through-space and through-bond coupling that is present in the singlet state. As such, the largest deviation from the parent pentalene geometry amongst all triplet diradicals in bond length is 0.015 Å. Similarly, the relative energies for the triplet diradicals are also uniform with all species within ~3 kcal/mol except for 1,2-DDP, which is 4.7 kcal/mol higher than the lowest energy triplet at the CASMP2 level. This is to be expected, as the close proximity of the two spins decreases the stability of the triplet state. Changes in both geometry and the $\Delta E_{S\text{-}T}$ splitting for the singlet species range from negligible to dramatic, and will be discussed case by case in the rest of the chapter.

A summary of the relative energies between singlet and triplet states is shown in Table 4.S1. More diagnostic than the relative energy of every isomer of every multiplicity, the $\Delta E_{S\text{-}T}$ splitting itself is a representation of the degree of interaction between the two spins in the singlet species as discussed previously. Also shown is the relative energy between the singlets for each DDP isomer (Figure 4.3).

Figure 4.3. Relative energies for the singlet diradicals (**red**) and $\Delta E_{S\text{-}T}$ energy splitting (**blue**) of all nine didehydropentalene (DDP) species. All values in kcal/mol calculated at CASMP2/6-31G(d)//CASSCF(10,10)/6-31G(d).

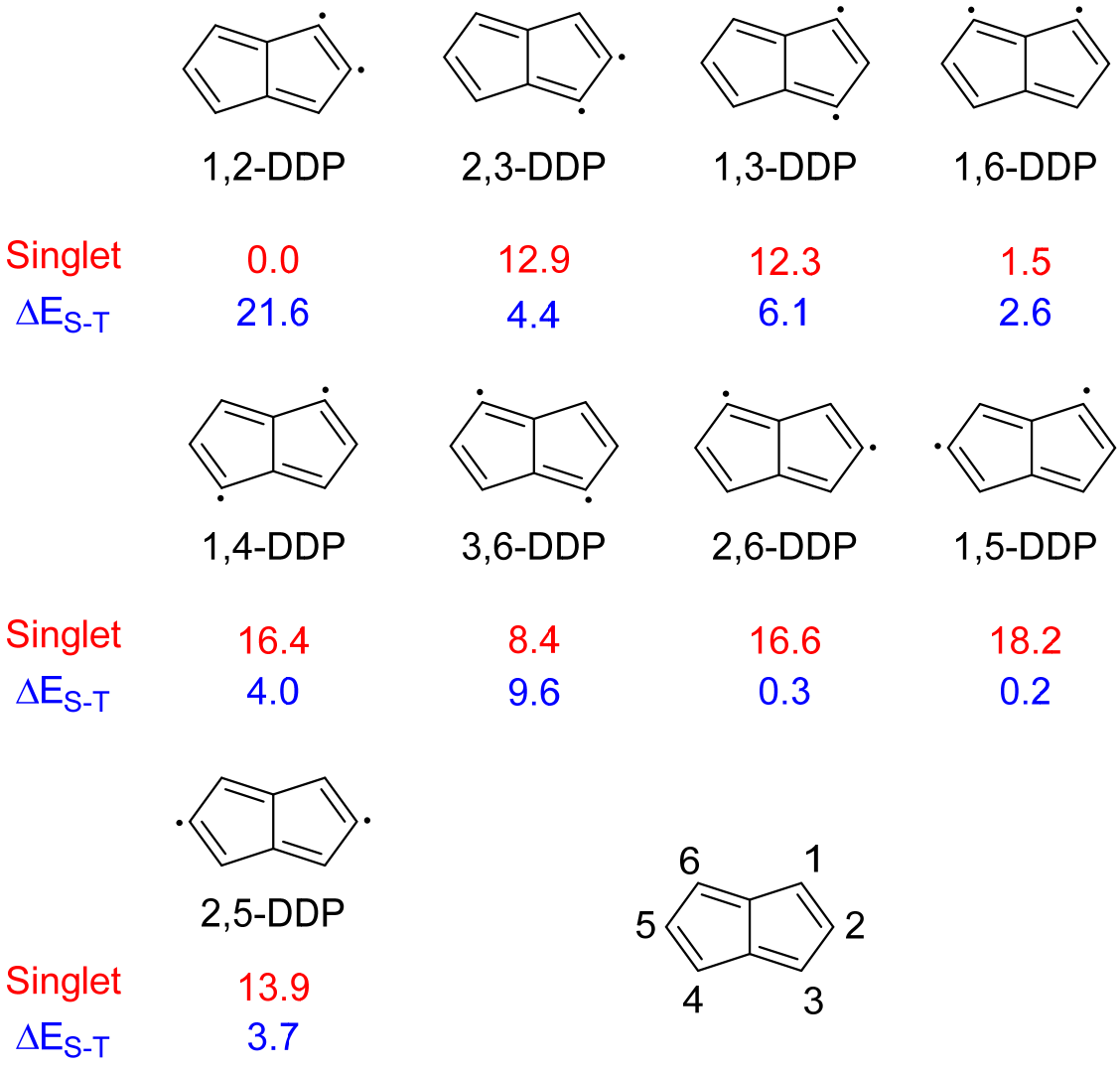

The first pair of singlet DDP isomers we will discuss are the 1,2-diradical species; 1,2-DDP and 2,3-DDP. As seen in previously studied arynes, the two adjacent orbitals overlap to form what is essentially a π bond (Figure 4.4). Unlike benzene, there is a high-degree of bond localization in pentalene due to its anti-aromatic character. Thus when comparing the change in

bond length from pentalene to the singlet diradical, 1,2-DDP demonstrates a much smaller change (decrease of 0.09 Å) because it is shortening the already shorter bond. For 2,3-DDP, the change in bond length is the most dramatic change of any of the DDP singlet diradicals at decrease of 0.126 Å.

Figure 4.4. Molecular orbitals depicting π-like bond formed from the through-space interaction of adjacent spins in 1,2-DDP (left) and 2,3-DDP (right).

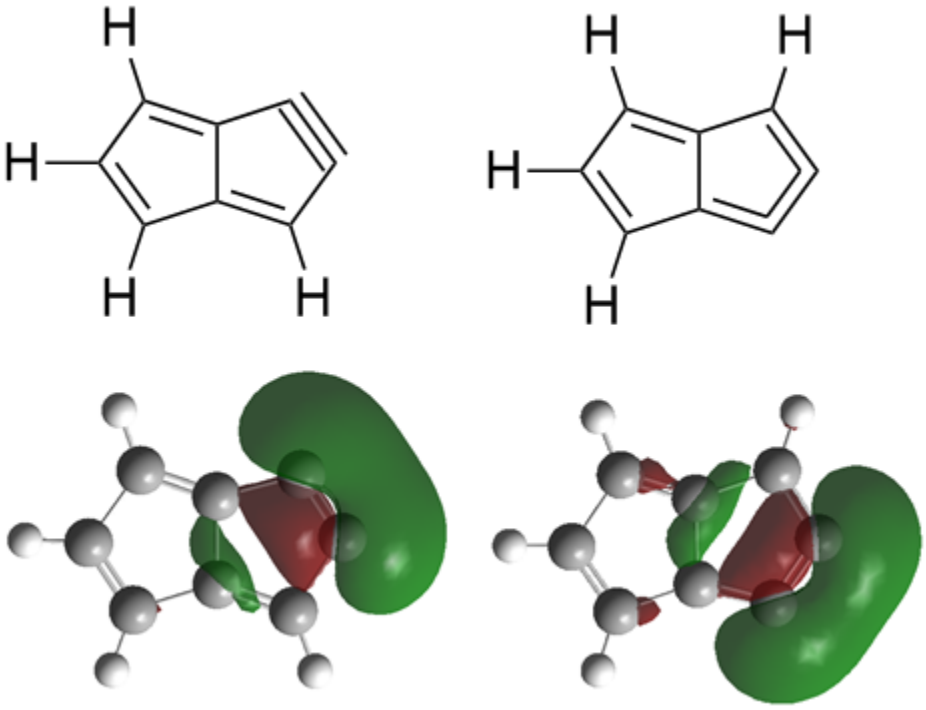

This direct through-space interaction is responsible for the increase in the $\Delta E_{S\text{-}T}$ splitting as well as the shortening of the intermediate bond, leading to a cumulenic structure for 2,3-DDP or triple-bond structure for 1,2-DDP. CASMP2 finds a significant difference between the $\Delta E_{S\text{-}T}$ splitting for 1,2-DDP and 2,3-DDP at 21.6 kcal/mol to 4.4 kcal/mol, respectively. In their study

of didehydronaphthalene, Squires *et al.* encountered a similar difference for 1,2-DDN and 2,3-DDN, as naphthalene also shows bond alternation (Figure 4.5).[16] Their CASPT2 calculations showed a larger $\Delta E_{S\text{-}T}$ splitting for 1,2-DDN (32.2 kcal/mol) than for 2,3-DDN (29.4 kcal/mol). They concluded for 1,2-DDN there is less distortion cost to shortening the already shorter 1,2 bond than for the longer 2,3-bond for the singlet diradical. The larger magnitude of this difference for 1,2-DDP and 2,3-DDP can be explained for two reasons. One is that due to the anti-aromaticity[41] of pentalene, the bond alternation is more pronounced than in naphthalene, with a 0.148 Å difference between the 1,2 and 2,3-bond lengths compared to 0.048 Å for naphthalene. Secondly, the smaller [5,5] bicyclic ring structure of pentalene creates greater ring strain from bond shortening compared to the [6,6] bicyclic structure of naphthalene. Both of these factors explain why 2,3-DDP has a much smaller $\Delta E_{S\text{-}T}$ splitting not only compared to 1,2-DDP, but to many similar arynes, such as *o*-benzyne (37.5 kcal/mol), 1,2-DDPh (34.9 kcal/mol) 9,10- DDPh (38.1 kcal/mol) and 1,2-DDN (32.2 kcal/mol).

Figure 4.5. Labeled positions of discussed didehydro species.

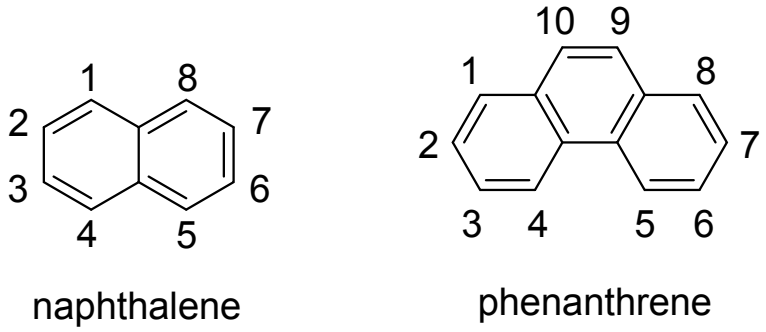

The singlet diradical 1,3-DDP is analogous to *m*-benzyne. Debate over the true form of *m*-benzyne, between a diradical or bicyclic structure was prevalent for some time. Sander and

coworkers were able to demonstrate that the structure is not bicyclic, but can be best thought of as a delocalized diradical structure shared across the three atoms.[11] Like similar diradical systems, through-space interactions of the back lobe of the radical orbitals, and through-bond interactions involving the intermediate C-H σ* bond allow for coupling of the two radical centers (Figure 4.7). Table 4.1 compares the ΔE_{S-T} splitting and several geometrical parameters between 1,3-DDP and several previously studied 1,3-diradicals. Though a mixture of experimental and several different theoretical methods, the ΔE_{S-T} splitting for the three 1,3-diradicals of six-membered rings generally ~20 kcal/mol. These diradicals are also consistent in the change in bond angle and distance between the radical centers, with that distance decreasing by 9-17%. For 1,3-DDP, which starts with a smaller radical-radical separation, the distance only changes by 2% between from pentalene to diradical. The degree of the ΔE_{S-T} splitting is also considerably smaller at only 6.1 kcal/mol. It seems that compared to the larger rings, 1,3-DDP is less able to take advantage of this orbital overlap due to ring strain.

Table 4.1. Comparison of geometric parameters of 1,3-diradicals to their parent arenes.

Species	Angle between C1 and C3 (degrees)	Distance between C1 and C3 (Å)	Percent change in distance	ΔE_{S-T} (kcal/mol)
benzene	120	2.42		
m-benzyne	100	2.10	13%	21.0[a]
naphthalene	120	2.42		
1,3-DDN	106	2.20	9%	17.2[b]
phenanthrene	-	2.43		
1,3-DDPh	-	2.00	17%	20.75[c]
pentalene	110	2.34		
1,3-DDP	105	2.29	2%	6.1[d]

a) CCSD(T)/6-311G-(2d,2p). b) CASPT2(12,12)/cc-pVDZ//CAS/cc-pVDZ. c) BLYP/6-31G(d). d) CASMP2(10,20)/6-31G(d)//CAS/6-31G(d).

In their study to elucidate the structure of *m*-benzyne, Sander and coworkers used scans of the C1-C3 bond distance to demonstrate the flat potential energy surface for these species.[11] Figure 4.6 shows the scan of the distance between radical centers for 1,3-DDP, as well as scans for *m*-benzyne and 1,3-DDN at CASSCF/6-31G(d). First comparing *m*-benzyne to 1,3-DDN, the singlet diradicals show nearly identical relative energy along the entire length of the scan. Negligible change in the interaction between the two radicals is seen from the addition of the additional ring in naphthalene. Comparing both *m*-benzyne and 1,3-DDN to 1,3-DDP, we see that all three species are nearly identical in the 2.1 to 2.4 Å region. This demonstrates that a similar level of through-space interaction is present in all three species, and the magnitude of this stabilizing interaction is also similar (the largest difference between all three in that region is 1.34 kcal/mol). The deviation between 1,3-DDP and the other 1,3-diradicals is demonstrated in the 1.4 to 2.0 Å region. All three species begin to rapidly increase in energy as the bond distance decreases and the diradical shifts to a bicyclic structure. The energy cost of this process is shown

to be higher for the five-membered pentalene ring. As 1,3-DDP already starts close to this optimal separation, the overall change in geometry is far less dramatic compared to the other 1,3-diradical species.

Figure 4.6. Scan between radical centers in several didehydro species on the singlet surface. All scans performed at CASSCF/6-31G(d) with the appropriate active space for each system to include all π-electrons and radicals.

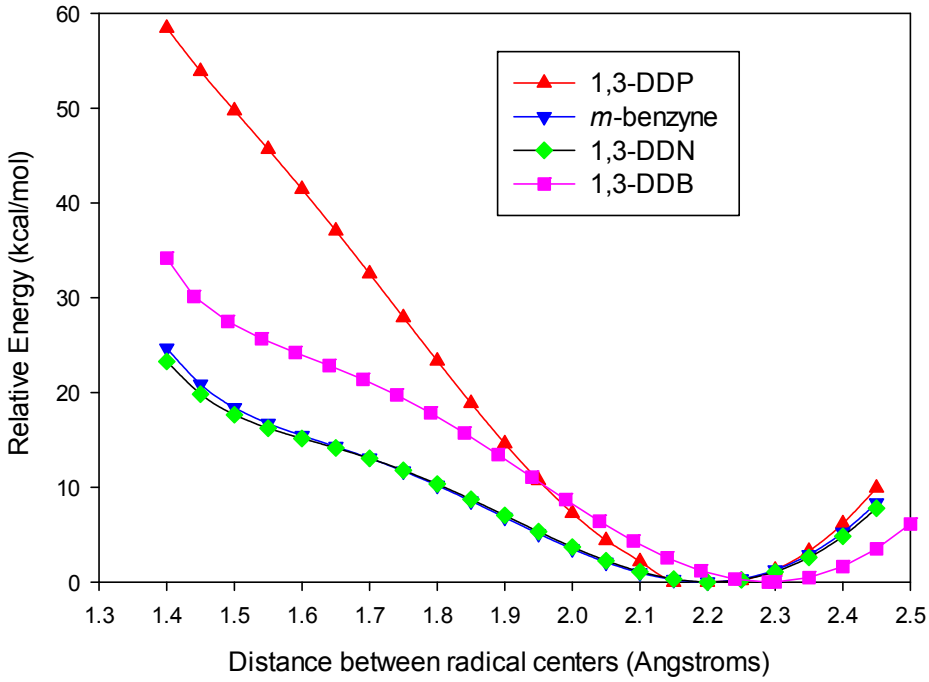

The singlet 1,6-DDP, another diradical with the two spins separated by three bonds, has a much smaller $\Delta E_{S\text{-}T}$ splitting of 2.6 kcal/mol. Due to the geometry of the diradical, no through-space interaction is possible between the two radical orbitals as presented in 1,3-DDP (Figure

4.7). A $\Delta E_{S\text{-}T}$ splitting of a similar magnitude is observed in the equivalent bicyclic arynes such as didehydrophenanthrene and didehydronaphthalene. NBO calculations show a small interaction between the two spins through donation to the C-C σ* orbital of the bridging carbon-carbon bond, though the overall magnitude of this interaction is less significant than the direct through-space interactions present in 1,3-DDP. Appropriately, the greatest change in geometry for 1,6-DDP is the shortening of the r_1 and r_8 bonds, and lengthening of the r_9 bridging bond (Table 4.S4).

Figure 4.7. Top: Molecular orbitals depicting through-space interaction in 1,3-DDP and the lack of through-space interaction in 1,3-DDP (left) compared to 1,6-DDP (right). Bottom: Orbitals depicting through-bond and through-space interactions.

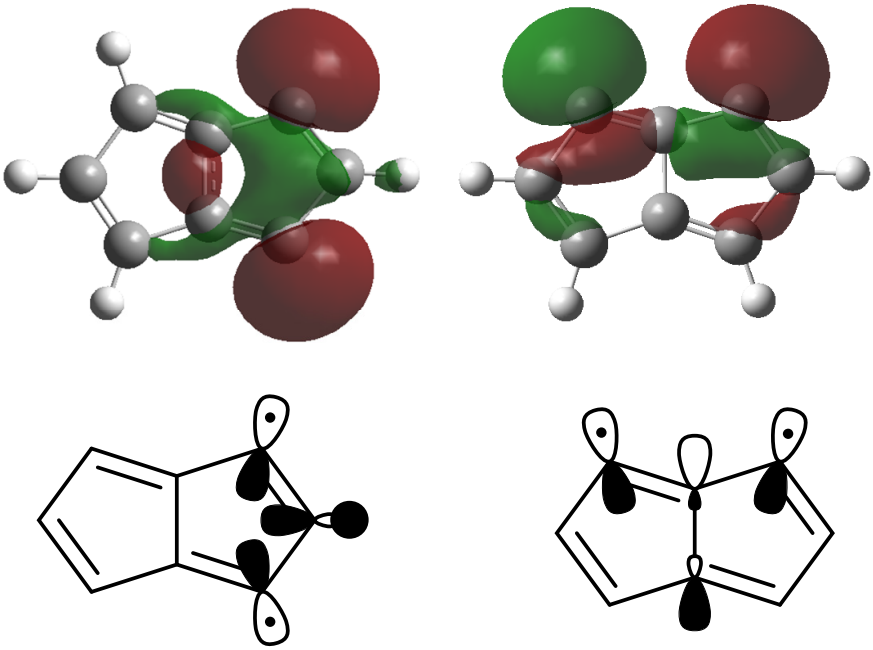

For two isomers of the DDP family, 1,5-DDP and 2,6-DDP, the differences between the singlet and triplet diradical geometry are negligible. Similarly, the singlet and triplet energies are nearly degenerate for both species. The similar geometry and small $\Delta E_{S\text{-}T}$ splitting for these diradicals are a result of the two spins being too distant for through-space coupling, while also lacking a convenient intermediate orbital for through-bond coupling. This is not the case for the other two long distance diradicals, 1,4-DDP and 3,6-DDP, with the two spins on opposite rings with the bridging C-C σ* bond mutually accessible. Both show a higher $\Delta E_{S\text{-}T}$ splitting of 4.0 kcal/mol and 9.6 kcal/mol at CASMP2. The $\Delta E_{S\text{-}T}$ splitting is similar to the equivalent 1,5-DDN species ($\Delta E_{S\text{-}T}$ splitting 7.7 kcal/mol) and 3,6-DDPh species (6.7 kcal/mol) studied previously. Cramer and Sola attributed the larger $\Delta E_{S\text{-}T}$ splitting to stabilizing through-bond coupling with the intermediate C-C σ* orbital (Figure 4.8).[16,17] The closest example from the benzyne family is the *p*-benzyne. While having the same through-bond interactions, *p*-benzyne suffers from destabilizing through-space interactions, and as a consequence has an experimentally determined $\Delta E_{S\text{-}T}$ splitting of 3.8 kcal/mol. In the bicyclic diradicals, the separation of the two spins on different rings removes this destabilizing interaction and explains the larger $\Delta E_{S\text{-}T}$ splitting.

Figure 4.8. Coupling in 1,4-diradicals.

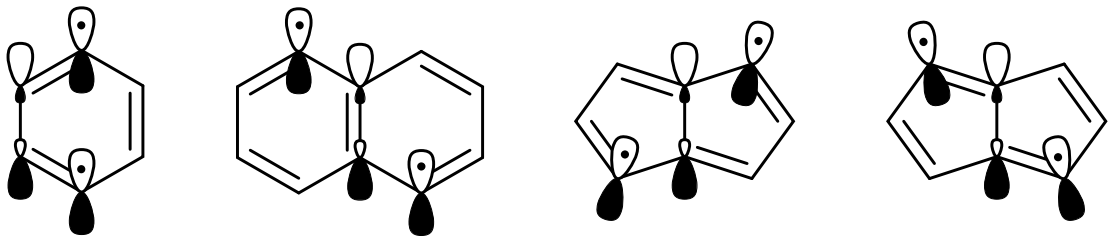

3.8[a] 7.8[b] 4.0[c] 9.6[c]

a) Experimental photoelectron spectroscopy[42]. b) [b]CASPT2(12,12)/cc-pVDZ//CAS/cc-pVDZ[16] c) CASMP2(10,20)/6-31G(d)//CAS/6-31G(d).

The difference in the $\Delta E_{S\text{-}T}$ splitting between 1,4-DDP and 3,6-DDP can be rationalized through NBO calculations, which shows the degree of donation between the two spins into the intermediate C-C anti-bonding orbital. Due to the bond localization present in pentalene, the distance between the two spins and the bridging bond is shorter in 3,6-DDP compared to 1,4-DDP by 0.120 Å. NBO calculations demonstrate a greater stabilization energy for this interaction of 10.7 kcal/mol compared to 8.0 kcal/mol due to increased orbital overlap from the stated differences in geometry. The relative differences are further reflected in the length of the bridging C-C bond, which lengthens by 0.026 Å in 3,6-DDP and by 0.015 Å in 1,4-DDP compared to the parent pentalene structure. This is a result of the increased donation of both radical centers to the C-C σ* orbital.

The remaining species, 2,5-DDP, shows non-negligible coupling between the two spins in the singlet state despite the largest distance separating them. Perhaps surprisingly, the CASMP2 $\Delta E_{S\text{-}T}$ splitting for 2,5-DDP was found to be 3.7 kcal/mol. "W-like" coupling is a well-known phenomenon in both NMR and EPR spectroscopy.[43,44] Squires *et al.* proposed for 2,7-

DDN that this W-framework also allows for good coupling between the two spins, leading to a $\Delta E_{S\text{-}T}$ splitting of 2.7 kcal/mol in their study.[45,46]

Didehydrobenzocyclobutadienes – Results

Benzocyclobutadiene, three monodehydrobenzocyclobutadienes, and nine DDB species, were successfully optimized using both B3LYP/6-31G(d) and CASSCF(10,10)/6-31G(d). Though the spin contamination in the DDB species is far less severe than in DDP (Table 4.S3), CASSCF and CASMP2 is still the more appropriate level of theory for these diradicals, and will again be the focus of our discussion. Though there is no experimental data for the structure of benzocyclobutadiene, the calculated CASSCF geometry for benzocyclobutadiene is consistent with previously reported calculations at MP2/cc-pVDZ[47] level, as well with the X-ray crystal structure of di-*tert*-butyltetramethylbenzocyclobutadiene (Figure 4.9).[29] While differences exist, the X-ray structure is of a very highly substituted benzocyclobutadiene. Due to strain induced by the annealed small ring, bond localization is seen in the benzene ring. This is phenomenon is known as the Mills-Nixon effect, and has been observed in many aromatic rings.[48,49] The resonance structure chosen is drawn to best represent this bond alternation in benzocyclobutadiene.

Figure 4.9. Bond lengths of benzocyclobutadiene and di-*tert*-butyltetramethylbenzocyclobutadiene.

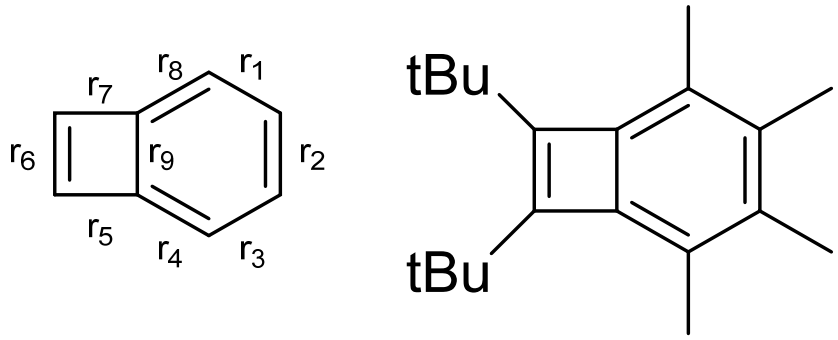

Bond	MP2/cc-pVDZ[a]	CASSCF(10,10)/6-31G(d)[b]	Experimental[c]
r_1	1.436	1.446	1.440
r_2	1.396	1.373	1.370
r_4	1.378	1.355	1.366
r_5	1.532	1.509	1.533
r_6	1.372	1.361	1.357
r_9	1.429	1.434	1.401

a) Ref. 44 b) This work c) Ref 26.

As seen in DDP, the triplet diradical species show little deviation from the parent benzocyclobutadiene structure, with the largest deviation in any C-C bond length being only 0.026 Å (Table 4.S5). The relative energy values compared between all triplet diradical species are within 3.5 kcal/mol of one another, with the exception of 5,6-DDB. In this structure the two spins are forced closest to one another by the short C5-C6 bond, causing the relative instability. A summary of the relative energies between singlet and triplet states is shown in Table 4.S2. The $\Delta E_{S\text{-}T}$ energy splitting and relative energy of the singlet species for all nine DDB isomers is shown below in Figure 4.10.

Figure 4.10. Relative energies for the singlet diradicals (**red**) and $\Delta E_{S\text{-}T}$ energy splitting (**blue**) of all nine didehydrobenzocyclobutadienes (DDB). All values in kcal/mol calculated at CASMP2/6-31G(d)//CASSCF(10,10)/6-31G(d).

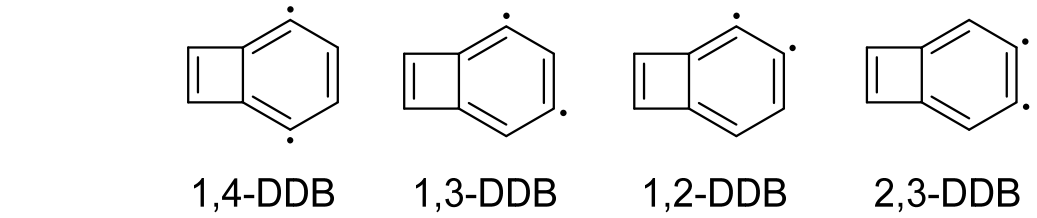

	1,4-DDB	1,3-DDB	1,2-DDB	2,3-DDB
Singlet	30.3	23.5	10.3	0.0
$\Delta E_{S\text{-}T}$	7.7	13.7	29.0	40.8

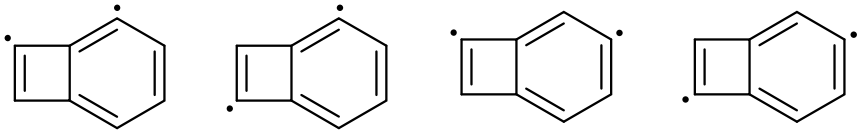

	1,6-DDB	1,5-DDB	2,6-DDB	2,5-DDB
Singlet	32.7	34.3	36.8	36.4
$\Delta E_{S\text{-}T}$	7.0	4.7	0.8	1.1

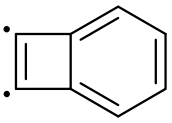

	5,6-DDB
Singlet	31.3
$\Delta E_{S\text{-}T}$	11.4

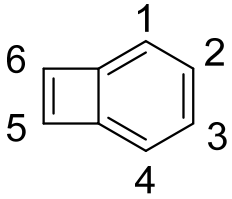

Of the nine isomers, two are 1,2-diradicals on the benzene ring; 1,2-DDB and 2,3-DDB. Comparing the $\Delta E_{S\text{-}T}$ energy splitting of benzene to these two DDB isomers using CASSCF/6-31G(d) calculations, the $\Delta E_{S\text{-}T}$ energy splitting for benzene is almost the exact average of the two (Table 4.2). This result can readily be explained by the difference in bond lengths. The

introduction of the four-membered ring causes bond localization in the parent six-membered ring, lengthening the C1-C2 bond and shortening the C2-C2 bond. The shorter distance between diradical centers allows for greater interaction between the two spins, and thus a larger $\Delta E_{S\text{-}T}$ energy splitting for 2,3-DDB.

Table 4.2. Comparison of singlet 1,2-diradicals. All data from CASSCF/6-31G(d) with the appropriate active space to include the full π system and radical centers.

Species	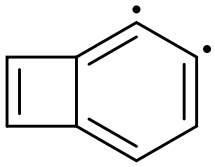	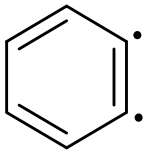	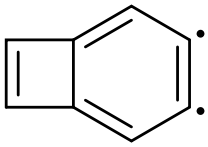
$\Delta E_{S\text{-}T}$ (kcal/mol)	26.2	33.4	37.9
Radical separation (Å)	1.286	1.259	1.250

The singlet diradical 5,6-DDB offers a unique example of a 1,2-diradical on a four-membered ring. As seen in DDP, a smaller ring size compared to six-membered rings led to a smaller $\Delta E_{S\text{-}T}$ energy splitting due to an increased ring strain associated with the coupling of the two spins. The same result is seen in 5,6-DDB. The $\Delta E_{S\text{-}T}$ splitting is found to be 11.4 kcal/mol at CASMP2; much smaller than the value for *o*-benzyne, 1,2-DDN, and 2,3-DDN.

The $\Delta E_{S\text{-}T}$ splitting for 5,6-DDB is much larger than 2,3-DDP (calc. 4.4 kcal/mol), despite the smaller ring size. This can be rationalized by comparing not just the size of the ring, but the overall change in bond length between the parent structure and the diradical. The overall change in bond length between benzocyclobutadiene and 5,6-DDB is very small at only 0.07 Å. In this instance, the large degree of stabilization from direct orbital overlap of the radicals is offset minimally from increased ring strain. In comparison, the change in bond length between

pentalene and 2,3-DDP is quite large (0.126 Å). As a result, the increased ring strain greatly diminishes the overall $\Delta E_{S\text{-}T}$ splitting. As mentioned earlier, the triplet 5,6-DDB is destabilized by the proximity of the two spins which also contributes to the large $\Delta E_{S\text{-}T}$ splitting.

Two DDB species are 1,3-diradicals: 1,3-DDB and 1,6-DDB. The $\Delta E_{S\text{-}T}$ splitting for 1,3-DDB is 13.7 kcal/mol at CASMP2, which is very similar to the value for *m*-benzyne of 14.8. The addition of the four-membered ring has a minimal impact on the energy of the singlet. The other singlet 1,3-diradical, 1,6-DDB, has a $\Delta E_{S\text{-}T}$ splitting of 7.0 kcal/mol at CASMP2. The larger value of the $\Delta E_{S\text{-}T}$ splitting came as a surprise, as the geometry of the diradical means there is only a weak through-bond coupling through the intermediate C-C σ* orbital of the bridging bond. The closest related species in this study is 1,6-DDP, which has a much lower $\Delta E_{S\text{-}T}$ splitting of 2.6 kcal/mol. In an attempt to evaluate this large discrepancy, NBO calculations were performed to measure the degree of donation to this orbital (Table 4.3). Unfortunately, NBO calculations show nearly identical total stabilization energies as result of donation of each radical to the C-C σ* orbital. One possible explanation could be the increased relief of ring strain of the four-membered ring compared to a five-membered ring in pentalene.

The NRT analysis of 1,6-DDB found a very small contribution (2.4%) of a resonance form depicting a bond between the two radical carbons. A depiction of the SOMO shows what could be some overlap between the back-lobe of one of the radical's nonbonding orbital with the other. However, the very small size of this contribution is not enough to explain the large difference in $\Delta E_{S\text{-}T}$ splitting, and is too close to the limits of the theory employed.

Table 4.3. Comparison of 1,3-diradicals on separate rings for DDB and DDP.

	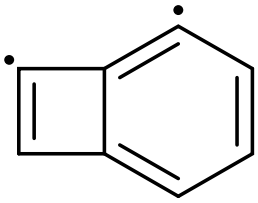	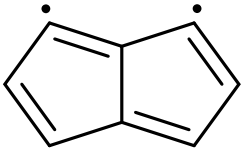
SOMO	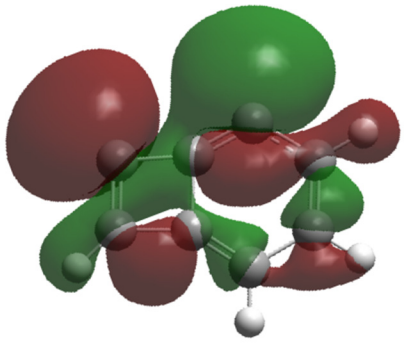	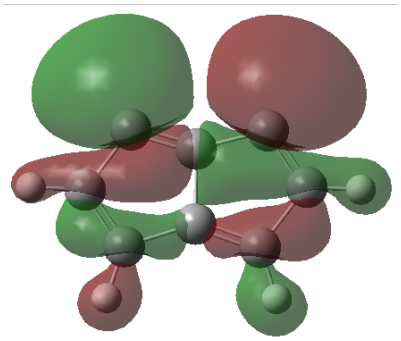
Change in bridge length (Å)[a]	+ 0.022	+ 0.010
Stabilization Energy (kcal/mol)[b]	6.90	6.74
$\Delta E_{S\text{-}T}$ splitting (kcal/mol)	7.0	2.6

a) Change in bond length of the singlet diradical compared to parent structure at CASSCF(10,10)/6-31G(d). b) Sum of stabilization energy from both spins to the intermediate C-C σ* orbital.

As done with pentalene, a scan of the distance between the carbon atoms containing the two spins was performed (Figure 4.6). The results are very similar to scans for 1,3-DDN and *m*-benzyne. Upon decreasing the distance, the slope for 1,3-DDB trends to higher relative energy more quickly than the other two arynes with a similar slope. The main difference demonstrated in 1,3-DDB is that the distance of the minimum structure is shifted by around 0.1 Å for 1,3-DDB compared to the others. This is in agreement with our understanding of the $\Delta E_{S\text{-}T}$ splitting of 1,3-DDB; though similar to that of *m*-benzyne, the $\Delta E_{S\text{-}T}$ splitting is slightly smaller due to less ideal orbital overlap.

The $\Delta E_{S\text{-}T}$ splitting for 1,4-DDB was found to be 7.7 kcal/mol. With no proper analogue in the DDP system, we compare the $\Delta E_{S\text{-}T}$ splitting using CASSCF of 1,4-DDB (5.9) to the equivalent diradicals of *p*-benzyne (5.3) and 1,4-DDN (5.6). As seen in 1,3-DDB, it appears that the four-membered ring has a small impact of these structures when both radical centers are located on the benzene ring. The other diradical with a 1,4-diradical separation is 1,5-DDB. Though located on different rings, a common C-C σ* orbital of the intermediate bridging bond allows for interactions between the two spins, and elevates the $\Delta E_{S\text{-}T}$ splitting to a significant non-zero value.

The remaining diradicals, 2,5-DDB and 2,6-DDB, show a $\Delta E_{S\text{-}T}$ splitting typical for two spins distantly separated across two rings. With no direct orbital overlap and no convenient pathways for donation into intermediate orbitals, the interaction between the two spins is very weak. Thus, these $\Delta E_{S\text{-}T}$ splitting values are the smallest of the DDB family with a calculated $\Delta E_{S\text{-}T}$ splitting of 0.8 and 1.1 kcal/mol at CASMP2. The lack of coupling is also evident from the small changes to the geometry of these diradicals, with the largest change in bond length for either of the two diradicals compared to benzocyclobutadiene only being 0.015 Å.

Throughout this chapter, we were able to rationalize the observed differences in the $\Delta E_{S\text{-}T}$ splittings for singlet 1,2-diradicals by comparing the impact of ring size and bond localization. Simply put, smaller rings incur a larger stability cost when decreasing any give bond length from higher ring strain. Bond alternation also has an impact on the $\Delta E_{S\text{-}T}$ splitting, as the energy cost is lower when decreasing the bond length of the already shorter bond. A summary of these results can be seen in Figure 4.11, using data from a wide variety of published studies and this work. Although these values are taken from different computational studies at various levels of theory, a generalized trend can still be seen. In general, larger rings are capable of larger

geometry changes upon formation of the diradical, and are more stabilized as a result. It is of great interest to the author to complete a larger study of a wider variety of arynes at a consistent and high level of theory. Currently, CASSCF and CASMP2 calculations of larger organic compounds such as phenanthrene are on the limits of practicality.

Figure 4.11. Comparison of singlet 1,2-diradicals across various arynes.

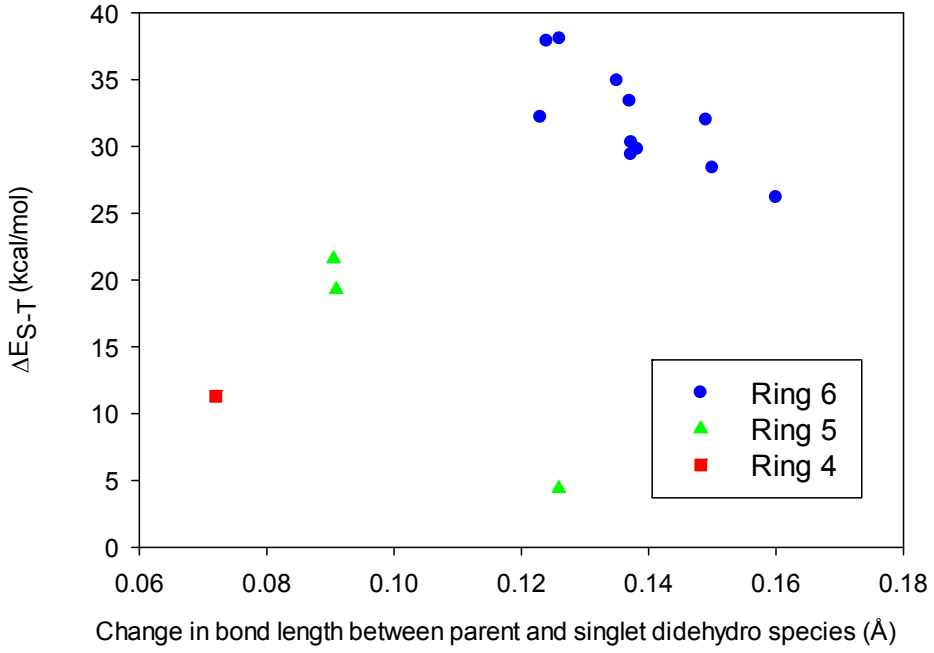

Summary

CASSCF and CASMP2 calculations were used to analyze all possible didehydropentalene and didehydrobenzocyclobutadiene isomers. Though B3LYP calculations were attempted, many of the singlet diradicals showed large amounts of spin contamination (a known problem with DFT methods) making the data unreliable. The $\Delta E_{S\text{-}T}$ splitting for all species is well understood through comparisons to previously studied patterns in through-space and through-bond interactions in benzyne, didehydronaphthalenes, and didehydrophenanthrenes.

The largest deviations can be rationalized from the decreasing ring size from six-membered rings to five- and four-membered rings. NBO and NRT calculations for several key species demonstrate trends in donation of spin density to intermediate anti-bonding orbitals that account for observed changes in geometry and $\Delta E_{S\text{-}T}$ splitting.

References

1. Wenk, H. H.; Winkler, M.; Sander, W. One century of aryne chemistry. *Angew. Chem., Int. Ed.* **2003**, *42*, 502-527.

2. Hoffmann, R.; Imamura, A.; Hehre, W. J. Benzynes, dehydroconjugated molecules, and the interaction of orbitals separated by a number of intervening sigma bonds. *J. Amer. Chem. Soc.* **1968**, *90*, 1499-1509.

3. Lee, M. D.; Ellestad, G. A.; Borders, D. B. Calicheamicins: discovery, structure, chemistry, and interaction with DNA. *Acc. Chem. Res.* **1991**, *24*, 235-243.

4. Schottelius, M. J.; Chen, P. 9,10-Dehydroanthracene: p-Benzyne-Type Biradicals Abstract Hydrogen Unusually Slowly. *J. Am. Chem. Soc.* **1996**, *118*, 4896-4903.

5. Wenthold, P. G.; Squires, R. R.; Lineberger, W. C. Ultraviolet Photoelectron Spectroscopy of the *o*-, *m*-, and *p*-Benzyne Negative Ions. Electron Affinities and Singlet−Triplet Splittings for *o*-, *m*-, and *p*-Benzyne. *J. Am. Chem. Soc.* **1998**, *120*, 5279-5290.

6. Jones, R. R.; Bergman, R. G. p-Benzyne. Generation as an intermediate in a thermal isomerization reaction and trapping evidence for the 1,4-benzenediyl structure. *J. Amer. Chem. Soc.* **1972**, *94*, 660-661.

7. Chapman, O. L.; Chang, C. C.; Kolc, J.; Rosenquist, N. R.; Tomioka, H. Photochemical method for the introduction of strained multiple bonds. Benzyne C≡C stretch. *J. Am. Chem. Soc.* **1975**, *97*, 6586-6588.

8. Marquardt, R.; Sander, W.; Kraka, E. 1,3-Didehydrobenzene (m-Benzyne). *Angew. Chem. Int. Ed.* **1996**, *35*, 746-748.

9. Marquardt, R.; Balster, A.; Sander, W.; Kraka, E.; Cremer, D.; Radziszewski, J. G. p-Benzyne. *Angew. Chem. Int. Ed.* **1998**, *37*, 955-958.

10. Sander, W.; Exner, M.; Winkler, M.; Balster, A.; Hjerpe, A.; Kraka, E.; Cremer, D. Vibrational Spectrum of m-Benzyne: A Matrix Isolation and Computational Study. *J. Am. Chem. Soc.* **2002**, *124*, 13072-13079.

11. Winkler, M.; Sander, W. The structure of meta-benzyne revisited-A close look into σ-bond formation. *J. Phys. Chem. A* **2001**, *105*, 10422-10432.

12. Davico, G. E.; Schwartz, R. L.; Ramond, T. M.; Lineberger, W. C. Photoelectron Spectroscopy of Benzoquinonide and Dehydrobenzoquinone Anions. *J. Am. Chem. Soc.* **1999**, *121*, 6047-6054.

13. Thoen, K. K.; Kenttämaa, H. I. Reactivity of a Substituted m-Benzyne Biradical. *J. Am. Chem. Soc.* **1999**, *121*, 800-805.

14. Thoen, K. K.; Kenttämaa, H. I. Synthesis and Characterization of Aromatic Biradicals in the Gas Phase: A meta-Benzyne with an Inert Positively Charged Substituent and Its ortho- and para-Isomers. *J. Am. Chem. Soc.* **1997**, *119*, 3832-3833.

15. Chakraborty, M.; Tessier, C. A.; Youngs, W. J. Unusual Formation of a Cyclyne Dimer and an Indenoindene Derivative. *J. Org. Chem.* **1999**, *64*, 2947-2949.

16. Squires, R. R.; Cramer, C. J. Electronic interactions in aryne biradicals. Ab initio calculations of the structures, thermochemical properties, and singlet-triplet splittings of the didehydronaphthalenes. *J. Phys. Chem. A* **1998**, *102*, 9072-9081.

17. Poater, J.; Bickelhaupt, F. M.; Solà, M. Didehydrophenanthrenes: Structure, Singlet−Triplet Splitting, and Aromaticity. *J. Phys. Chem. A.* **2007**, *111*, 5063-5070.

18. Johnson, W. T. G.; Cramer, C. J. Influence of Hydroxyl Substitution on Benzyne Properties. Quantum Chemical Characterization of the Didehydrophenols. *J. Am. Chem. Soc.* **2001**, *123*, 923-928.

19. Logan, C. F.; Chen, P. Ab Initio Calculation of Hydrogen Abstraction Reactions of Phenyl Radical and p-Benzyne. *J. Am. Chem. Soc.* **1996**, *118*, 2113-2114.

20. Hoffner, J.; Schottelius, M. J.; Feichtinger, D.; Chen, P. Chemistry of the 2,5-Didehydropyridine Biradical: Computational, Kinetic, and Trapping Studies toward Drug Design. *J. Am. Chem. Soc.* **1998**, *120*, 376-385.

21. Esselman, B. J.; Emmert, F. L.; Wiederhold, A. J.; Thompson, S. J.; Slipchenko, L. V.; McMahon, R. J. Thermal Isomerizations of Diethynyl Cyclobutadienes and Implications for Fullerene Formation. *J. Org. Chem.* **2015**, *80*, 11863-11868.

22. Nimlos, M. R.; Filley, J.; McKinnon, J. T. Hydrogen Atom Mediated Stone−Wales Rearrangement of Pyracyclene: A Model for Annealing in Fullerene Formation. *J. Phys. Chem. A.* **2005**, *109*, 9896-9903.

23. Alder, R. W.; Harvey, J. N. Radical-Promoted Stone−Wales Rearrangements. *J. Am. Chem. Soc.* **2004**, *126*, 2490-2494.

24. Kroto, H. W.; Allaf, A. W.; Balm, S. P. C60: Buckminsterfullerene. *Chem. Rev.* **1991**, *91*, 1213-1235.

25. Bally, T.; Chai, S.; Neuenschwander, M.; Zhu, Z. Pentalene: Formation, Electronic, and Vibrational Structure. *J. Am. Chem. Soc.* **1997**, *119*, 1869-1875.

26. Zilberg, S.; Haas, Y. Biradicals Stabilized by Intramolecular Charge Transfer: Properties of Heterosubstituted Pentalene and Cyclooctatetraene Biradicals. *J. Phys. Chem. A*. **2006**, *110*, 8397-8400.

27. Chapman, O. L.; Chang, C. C.; Rosenquist, N. R. Benzocyclobutadiene. *J. Am. Chem. Soc.* **1976**, *98*, 261-262.

28. Trahanovsky, W. S.; Fischer, D. R. Observation of benzocyclobutadiene by flow nuclear magnetic resonance. *J. Am. Chem. Soc.* **1990**, *112*, 4971-4972.

29. Winter, W.; Straub, H. Molecular Structure of a Benzocyclobutadiene. *Angew. Chem. Int. Ed.* **1978**, *17*, 127-128.

30. Vollhardt, K. P. C.; Yee, L. S. 1,2-Bis(trimethylsilyl)benzocyclobutadiene, a paratropic 8 π-electron system. *J. Am. Chem. Soc.* **1977**, *99*, 2010-2012.

31. Becke, A. D. Density-functional thermochemistry. III. The role of exact exchange. *J. Chem. Phys.* **1993**, *98*, 5648-5652.

32. Hariharan, P. C.; Pople, J. A. Influence of polarization functions on MO hydrogenation energies. *Theor. Chim. Acta* **1973**, *28*, 213-222.

33. Frisch, M. J.; Trucks, G. W.; Schlegel, H. B.; Scuseria, G. E.; Robb, M. A.; Cheeseman, J. R.; Scalmani, G.; Barone, V.; Mennucci, B.; Petersson, G. A.; Nakatsuji, H.; Caricato, M.; Li, X.; Hratchian, H. P.; Izmaylov, A. F.; Bloino, J.; Zheng, G.; Sonnenberg, J. L.; Hada, M.; Ehara, M.; Toyota, K.; Fukuda, R.; Hasegawa, J.; Ishida, M.; Nakajima, T.; Honda, Y.; Kitao, O.; Nakai, H.; Vreven, T.; Montgomery Jr., J. A.; Peralta, J. E.; Ogliaro, F.; Bearpark, M. J.; Heyd, J.; Brothers, E. N.; Kudin, K. N.; Staroverov, V. N.; Kobayashi, R.; Normand, J.; Raghavachari, K.; Rendell, A. P.; Burant, J. C.; Iyengar, S. S.; Tomasi, J.; Cossi, M.; Rega, N.; Millam, N. J.; Klene, M.; Knox, J. E.; Cross, J. B.; Bakken, V.; Adamo, C.; Jaramillo, J.; Gomperts, R.; Stratmann, R. E.; Yazyev, O.; Austin, A. J.; Cammi, R.; Pomelli, C.; Ochterski, J. W.; Martin, R. L.; Morokuma, K.; Zakrzewski, V. G.; Voth, G. A.; Salvador, P.; Dannenberg, J. J.; Dapprich, S.; Daniels, A. D.; Farkas, Ö.; Foresman, J. B.; Ortiz, J. V.; Cioslowski, J.; Fox, D. J.; *Gaussian 09; Revision B.1*, 2009.

34. Borden, W. T.; Davidson, E. R. Singlet-Triplet Energy Separations in Some Hydrocarbon Diradicals. *Annu. Rev. Phys. Chem.* **1979**, *30*, 125-153.

35. Squires, R. R.; Cramer, C. J. Electronic Interactions in Aryne Biradicals. Ab Initio Calculations of the Structures, Thermochemical Properties, and Singlet−Triplet Splittings of the Didehydronaphthalenes. *J. Phys. Chem. A.* **1998**, *102*, 9072-9081.

36. Glendening, E. D.; Badenhoop, J. K.; Reed, A. E.; Carpenter, J. E.; Bohmann, J. A.; Morales, C. M.; Landis, C. R.; Weinhold, F. A. *NBO 6.0*. Theoretical Chemistry Institute: University of Wisconsin, Madison, 2013.

37. Glendening, E. D.; Weinhold, F. Natural resonance theory: II. Natural bond order and valency. *J. Comput. Chem.* **1998**, *19*, 610-627.

38. Glendening, E. D.; Weinhold, F. Natural resonance theory: I. General formalism. *J. Comput. Chem.* **1998**, *19*, 593-609.

39. Glendening, E. D.; Badenhoop, J. K.; Weinhold, F. Natural resonance theory: III. Chemical applications. *J. Comput. Chem.* **1998**, *19*, 628-646.

40. Aguirre-Etcheverry, P.; O'Hare, D. Electronic Communication through Unsaturated Hydrocarbon Bridges in Homobimetallic Organometallic Complexes. *Chem. Rev.* **2010**, *110*, 4839-4864.

41. Schleyer, P. v. R.; Maerker, C.; Dransfeld, A.; Jiao, H.; van Eikema Hommes, N. J. R. Nucleus-independent chemical shifts: a simple and efficient aromaticity probe. *J. Am. Chem. Soc.* **1996**, *118*, 6317-6318.

42. Wenthold, P. G.; Squires, R. R.; Lineberger, W. C. Ultraviolet Photoelectron Spectroscopy of the *o*-, *m*-, and *p*-Benzyne Negative Ions. Electron Affinities and Singlet-Triplet Splittings for *o*-, *m*-, and *p*-Benzyne. *J. Am. Chem. Soc.* **1998**, *120*, 5279-5290.

43. Sternhell, S. Correlation of interproton spin-spin coupling constants with structure. *Quart. Rev. Chem. Soc.* **1969**, *23*, 236-270.

44. King, F. W. Long-range proton hyperfine coupling. *Chem. Rev.* **1976**, *76*, 157-186.

45. Cramer, C. J.; Squires, R. R. Prediction of Singlet-Triplet Splittings for Aryne Biradicals from ^{1}H Hyperfine Interactions in Aryl Radicals. *J. Phys. Chem. A* **1997**, *101*, 9191-9194.

46. Cramer, C. J.; Squires, R. R. Prediction of Singlet−Triplet Splittings for Aryne Biradicals from ^{1}H Hyperfine Interactions in Aryl Radicals. *J. Phys. Chem. A.* **1997**, *101*, 9191-9194.

47. Despotović, I.; Eckert-Maksić, M.; Maksić, Z. B.; Smith, D. M. In Pursuit of the Elusive Bond-Stretch Isomers by ab Initio Methods. Benzocyclobutene, Benzo[1,2:4,5] dicyclobutadiene, and Some Related Substituted Systems. *J. Phys. Chem. A.* **2003**, *107*, 10396-10405.

48. Stanger, A. Is the Mills Nixon effect real? *J. Am. Chem. Soc.* **1991**, *113*, 8277-8280.

49. Sadana, A. K.; Saini, R. K.; Billups, W. E. Cyclobutarenes and Related Compounds. *Chem. Rev.* **2003**, *103*, 1539-1602.

Supporting Information

Chapter 4: Diradicals on the C_8H_4 Potential Energy Surface

Includes the work of a collaborator:

Brian Esselman

Figure 4.S1. Early results of a B3LYP/6-31G(d) study. All energies in kcal/mol. A (-) indicates that no minimum was found.

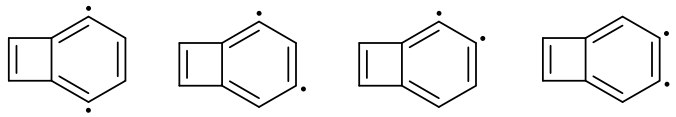

	1,4-DDB	1,3-DDB	1,2-DDB	2,3-DDB
Singlet	-	28.9	13.3	8.4
(Triplet)	(35.8)	(53.6)	(35.1)	(40.6)

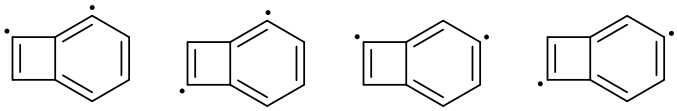

	1,6-DDB	1,5-DDB	2,6-DDB	2,5-DDB
Singlet	37.4	42.1	47.5	48.8
(Triplet)	(36.9)	(36.3)	(35.3)	(35.0)

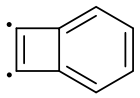

	5,6-DDB
Singlet	-
(Triplet)	(41.4)

Table 4.S1. Relative energy of all didehydropentalene species at various levels of theory. All energies in kcal/mol relative to singlet 2,3-DDP including ZPVE. CASMP2 values are single-point energy calculations on the CASSCF optimized structure.

	B3LYP/6-31G(d)		CASSCF(10,10)/ 6-31G(d)		CASMP2//CASSCF(10,10)/ 6-31G(d)	
Species	Singlet	Triplet	Singlet	Triplet	Singlet	Triplet
1,2-DDP	0.0	9.0	0.0	20.1	0.0	21.6
1,3-DDP	2.7	6.4	10.7	17.8	12.3	18.4
1,4-DDP	6.6	9.2	16.4	18.9	16.4	20.3
1,5-DDP	7.0	9.5	16.8	17.6	18.2	18.4
1,6-DDP	5.9	7.8	16.4	17.9	16.2	18.8
2,3-DDP	2.4	8.4	12.4	16.9	12.9	17.3
2,5-DDP	6.4	6.3	14.5	16.5	13.9	17.6
2,6-DDP	6.2	7.6	15.7	16.8	16.6	16.9
3,6-DDP	0.2	7.7	10.6	17.7	8.4	18.0

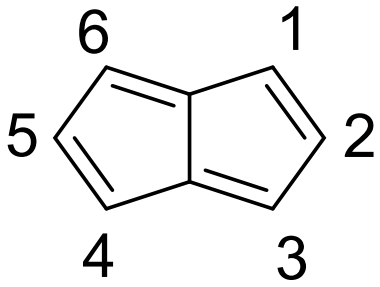

Table 4.S2. Relative energy of all didehydrobenzocyclobutadiene species at various level of theory. All energies in kcal/mol relative to singlet 2,3-DDB including ZPVE. CASMP2 values are single-point energy calculations on the CASSCF optimized structure.

	B3LYP/6-31G(d)		CASSCF(10,10)/ 6-31G(d)		CASMP2//CASSCF(10,10)/ 6-31G(d)	
Species	Singlet	Triplet	Singlet	Triplet	Singlet	Triplet
1,2-DDB	4.9	29.4	10.7	36.9	10.3	39.3
1,3-DDB	18.2	26.2	23.5	35.3	23.5	37.2
1,4-DDB	20.0	27.4	30.6	36.5	30.3	38.0
1,5-DDB	24.5	28.0	33.8	38.2	34.3	39.0
1,6-DDB	24.5	28.0	33.8	38.4	32.7	39.8
2,3-DDB	0.0	36.4	0.0	37.9	0.0	40.8
2,5-DDB	25.2	26.6	35.9	36.1	36.4	37.5
2,6-DDB	25.8	27.0	35.3	36.5	36.8	37.6
5,6-DDB	26.2	33.0	30.5	41.8	31.3	42.8

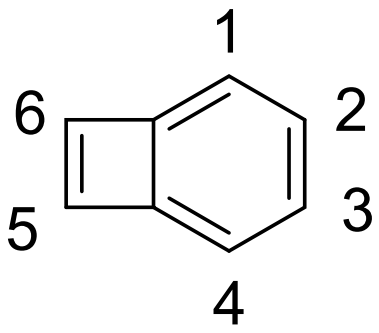

Table 4.S3. $\langle \hat{S}^2 \rangle$values calculated for B3YLP/6-31G(d) structures.

Species	Singlet	Triplet
1,2-DDP	0.539	2.001
1,3-DDP	0.107	2.006
1,4-DDP	0.279	2.013
1,5-DDP	3.093	2.000
1,6-DDP	0.471	2.006
2,3-DDP	2.929	2.001
2,5-DDP	0.159	2.144
2,6-DDP	0.426	2.000
3,6-DDP	0.249	2.000

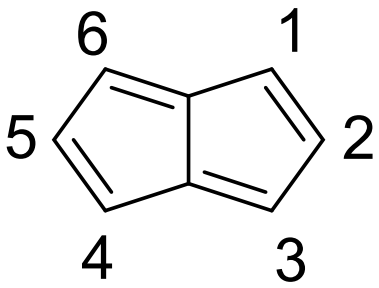

Species	Singlet	Triplet
1,2-DDB	0.000	2.000
1,3-DDB	0.028	2.001
1,4-DDB	0.249	2.000
1,5-DDB	0.426	2.000
1,6-DDB	0.090	2.000
2,3-DDB	0.000	2.000
2,5-DDB	0.141	2.001
2,6-DDB	0.471	2.000
5,6-DDB	0.185	2.000

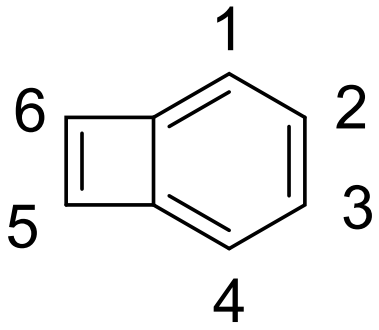

Table 4.S4. Bond lengths for pentalene, monodehydropentalenes, and all singlet and triplet didehydropentalene species.

	Bond Lengths (Å) CASSCF(8,8)/6-31G(d) and CASSCF(9,9)/6-31G(d)		
Bond	**pentalene**	**1-dehydropentalene**	**2-dehydropentalene**
r_1	1.473	1.474	1.468
r_2	1.357	1.354	1.358
r_3	1.500	1.491	1.498
r_4	1.352	1.353	1.353
r_5	1.473	1.474	1.468
r_6	1.357	1.354	1.358
r_7	1.352	1.353	1.353
r_8	1.352	1.353	1.353
r_9	1.469	1.474	1.473

	Singlet Bond Lengths (Å) at CASSCF(10,10)/6-31G(d)								
Bond	**1,2-DDP**	**1,3-DDP**	**1,4-DDP**	**1,5-DDP**	**1,6-DDP**	**2,3-DDP**	**2,5-DDP**	**2,6-DDP**	**3,6-DDP**
r_1	1.475	1.429	1.458	1.468	1.476	1.494	1.481	1.475	1.469
r_2	1.267	1.340	1.352	1.358	1.357	1.362	1.349	1.359	1.359
r_3	1.495	1.502	1.504	1.489	1.491	1.374	1.491	1.490	1.488
r_4	1.365	1.357	1.352	1.352	1.341	1.359	1.355	1.352	1.339
r_5	1.473	1.469	1.458	1.466	1.463	1.465	1.481	1.463	1.469
r_6	1.358	1.360	1.352	1.356	1.351	1.360	1.349	1.358	1.359
r_7	1.502	1.500	1.504	1.498	1.498	1.501	1.491	1.491	1.488
r_8	1.347	1.352	1.352	1.357	1.356	1.352	1.355	1.353	1.339
r_9	1.481	1.445	1.484	1.481	1.479	1.484	1.474	1.481	1.495

	Triplet Bond Lengths (Å) at CASSCF(10,10)/6-31G(d)								
Bond	**1,2-DDP**	**1,3-DDP**	**1,4-DDP**	**1,5-DDP**	**1,6-DDP**	**2,3-DDP**	**2,5-DDP**	**2,6-DDP**	**3,6-DDP**
r_1	1.476	1.465	1.471	1.476	1.474	1.475	1.472	1.474	1.465
r_2	1.357	1.356	1.36	1.358	1.359	1.267	1.356	1.354	1.354
r_3	1.497	1.492	1.490	1.491	1.491	1.495	1.489	1.491	1.502
r_4	1.348	1.350	1.350	1.348	1.347	1.365	1.355	1.352	1.353
r_5	1.469	1.466	1.471	1.471	1.459	1.473	1.472	1.465	1.465
r_6	1.357	1.359	1.360	1.355	1.355	1.358	1.356	1.353	1.354
r_7	1.497	1.497	1.490	1.489	1.502	1.502	1.489	1.503	1.502
r_8	1.354	1.351	1.350	1.354	1.355	1.347	1.355	1.355	1.353
r_9	1.478	1.484	1.476	1.478	1.478	1.481	1.48	1.478	1.477

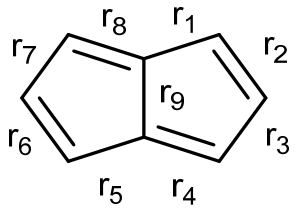

Table 4.S5. Bond lengths for benzocyclobutadiene, three monodehydrobenzocyclobutadienes (MDB), and all singlet and triplet didehydrobenzocyclobutadiene species.

	Bond Lengths (Å) CASSCF(8,8)/6-31G(d) and CASSCF(9,9)/6-31G(d)			
Bond	**benzocyclobutadiene**	**1-MDB**	**2- MDB**	**5-MDB**
r_1	1.446	1.434	1.434	1.445
r_2	1.374	1.376	1.363	1.374
r_3	1.446	1.448	1.451	1.445
r_4	1.355	1.356	1.357	1.353
r_5	1.509	1.509	1.508	1.505
r_6	1.361	1.362	1.361	1.360
r_7	1.509	1.505	1.509	1.511
r_8	1.355	1.345	1.358	1.357
r_9	1.434	1.440	1.437	1.435

	Singlet Bond Lengths (Å) at CASSCF(10,10)/6-31G(d)								
Bond	**1,2-DDB**	**1,3-DDB**	**1,4-DDB**	**1,5-DDB**	**1,6-DDB**	**2,3-DDB**	**2,5-DDB**	**2,6-DDB**	**3,6-DDB**
r_1	1.286	1.438	1.426	1.436	1.435	1.442	1.431	1.434	1.440
r_2	1.375	1.357	1.389	1.372	1.373	1.250	1.361	1.364	1.380
r_3	1.444	1.427	1.426	1.449	1.449	1.442	1.452	1.448	1.440
r_4	1.373	1.363	1.336	1.351	1.357	1.364	1.354	1.360	1.356
r_5	1.524	1.512	1.502	1.493	1.492	1.508	1.509	1.507	1.538
r_6	1.360	1.361	1.360	1.366	1.360	1.359	1.357	1.361	1.289
r_7	1.513	1.511	1.502	1.485	1.501	1.508	1.514	1.508	1.538
r_8	1.364	1.347	1.336	1.350	1.325	1.364	1.363	1.355	1.356
r_9	1.424	1.428	1.473	1.460	1.456	1.455	1.435	1.440	1.403

	Triplet Bond Lengths (Å) at CASSCF(10,10)/6-31G(d)								
Bond	**1,2-DDB**	**1,3-DDB**	**1,4-DDB**	**1,5-DDB**	**1,6-DDB**	**2,3-DDB**	**2,5-DDB**	**2,6-DDB**	**3,6-DDB**
r_1	1.449	1.437	1.437	1.436	1.433	1.436	1.433	1.433	1.444
r_2	1.363	1.365	1.376	1.372	1.377	1.377	1.364	1.363	1.374
r_3	1.454	1.437	1.437	1.449	1.447	1.436	1.450	1.450	1.444
r_4	1.355	1.358	1.347	1.351	1.358	1.360	1.355	1.358	1.355
r_5	1.506	1.508	1.505	1.493	1.513	1.508	1.503	1.511	1.502
r_6	1.361	1.362	1.362	1.366	1.362	1.362	1.361	1.360	1.370
r_7	1.503	1.503	1.505	1.485	1.499	1.508	1.509	1.504	1.502
r_8	1.346	1.348	1.347	1.350	1.346	1.360	1.360	1.357	1.355
r_9	1.447	1.445	1.443	1.460	1.439	1.438	1.439	1.439	1.439

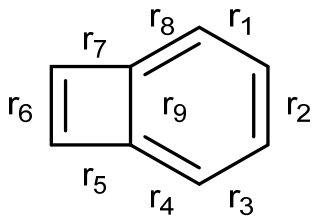

Chapter 5: Contributions of Theory to Studies of Highly Unsaturated Carbon Chains

Includes the work of several collaborators and publications:

Spectroscopy and Photochemistry of Triplet 1,3-Dimethylpropynylidene (Me–C–C–C–Me). Stephanie N. Knezz, Terese A. Waltz, Benjamin C. Haenni, Nicola J. Burrmann, and Robert J. McMahon. *Manuscript submitted*.

Reactive Carbon-Chain Molecules: Synthesis of 1-Diazohepta-2,4,6-triyne and Spectroscopic Characterization of Triplet HC_7H (H–C≡C−Ċ=C=Ċ−C≡C−H). Christopher J. Shaffer, Benjamin C. Haenni, John F. Stanton, and Robert J. McMahon. *Manuscript in preparation*.

Reactive Carbon-Chain Molecules: Synthesis of 1-Diazo-octa-2,4,6-triyne and Spectroscopic Characterization of Triplet MeC_7H (Me–C≡C−Ċ=C=Ċ−C≡C−H). Christopher J. Shaffer, Benjamin C. Haenni, John F. Stanton, and Robert J. McMahon. *Manuscript in preparation*.

Introduction

Highly unsaturated carbon species are of central importance in the study of organic compounds in harsh reaction environments, such as combustion,[1,2] planetary atmospheres,[3-5] and interstellar space.[6-8] For the series of linear carbon chain molecules, HC_nH, the electronic structure alternates from closed shell (n = even) to open shell (n = odd) as a function of carbon chain length (Scheme 5.1).[9] Although it is not possible to detect the carbon chains HC_nH in interstellar space by radioastronomy because they lack a permanent dipole moment, several members of the even series HC_nH (n = 2, 4, 6; acetylene, diacetylene, triacetylene) have been detected by infrared spectroscopy.[10] The likely existence of the series HC_nH (both even and odd) in space may be inferred from the detection of chemically related structures: the corresponding radicals (HC_n, n = 1-8), anions (HC_n^- n = 4, 6, 8), and C_nH_2 isomers of higher energy than linear HC_nH.

Scheme 5.1. Family of HC_nH Carbon Chains. Orbital sketch illustrates the Highest Occupied Molecular Orbital (HOMO) (one molecular orbital of a degenerate pair).

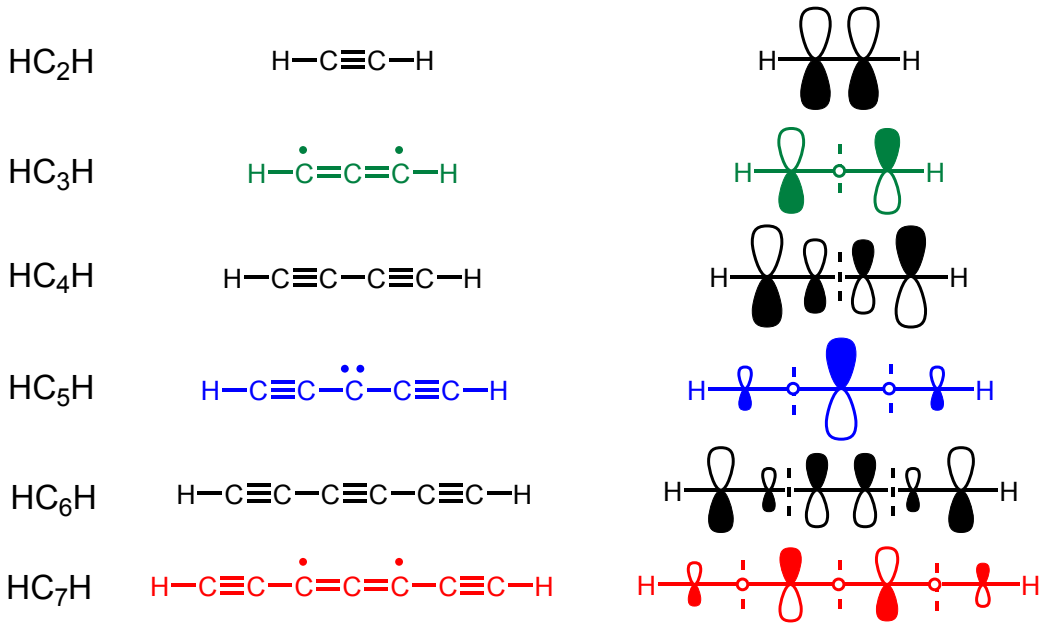

Computational chemistry plays an invaluable role in the study of these species. As opposed to generating these species through a discharge, in the McMahon group we approach these species from an organic synthetic route. Typically, a diazo precursor is trapped in a rare-gas matrix at cryogenic temperatures. From there, photolysis of the diazo compound can yield the carbene or diradical product. While in the matrix, the species can typically be studied by IR, UV/Vis, and EPR spectroscopy. To elucidate the nature of the species trapped in the matrix with only these techniques can be challenging or impossible. Thus, it is critically important to use accurate computational methods to generate predicted spectra for comparison to experimental spectra to computer spectra, as well as to explore the potential energy surface to validate the predicted structure. It often requires a combination of many spectroscopic and theoretical results to properly study these compounds.

The following chapter shows how a wide variety of modern computational methods were used in conjunction with spectroscopy to study three members of the highly unsaturated carbon chain family. In each study, the combination of theory and experiment was critical in developing a proper understanding of these systems. We will focus on the computational work done for three different carbon chains; HC_7H, MeC_7H,[11] and MeC_3Me.[12,13]

Computational Methods

Across all three studies, the B3LYP[14] density functional was used to optimize the geometries of most species. Coupled-cluster methodologies, both including a perturbative treatment of triplet excitations and without (CCSD(T) and CCSD, respectability),[15] were utilized to perform geometry optimizations. Harmonic vibrational frequency calculations were used to ensure the nature of all stationary points on the potential energy surface, as well as for

comparison to experimental IR spectra. Several basis sets were employed in this study, including 6-31G(d),[16] the correlation-consistent cc-pVDZ and cc-pVTZ basis sets,[17] and ANO1.[18] The DFT and lower level coupled-cluster calculations were obtained using the Gaussian 09 software package,[19] whereas the higher level coupled-cluster calculations were done in the frozen-core approximation using the CFOUR software package.[20] Geometry optimization and harmonic vibrational frequency calculation for excited states of HC_7H and MeC_7H were performed using equation-of-motion coupled-cluster calculations (EOM-CCSD) with the ANO1 basis set. Vibrational structure in the electronic transition was computed using a Franck-Condon simulation that includes Duschinsky mixing, as implemented in the FCFast program.[21] All Natural Bond Orbital (NBO) and Natural Resonance Theory (NRT) calculations were performed with NBO 6.0[22] as implemented in Gaussian 09.

Results and Discussion

Relative energies on the C_7H_2, C_8H_4, and C_5H_6 potential energy surfaces

Figure 5.1 shows the relative energies for each of the species studied in the current investigations. The relative energies provide some evidence for the possibility of observing a given isomer after generating the diradical or carbene from photolysis of the diazo precursor. If an isomer is much higher in energy than the other isomers, it would be unexpected to observe that isomer in the matrix. Previous studies on a variety of potential energy surfaces have proven these computational methods effective for the study of carbene and cumulene isomers.[23-25] Our results are in poor agreement with several[26-28] earlier studies, as many density functional methods exhibit a significant bias in over-emphasizing delocalized structures, which is highly problematic in conjugated organic structures of the type considered in this investigation.[24,29,30] The linear

triplet ^{3}**1** was found to be the lowest energy isomer at CCSD(T)/cc-pVTZ on the C_7H_2 surface. On both the C_8H_4 and C_5H_6 potential energy surfaces, a very stable enetriyne (**13**) and enyne (**17**) isomer is present around 30 kcal/mol lower in energy than the next most stable isomer. In both cases, these isomers are observed experimentally upon photoexcitation of triplet ^{3}**9** and ^{3}**15**, respectively.[12,31] Comparison of the C_7H_2 and C_8H_4 relative energies show only a small impact from methyl substitution. Overall, Figure 5.1 represents an impressive amount of work spanning nearly a decade and hundreds of hours of calculations on the PHOENIX cluster.

Figure 5.1. Relative energies of the isomers on the potential energy surfaces studied (kcal/mol, ZPVE and frozen-core approximation included). C_7H_2 and C_8H_4 energies at CCSD(T)/cc-pVTZ. C_5H_6 energies at CCSD/cc-pVDZ.

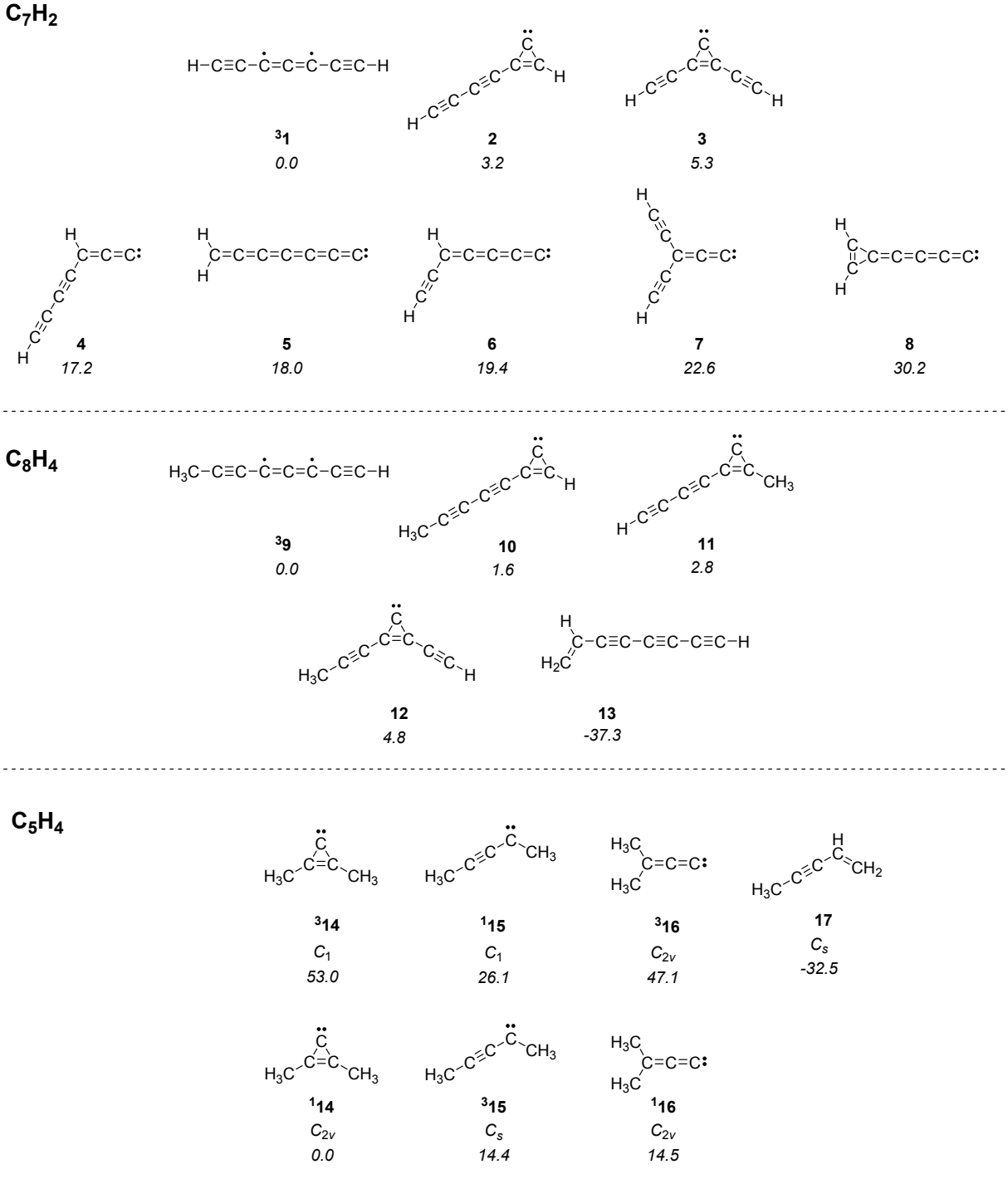

Structure of Triplet Diradical Species – Electronic Structure and NBO / NRT calculations

Computed structural data for triplet HC_7H (^{3}**1**) and triplet MeC_7H (^{3}**9**) are shown in Table 5.1. Methyl substitution has little impact on the bond lengths of the carbon chain, and both exhibit a bond-length alternation pattern indicative of a 1,3-allenic diradical. For both species, the carbon backbone is linear ($D_{\infty h}$ for ^{3}**1** and C_{3v} for ^{3}**9**). The apparent importance of the 1,3-allenic diradical structure, which is reminiscent of the structure of triplet HC_3H (C_2),[23,32] prompted us to consider the whether HC_7H (**1**) should be considered a 'diethynyl substituted' version of HC_3H. Geometry optimization, using an input structure based upon the C_2-symmetry structure of HC_3H with the hydrogen substituents replaced with ethynyl substituents, converged to a structure that formally possesses C_2 symmetry. The deviations from $D_{\infty h}$ symmetry, however, are vanishingly small (< 0.02°), the C_2 and $D_{\infty h}$ structures are equal in energy, and in all respects, the structures are indistinguishable. We interpret the computational data as predicting a $D_{\infty h}$ structure for triplet HC_7H (^{3}**1**).

Table 5.1. Computed structural parameters for triplet HC_7H (^{3}**1**) and MeC_7H (^{3}**9**).[a]

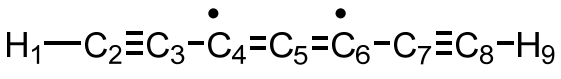

Parameter	$D_{\infty h}$
r [H1-C2]	1.064
r [C2-C3]	1.227
r [C3-C4]	1.339
r [C4-C5]	1.275
r [C5-C6]	1.275
r [C6-C7]	1.339
r [C7-C8]	1.227
r [C8-H9]	1.064

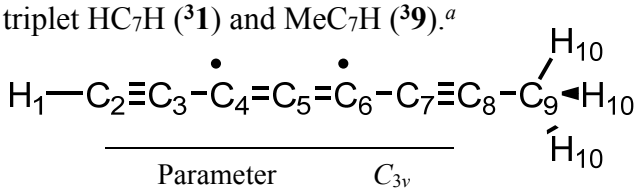

Parameter	C_{3v}
r [H1-C2]	1.064
r [C2-C3]	1.228
r [C3-C4]	1.338
r [C4-C5]	1.277
r [C5-C6]	1.275
r [C6-C7]	1.339
r [C7-C8]	1.228
r [C8-C9]	1.461
r [C9-H10]	1.092
θ [C8-C9-H10]	110.522

[a] Bond length (r) in Ångstrom (Å), bond angle (θ) in degree; CCSD(T)/cc-pVTZ (fc).

Optimization of the geometry for triplet MeC_3Me (^{3}**15**) proved to be more challenging than expected. As demonstrated in Figure 5.2, the geometry of ^{3}**15** was very dependent on the method and level of theory employed. The geometry at B3LYP was found to be a D_3 structure, with a deviation from an idealized D_{3d} symmetry that was dependent on the basis set (Figure 5.2a). (Huang *et al.* reported D_{3d} for the optimized structure at B3LYP/6-311G(d,p).[33]) Our DFT studies find that D_{3d} and D_{3h} structures each exhibit one imaginary vibrational frequency. At the CCSD/cc-pVDZ level, the carbon chain is bent and adopts an unsymmetrical structure in which the methyl groups are nonequivalent (C_s geometry) (Figure 5.2b). At the highest level of theory employed in this study (CCSD(T)/ANO1), a further distortion involving the dihedral angle of one of the methyl groups relative to the CCC plane removes all symmetry (C_1 geometry) (Figure 5.2c).

Figure 5.2. Computed structures for triplet MeC_3Me (^{3}**15**) at various methods and basis sets. (a) B3LYP/6-31G(d) (D_3). (b) CCSD/cc-pVDZ (C_s). (c) CCSD(T)/ANO1 (C_1).

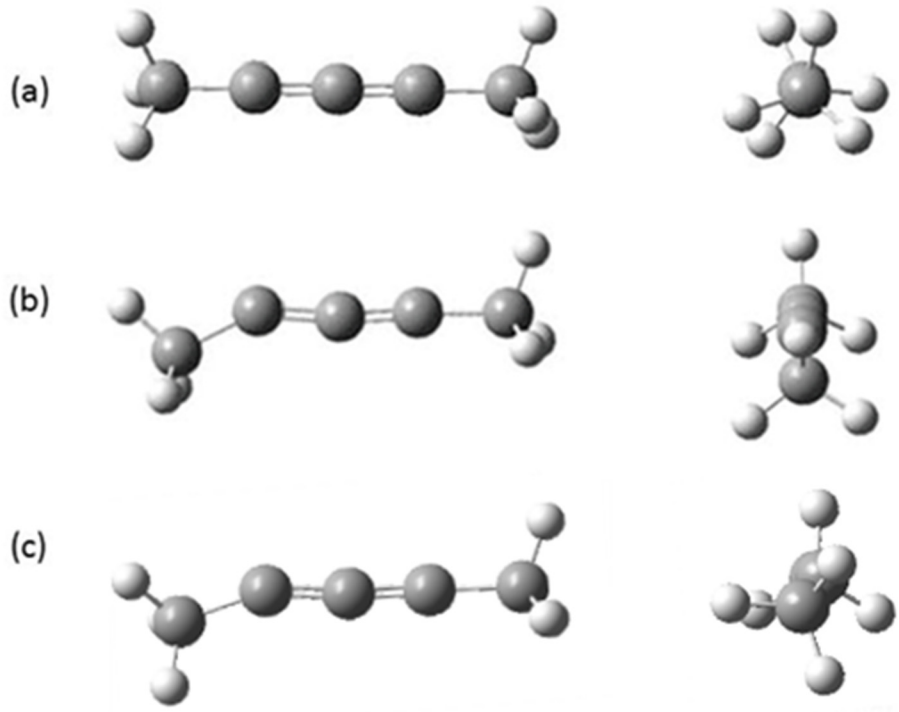

Coupled-cluster methods finding a bent, asymmetrical structure for ^{3}**15** came as quite a surprise. Prior experimental[11,23,34,35] and theoretical studies[36,37] establish symmetrical structures for HC_3H, HC_5H, and HC_7H. To properly assess the possibility of a symmetrical structure, optimizations constrained to D_3, D_{3h} or D_{3d} symmetry were performed. In each case, the structures exhibit five imaginary vibrational frequencies (two doubly-degenerate bends and one stretch), establishing that the computed energies of these structures represent upper limits for actual low-energy transition states on the potential energy surface. The D_3, D_{3h}, and D_{3d} structures are exceedingly close in energy to the fully-optimized C_1 structure (unsymmetrical carbene), lying only 0.2 kcal/mol (70 cm^{-1}) higher than the C_1 structure (Table 5.2). Upon inclusion of zero-point vibrational energy, the relative energies actually reverse; the high

symmetry structures lie 0.4 kcal/mol *lower* in energy than the C_1 structure. These calculations demonstrate that triplet MeC_3Me (**^{3}15**) resides on an exceptionally shallow portion of the potential energy surface.

Table 5.2. Computed Energies for Triplet MeC_3Me (**^{3}15**).[a]

Symmetry	N (*i*) [b]	E [c]	E (rel) [d]	E + ZPVE [c]	E + ZPVE (rel) [d]
C_1	0	-193.626328	0.00	-193.541322	0.00
D_3	5	-193.626001	0.21	-193.541975	-0.41
D_{3h}	5	-193.626000	0.21	-193.541975	-0.41
D_{3d}	5	-193.626003	0.20	-193.541573	-0.16

[a] CCSD(T)/ANO1; D_3, D_{3h}, D_{3d} geometry optimizations constrained to the given symmetry. [b] Number of imaginary vibrational frequencies. [c] Total energy in Hartree. [d] Relative energy in kcal/mol.

On the basis of the flat potential energy surface and the very low frequency vibrational mode (8 cm^{-1}, B3LYP/6-31G(d); 9 cm^{-1}, CCSD(T)/ANO1), as well as by analogy with related systems,[34,38,39] we infer that triplet MeC_3Me (**^{3}15**) is a quasilinear molecule.[40-44] This inference supports the interpretation of the IR spectrum, which will be disused below. Even though a sophisticated electronic structure calculation predicts an asymmetrical equilibrium structure for triplet MeC_3Me (**^{3}15**), the flatness of the potential energy surface affords a quasilinear structure.

To gain additional insight into the electronic structure of these highly delocalized triplet species, Natural Bond Orbital (NBO) and Natural Resonance Theory (NRT) calculations were performed. Figure 5.3 shows the dominant resonance structures for **^{3}1**, **^{3}9**, and **^{3}15**. For **^{3}1**, the

symmetrical diradical and carbenic resonance structures are the largest contributors at around 30%. Unlike HC_3H, the longer chain allows for other resonance forms, such as the unsymmetrical allenic 1,3 diradical resonance at 9%. The extension of the carbon chain leads to even more delocalization of the two spins compared to HC_3H. The addition of the methyl substituent in ^{3}**9** causes the two carbenes resonance structures to be non-degenerate. However, the total resonance weight of the main diradical and carbene resonance structures in MeC_7H ^{3}**9** is close to that seen in HC_7H ^{3}**1**. The major difference is the weight of the lesser diradical resonance, which is roughly double in MeC_7H ^{3}**9**. NBO calculations also show nearly identical spin densities along the carbon backbone, with the largest value at the carbon atoms on the major diradical resonance (Table 5.3). The high spin density on many of the carbon atoms, and the many resonance structures of similar weights, demonstrates the large degree of spin delocalization present in these systems.

The large difference in geometry of triplet MeC_3Me ^{3}**15** compared to the other species in this study is reflected in the NBO and NRT results. The unsymmetrical structure as a result of the methyl substitution causes an uneven weighing of the two possible carbene resonance forms. Interestingly, the balance between the diradical and major carbene resonance form is largely retained when compared to HC_7H and MeC_7H. Optimizations of the mono-methylated derivative MeC_3H were performed for comparison at CCSD/cc-pVDZ. The structure for triplet MeC_3H was found to be similar to that of ^{3}**15**, with an unsymmetrical structure (C_s point group, see Figure 5.S1). The first methyl addition is largely responsible for the change in geometry, and NBO / NRT results demonstrated very similar values as well (Figure 5.S2 and Table 5.S2).

The calculated spin density on the center three carbon atoms across all three studied triplets (bolded values in Table 5.3) are similar, despite differences in chain length and methyl

substitution. The largest difference is seen in C-7 of MeC_3Me. The bent geometry is responsible for more carbenic character at that position, leading to a larger spin density compared to the linear carbon chains.

Figure 5.3. Leading resonance contributors for triplet HC_7H (^{3}**1**), MeC_7H (^{3}**9**) and MeC_3Me (^{3}**15**) as obtained from Natural Resonance Theory analysis. ^{3}**1** and ^{3}**9**, CCSD(T)/cc-pVTZ (fc). ^{3}**15**, CCSD(T)/cc-pVTZ//CCSD(T)/ANO1 (fc).

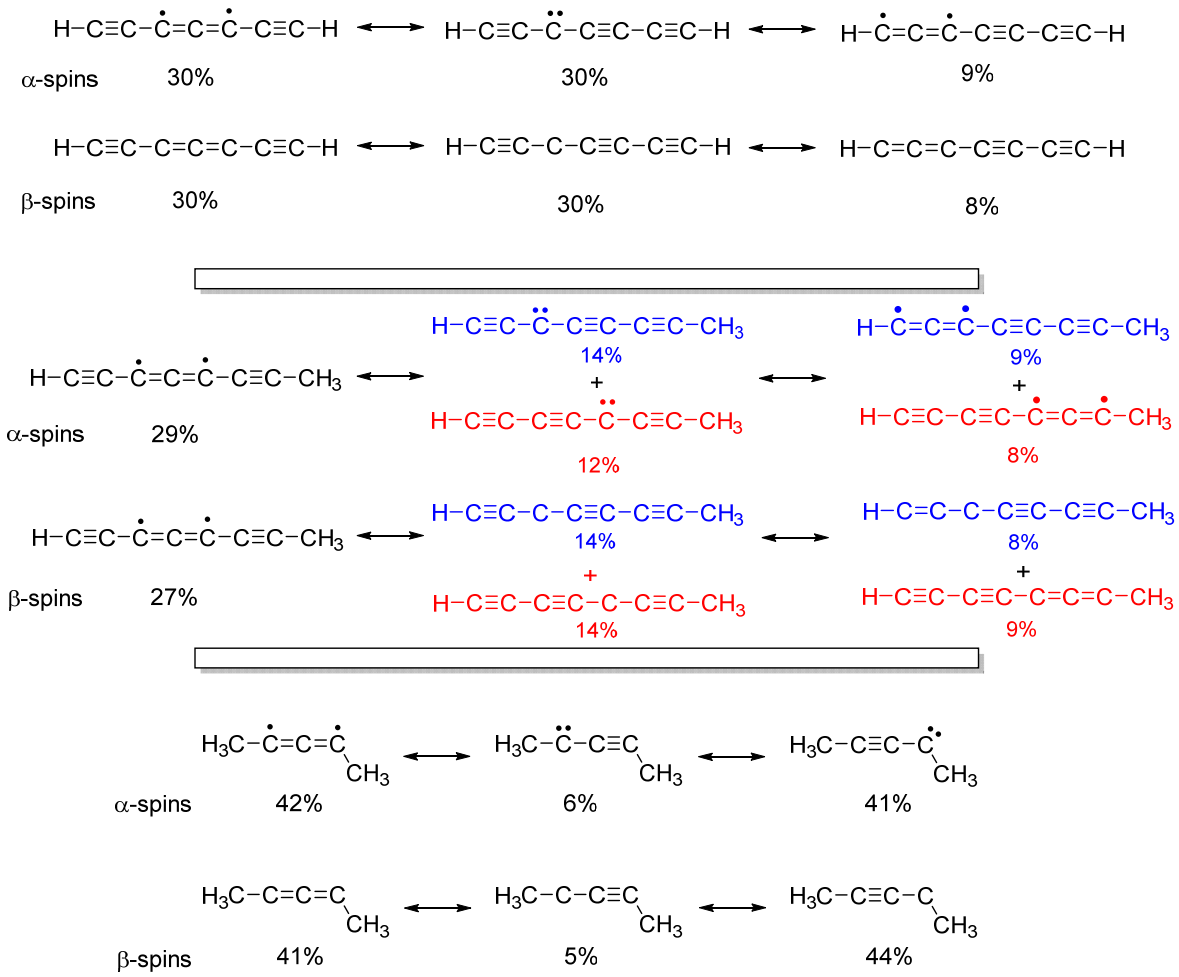

Table 5.3. Natural Bond Orbital/Natural Resonance Theory Analysis.[a]

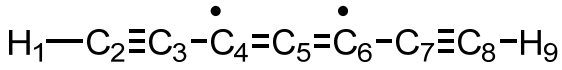

Natural Spin Densities									
atom	H1	C2	C3	**C4**	**C5**	**C6**	C7	C8	H9
	–0.07	1.21	–0.91	**1.30**	**–1.05**	**1.30**	–0.91	1.21	–0.07

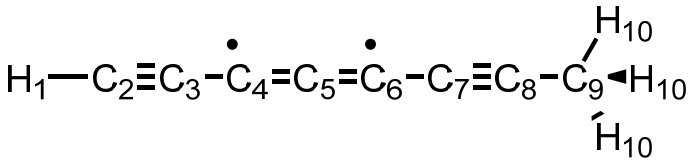

Natural Spin Densities										
atom	H1	C2	C3	**C4**	**C5**	**C6**	C7	C8	C9	H10
	-0.07	1.21	-0.91	**1.30**	**-1.04**	**1.29**	-0.87	1.10	-0.11	0.03

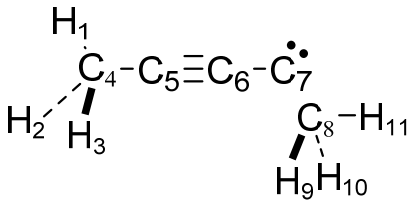

Natural Spin Densities											
atom	H1	H2	H3	C4	**C5**	**C6**	**C7**	C8	H9	H10	H11
	0.04	0.05	0.04	-0.14	**1.38**	**-0.93**	**1.57**	-0.14	0.05	0.05	0.03

[a] Computed at CCSD(T)/cc-pVTZ (fc).

Comparison of experimental and computed IR spectra

A common technique in the McMahon research group is to take full advantage of computed IR spectra to help identify matrix isolated species. Matrix isolation is incompatible with common analytical techniques such as mass spectrometry or ^{1}H-NMR, so IR provides us with a practical way to identify the trapped species. Calculation of harmonic vibrational frequencies calculations allow for predicted spectra for the IR region. High-level coupled-cluster calculations in particular have shown considerable success in accurately modeling the vibrational modes of these species.

Unfortunately, in the case of triplet HC_7H (^{3}**1**) and MeC_7H (^{3}**9**), the experimental spectra does not allow for unambiguous assignment of the isomer. Figure 5.4 shows the IR spectrum for HC_7H. The IR absorptions of the photoproducts upon photolysis of the diazo precursor are weak, and the overall quality of the subtraction spectrum is compromised by the strong background absorptions resulting from soot formation during the pyrolysis step. Though the spectral region at 1200-2700 cm^{-1} is clean, this does not allow for confirmation of the triplet HC_7H ^{3}**1**. The absence of IR absorptions for the photoproduct(s) in the region 1900-2200 cm^{-1} excludes formation of cumulenes **4**-**8**, as each of these species is predicted to exhibit one or more very intense cumulenic stretching vibrations in this region of the spectrum (see supporting information of tables of IR intensities).

Figure 5.4. (a-c) Computed IR spectra of the lower energy C_7H_2 isomers. (d) Experimental IR subtraction spectrum showing the disappearance of 1-diazohepta-2,4,6-triyne upon irradiation (λ > 444 nm, 4 h; Ar, 10 K). (e) Computed IR spectrum of diazo precursor. (Spectra of ^{3}**1**, **2**, **3** computed at CCSD(T)/cc-pVTZ (fc); spectrum of the diazo precursor computed at B3LYP/6-31G*).

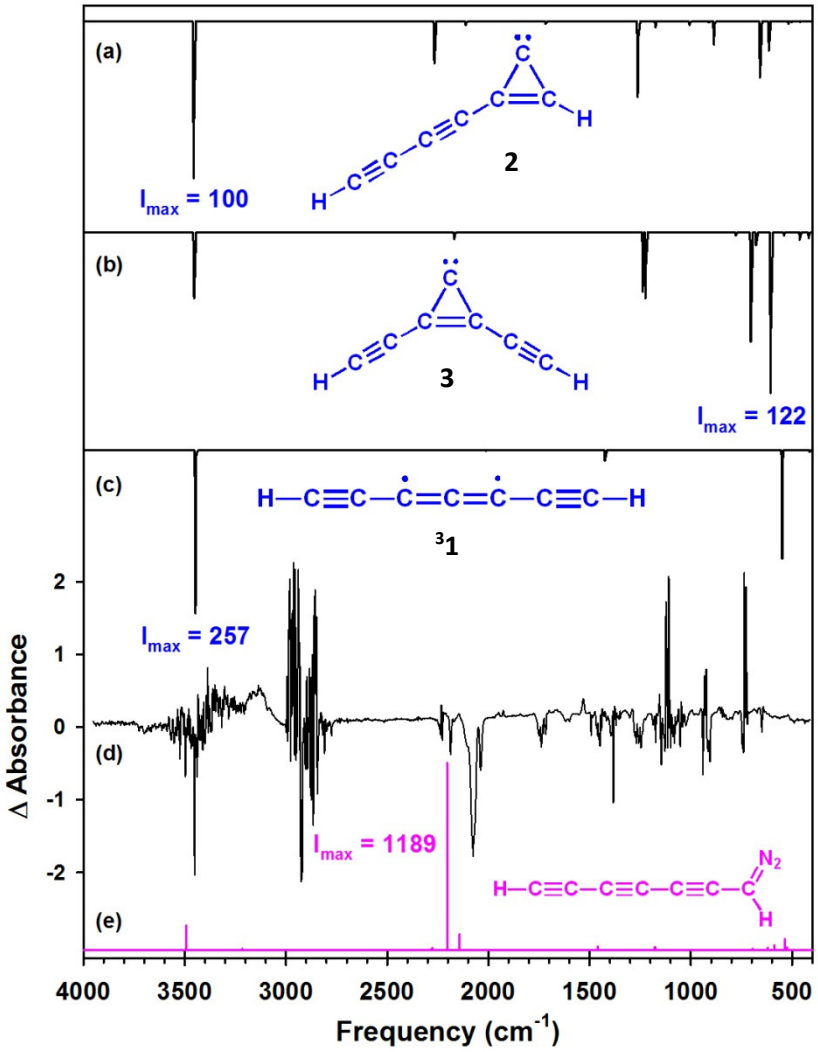

The predicted IR spectra for the isomers on the C_8H_4 surface are compared against the experimental subtraction spectrum in Figure 5.5. Though the quality of the spectrum is improved compared to HC_7H, the IR alone is not enough to confirm the presence of ^{3}**9**. All isomers shown, besides **10**, show intense absorption from the acetylenic C-H stretch around 3400 cm^{-1}, matching the observed experimental peak at 3202 cm^{-1}. The remaining three isomers have intense predicted absorptions that are either not seen experimentally or are ambiguous. Overall, the predicted IR spectra are not conclusive.

The comparison of the predicted IR spectrum of ^{3}**15** is interesting because of drastically different geometries found dependent on the method and level of theory used (Figure 5.6). Between the two predicted IR spectra, the higher-symmetry D_3 structure (B3LYP/6-31G(d)) does not demonstrate a C=C=C symmetric stretching vibration. The C_1 structure (CCSD(T)/ANO1), however, displays this peak at 1818 cm^{-1}. The unusually sharp peak at 1598 cm^{-1} in the experimental spectrum occurs in a region of the spectrum that is often contaminated by water. We are not confident in assigning this feature to triplet MeC_3Me (^{3}**15**) and note that the agreement with the putative feature at 1818 cm^{-1} in the predicted spectrum is much poorer than would be expected for a computation at this high level of theory. Thus, our tentative conclusion is that the absence of a C=C=C symmetric vibration in the IR spectrum of triplet MeC_3Me (^{3}**15**), and the extremely flat potential energy surface demonstrated at CCSD(T)/ANO1, implies either a high-symmetry structure or a quasilinear molecular structure, in which degenerate unsymmetrical structures equilibrate because the barrier to linearity lies below the zero-point energy. The parent HC_3H is experimentally known to be a quasilinear molecule.[34,45] Additionally, MeC_3H, which our CCSD/cc-pVDZ optimizations found to have a similar bent structure to MeC_3Me, has been characterized as quasilinear by theoretical methods.[46]

Figure 5.5. Computed IR spectra of several MeC_7H isomers compared to experimental IR subtraction spectrum showing growth of triplet MeC_7H (^{3}**9**) resulting from photoirradiation ($\lambda >$ 571 nm, 76 h) of 1-diazo-hepta-2,4,6-triyne (Ar, 10 K). (Spectra of ^{3}**9**, **10**, **11** computed at CCSD(T)/cc-pVTZ (fc); spectrum of the diazo precursor computed at B3LYP/6-31G*.)

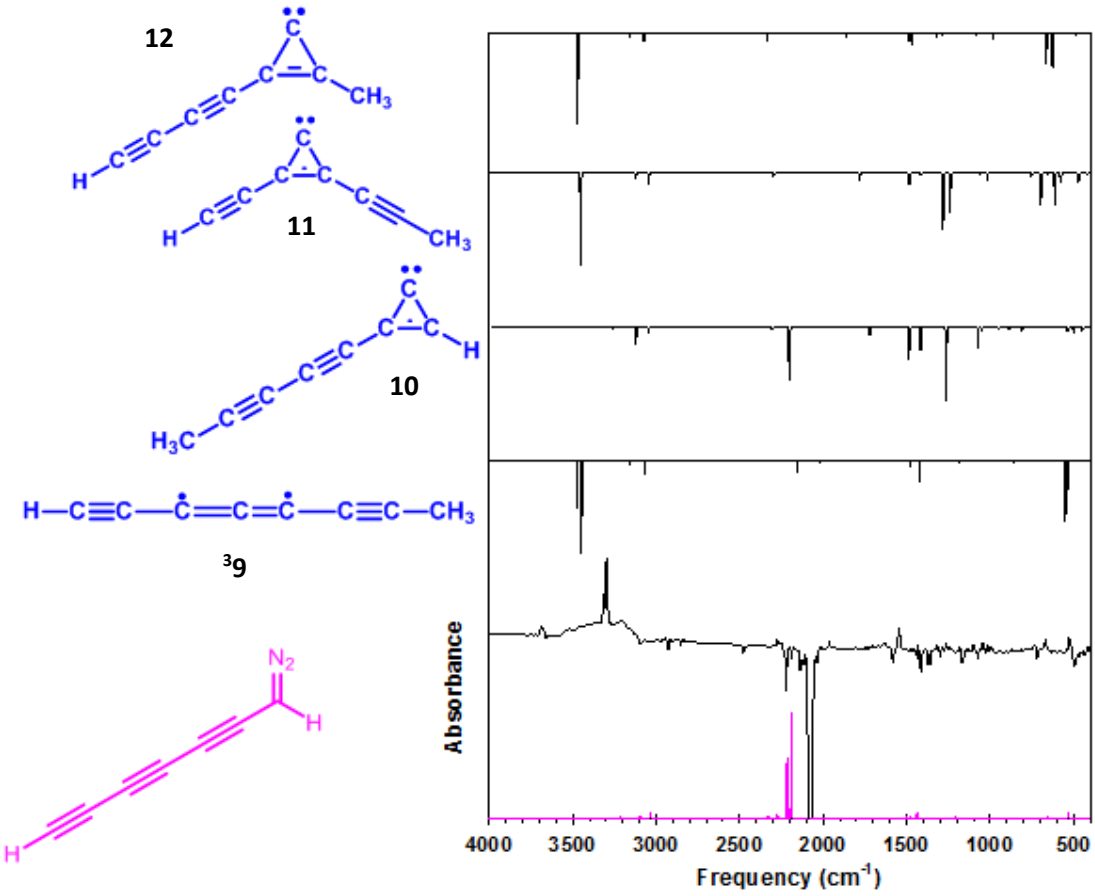

Figure 5.6. Top: Computed IR spectra for triplet MeC_3Me (**^{3}15**) at CCSD(T)/ANO1 (above) and B3LYP/6-31G(d) (below) Middle: IR subtraction spectrum showing the disappearance of 2-diazo-3-pentyne and appearance of triplet MeC_3Me (**^{3}15**) upon irradiation ($\lambda > 472$ nm, 6 h, N_2, 10 K) Bottom: Computed spectrum for 2-diazo-3-pentyne (CCSD/cc-pVDZ).

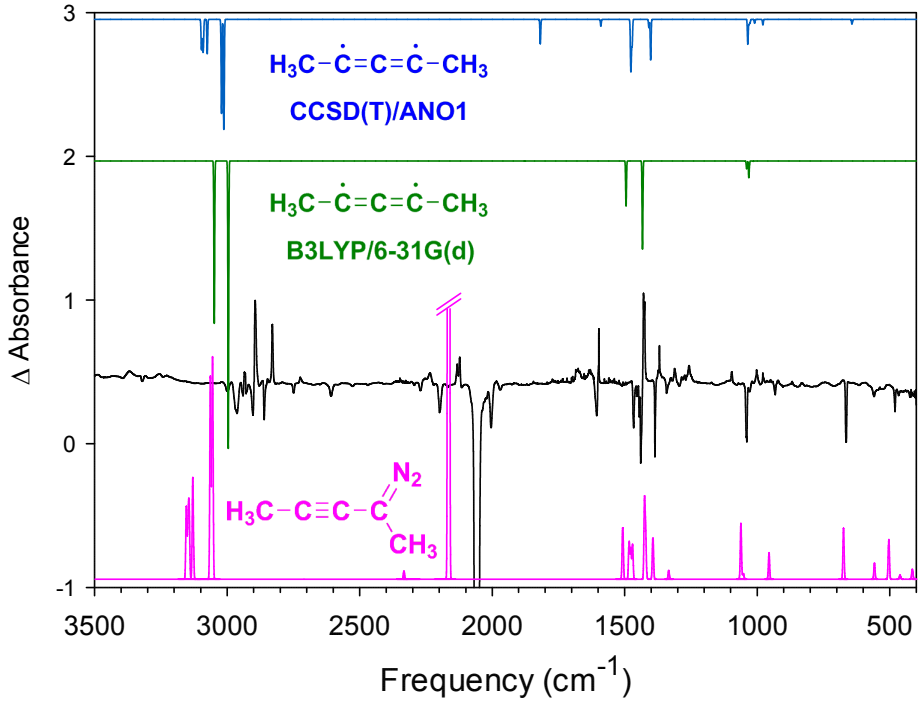

Excited State Calculations of HC_7H and MeC_7H

Figure 5.7 shows the electronic absorption spectra for triplet HC_7H (**^{3}1**) and MeC_7H (**^{3}9**). The absorptions observed in the visible region of the spectrum (390-510 nm) arise from a weakly allowed $A\ ^3\Sigma_u^- \leftarrow X\ ^3\Sigma_g^-$ transition in triplet HC_7H (**^{3}1**), as previously assigned by Fulara *et al.*,[47] and from the weakly allowed $A\ ^3A_1 \leftarrow X\ ^3A_1$ transition in triplet MeC_7H (**^{3}9**). The vibronic spectrum arising from these transitions exhibit good agreement with spectral data obtained previously in a neon matrix[47] and in the gas phase.[48-50] The dominant feature in both spectra

involves a progression between 1960 and 1990 cm^{-1}, which is clearly evident for several quanta beyond the origin. The frequency of this mode is substantially lower than that expected for a typical C≡C stretching vibration. Although the mode has previously been described as ν(C≡C),[47] it displays great similarity to the symmetric stretching vibration of the propargyl radical ($H_2\dot{C}–C≡C–H \leftrightarrow H_2C=C=\dot{C}–H$; 1935 cm^{-1}),[51] which exhibits substantial cumulenic character. In our opinion, it is appropriate to recognize that this vibration may be better characterized as ν(C=C=C).

To evaluate these vibronic couplings patterns, the excited state for both HC_7H and MeC_7H was evaluated using equation-of-motion coupled-cluster methodology (EOM-CCSD/ANO1). The calculations predict an adiabatic transition energies similar to experiment (calc. 2.86 eV to 2.45 eV for HC_7H, calc. 2.87 eV to 2.47 eV for MeC_7H) and an axially symmetric excited state that displays increased delocalization (reduced bond-length alternation) relative to the ground state structure (Table 5.S1).[52] Franck-Condon simulations including Duschinsky mixing provide insight into the vibrational structure observed in the experimental spectrum (Figures 5.8 and 5.9). Based upon the change in C–C bond alternation between ground and excited states seen for both species, the C–C cumulenic stretching vibration would be expected to be prominent in the vibronic progression; the Franck-Condon simulations agree with experiment in both frequency and intensity. The simulation reveals that the vibronic progression ν_α = 562 cm^{-1} for HC_7H is comprised of two-quantum transitions from each of the doubly-degenerate C–H bending modes,[47,48] as well as a minor contribution from a symmetric C–C stretching mode. As methyl substitution breaks the symmetry, the related vibronic progression at ν_α = 495 cm in the MeC_7H spectrum is comprised of a single two-quantum transition from a C-H bending mode. Unfortunately, the Franck-Condon simulations do not afford insight into the

other two vibrational progressions in the spectra, which suggests that these features arise through the effects of anharmonicity or vibronic coupling in the excited state. The strong similarities between both spectra support that triplet ^{3}**1** and ^{3}**9** are present in the matrix. Furthermore, the observed vibronic progressions exhibit good agreement with spectral data obtained in previous experiments, both for HC_7H[47-49] and MeC_7H.[50]

Figure 5.7. Top: UV/visible spectrum of 1-diazohepta-2,4,6-triyne (Ar, 10 K) prior to irradiation (Dotted line). Spectrum obtained upon irradiation of ^{3}**1** (λ > 444 nm, 2 h) (Solid line). Bottom: UV/visible spectra of 1-diazo-octa-2,4,6-triyne (Dotted line) prior to photolysis (Ar, 10 K. Triplet MeC_7H (^{3}**9**) obtained upon irradiation (λ > 534 nm, 72 h) (Solid line).

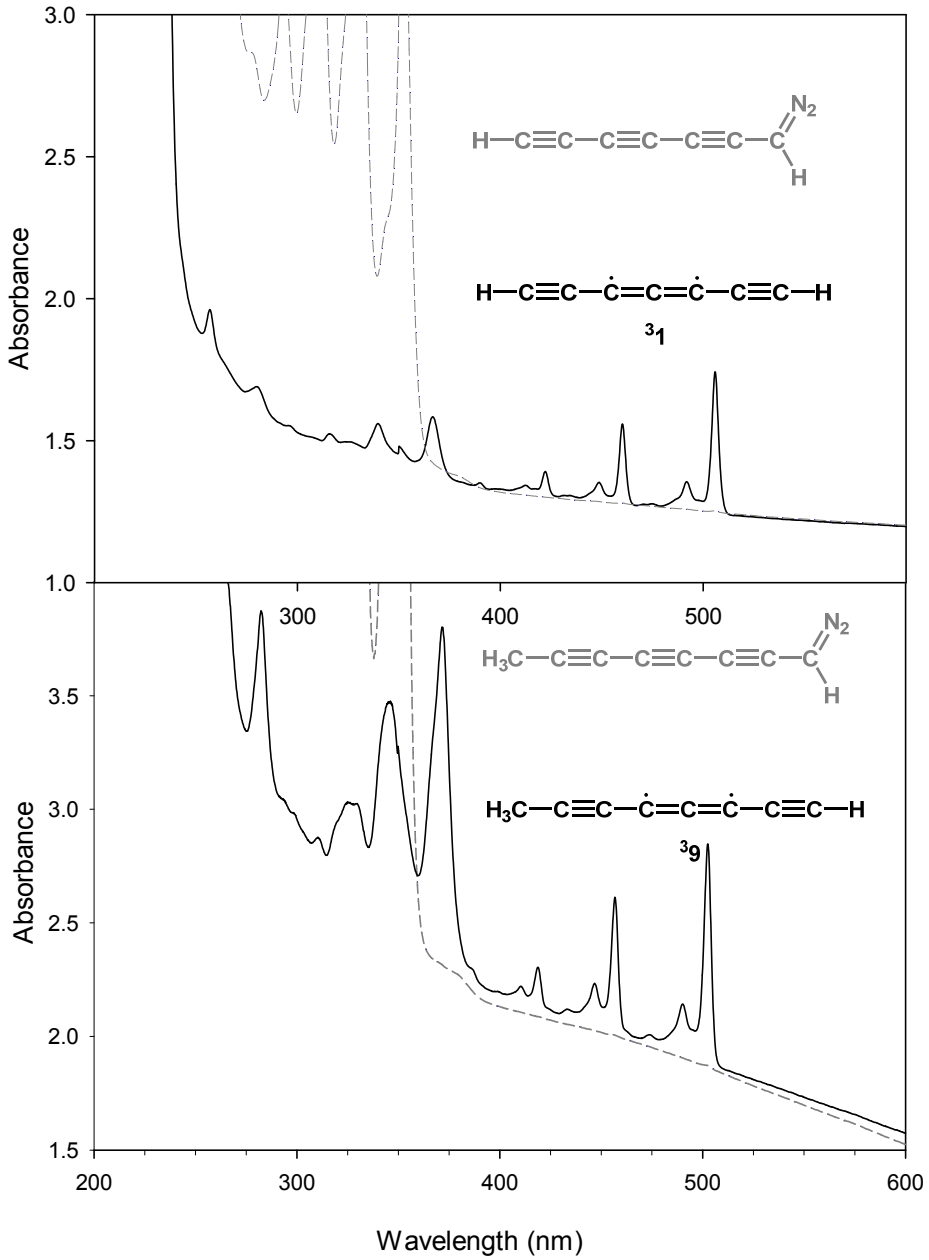

Figure 5.8. Top: Franck-Condon simulation for the $A\ ^3\Sigma_u^- \leftarrow X\ ^3\Sigma_g^-$ transition of HC_7H (in red) superimposed on the experimental spectrum (Ar, 10 K). Bottom: Vibrational modes in the $A\ ^3\Sigma_u^-$ state (computed) that contribute to the observed vibrational progressions at $\nu = 1960\ cm^{-1}$ and $\nu_\alpha = 562\ cm^{-1}$.

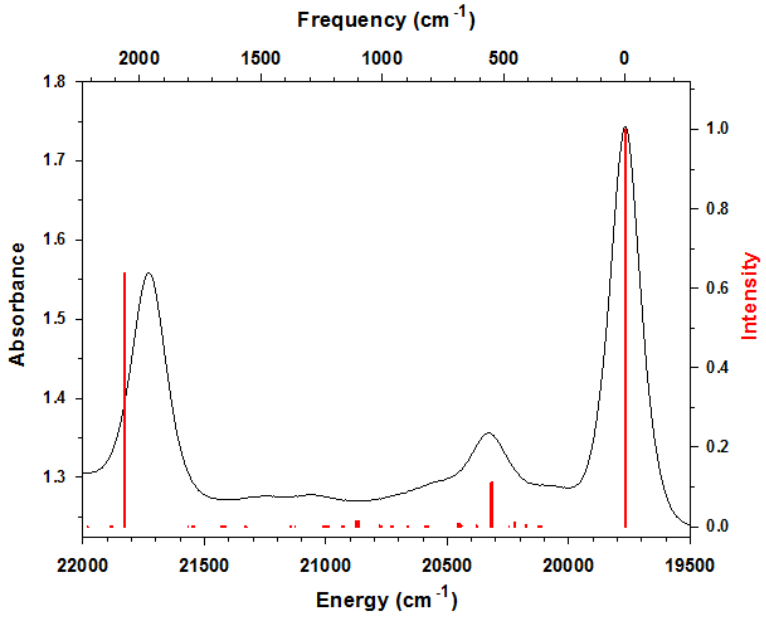

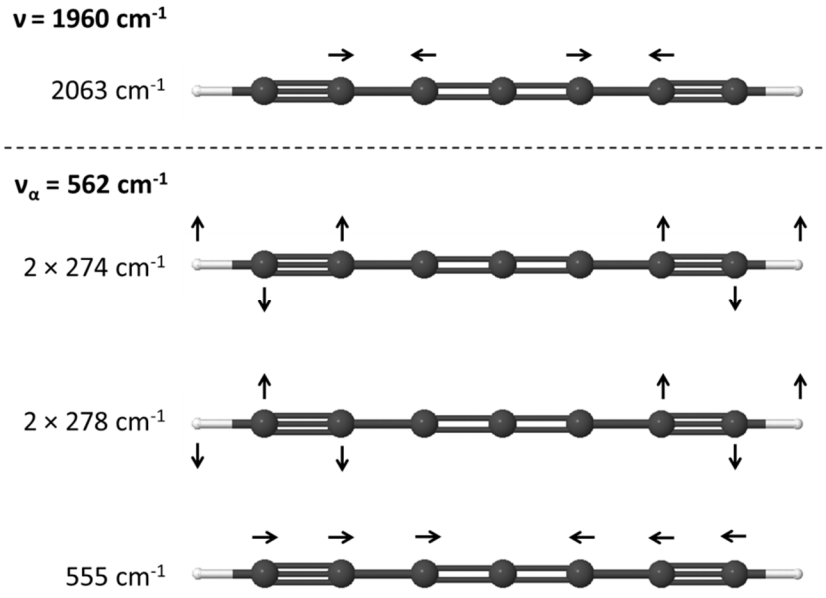

Figure 5.9. Top: Franck-Condon simulation for the $A\ ^3A_1 \leftarrow X\ ^3A_1$ transition of MeC_7H (in red) superimposed on the experimental spectrum (Ar, 10 K). Bottom: Vibrational modes in the $A\ ^3A_1$ state (computed) that contribute to the observed vibrational progressions at $\nu = 1993\ cm^{-1}$ and $\nu_\alpha = 495\ cm^{-1}$.

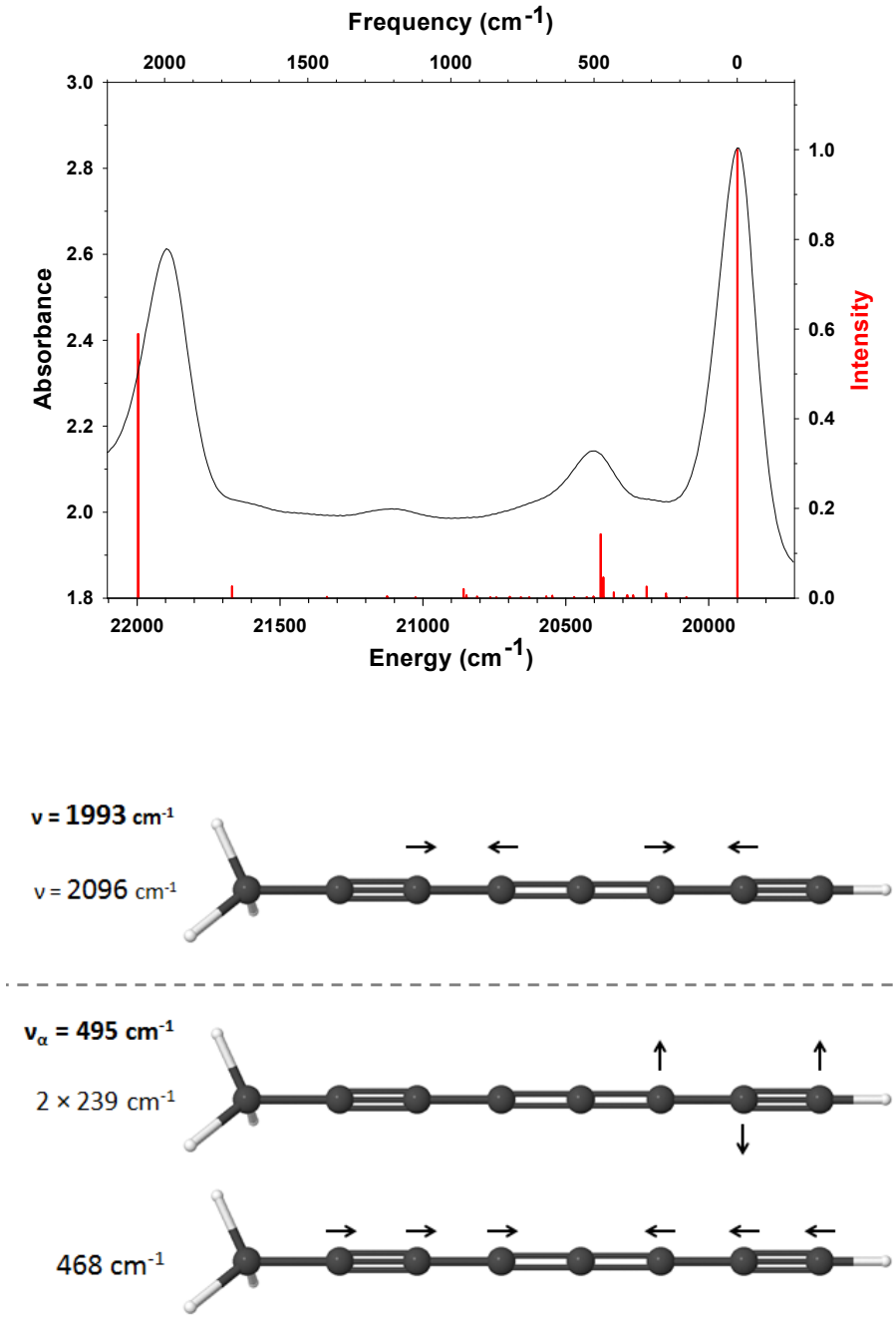

Summary

This chapter demonstrated that for a series of highly unsaturated carbon chains, HC_7H, MeC_7H, and MeC_3Me, modern computational methods were critical for their study. Coupled-cluster calculations allow us to accurately predict the structure and relative energies of many isomers on the potential energy surface. It was shown that predicted IR spectra are not only a powerful tool in identifying an isomer in the matrix, but rationalizing the symmetry of the molecule based of results from different levels of theory, as in the case with MeC_3Me. NBO and NRT calculations were applied to understand the complexities of these highly delocalized electronic structures. Lastly, excited state calculations of HC_7H and MeC_7H show good agreement with the vibronic progressions seen in both electronic absorption spectra.

References

1. Taatjes, C. A.; Klippenstein, S. J.; Hansen, N.; Miller, J. A.; Cool, T. A.; Wang, J.; Law, M. E.; Westmoreland, P. R. Synchotron photoionization measurements of combustion intermediates: Photoionization efficiency and identification of C_3H_2 isomers. *PCCP* **2005**, *7*, 806-813.

2. Maksyutenko, P.; Zhang, F.; Gu, X.; Kaiser, R. I. A crossed molecular beam study on the reaction of methylidyne radicals [$CH(X^2\Pi)$] with acetylene ($C_2H_2(X^1\Sigma_g^+)$] - competing C_3H_2 + H and C_3H + H_2 channels. *PCCP* **2011**, *13*, 240-252.

3. Special Issue: Titan Atmosphere. *J. Phys. Chem. A* **2009**, *113*, 11097-11237.

4. Special Issue: Progress in Understanding Titan's Atmosphere and Space Environment. *Philos. Trans. R. Soc. London, Ser. A* **2009**, *367*, 603-798.

5. Lorenz, R.; Mitton, J. *Titan Unveiled: Saturn's Mysterious Moon Explored*; Princeton University Press: Princeton, NJ, 2008.

6. Thaddeus, P.; McCarthy, M. C. Carbon chains and rings in the laboratory and in space. *Spectrochim. Acta, Part A* **2001**, *57A*, 757-774.

7. Herbst, E. The Chemistry of Interstellar Space. *Chem. Soc. Rev.* **2001**, *30*, 168-176.

8. Ehrenfreund, P.; Charnley, S. B. Organic Molecules in the Interstellar Medium, Comets, and Meteorites: A Voyage from Dark Clouds to Early Earth. *Annual Review of Astronomy and Astrophysics* **2000**, *38*, 427-483.

9. Fan, Q.; Pfeiffer, G. V. Theoretical Study of Linear C_n (n = 6-10) and HC_nH (n = 2-10) Molecules. *Chem. Phys. Lett.* **1989**, *162*, 472-478.

10. Lovas, F. J. NIST Recommended Rest Frequencies for Observed Interstellar Molecular Microwave Transitions - 2002 Revision. *J. Phys. Chem. Ref. Data* **2004**, *33*, 177-355.

11. Shaffer, C. J. Ph.D. Dissertation, University of Wisconsin-Madison, 2010.

12. Knezz, S. N., Ph.D. Dissertation, University of Wisconsin-Madison, 2016.

13. Burrmann, N. J., Ph.D. Dissertation, University of Wisconsin-Madison, 2010.

14. Becke, A. D. Density-functional thermochemistry. III. The role of exact exchange. *J. Chem. Phys.* **1993**, *98*, 5648-5652.

15. Raghavachari, K.; Trucks, G. W.; Pople, J. A.; Head-Gordon, M. A fifth-order perturbation comparison of electron correlation theories. *Chem. Phys. Lett.* **1989**, *157*, 479-483.

16. Hariharan, P. C.; Pople, J. A. Influence of polarization functions on MO hydrogenation energies. *Theor. Chim. Acta* **1973**, *28*, 213-222.

17. Dunning, T. H., Jr. Gaussian basis sets for use in correlated molecular calculations. I. The atoms boron through neon and hydrogen. *J. Chem. Phys.* **1989**, *90*, 1007-1023.

18. Almlof, J.; Taylor, P. R. General contraction of Gaussian basis sets. I. Atomic natural orbitals for first- and second-row atoms. *J. Chem. Phys.* **1987**, *86*, 4070-4077.

19. Frisch, M. J.; Trucks, G. W.; Schlegel, H. B.; Scuseria, G. E.; Robb, M. A.; Cheeseman, J. R.; Scalmani, G.; Barone, V.; Mennucci, B.; Petersson, G. A.; Nakatsuji, H.; Caricato, M.; Li, X.; Hratchian, H. P.; Izmaylov, A. F.; Bloino, J.; Zheng, G.; Sonnenberg, J. L.; Hada, M.; Ehara, M.; Toyota, K.; Fukuda, R.; Hasegawa, J.; Ishida, M.; Nakajima, T.; Honda, Y.; Kitao, O.; Nakai, H.; Vreven, T.; Montgomery Jr., J. A.; Peralta, J. E.; Ogliaro, F.; Bearpark, M. J.; Heyd, J.; Brothers, E. N.; Kudin, K. N.; Staroverov, V. N.; Kobayashi, R.; Normand, J.; Raghavachari, K.; Rendell, A. P.; Burant, J. C.; Iyengar, S. S.; Tomasi, J.; Cossi, M.; Rega, N.; Millam, N. J.; Klene, M.; Knox, J. E.; Cross, J. B.; Bakken, V.; Adamo, C.; Jaramillo, J.; Gomperts, R.; Stratmann, R. E.; Yazyev, O.; Austin, A. J.; Cammi, R.; Pomelli, C.; Ochterski, J. W.; Martin, R. L.; Morokuma, K.; Zakrzewski, V. G.; Voth, G. A.; Salvador, P.; Dannenberg, J. J.; Dapprich, S.; Daniels, A. D.; Farkas, Ö.; Foresman, J. B.; Ortiz, J. V.; Cioslowski, J.; Fox, D. J.; *Gaussian 09; Revision B.1*, 2009.

20. Stanton, J. F.; Gauss, J.; Harding, M. E.; Szalay, P. G.; with contributions from A.A. Auer, R. J. B., U. Benedikt, C. Berger, D.E. Bernholdt, Y.J. Bomble, L. Cheng, O.

Christiansen, M. Heckert, O. Heun, C. Huber, T.-C. Jagau, D. Jonsson, J. Jusélius, K. Klein, W.J. Lauderdale, D.A. Matthews, T. Metzroth, L.A. Mück, D.P. O'Neill, D.R. Price, E. Prochnow, C. Puzzarini, K. Ruud, F. Schiffmann, W. Schwalbach, C. Simmons, S. Stopkowicz, A. Tajti, J. Vázquez, F. Wang, J.D. Watts and the integral packages MOLECULE (J. Almlöf and P.R. Taylor), PROPS (P.R. Taylor), ABACUS (T. Helgaker, H.J. Aa. Jensen, P. Jørgensen, and J. Olsen), and ECP routines by A. V. Mitin and C. van Wüllen. For the current version, see http://www.cfour.de. 2014.

21. Dierksen, M.; Grimme, S. An efficient approach for the calculation of Franck–Condon integrals of large molecules. *J. Chem. Phys.* **2005**, *122*, 244101.

22. Glendening, E. D.; Badenhoop, J. K.; Reed, A. E.; Carpenter, J. E.; Bohmann, J. A.; Morales, C. M.; Landis, C. R.; Weinhold, F. A. *NBO 6.0*. Theoretical Chemistry Institute: University of Wisconsin, Madison, 2013.

23. Seburg, R. A.; Patterson, E. V.; Stanton, J. F.; McMahon, R. J. Structures, Automerizations, and Isomerizations of C_3H_2 Isomers. *J. Am. Chem. Soc.* **1997**, *119*, 5847-5856.

24. Seburg, R. A.; McMahon, R. J.; Stanton, J. F.; Gauss, J. Structures and Stabilities of C_5H_2 Isomers: Quantum Chemical Studies. *J. Am. Chem. Soc.* **1997**, *119*, 10838-10845.

25. Sun, B.; Huang, M.; Tsai, M.; Sun, H.; Gao, L.; Wang, Y.; Yeh, Y.; Shih, Y.; Sia, Z.; Chen, P.; Kaiser, R. I.; Chang, A. H. H. Synthesis of interstellar 1,3,5-heptatriynylidene, C_7H ($X\ ^2\Pi$), via the neutral-neutral reaction of ground state carbon atom, $C(^3P)$, with triacetylene, HC_6H ($X\ ^1\Sigma_g^+$). *J. Chem. Phys.* **2009**, *131*, 104305.

26. Cooper, D. L.; Murphy, S. C. *Ab Initio* Geometries for $C_{2n+1}H$, $C_{2n+1}H^+$, and $C_{2n+1}H_2$ Species for n = 1, 2, 3. *Astrophys. J.* **1988**, *333*, 482-490.

27. Aoki, K.; Ikuta, S. The singlet with a C_3 ring: the probable candidate of HC_6N and C_7H_2. *J. Mol. Struct.* **1994**, *310*, 229-238.

28. Dua, S.; Blanksby, S. J.; Bowie, J. H. Formation of Neutral C_7H_2 Isomers from Four Isomeric C_7H_2 Radical Anion Precursors in the Gas Phase. *J. Phys. Chem. A* **2000**, *104*, 77-85.

29. Plattner, D. A.; Houk, K. N. C_{18} Is a Polyyne. *J. Am. Chem. Soc.* **1995**, *117*, 4405-4406.

30. Woodcock, H. L.; Schaefer, H. F., III; Schreiner, P. R. Problematic Energy Differences between Cumulenes and Poly-ynes: Does This Point to a Systematic Improvement of Density Functional Theory? *J. Phys. Chem. A* **2002**, *106*, 11923-11931.

31. Schaffer, C. J., Ph.D. Dissertation, University of Wisconsin-Madison, 2010.

32. Seburg, R. A.; DePinto, J. T.; Patterson, E. V.; McMahon, R. J. Structure of Triplet Propynylidene. *J. Am. Chem. Soc.* **1995**, *117*, 835-836.

33. Huang, L. C. L.; Lee, H. Y.; Mebel, A. M.; Lin, S. H.; Lee, Y. T.; Kaiser, R. I. A combined crossed beam and *ab initio* investigation on the reaction of carbon species with C_4H_6 isomers. II. The dimethylacetylene molecule, H_3CCCCH_3 ($X\,^1A_{1g}$) *J. Chem. Phys.* **2000**, *113*, 9637-9648.

34. Seburg, R. A.; Patterson, E. V.; McMahon, R. J. Structure of Triplet Propynylidene (HCCCH) as Probed by IR, UV/vis, and EPR Spectroscopy of Isotopomers. *J. Am. Chem. Soc.* **2009**, *131*, 9442-9455.

35. Bowling, N. P.; Halter, R. J.; Hodges, J. A.; Seburg, R. A.; Thomas, P. S.; Simmons, C. S.; Stanton, J. F.; McMahon, R. J. Reactive Carbon-Chain Molecules: Synthesis of 1-Diazo-2,4-pentadiyne and Spectroscopic Characterization of Triplet Pentadiynylidene (H−C:C−C̈−C:C−H). *J. Am. Chem. Soc.* **2006**, *128*, 3291-3302.

36. Fan, Q.; Pfeiffer, G. V. Theoretical study of linear Cn (n=6−10) and HCnH (n=2−10) molecules. *Chem. Phys. Lett.* **1989**, *162*, 472-478.

37. Horný, L. u.; Petraco, N. D. K.; Schaefer, H. F. Odd Carbon Long Linear Chains $HC_{2n+1}H$ (n = 4−11): Properties of the Neutrals and Radical Anions. *J. Am. Chem. Soc.* **2002**, *124*, 14716-14720.

38. Nimlos, M. R.; Davico, G.; Giese, C. M.; Wenthold, P. G.; Lineberger, W. C.; Blanksby, S. J.; Hadad, C. M.; Petersson, G. A.; Ellison, G. B. Photoelectron spectroscopy of $HCCN^-$ and $NCNC^-$ reveals the quasilinear triplet carbenes, HCCN and HCNC. *J. Chem. Phys.* **2002**, *117*, 4323-4339.

39. Osborn, D. L.; Vogelhuber, K. M.; Wren, S. W.; Miller, E. M.; Lu, Y.-J.; Case, A. S.; Sheps, L.; McMahon, R. J.; Stanton, J. F.; Harding, L. B.; Ruscic, B.; Lineberger, W. C. Electronic States of the Quasi-linear Molecule Propargylene (HCCCH) from Negative Ion Photoelectron Spectroscopy. *J. Am. Chem. Soc.* **2014**, *136*, 10361-10372.

40. Laane, J. In *Structures and Conformations of Non-Rigid Molecules*; Laane, J., Dakkouri, M., van der Veken, B., Oberhammer, H., Eds.; Kluwer: Dordrecht, 1993, p 65-98.

41. Bunker, P. R. Quasilinear and Quasiplanar Molecules. *Annu. Rev. Phys. Chem.* **1983**, *34*, 59-75.

42. Winnewisser, B. P. In *Molecular Spectroscopy: Modern Research*; Rao, K. N., Ed.; Academic Press: Orlando, 1985; Vol. III, p 321-419.

43. Winnewisser, M.; Winnewisser, B. P.; Medvedev, I. R.; De Lucia, F. C.; Ross, S. C.; Bates, L. M. The hidden kernel of molecular quasi-linearity: Quantum monodromy. *J. Mol. Struct.* **2006**, *798*, 1-26.

44. Child, M. S. Quantum monodromy and molecular spectroscopy. *Adv. Chem. Phys.* **2007**, *136*, 39-94.

45. Osborn, D. L.; Vogelhuber, K. M.; Wren, S. W.; Miller, E. M.; Lu, Y.-J.; Case, A. S.; Sheps, L.; McMahon, R. J.; Stanton, J. F.; Harding, L. B.; Ruscic, B.; Lineberger, W. C. Electronic States of the Quasilinear Molecule Propargylene (HCCCH) from Negative Ion Photoelectron Spectroscopy. *J. Am. Chem. Soc.* **2014**, *136*, 10361−10372.

46. Kaiser, R. I.; Mebel, A. M.; Lee, Y. T.; Chang, A. H. H. Unimolecular decomposition of chemically activated triplet C_4HD_3 complexes: A combined cross-beam and ab initio study. *J. Chem. Phys.* **2001**, *115*, 5117-5125.

47. Fulara, J.; Freivogel, P.; Forney, D.; Maier, J. P. Electronic Absorption Spectra of Linear Carbon Chains in Neon Matrices. III. $HC_{2n+1}H$. *J. Chem. Phys.* **1995**, *103*, 8805-8810.

48. Ding, H.; Schmidt, T. W.; Pino, T.; Boguslavskiy, A. E.; Güthe, F.; Maier, J. P. Gas Phase Electronic Spectra of the Linear Carbon Chains $HC_{2n+1}H$ (n = 3-6, 9). *J. Chem. Phys.* **2003**, *119*, 814-819.

49. Wehres, N.; Zhao, D.; Ubachs, W.; Linnartz, H. Rotationally resolved $A\ ^3\Sigma_u^- \leftarrow X\ ^3\Sigma_g^-$ spectrum of HC_7H. *Chem. Phys. Lett.* **2010**, *497*, 30-32.

50. Schmidt, T. W.; Ding, H.; Boguslavskiy, A. E.; Pino, T.; Maier, J. P. Methyl Substitution in Hydrocarbon Discharge Chemistry: Diagnosis by Laser Spectroscopy. *J. Phys. Chem. A* **2003**, *107*, 6550-6553.

51. Jochnowitz, E. B.; Zhang, X.; Nimlos, M. R.; Varner, M. E.; Stanton, J. F.; Ellison, G. B. Propargyl Radical: Ab Initio Anharmonic Modes and the Polarized Infrared Absorption Spectra of Matrix-Isolated $HCCCH_2$. *J. Phys. Chem. A* **2005**, *109*, 3812-3821.

52. Crawford, T. D.; Stanton, J. F.; Allen, W. D.; Schaefer, H. F., III Hartree–Fock orbital instability envelopes in highly correlated single-reference wave functions. *J. Chem. Phys.* **1997**, *107*, 10626-10632.

Supporting Information

Chapter 5: Contributions of Theory to Studies of Highly Unsaturated Carbon Chains

Includes the work of several collaborators and publications:

Spectroscopy and Photochemistry of Triplet 1,3-Dimethylpropynylidene (Me–C–C–C–Me). Stephanie N. Knezz, Terese A. Waltz, Benjamin C. Haenni, Nicola J. Burrmann, and Robert J. McMahon. *Manuscript submitted*.

Reactive Carbon-Chain Molecules: Synthesis of 1-Diazohepta-2,4,6-triyne and Spectroscopic Characterization of Triplet HC_7H (H–C≡C−Ċ=C=Ċ−C≡C−H). Christopher J. Shaffer, Benjamin C. Haenni, John F. Stanton, and Robert J. McMahon. *Manuscript in preparation*.

Reactive Carbon-Chain Molecules: Synthesis of 1-Diazo-octa-2,4,6-triyne and Spectroscopic Characterization of Triplet MeC_7H (Me–C≡C−Ċ=C=Ċ−C≡C−H). Christopher J. Shaffer, Benjamin C. Haenni, John F. Stanton, and Robert J. McMahon. *Manuscript in preparation*.

Figure 5.S1. Computed structures for MeC_3Me (**15**) and MeC_3H. (a) ^{3}**15** at B3LYP/6-31G(d) (D_3). (b) ^{3}**15** at CCSD/cc-pVDZ (C_s). (c) ^{1}**15** at CCSD/cc-pVDZ (C_1). (d) ^{3}**15** at CCSD(T)/ANO1 (C_1). (e) MeC_3Me at B3LYP/6-31G(d) (C_s). (f) MeC_3Me at CCSD/cc-pVDZ (C_s).

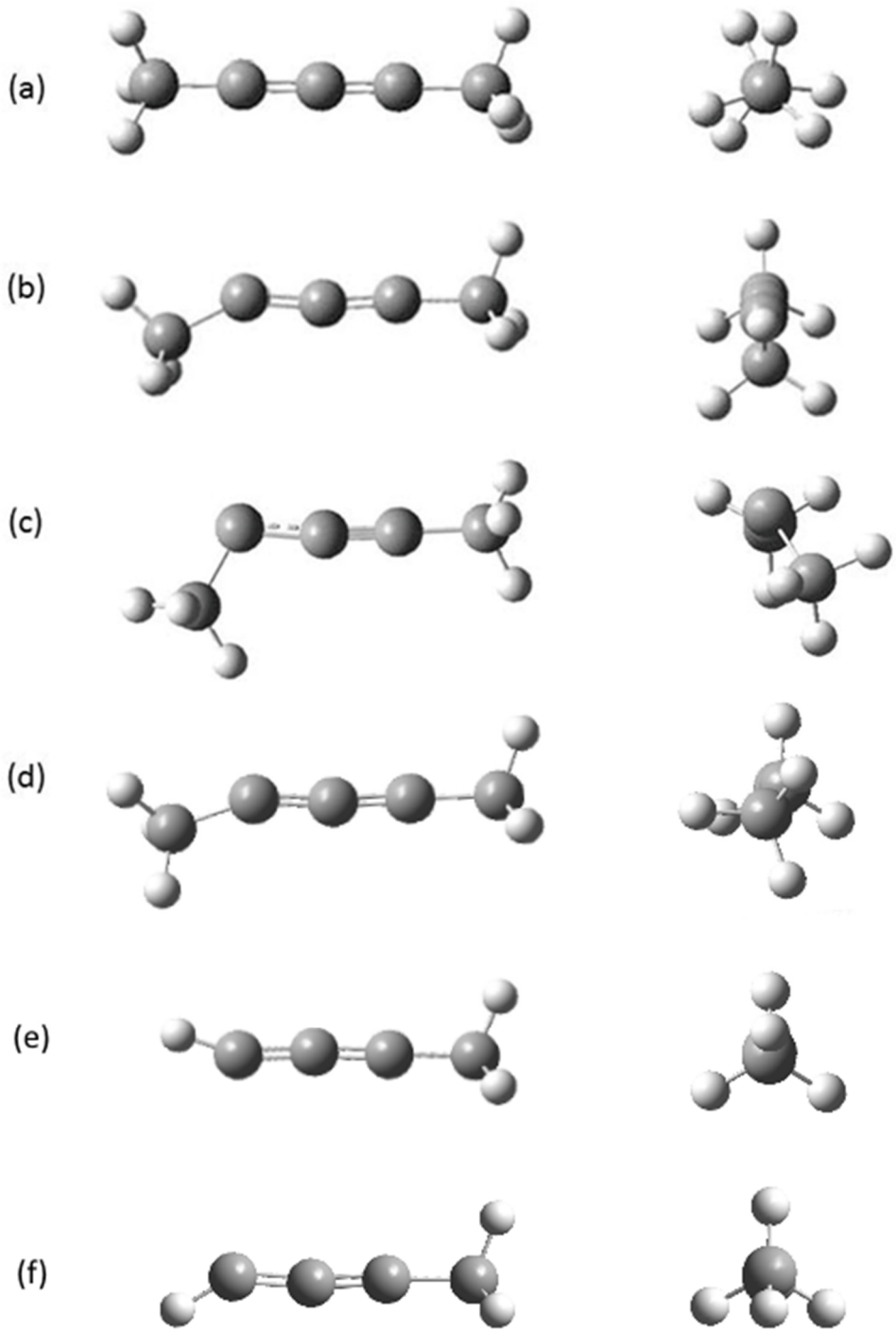

Table 5.S1. Computed excited state structural parameters for the $A\ ^3\Sigma_u^-$ state of triplet HC_7H and the $A\ ^3A_1$ of triplet MeC_7H.[a]

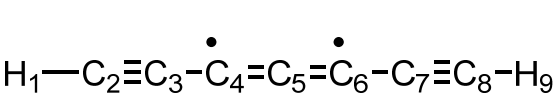

Parameter	$D_{\infty h}$
r [H1-C2]	1.062
r [C2-C3]	1.253
r [C3-C4]	1.303
r [C4-C5]	1.290
r [C5-C6]	1.290
r [C6-C7]	1.303
r [C7-C8]	1.253
r [C8-H9]	1.062

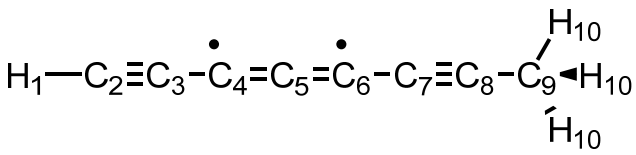

Parameter	C_{3v}
r [H1-C2]	1.062
r [C2-C3]	1.255
r [C3-C4]	1.303
r [C4-C5]	1.291
r [C5-C6]	1.292
r [C6-C7]	1.305
r [C7-C8]	1.252
r [C8-C9]	1.456
r [C9-H10]	1.091
θ [C8-C9-H10]	110.522

Table 5.S2. Computed Spin Densities for Triplets HC_3H, MeC_3H, and MeC_3Me (^{3}**15**).[a]

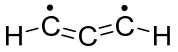

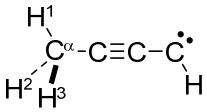

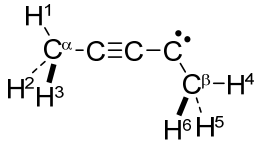

	Natural Spin Density		
Atom	HC_3H	MeC_3H	MeC_3Me (^{3}**15**)
H-1		0.04	0.04
H-2		0.04	0.05
H-3		0.04	0.04
C-α		-0.14	-0.14
H	-0.04		
C-1	1.24	1.36	1.38
C-2	-0.40	-0.98	-0.93
C-3	1.24	1.70	1.57
H	-0.04	-0.07	
C-β			-0.14
H-4			0.03
H-5			0.05
H-6			0.05
Σ (|spin density|)	2.96	4.37	4.42
Σ (spin density)	2.00	1.99	2.00
'excess' spin density	0.96	2.38	2.42

[a] From the Natural Bond Orbital (NBO) analyses of triplets HC_3H, QCISD/6-311+G(2df,p),[1] MeC_3H CCSD(T)/cc-pVTZ//CCSD/cc-pVDZ, and MeC_3Me (^{3}**15**) CCSD(T)/cc-pVTZ//CCSD(T)/ANO1).

1) Seburg, R. A.; Patterson, E. V.; McMahon, R. J. *J. Am. Chem. Soc.* **2009**, *131*, 9442.

Figure S2. Natural Resonance Theory (NRT) descriptions of triplets HC_3H, MeC_3H, and MeC_3Me (^{3}**15**). (calculated at QCISD/6-311+G(2df,p); CCSD(T)/cc-pVTZ//CCSD/cc-pVDZ, CCSD(T)/cc-pVTZ//CCSD(T)/ANO1, respectively).

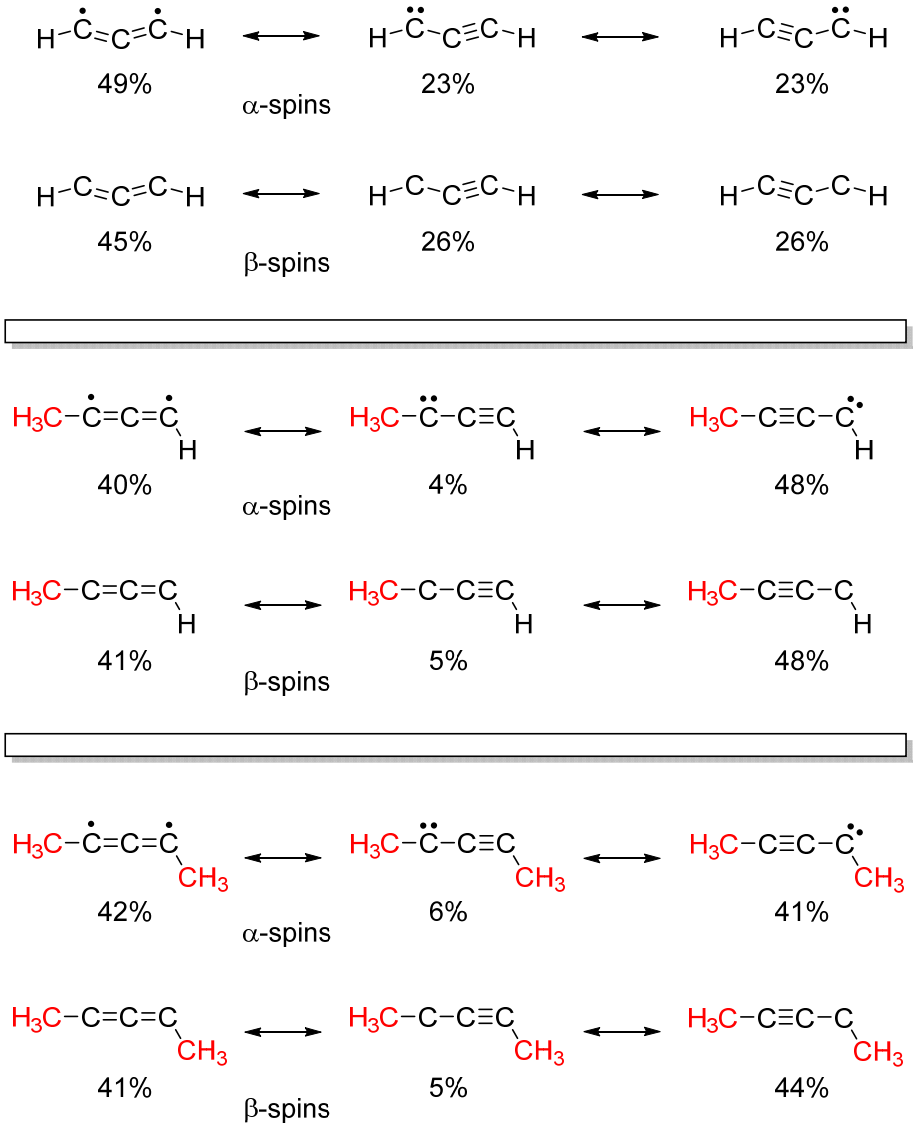

Charge	Multiplicity	Theory/Basis Set	Full Point Group
0	3	CCSD(T)/cc-pVTZ	$D_{\infty h}$
Zero-point Energy	**Electronic Energy**	**Electronic and Zero-Point Energy**	**Dipole Moment (D)**
0.047268	-267.153693	-267.106424	0.0000

Energies in Hartrees/particle

Symm.	Frequency (cm^{-1})	Intensity
Σ_u^-	71.7089	3.0756
Σ_u^-	71.7089	3.0756
Π_g	170.5626	0.0000
Π_g	170.5626	0.0000
Π_u	376.1248	0.9863
Π_u	376.1248	0.9863
Π_u	413.2039	1.3549
Π_u	413.2039	1.3549
Π_g	428.2711	0.0000
Π_g	428.2711	0.0000
Π_g	549.0547	0.0000
Π_g	549.0547	0.0000
Π_u	548.8854	85.6651
Π_u	548.8854	85.6651
Σ_g^+	545.7899	0.0000
Σ_u^-	1039.7954	5.8572
Σ_u^-	1424.0433	18.3159
Σ_g^+	1662.3812	0.0000
Σ_u^-	2012.1446	0.9786
Σ_g^+	2047.6708	0.0000
Σ_u^-	3447.1321	256.9941
Σ_g^+	3453.7449	0.0000

Atom	Coordinates (Angstroms)		
	X	Y	Z
C	0.000000	-1.275220	0.000000
C	0.000000	0.000000	0.000000
C	0.000000	1.275220	0.000000
C	0.000000	-2.614216	0.000000
C	0.000000	-3.841687	0.000000
H	0.000000	-4.905545	0.000000
C	0.000000	2.614216	0.000000
C	0.000000	3.841687	0.000000
H	0.000000	4.905545	0.000000

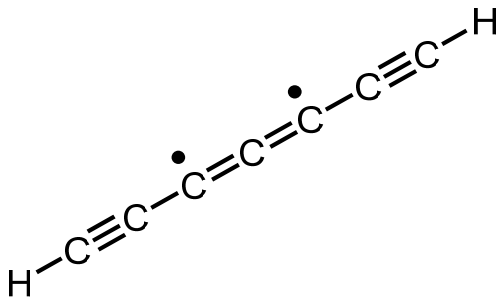

Charge	Multiplicity	Theory/Basis Set	Full Point Group
0	3	EOM-CCSD/ANO1	$D_{\infty h}$
Zero-point Energy	**Electronic Energy**	**Electronic and Zero-Point Energy**	**Dipole Moment (D)**
0.049061	-267.014122	-266.956061	0.0000

Energies in Hartrees/particle

Symm.	Frequency (cm^{-1})	Intensity
Π_u	72.3916	2.5801
Π_u	72.3916	2.5801
Π_g	179.4676	0.0000
Π_g	179.4676	0.0000
Π_u	274.4867	71.3798
Π_u	274.4867	71.3798
Π_g	277.6942	0.0000
Π_g	277.6942	0.0000
Π_u	337.9103	8.6834
Π_u	337.9103	8.6834
Π_u	405.8996	17.3758
Π_u	405.8996	17.3758
Π_g	412.1945	0.0000
Π_g	412.1945	0.0000
Σ_g^+	554.8957	0.0000
Σ_u^-	1107.0495	3.8145
Σ_g^+	1564.9231	0.0000
Σ_u^-	1644.0292	15.4625
Σ_g^+	2063.1426	0.0000
Σ_u^-	3463.3059	188.1641
Σ_g^+	3472.8845	0.0000
Σ_u^-	3744.9562	1003.3581

Atom	Coordinates (Angstroms)		
	X	Y	Z
C	0.000000	0.000000	0.000000
C	0.000000	0.000000	-1.290985
C	0.000000	0.000000	1.290985
C	0.000000	0.000000	-2.594059
C	0.000000	0.000000	2.594059
C	0.000000	0.000000	-3.847425
C	0.000000	0.000000	3.847425
H	0.000000	0.000000	-4.909317
H	0.000000	0.000000	4.909317

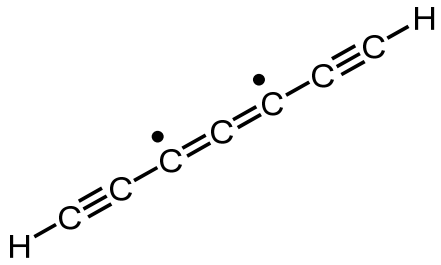

Charge	Multiplicity	Theory/Basis Set	Full Point Group
0	1	CCSD(T)/cc-pVTZ	C_S
Zero-point Energy	**Electronic Energy**	**Electronic and Zero-Point Energy**	**Dipole Moment (D)**
0.051311	-267.152631	-267.101320	3.6676

Energies in Hartrees/particle

Symm.	Frequency (cm^{-1})	Intensity
A’	94.2436	3.6899
A’’	97.1157	0.3547
A’	233.4865	5.2229
A’’	261.3440	2.6389
A’	459.2760	0.6108
A’’	495.4392	0.0854
A’	501.6063	0.8198
A’	518.5012	1.7561
A’’	540.1706	1.0058
A’	613.1945	42.6131
A’’	658.3916	36.1432
A’’	886.6627	15.0701
A’	909.7067	2.1368
A’	1006.3879	2.5574
A’	1174.8903	4.0239
A’	1262.7704	48.4579
A’	1715.0085	8.4485
B’’	2111.8546	2.7022
A’	2266.9020	27.0020
A’	3259.6079	1.3955
A’	3456.2153	100.6038

Atom	Coordinates (Angstroms)		
	X	Y	Z
C	0.000000	0.000000	0.000000
H	0.000000	0.000000	1.078341
C	0.732888	0.000000	-1.215744
C	-0.709475	0.000000	-1.134801
C	-1.936156	0.000000	-1.800425
C	-3.000037	0.000000	-2.399221
C	-4.199635	0.000000	-3.066141
C	-5.260333	0.000000	-3.660829
H	-6.188789	0.000000	-4.180705

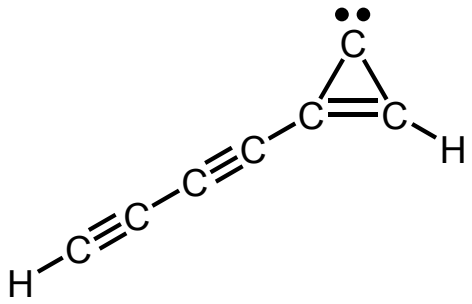

Charge	Multiplicity	Theory/Basis Set	Full Point Group
0	1	CCSD(T)/cc-pVTZ	C_{2V}
Zero-point Energy	**Electronic Energy**	**Electronic and Zero-Point Energy**	**Dipole Moment (D)**
0.050850	-267.148757	-267.097906	3.7740

Energies in Hartrees/particle

Symm.	Frequency (cm^{-1})	Intensity
A_1	99.9199	2.1525
B_1	179.2099	0.6230
B_2	226.7098	0.1348
A_2	229.6260	0.0000
A_1	418.0388	3.2700
B_1	460.5336	17.5129
B_2	539.6686	1.7959
A_1	606.2612	66.1385
B_2	606.9382	24.0802
A_2	633.3705	0.0000
A_1	678.3382	7.2189
A_2	702.8648	0.0000
B_1	704.2804	60.4275
B_2	777.1399	4.7896
B_2	1224.0525	36.3346
A_1	1237.0163	32.7649
A_1	1768.3941	0.2344
B_2	2159.0633	25.8590
A_1	2168.5729	3.6286
B_2	3450.0554	122.4276
A_1	3454.5629	31.9340

Atom	Coordinates (Angstroms)		
	X	Y	Z
C	0.000000	0.000000	0.000000
C	-1.266568	0.671739	0.000000
C	-1.266568	-0.671739	0.000000
C	-1.989351	1.872783	0.000000
C	-1.989351	-1.872783	0.000000
C	-2.613787	2.913581	0.000000
C	-2.613787	-2.913581	0.000000
H	-3.154574	3.830380	0.000000
H	-3.154574	-3.830380	0.000000

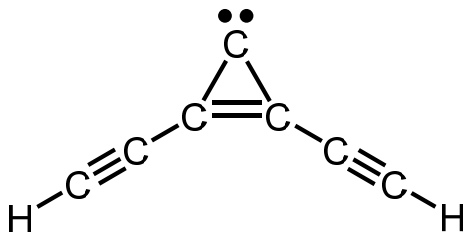

Charge	Multiplicity	Theory/Basis Set	Full Point Group
0	1	CCSD(T)/cc-pVTZ	C_S
Zero-point Energy	**Electronic Energy**	**Electronic and Zero-Point Energy**	**Dipole Moment (D)**
0.050544	-267.129612	-266.079068	5.2497

Energies in Hartrees/particle

Symm.	Frequency (cm^{-1})	Intensity
A'	73.1951	3.8994
A"	137.6105	9.5608
A'	177.3629	4.4917
A"	197.5392	2.9756
A'	290.4298	0.5471
A"	318.0038	0.1684
A'	467.1133	0.0194
A	505.7176	1.7036
A''	506.2975	1.6578
A'	631.0004	40.8395
A"	659.0965	36.9449
A'	751.8407	49.0412
A"	869.8113	5.0275
A'	1087.6444	14.4192
A'	1217.1365	23.1731
A'	1396.3305	20.0013
A'	1981.8587	891.1513
A'	2103.3770	20.7707
A'	2253.3431	211.9539
A'	3128.4951	1.1733
A'	3453.1076	98.7786

Atom	Coordinates (Angstroms)		
	X	Y	Z
C	0.000000	0.000000	0.000000
H	0.000000	0.000000	1.088669
C	1.265360	0.000000	-0.631951
C	-1.168438	0.000000	-0.669536
C	-2.311327	0.000000	-1.272133
C	2.374617	0.000000	-1.144992
C	3.612470	0.000000	-1.735210
C	4.711964	0.000000	-2.254880
H	5.671988	0.000000	-2.714654

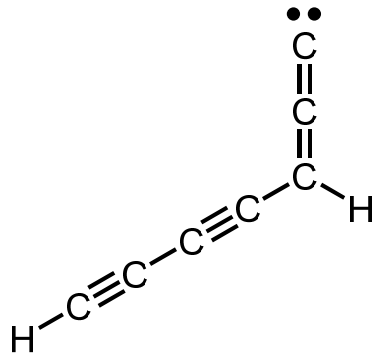

Charge	Multiplicity	Theory/Basis Set	Full Point Group
0	1	CCSD(T)/cc-pVTZ	C_{2V}
Zero-point Energy	**Electronic Energy**	**Electronic and Zero-Point Energy**	**Dipole Moment (D)**
0.051053	-267.127719	-266.077746	7.336695

Energies in Hartrees/particle

Symm.	Frequency (cm^{-1})	Intensity
B_2	73.1998	1.3896
B_1	76.3190	0.2262
B_2	170.2502	10.7253
B_1	188.8364	7.1963
B_1	267.4835	0.3144
B_2	285.1324	0.0531
B_1	403.4572	0.6046
B_1	454.6375	0.7674
B_2	518.2576	1.3198
A_1	554.0531	0.0600
B_2	556.1076	2.1219
B_2	909.2585	36.0964
B_1	1019.9295	0.3306
A_1	1047.5136	1.9005
A_1	1423.7883	12.2402
A_1	1537.1655	21.4006
A_1	1890.6939	315.7606
A_1	2092.4762	304.0576
A_1	2118.0300	1357.9537
A_1	3130.2562	0.0269
B_1	3218.6701	0.0678

Atom	Coordinates (Angstroms)		
	X	**Y**	**Z**
C	0.000000	0.000000	0.000000
C	0.000000	0.000000	1.293817
C	0.000000	0.000000	2.597985
C	0.000000	0.000000	3.870430
C	0.000000	0.000000	5.167300
C	0.000000	0.000000	6.440766
C	0.000000	0.000000	7.768480
H	0.000000	0.930554	8.325621
H	0.000000	-0.930554	8.325621

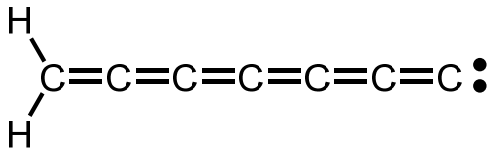

Charge	Multiplicity	Theory/Basis Set	Full Point Group
0	1	CCSD(T)/cc-pVTZ	C_S
Zero-point Energy	**Electronic Energy**	**Electronic and Zero-Point Energy**	**Dipole Moment (D)**
0.050463	-267.125986	-267.075523	6.268778

Energies in Hartrees/particle

Symm.	Frequency (cm^{-1})	Intensity
A’	64.0379	0.9871
A’’	117.2588	3.5600
A’	178.9541	3.0033
A’’	257.4616	9.6297
A’	273.1612	2.2968
A’’	315.3413	9.8520
A’	450.7345	0.7018
A’	504.2569	5.6635
A’’	562.7691	1.8190
A’	641.2734	37.5970
A’’	652.3605	35.4145
A’	781.3168	9.5974
A’’	819.3371	4.1516
A’	10005.9108	35.9317
A’	1267.0146	5.1481
A’	1456.9494	119.0295
A’	1922.1333	138.8534
A’	2119.1616	867.5498
A’	2165.8097	504.2823
A’	3141.5778	2.4913
A’	3453.5649	74.7666

Atom	Coordinates (Angstroms)		
	X	Y	Z
C	0.000000	0.000000	0.000000
H	0.000000	0.000000	1.087271
C	1.166964	0.000000	-0.657508
C	-1.263407	0.000000	-0.651686
C	-2.360703	0.000000	-1.173149
H	-3.314265	0.000000	-1.646394
C	2.289083	0.000000	-1.245686
C	3.443750	0.000000	-1.859932
C	4.587530	0.000000	-2.463401

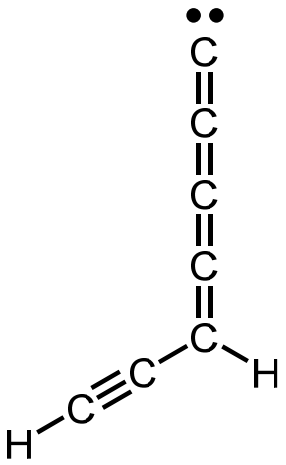

Charge	Multiplicity	Theory/Basis Set	Full Point Group
0	1	CCSD(T)/cc-pVTZ	C_{2V}
Zero-point Energy	**Electronic Energy**	**Electronic and Zero-Point Energy**	**Dipole Moment (D)**
0.049945	-267.120325	-267.070380	5.162131

Energies in Hartrees/particle

Symm.	Frequency (cm^{-1})	Intensity
B_2	117.8514	3.1116
A_1	124.1014	3.6880
B_1	130.2030	1.9923
B_1	245.4076	16.0253
B_2	290.3558	0.8749
A_2	313.8463	0.0000
B_2	540.7554	8.3455
A_1	556.8997	1.3739
B_2	642.3522	18.1598
A_1	643.4985	46.4757
B_1	657.6573	10.1146
A_1	662.1556	16.9047
A_2	678.0992	0.0000
B_1	690.6206	56.5102
B_2	1189.8370	153.9787
A_1	1260.9593	4.0790
A_1	1985.8106	725.7993
B_2	2141.1199	145.1945
A_1	2148.7243	48.6161
B_2	3450.4901	83.4115
A_1	3452.4557	35.3336

Atom	Coordinates (Angstroms)		
	X	Y	Z
C	0.000000	0.000000	0.000000
C	0.000000	0.000000	1.289868
C	0.000000	0.000000	2.643698
C	0.000000	1.220770	3.387658
C	0.000000	2.253822	4.024841
H	0.000000	3.165296	4.575163
C	0.000000	-1.220770	3.387658
C	0.000000	-2.253822	4.024841
H	0.000000	-3.165296	4.575163

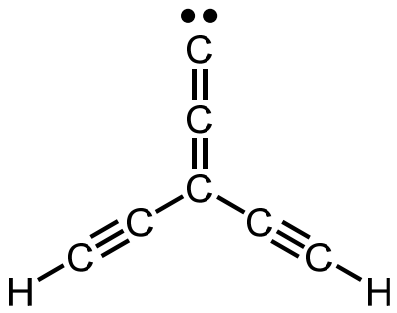

Charge	Multiplicity	Theory/Basis Set	Full Point Group
0	1	CCSD(T)/cc-pVTZ	C_{2V}
Zero-point Energy	**Electronic Energy**	**Electronic and Zero-Point Energy**	**Dipole Moment (D)**
0.051592	-267.109822	-267.058230	11.407759

Energies in Hartrees/particle

Symm.	Frequency (cm^{-1})	Intensity
B_1	71.5167	0.0142
B_2	82.9198	0.2325
B_1	205.1276	6.5385
B_2	209.9268	12.8587
B_2	425.9999	7.1216
B_1	449.6728	0.0090
B_1	475.8470	2.6050
A_1	546.6479	1.3677
B_2	557.8787	2.6254
B_2	730.6877	47.2525
A_2	912.6028	0.0000
A_1	933.6757	24.4290
B_1	934.5135	7.3148
B_1	1110.8759	14.8437
A_1	1115.0365	91.5602
A_1	1476.6423	439.1083
A_1	1673.9548	430.9281
A_1	2000.6387	2.1127
A_1	2185.9434	3109.1644
B_1	3252.1312	12.1843
A_1	3292.8893	33.1019

Atom	Coordinates (Angstroms)		
	X	Y	Z
C	0.000000	0.000000	0.000000
C	0.000000	0.000000	1.282476
C	0.000000	0.000000	2.597420
C	0.000000	0.000000	3.856151
C	0.000000	0.000000	5.183981
C	0.000000	0.668192	6.444270
C	0.000000	-0.668192	6.444270
H	0.000000	1.592361	6.998881
H	0.000000	-1.592361	6.998881

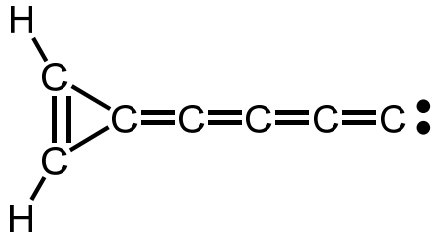

Charge	Multiplicity	Theory/Basis Set	Full Point Group
0	3	CCSD(T)/cc-pVTZ	C_{3v}

Zero-point Energy	Electronic Energy	Electronic and Zero-Point Energy	Dipole Moment (D)
0.076141	-306.403923	-306.327782	1.7123

Energies in Hartrees/particle

Symm.	Frequency (cm^{-1})	Intensity
E	58.6327	3.1919
E	58.6327	3.2760
E	134.1850	0.0049
E	134.1850	0.0835
E	243.9948	3.4320
E	249.9757	3.7868
E	385.6168	0.0166
E	385.6168	0.0257
E	418.2790	0.6398
E	418.2790	0.6398
E	428.4515	0.0428
E	428.4515	0.0428
A_1	461.5996	0.1380
E	539.6408	43.9001
E	539.6408	43.9001
A_1	851.2966	3.7836
E	1045.3969	0.9130
E	1045.3969	0.9130
A_1	1175.1703	3.7287
A_1	1412.8764	16.1923
A_1	1451.4234	45.7802
E	1482.6130	7.4698
E	1482.6130	7.4698
A_1	1696.8444	0.0692
A_1	2026.0452	6.6380
A_1	2158.6914	39.2452
A_1	3037.5398	23.6038
E	3111.8014	4.2538
E	3111.8014	4.2538
A_1	3453.3838	137.9238

Atom	Coordinates (Angstroms)		
	X	Y	Z
H	0.000000	0.000000	0.000000
C	0.000000	0.000000	1.063539
C	0.000000	0.000000	2.291732
C	0.000000	0.000000	3.630157
C	0.000000	0.000000	4.906774
C	0.000000	0.000000	6.181549
C	0.000000	0.000000	7.520934
C	0.000000	0.000000	8.749355
C	0.000000	0.000000	10.210643
H	-0.511284	0.885569	10.593423
H	-0.511284	-0.885569	10.593423
H	1.022568	0.000000	10.593423

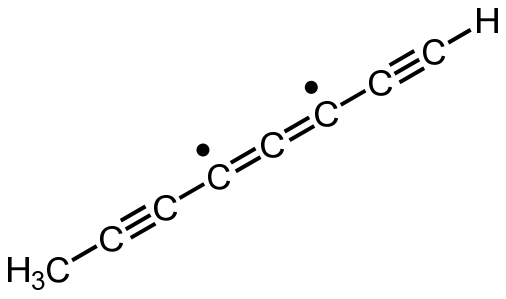

Charge	Multiplicity	Theory/Basis Set	Full Point Group
0	3	EOM-CCSD/ANO1	C_{3v}

Zero-point Energy	Electronic Energy	Electronic and Zero-Point Energy	Dipole Moment (D)
0.077892	-306.259952	-306.182060	1.750542

Energies in Hartrees/particle

Symm.	Frequency (cm^{-1})	Intensity
E	53.1500	3.3820
E	53.1500	3.3820
E	125.0008	1.0296
E	125.0008	1.0296
E	192.7329	0.1997
E	192.7329	0.1997
E	239.3719	42.3868
E	239.3719	42.3868
E	334.3202	1.5329
E	334.3202	1.5329
E	378.5145	0.0144
E	378.5145	0.0144
E	408.5583	7.2660
A1	408.5583	7.2660
A1	468.4021	0.0199
A1	856.6967	2.1246
E	1036.3006	1.2355
E	1036.3006	1.2355
A1	1225.6380	1.7213
A1	1423.2835	26.7174
E	1484.1116	7.8345
E	1484.1116	7.8345
A1	1597.6268	3.0892
A1	1768.5981	27.1557
A1	2096.8328	11.8443
A1	3043.5860	30.0905
E	3114.8407	4.3312
E	3114.8407	4.3312
A1	3466.7553	6.6304
A1	3509.4563	911.7335

Atom	Coordinates (Angstroms)		
	X	Y	Z
H	10.713483	0.000000	0.000000
C	8.707235	0.000000	0.000000
C	6.336553	0.000000	0.000000
C	3.874604	0.000000	0.000000
C	1.434740	0.000000	0.000000
C	-1.006036	0.000000	0.000000
C	-3.471472	0.000000	0.000000
C	-5.837995	0.000000	0.000000
C	-8.588809	0.000000	0.000000
H	-9.321443	0.963891	-1.669508
H	-9.321443	-1.927782	0.000000
H	-9.321443	0.963891	1.669508

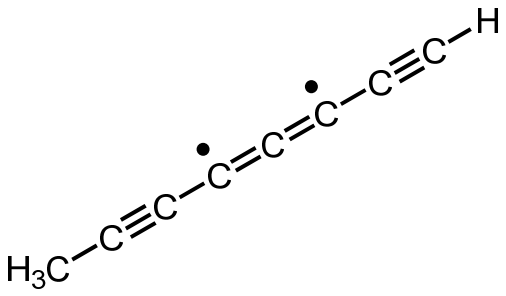

Charge	Multiplicity	Theory/Basis Set	Full Point Group
0	1	CCSD(T)/cc-pVTZ	C_S

Zero-point Energy	Electronic Energy	Electronic and Zero-Point Energy	Dipole Moment (D)
0.079948	-306.467163	-306.387215	0.9170

Energies in Hartrees/particle

Symm.	Frequency (cm^{-1})	Intensity
A'	61.1623	2.0994
A"	73.6013	2.8019
A'	152.0380	0.2580
A"	187.7879	0.0002
A'	261.0909	0.9925
A"	311.2744	3.0453
A'	426.1179	1.7885
A''	457.2499	0.0051
A'	464.9908	0.0456
A'	492.6164	0.1262
A"	493.3799	0.1505
A'	576.9376	3.5667
A"	616.5746	41.5210
A'	618.6099	40.6855
A"	672.3698	4.8610
A'	897.6370	0.0030
A"	942.0971	31.1721
A"	989.3591	22.1721
A'	1079.9379	1.3514
A'	1278.9538	3.7298
A'	1312.8621	9.6876
A'	1451.0100	4.7666
A'	1648.3963	9.7157
A'	2087.8819	0.1257
A'	2226.9070	0.4846
A'	2273.5659	12.7453
A'	3156.6066	1.2624
A'	3171.7053	9.2200
A'	3254.8754	4.8705
A'	3455.7112	116.6582

Atom	Coordinates (Angstroms)		
	X	Y	Z
C	0.000000	0.000000	0.000000
H	0.000000	0.000000	1.084764
C	1.611426	0.000000	-0.678941
H	2.105969	0.000000	-0.151646
H	1.179643	0.000000	-1.761306
C	-1.279005	0.000000	-0.634490
C	-2.389856	0.000000	-1.143649
C	-3.629134	0.000000	-1.723907
C	-4.738878	0.000000	-2.238570
C	-5.983383	0.000000	-2.815376
C	-7.088241	0.000000	-3.325258
H	-8.053920	0.000000	-3.771750

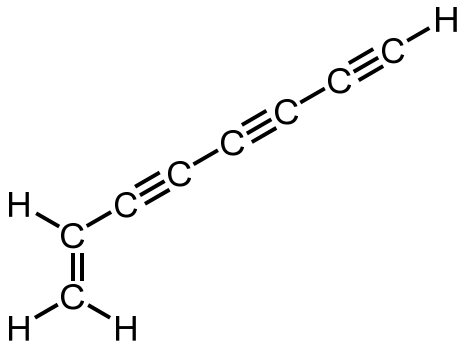

Charge	Multiplicity	Theory/Basis Set	Full Point Group
0	1	CCSD(T)/cc-pVTZ	C_s
Zero-point Energy	**Electronic Energy**	**Electronic and Zero-Point Energy**	**Dipole Moment (D)**
0.0799622	-306.399745	-306.320123	4.4815

Energies in Hartrees/particle

Symm.	Frequency (cm^{-1})	Intensity
A''	15.1865	0.0548
A'	67.5147	2.3412
A''	121.8029	0.3310
A'	175.6171	0.1819
A''	204.2103	0.8622
A'	297.1760	5.2878
A''	350.9628	8.9710
A'	416.6528	1.2817
A''	471.0719	9.2710
A'	522.6097	3.1773
A'	579.5729	8.3781
A'	613.0722	43.1367
A''	651.3493	1.5298
A''	695.6885	29.4365
A'	749.6087	3.4214
A'	1018.3304	6.8680
A''	1049.3410	1.5171
A'	1057.5167	0.8020
A'	1237.4381	33.4055
A'	1282.5093	47.9465
A'	1414.9902	6.5932
A'	1483.4715	9.9399
A''	1487.7600	7.5588
A'	1781.5428	7.1401
A'	2162.2725	7.7632
A'	2293.2266	84.5292
A'	3047.3002	11.2741
A''	3121.9510	2.6828
A'	3126.1003	4.5438
A'	3454.5763	79.1936

Atom	Coordinates (Angstroms)		
	X	Y	Z
C	0.000000	0.000000	0.000000
C	0.000000	0.000000	1.434709
C	1.186075	0.000000	0.633579
C	2.587048	0.000000	0.561808
C	3.799403	0.000000	0.499959
H	4.862549	0.000000	0.453643
C	-0.721602	0.000000	-1.198803
C	-1.353540	0.000000	-2.237310
C	-2.124025	0.000000	-3.480395
H	-2.762812	0.883675	-3.524661
H	-2.762812	-0.883675	-3.524661
H	-1.464207	0.000000	-4.348725

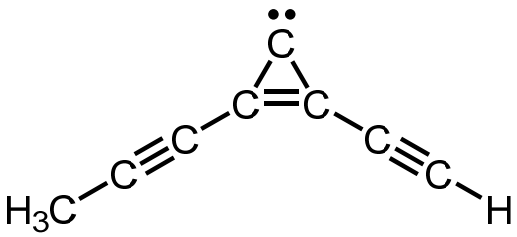

`

Charge	Multiplicity	Theory/Basis Set	Full Point Group
0	1	CCSD(T)/cc-pVTZ	C_s
Zero-point Energy	**Electronic Energy**	**Electronic and Zero-Point Energy**	**Dipole Moment (D)**
0.079917	-306.403271	-306.323354	4.7364

Energies in Hartrees/particle

Symm.	Frequency (cm^{-1})	Intensity
A''	10.9491	24.0864
A'	67.9613	3.0507
A''	68.8294	0.6502
A'	174.5476	5.4638
A''	185.8776	2.5461
A'	308.4563	1.9096
A''	343.4726	0.7847
A'	441.2446	0.6020
A'	454.0915	1.1911
A''	489.5090	0.1598
A'	500.0890	2.5622
A''	536.6551	1.6958
A'	811.9366	1.2964
A''	883.3642	0.8798
A'	948.7968	0.8798
A''	1050.2823	1.0517
A'	1052.7812	1.6964
A'	1070.7116	8.8333
A'	1263.5366	40.2877
A'	1265.7157	15.4051
A'	1415.6809	9.4864
A'	1484.1093	8.2470
A''	1486.1060	7.6517
A'	1718.3524	18.7424
A'	2204.1845	21.4620
A'	2304.3499	127.8563
A'	3046.2804	14.3971
A''	3121.9022	3.1637
A'	3123.0998	3.9755
A'	3257.7956	0.8411

Atom	Coordinates (Angstroms)		
	X	Y	Z
C	0.000000	0.000000	0.000000
H	0.000000	0.000000	1.078354
C	0.734866	-0.000000	-1.213471
C	-0.708566	0.000000	-1.136251
C	-1.933710	0.000000	-1.802681
C	-2.997457	0.000000	-2.403789
C	-4.193720	0.000000	-3.073837
C	-5.253954	0.000000	-3.673082
C	-6.526092	0.000000	-4.395001
H	-7.364627	0.000000	-3.697164
H	-6.600686	0.884939	-5.029054
H	-6.600686	-0.884939	-5.029054

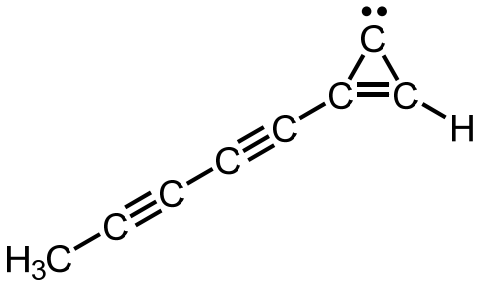

`

Charge	Multiplicity	Theory/Basis Set	Full Point Group
0	1	CCSD(T)/cc-pVTZ	C_1
Zero-point Energy	**Electronic Energy**	**Electronic and Zero-Point Energy**	**Dipole Moment (D)**
0.079599	-306.404874	-306.325275	3.8415

Energies in Hartrees/particle

Symm.	Frequency (cm^{-1})	Intensity
A	29.5405	1.2912
A	70.6314	2.7463
A	93.9879	0.4503
A	182.5619	1.1929
A	245.5909	8.1790
A	316.8092	3.3797
A	351.8019	1.0572
A	469.7624	0.7884
A	504.8552	0.7022
A	519.3376	0.3191
A	523.7848	3.3530
A	592.3546	1.7287
A	608.5680	43.1783
A	651.5627	38.4867
A	780.4051	0.3770
A	977.2203	11.4430
A	1030.3150	2.5296
A	1080.3481	6.4889
A	1268.1291	22.3376
A	1305.2586	26.2554
A	1401.9644	2.4024
A	1480.5131	13.8771
A	1491.9305	9.7736
A	1816.4588	6.8419
A	2111.4349	1.1109
A	2267.2340	7.6004
A	3046.3161	6.4845
A	3119.0781	7.1330
A	3142.9115	4.2051
A	3459.1106	104.2597

Atom	Coordinates (Angstroms)		
	X	Y	Z
C	0.000000	0.000000	0.000000
C	0.000000	0.000000	1.479799
C	0.759824	0.000000	-1.201751
C	-0.678341	-0.015970	-1.157609
C	-1.888949	-0.028799	-1.855878
C	-2.944960	-0.040314	-2.468746
C	-4.133530	-0.052970	-3.155154
H	-5.185655	-0.064326	-3.765068
C	-6.106153	-0.074126	-4.298106
H	0.173922	-1.023471	1.822002
H	0.818398	0.617869	1.850917
H	-0.949437	0.345968	1.886936